



Friedrich-Schiller-Universität Jena

---

Chemisch-Geowissenschaftliche Fakultät

Functional Polyether-Based Materials:  
From Synthesis to Controlled Cellular Uptake and  
Self-Healing Coatings

**Dissertation**

zur Erlangung des akademischen Grades  
doctor rerum naturalium (Dr. rer. nat.)

vorgelegt dem Rat der Chemisch-Geowissenschaftlichen Fakultät der  
Friedrich-Schiller-Universität Jena

von Diplom-Chemiker Markus J. Barthel  
geboren am 12.07.1985 in Zwickau



Gefördert durch das Dutch Polymer Institute (DPI, Technology Area HTE, Projekt #690) und den Deutschen Akademischen Austauschdienst (DAAD).

Gutachter:

1. Prof. Dr. Ulrich S. Schubert (Universität Jena)
2. Jun.-Prof. Dr. Felix H. Schacher (Universität Jena)

Tag der öffentlichen Verteidigung: 25.04.2014





*Für Claudia und meine Familie*



## Table of content

Documentation of authorship .....	1
1 Introduction .....	5
2 Self-assembly of functional polyether-based materials for controlled cell-uptake .....	11
3 Furfuryl glycidyl ether – a new monomer for living anionic ring-opening polymerization .....	25
4 Application of PFGE containing block copolymers .....	31
5 Summary.....	41
6 Zusammenfassung.....	45
7 References .....	49
List of abbreviations .....	53
Curriculum vitae .....	55
Publication list .....	57
Acknowledgements / Danksagung.....	61
Declaration of authorship / Selbstständigkeitserklärung .....	65
Publication P1 – P6.....	67



## Documentation of authorship

This section contains a list of the individual authors' contribution to the publications reprinted in this thesis.

1. "Poly(ethylene oxide) (PEO)-based ABC triblock terpolymers – Synthetic complexity vs. application benefits"

Markus J. Barthel, Felix H. Schacher, Ulrich S. Schubert

*Polym. Chem.* **2014**, DOI: 10.1039/C3PY01666H.

M. J. Barthel: Conceptual development, preparation of the manuscript  
F. H. Schacher: Conceptual development, correction of the manuscript, supervision  
U. S. Schubert: Correction of the manuscript, supervision

2. "Understanding and tuning the self-assembly of polyether-based triblock terpolymers in aqueous solution"

Markus J. Barthel, Ulrich Mansfeld, Stephanie Hoepfner, Justyna A. Czaplewska, Felix H. Schacher, Ulrich S. Schubert

*Soft Matter* **2013**, *9*, 3509-3520.

M. J. Barthel: Conceptual development, synthesis and characterization of the polymers, post-polymerization functionalization, DLS measurements, turbidimetry, preparation of the manuscript  
U. Mansfeld: Cryo-TEM measurements  
S. Hoepfner: Cryo-TEM measurements  
J. A. Czaplewska: Synthesis of acetylated thiogalactose  
F. H. Schacher: Conceptual development, correction of the manuscript, supervision  
U. S. Schubert: Conceptual contribution, correction of the manuscript, supervision

3. "Small but powerful: Co-assembly of polyether-based triblock terpolymers into sub-30 nm micelles and synergistic effects on cellular interactions"

Markus J. Barthel<sup>#</sup>, Alexandra Rinkenauer<sup>#</sup>, Michael Wagner, Ulrich Mansfeld, Stephanie Hoepfner, Justyna A. Czaplewska, Michael Gottschaldt, Anja Schallon, Felix H. Schacher, Ulrich S. Schubert

*submitted to Adv. Funct. Mater.*

<sup>#</sup>Both authors contributed equally to this work.

M. J. Barthel: Conceptual development, synthesis and characterization of the polymers, post-polymerization functionalization, self-assembly, DLS measurements, preparation of the manuscript  
A. C. Rinkenauer: Conceptual development, cell-uptake studies, toxicity tests, preparation of the manuscript  
M. Wagner: AF<sub>4</sub> and zeta-potential measurements, preparation of the manuscript  
U. Mansfeld: Cryo-TEM measurements  
S. Hoepfener: Cryo-TEM measurements  
J. A. Czaplewska: Synthesis of acetylated thiogalactose  
M. Gottschaldt: Correction of the manuscript  
A. Schallon: Conceptual development, correction of the manuscript  
F. H. Schacher: Conceptual development, correction of the manuscript, supervision  
U. S. Schubert: Correction of the manuscript, supervision

4. “Homo- and block copolymers of poly(furfuryl glycidyl ether) by living anionic polymerization: Towards reversibly core-crosslinked micelles”

Markus J. Barthel<sup>#</sup>, Tobias Rudolph<sup>#</sup>, Sarah Crotty, Felix H. Schacher, Ulrich S. Schubert  
*J. Polym. Sci., Part A: Polym. Chem.* **2012**, *50*, 4958-4965.

M. J. Barthel: Conceptual development, synthesis and characterization of the polymers, cross-linking studies, preparation of the manuscript  
T. Rudolph: Conceptual development, synthesis and characterization of the polymers, crosslinking studies, DLS measurements  
S. Crotty: MALDI-ToF MS measurements  
F. H. Schacher: Conceptual development, correction of the manuscript, supervision  
U. S. Schubert: Correction of the manuscript, supervision

5. “Self-healing materials *via* reversible crosslinking of poly(ethylene oxide)-*block*-poly(furfuryl glycidyl ether) (PEO-*b*-PFGE) block copolymer films”

Markus J. Barthel, Tobias Rudolph, Anke Teichler, Renzo M. Paulus, Jürgen Vitz, Stephanie Hoepfener, Martin D. Hager, Felix H. Schacher, Ulrich S. Schubert  
*Adv. Funct. Mater.* **2013**, *23*, 4921-4932.

M. J. Barthel: Conceptual development, synthesis and characterization of the polymers, self-healing studies, preparation of the manuscript  
T. Rudolph: Conceptual development, self-healing studies  
A. Teichler: Profilometry and contact angle measurements  
R. M. Paulus: DSC measurements  
J. Vitz: Nano-indentation measurements

<sup>#</sup>Both authors contributed equally to this work.

S. Hoepfener: AFM and TEM measurements  
M. D. Hager: Conceptual contribution, correction of the manuscript  
F. H. Schacher: Conceptual development, correction of the manuscript, supervision  
U. S. Schubert: Correction of the manuscript, supervision

6. “Poly(2-vinyl pyridine)-*block*-poly(ethylene oxide) featuring a furan group at the block junction – Synthesis and functionalization”

Tobias Rudolph<sup>#</sup>, Markus J. Barthel<sup>#</sup>, Florian Kretschmer, Ulrich Mansfeld, Stephanie Hoepfener, Martin D. Hager, Ulrich S. Schubert, Felix H. Schacher

*Macromol. Rapid Commun.* **2014**, DOI: 10.1002/marc201300875.

T. Rudolph: Conceptual development, functionalization of the polymers and nanoparticles, DLS, UV-Vis and zeta-potential measurements, preparation of the manuscript  
M. J. Barthel: Conceptual development, synthesis and characterization of the polymers, preparation of the manuscript  
F. Kretschmer: Synthesis and functionalization of gold nano-particles  
U. Mansfeld: TEM measurements  
S. Hoepfener: TEM measurements  
M. D. Hager: Correction of the manuscript  
U. S. Schubert: Correction of the manuscript, supervision  
F. H. Schacher: Conceptual development, correction of the manuscript, supervision

Declaration of the supervisor:

---

Prof. Dr. Ulrich S. Schubert

<sup>#</sup>Both authors contributed equally to this work.





## 1 Introduction

Parts of this chapter have been published: P1) M. J. Barthel, F. H. Schacher, U. S. Schubert, *Polym. Chem.* **2014**, DOI: 10.1039/C3PY01666H.

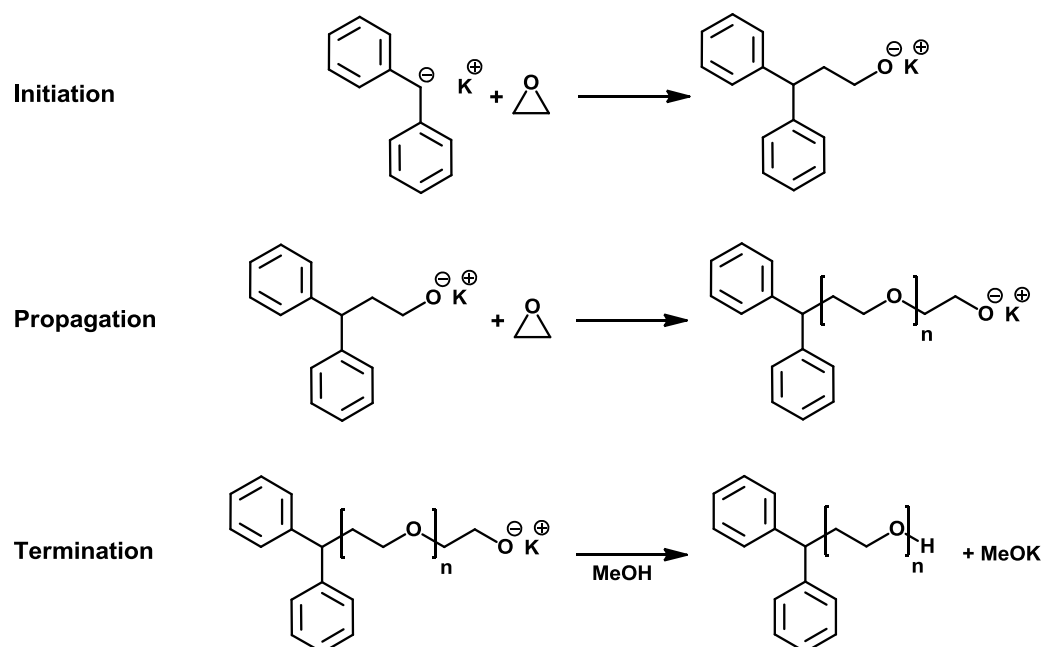
Nowadays, block copolymers are of broad interest regarding a variety of applications within the fields of material science, nanotechnology, and life science. In general, a combination of monomers with different chemical and physical properties is used to prepare such materials, in most cases of AB (diblock copolymers) or ABA (triblock copolymers) type. Both the combination of different properties of the constituting building blocks as well as the immiscibility of unlike polymer segments are exploited, leading to self-assembly in bulk, in thin-films, and in solution.<sup>1-3</sup> If a hydrophilic block A and a hydrophobic block B are combined, amphiphilic block copolymers are obtained.<sup>4</sup> Commercially established examples for block copolymers are polystyrene-*block*-polybutadiene-*block*-polystyrene (SBS) rubbers, or polystyrene-*block*-poly(methyl methacrylate) (PS-*b*-PMMA) thin-films in lithography strategies by, *e.g.*, IBM to pattern integrated circuit elements on length scales which cannot be reached by classical approaches.<sup>5,6</sup>

One widely used building block in various application fields as hydrophilic, non-toxic segment is poly(ethylene oxide) (PEO) or poly(ethylene glycol) (PEG), the nomenclature typically depends on the molar mass of the polymer). This is also the basis of Pluronics, a class of commercially available ABA triblock copolymers of poly(ethylene oxide)-*block*-poly(propylene oxide)-*block*-poly(ethylene oxide). These materials are mostly used as stabilizers for, *e.g.*, the synthesis of inorganic nanoparticles (Au, Ti).<sup>7</sup> The versatility of PEO and related materials can be explained by its outstanding physical and chemical properties. PEO is chemically inert, non-toxic, and thus a predestined candidate for biomedical applications.<sup>8</sup> PEO ensures good solubility in common organic solvents as well as water and, furthermore, is capable of preventing undesired interactions with the human immune system – the so called “stealth effect”.<sup>9</sup>

A powerful tool for the synthesis of well-defined polymers with a highly regular architecture, predictable molar mass, narrow molar mass distribution and controlled start and end-groups is the living anionic polymerization. Since the discovery of this technique by M. Szwarc in 1956,<sup>10</sup> the methodology has become an invaluable tool for the preparation of well-defined polymers and block copolymers.<sup>11</sup> Despite of the various advantages of the living anionic polymerization also disadvantages have to be pointed out. The living species, the carb-anion,

is highly sensitive to protic impurities. Therefore, it is necessary to work under inert conditions, to purify intensely all reactants and reaction vessels.

To obtain well-defined PEO containing block copolymers the living anionic ring-opening polymerization (AROP) of ethylene oxide represents a highly powerful and versatile technique.<sup>12</sup> As shown in **Scheme 1.1** the living AROP can be divided in three phases. In the first step the polymerization is initiated by the attack of a carbanion on the epoxy ring, resulting in the ring-opening. In the scheme a classical initiator for the synthesis of poly(ethylene oxide) (PEO), diphenylmethyl potassium, is shown.<sup>13</sup> The second step is represented by the chain propagation where the living species reacts with further ethylene oxide monomers, leading to the chain formation. For the living anionic polymerization it is crucial that the initiation rate is significantly higher than the propagation rate, which leads to predictable molar masses of the desired polymer. The last step is the termination of the living polymer chains. In **Scheme 1.1** the simplest method, the termination with methanol, is shown. The living polymer chain abstracts the proton of the hydroxyl group leading to the formation of an OH end-group of the PEO and formation of the potassium salt. Besides of methanol, also functional termination agents such as allyl or propargyl bromide can be used. The selective criterion is that the termination agent contains a partially positively charged carbon atom.



**Scheme 1.1:** Schematic representation of the reaction mechanism of the living anionic ring-opening polymerization of ethylene oxide.

Due to the lack of possibilities for the functionalization of PEO, there is a growing interest in the incorporation of functional groups into PEO-related materials. This can be achieved *via*

the preparation of block copolymers with segments containing functional monomers like butadiene, isoprene, vinylpyridine, or suitable glycidyl ethers featuring essentially the same polyether backbone. Traditionally used glycidyl ethers are allyl glycidyl ether (AGE, pendant double bond), ethoxy ethyl glycidyl ether (EEGE, protected hydroxyl groups), furfuryl glycidyl ether (FGE, furan moieties), or *N,N'*-dibenzyl amino glycidol (DBAG, protected amines) (**Figure 1.1**).<sup>14-17</sup>

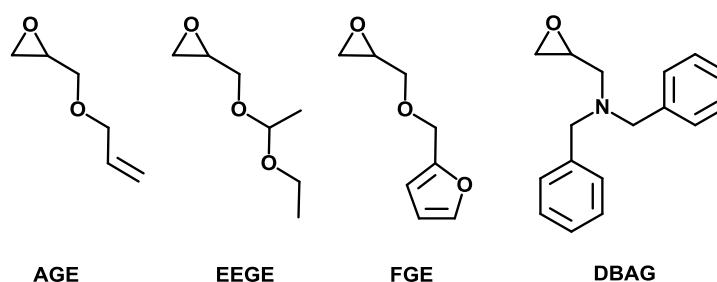


**Figure 1.1:** Schematic representation of suitable glycidyl ethers as monomers for living anionic ring-opening polymerization. Allyl glycidyl ether (AGE), ethoxy ethyl glycidyl ether (EEGE), furfuryl glycidyl ether (FGE) and *N,N'*-dibenzyl amino glycidol (DBAG).

In general, applications involving PEO-based block copolymers can be divided according to examples in the bulk or in solution. In both cases, mainly the phase separation of such systems is used to design nanostructured materials. Typically, applications in the bulk use PEO as a soft segment within block copolymer films of different composition, thickness, and morphology.<sup>18</sup> Furthermore, PEO containing block copolymer films have been employed for the coating of surfaces, exploiting the anti-fouling properties to prevent the uncontrolled adhesion and adsorption of proteins, cells, bacteria, and other microorganisms.<sup>19</sup>

In solution, PEO most often serves as hydrophilic part of amphiphilic or double hydrophilic block copolymers. Regarding amphiphilic systems, classical examples contain PS, PI or PB as hydrophobic segments. In aqueous media, such materials undergo self-assembly into micellar structures where the hydrophobic block forms the core. Many recent examples report the loading of these aggregates with hydrophobic compounds such as dyes or drugs (into the core). The PEO corona, on the other hand, provides solubility in aqueous media and, additionally, the stealth-effect attributed to PEO prevents undesired interactions with proteins and renders such particles attractive for potential biomedical applications.<sup>8</sup> One example is PEO-*b*-poly( $\epsilon$ -caprolactone) (PEO-*b*-PCL), where the PCL block forms a biodegradable core.<sup>20</sup> Moreover, the use of poly(ethylene oxide)-*block*-poly(allyl glycidyl ether) (PEO-*b*-PAGE) block copolymers in drug-delivery approaches has been reported by Hruby.<sup>21</sup> Here, micelles with a hydrophobic PAGE core and a PEO corona were formed in aqueous solution and the pendant double bonds within the PAGE side chain were used to covalently attach

doxorubicin (an anti-cancer drug) *via* a pH-labile linker. As the pH value in cells is distinctly lower than in the blood stream, the linker was cleaved upon uptake in the cell and the drug released selectively at the desired site.

Despite of this broad field of applications, it is of great interest to introduce further segments into block copolymers, *e.g.*, when dealing with ABC triblock terpolymers. This significantly increases the morphological variety as well as the range of functional groups or stimuli with which such materials can be externally addressed. In the last 15 years, a high scientific effort was invested to realize the synthesis of well-defined ABC triblock terpolymers although the first examples were already reported in the 1970 and 80s.<sup>22</sup> In these cases, the phase diagram of polystyrene-*block*-polybutadiene-*block*-poly(4-vinyl pyridine) (PS-*b*-PB-*b*-P4VP) or polystyrene-*block*-polyisoprene-*block*-poly(4-vinyl pyridine) (PS-*b*-PI-*b*-P4VP) was intensively studied.<sup>23</sup> However, this field intensified during the early 1990s, *e.g.*, through pioneering work on polystyrene-*block*-polybutadiene-*block*-poly(methyl methacrylate) (PS-*b*-PB-*b*-PMMA) by Stadler and coworkers.<sup>24-27</sup> The first examples of ABC triblock terpolymers containing a PEO segment were reported by Huang *et al.* in the late 1990s for poly(ethylene oxide)-*block*-polystyrene-*block*-poly(methyl methacrylate) (PEO-*b*-PS-*b*-PMMA) or (PS-*b*-PEO-*b*-PMMA) systems.<sup>28, 29</sup> The use of PEO within ternary systems can significantly broaden the range of possible applications and lead to fascinating materials (**Figure 1.2**). More specific, the following benefits can be identified: In the bulk it is possible to introduce a crystallizable segment and, therefore, an additional driving force to improve control over and the variety of volume morphologies. Furthermore, the block interactions can be tuned, as well as the formation of organic/inorganic hybrid structures is enabled. In the case of coatings the control over cell-adhesion by nanostructured block copolymers can be achieved. In solution an improved control over possible morphologies of solution structures and the creation of stimuli-responsive nanostructured materials (triggers are pH value, temperature and light) is given. By combination of these benefits versatile materials for drug-delivery approaches can be obtained.

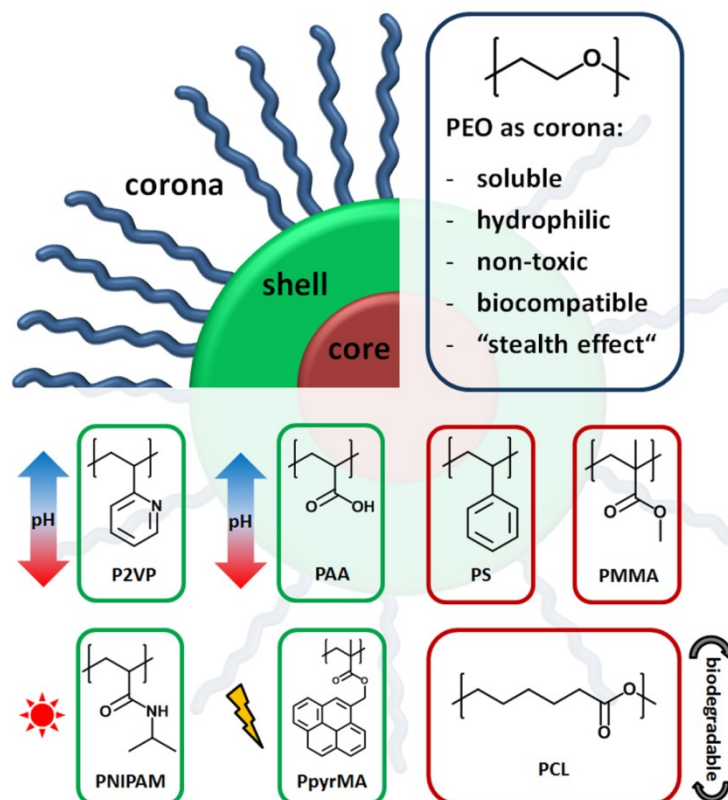


**Figure 1.2:** Schematic representation of a micellar structure for drug-delivery approaches showing selected examples for stimuli responsive building blocks for the shell or core segment. As pH sensitive building block poly(2-vinyl pyridine) (P2VP) and poly(acrylic acid) (PAA) are depicted. Poly(*n*-isopropylacrylamide) (PNIPAm) represents a thermo responsive unit whereas poly(pyrenylmethyl methacrylate) (PpyrMA) acts as light sensitive moiety. Possible hydrophobic core-forming blocks are polystyrene (PS) or poly(methyl methacrylate) (PMMA). A biodegradable hydrophobic segment represents poly( $\epsilon$ -caprolactone) (PCL).

The aim of this thesis is to point out the potential of well-defined PEO containing diblock copolymer and triblock terpolymer structures obtained by living anionic ring-opening polymerization in a broad field of applications. In the following chapters an overview from controlled synthesis and post-polymerization functionalization approaches to the application of polyether-based materials in solution as well as in the bulk will be given. **Chapter 2** will discuss the controlled synthesis of poly(ethylene oxide)-*block*-poly(allyl glycidyl ether)-*block*-poly(*t*-butyl glycidyl ether) (PEO-*b*-PAGE-*b*-PtBGE) by living AROP with sequential monomer addition. Subsequently, the obtained polymer will be used in a post-polymerization functionalization of the PAGE block with bioactive moieties, *via* thiol-ene click reactions. The influence of the attachment of acetylated thiogalactose on the self-assembly and lower critical solution temperature (LCST) is studied in detail. The synthesized polymers were used in a second step as platform for the formation of mixed micelles and the self-assembled structures were studied in detail with help of, *e.g.*, cryo-TEM, DLS and AF4 measurements. Additionally, the self-assembled structures are used to encapsulate a hydrophobic dye (nile

red) as model compound for a drug and the influence of the attached moieties on the cellular uptake is studied.

The application of a new monomer – furfuryl glycidyl ether – for the living anionic ring-opening polymerization is described in **Chapter 3**. The influence of different initiators for the living anionic polymerization on the synthesis of well-defined poly(furfuryl glycidyl ether) (PFGE) homopolymers is reported. Furthermore, well-defined diblock copolymers are synthesized and the formation of micellar structures, due to the highly hydrophobic character of the PFGE block could be studied. By reversible crosslinking of the PFGE block with a suitable bismaleimide utilizing the Diels-Alder reaction stabilized micellar nano-structures could be obtained. **Chapter 4** is devoted to the application of PFGE containing polymers. Here, PFGE homopolymers and PEO-*b*-PFGE diblock copolymers are applied as self-healing surface coatings. In this case the reversible crosslinking by the Diels-Alder reaction enables the changing of the mechanical properties of the polymer coating and the healing of an inflicted damage. Furfuryl glycidyl ether is subsequently used to create a reactive junction point in a poly(2-vinyl pyridine)-*b*-poly(ethylene oxide) chain. This unit is employed afterwards to attach the polymer covalently to a gold nano-particle surface and to connect a dye for an efficient targeting of the molecule.

## 2 Self-assembly of functional polyether-based materials for controlled cell-uptake

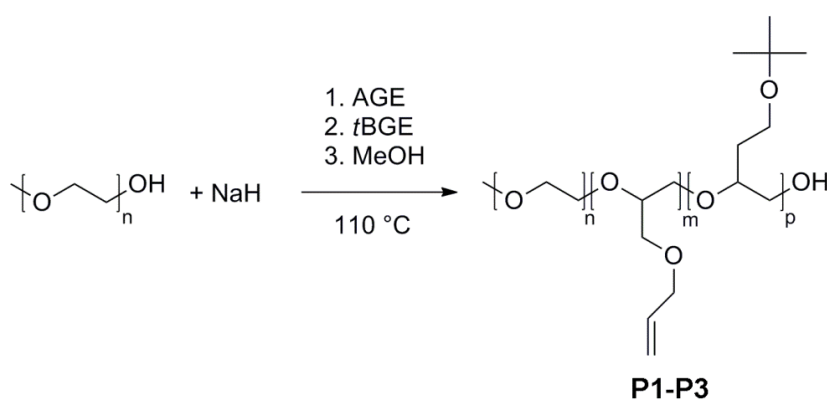
Parts of this chapter will be/have been published: P2) M. J. Barthel, U. Mansfeld, S. Hoepfner, J. A. Czaplewska, F. H. Schacher, U. S. Schubert, *Soft Matter* **2013**, *9*, 3509-3520. P3) M. J. Barthel, A. C. Rinkenauer, M. Wagner, U. Mansfeld, S. Hoepfner, J. A. Czaplewska, A. Schallon, F. H. Schacher, U. S. Schubert, *submitted to Adv. Funct. Mater.*

Nanostructures generated *via* bottom-up self-assembly processes of well-defined macromolecules are of great interest in the fields of polymer science, nanotechnology, and also biomedicine.<sup>3, 30, 31</sup> In particular in the latter case, soft and solution-borne structures, *i.e.* micelles, vesicles, or multicompartiment polymer particles are discussed regarding potential applications as sensors or delivery vehicles.<sup>32-34</sup> As shown in **Chapter 1** linear ABC triblock terpolymers hold great potential for the controlled formation of core/shell/corona or compartmentalized structures, where either the core or the shell are further subdivided.<sup>3, 35, 36</sup> Besides the typically observed nanostructures from diblock copolymers, which have been investigated in detail, these materials offer a greater diversity of accessible morphologies and the presence of a third segment allows the introduction of additional functionalities or responsive properties.<sup>37</sup> Regarding possible applications of these polymers in, *e.g.*, biological systems, the materials should be water soluble, non-toxic and chemically inert. As shown in the previous chapter these requirements are fulfilled by poly(ethylene oxide) (PEO) and, partially, by poly(glycidyl ethers) containing additional functionalities in the side chain, for instance, double bonds, hydroxyl groups or amino moieties.<sup>38</sup> For several monomers such as allyl glycidyl ether, 1-ethoxy ethyl glycidyl ether or *N,N'*-dibenzyl amino glycidol the preparation of well-defined side-chain functionalized polyether materials has already been achieved.<sup>17, 39-42</sup>

One further possibility to tune the solution properties of block copolymers and related materials (or nanostructures) are post-polymerization functionalizations, *e.g.*, by thiol-ene chemistry involving the pendant double bonds of allyl glycidyl ether segments.<sup>17, 43-47</sup> This process enables the incorporation of additional functionalities or the block-specific attachment of markers, such as fluorescent dyes. Nevertheless, controlled structure formation or, more precise, the successful prediction of solution structures generated *via* the self-assembly of triblock terpolymers still remains challenging.

In a previous study the synthesis of a well-defined amphiphilic triblock terpolymer poly(ethylene oxide)-*block*-poly(allyl glycidyl ether)-*block*-poly(*tert*-butyl glycidyl ether)

(PEO-*b*-PAGE-*b*-PtBGE) *via* sequential living anionic ring-opening polymerization whereas the pendant double bonds of the PAGE block were used in post-polymerization functionalizations *via* thio-ene click chemistry was reported. Thereby it was shown that bioactive moieties such as acetylated thiogalactose, acetylated thioglucose and acetylated cysteine as model compound for a cell-penetrating peptide could be attached to the polymer backbone. Subsequently, the influence of the attached moieties on the physical and chemical properties was studied. Here, a significant influence on the self-assembly behavior of the amphiphilic system in aqueous systems could be observed.<sup>47</sup> To investigate this phenomenon in detail a library of ABC triblock terpolymers, PEO-*b*-PAGE-*b*-PtBGE was synthesized *via* sequential living anionic ring-opening polymerization (AROP) (**Scheme 2.1**).



**Scheme 2.1:** Schematic representation of the synthesis of PEO-*b*-PAGE-*b*-PtBGE triblock terpolymers using sequential living anionic ring-opening polymerization (AROP).

The obtained triblock terpolymers consist of a first block, PEO, with a degree of polymerization (DP) of 42. The length of the middle block, PAGE, was varied whereas the DP of the last segment PtBGE was almost constant. The experimental data of selected polymers is given in **Table 2.1**. The final compositions were determined using <sup>1</sup>H NMR spectroscopy. For samples with a shorter PAGE segment (*e.g.*, DP = 2), the obtained block lengths were in good agreement with the theoretical values, whereas in case of longer blocks (DP = 20) the conversion of AGE did not reach 100%. This can be attributed to a rather slow polymerization rate in case of AGE, as already observed during earlier studies and in the literature.<sup>14, 47</sup> Nevertheless, full crossover to *t*BGE could be achieved.



**Table 2.1:** Molecular characterization data of selected synthesized triblock terpolymers.

Entry	$M_{\text{theo}}$ [g/mol]	$M_n^a$ [g/mol]	$M_w^a$ [g/mol]	PDI <sup>a</sup>	Ratio <sub>theo</sub> n/m/p	Ratio <sup>b</sup> n/m/p
<b>P1</b>	4,000	2,800	2,900	1.04	42/2/15	42/2/15
<b>P2</b>	4,950	2,900	3,100	1.05	42/10/15	42/7/14
<b>P3</b>	6,100	3,400	3,500	1.06	42/20/15	42/15/12

<sup>a</sup> Obtained by SEC (CHCl<sub>3</sub>:*i*-Prop.:TEA 94:4:2, using PEO standards)

<sup>b</sup> Determined by <sup>1</sup>H NMR spectroscopy

The reaction process was monitored by size exclusion chromatography (SEC). In **Figure 2.1** the SEC traces for the samples **P1-P3** are shown. The obtained polymers showed a narrow and monomodal molar mass distribution.

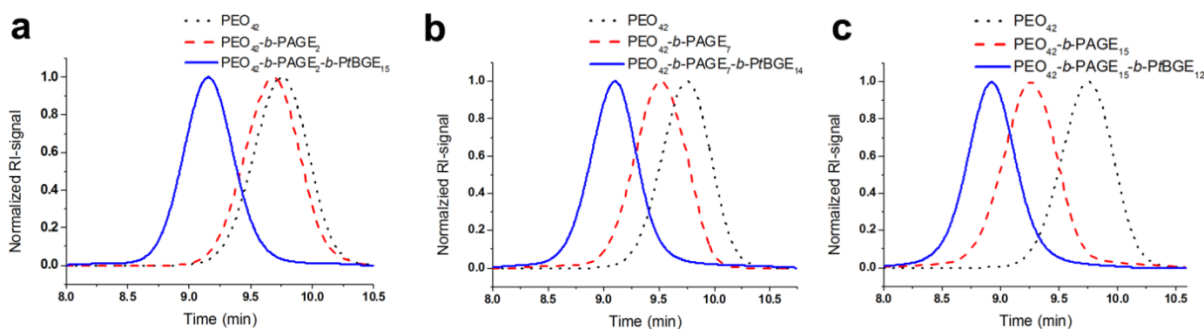
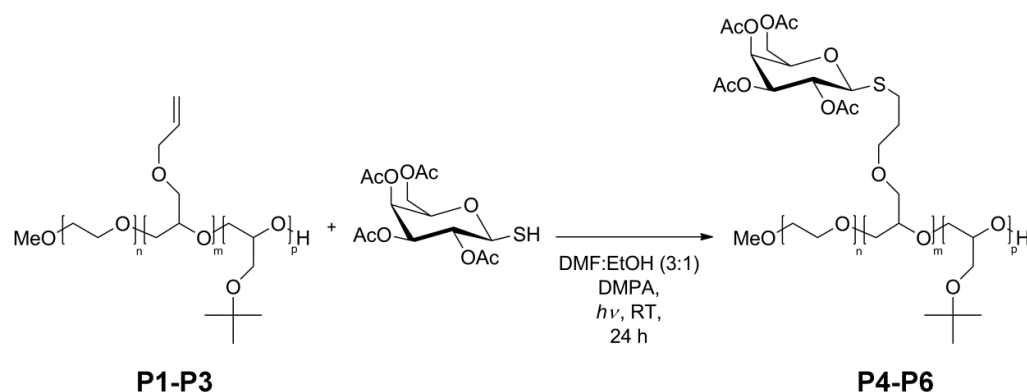


**Figure 2.1:** SEC traces for **P1** (a), **P2** (b) and **P3** (c) obtained *via* living AROP; PEO macroinitiator (solid black lines), PEO-*b*-PAGE diblock copolymer (solid red lines), and PEO-*b*-PAGE-*b*-PtBGE triblock terpolymers (solid blue lines).

Post-polymerization modification by thiol-ene chemistry represents one straightforward possibility to influence the solution behavior of the obtained triblock terpolymers. For this purpose, acetylated thiogalactose was attached to the PAGE segment of the as-synthesized triblock terpolymers (**Scheme 2.2**). The introduction of these molecules to the polymer increases the volume fraction of the hydrophobic middle block, PAGE, but also enables subsequent deprotection of the galactose moieties towards double hydrophilic sugar-labeled terpolymers.<sup>48</sup>



**Scheme 2.2:** Schematic representation of the post-polymerization functionalization of PEO-*b*-PAGE-*b*-PtBGE triblock terpolymers by the attachment of acetylated galactose *via* thiol-ene chemistry.

The detailed characterization of selected triblock terpolymers is given in **Table 2.2**. It could be shown that for the sample **P6** full conversion of the double bonds could be obtained. For the samples **P4** and **P5** only partial conversion could be achieved. This can be attributed to solubility problems and aggregation of the polymer chains in the solvent mixture due to the differences in solubility caused by the three blocks.

**Table 2.2:** Molecular characteristics of the functionalized triblock terpolymers.

Entry	$M_{\text{theo}}$ [g/mol]	$M_n^a$ [g/mol]	$M_w^a$ [g/mol]	PDI <sup>a</sup>	$f^b$ [%]
<b>P4</b>	4,800	2,850	2,950	1.03	65
<b>P5</b>	7,000	3,500	3,650	1.05	50
<b>P6</b>	10,600	4,600	4,800	1.05	100

<sup>a</sup> Obtained by SEC (CHCl<sub>3</sub>:*i*-Prop.:TEA 94:4:2, using PEO standards)

<sup>b</sup> Determined by <sup>1</sup>H NMR spectroscopy

To study the self-assembly properties of the functionalized triblock terpolymers in aqueous solution dynamic light scattering (DLS) measurements were performed. For all polymers shown here, the formation of core/shell/corona architectures was expected. The hydrophobic PtBGE segment is supposed to form the core, covered by a shell of the middle block, PAGE. The hydrophilic corona consists of the PEO segment, like already observed in earlier studies.<sup>47</sup> In the following aqueous solutions **P4**, **P5** and **P6** at concentrations of 5 g/L were studied by DLS (**Figure 2.2**). As the collapse of the PEO segments during heating/cooling cycles might lead to structural rearrangements and changes in the micellar morphology, each sample has been investigated prior to (solid black lines) and after heating to 100 °C (solid red lines).

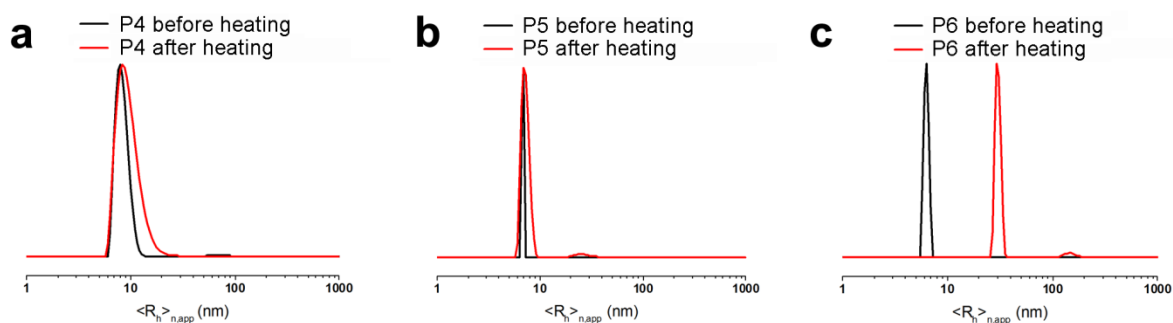


**Figure 2.2:** Number-weighted DLS CONTIN plots for **P4** before (solid black line,  $\langle R_h \rangle_{n,app} = 8$  nm) and after three consecutive heating/cooling cycles (solid red line,  $\langle R_h \rangle_{n,app} = 9$  nm, a); **P5** before (solid black line,  $\langle R_h \rangle_{n,app} = 7$  nm) and after heating (solid red line,  $\langle R_h \rangle_{n,app} = 7$  nm, b); **P6** before (solid black line,  $\langle R_h \rangle_{n,app} = 8$  nm) and after heating (solid red line,  $\langle R_h \rangle_{n,app} = 30$  nm, c).

For solutions from **P4**, particles with a  $\langle R_h \rangle_{n,app} = 8$  nm can be observed, and no significant changes occur during the heating/cooling cycles ( $\langle R_h \rangle_{n,app} = 9$  nm, **Figure 2.2, a**). Also in case of **P5**, the initially formed particles with  $\langle R_h \rangle_{n,app} = 7$  nm can also be found after the heat treatment, as well as a small fraction of larger aggregates, presumably micellar clusters ( $\langle R_h \rangle_{n,app} = 7$  and 25 nm, **Figure 2.2, b**). The highest impact of the heating on the particle sizes was observed for the triblock terpolymer with the highest weight fraction of hydrophobic segments (**P6**), where significant changes can be observed: At first, micelles with  $\langle R_h \rangle_{n,app} = 8$  nm are formed, which transform into larger aggregates after the heat treatment (**Figure 2.2, c**). More precisely, a bimodal distribution with  $\langle R_h \rangle_{n,app} = 30$  and 145 nm is found afterwards. This can be attributed to irreversible aggregation processes, leading to changes in micellar size and, potentially, morphology. The experimental data is shown in **Table 2.3**.

**Table 2.3:** DLS data for the triblock terpolymers after modification *via* thiol-ene chemistry before and after heat treatment.

Entry	Before heat-treatment	After heat-treatment
	N [nm]	N [nm]
<b>P4</b>	8	9
<b>P5</b>	7	7
<b>P6</b>	8	30

While DLS measurements are a powerful tool to assess average size and dynamics of micellar aggregates in solution, a detailed assignment of the involved morphologies requires further information. A straightforward and elegant tool to achieve this is cryo-TEM. Thereby, the self-assembled structures of individual macromolecules can be (ideally) visualized without drying artifacts in, typically, aqueous media.<sup>49-51</sup>

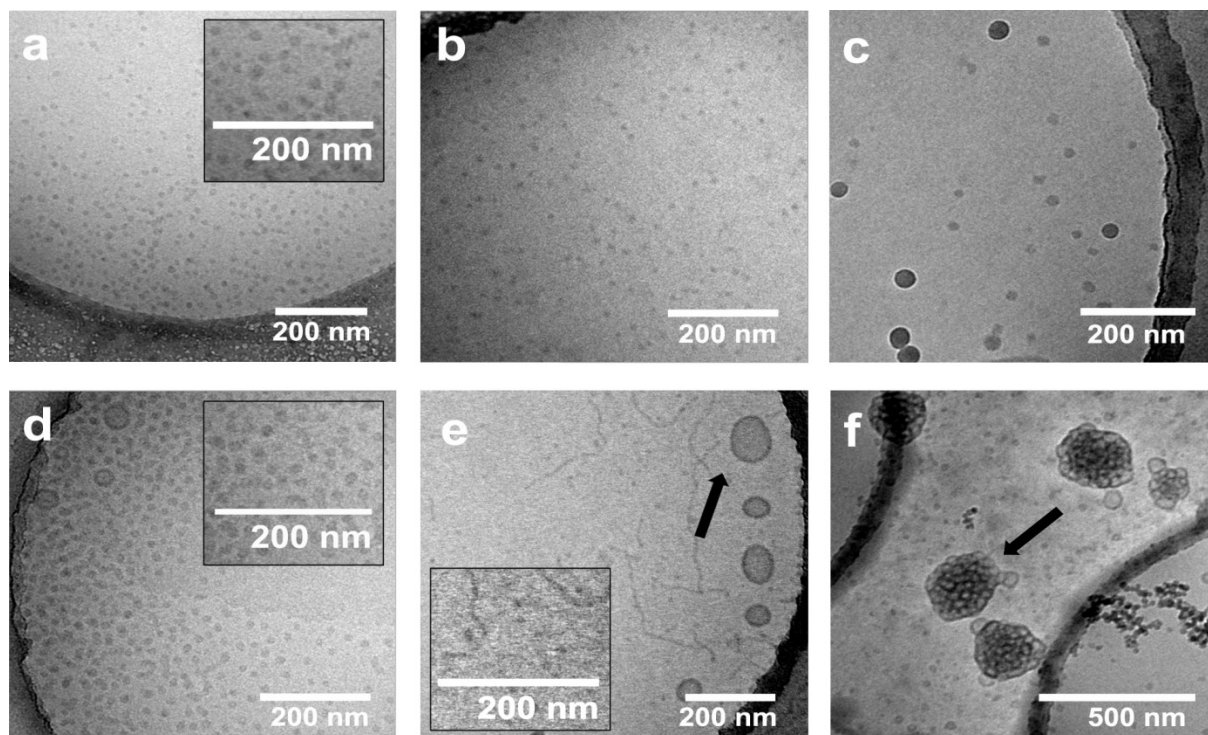


**Figure 2.3:** Cryo-TEM measurements of the functionalized triblock terpolymers after the attachment of thiogalactose before (a: **P4**; b: **P5**; c: **P6**) and after heating (d: **P4**; e: **P5**; f: **P6**) at a concentration of 5 mg/mL.

As shown by DLS measurements solutions from **P4** did not reveal any significant changes in particle size upon heating (**Figure 2.2**). This can also be confirmed by the cryo-TEM images (**Figure 2.3, a and d**) showing micelles before and after heating. For **P5**, a transformation of the self-assembled structures could be observed. Initially spherical micelles can be detected, whereas worm-like structures and vesicles are visible after the heating process. This is ascribed to the increase of the hydrophobic weight fractions *via* thiol-ene chemistry, presumably crossing the transition point from spherical micelles to larger structures. For the sample with the highest content of PAGE (**P6**), light scattering pointed towards larger structures (30 nm) being formed after heating. As shown *via* cryo-TEM (**Figure 2.3, c and f**), vesicles of a rather broad size distribution are formed initially, which agglomerate to larger clusters while heating. A schematic representation of the self-assembly behavior of the three described PEO-*b*-PAGE<sub>Gal</sub>-*b*-PtBGE triblock terpolymers before and after heat-treatment is depicted in **Figure 2.4**.

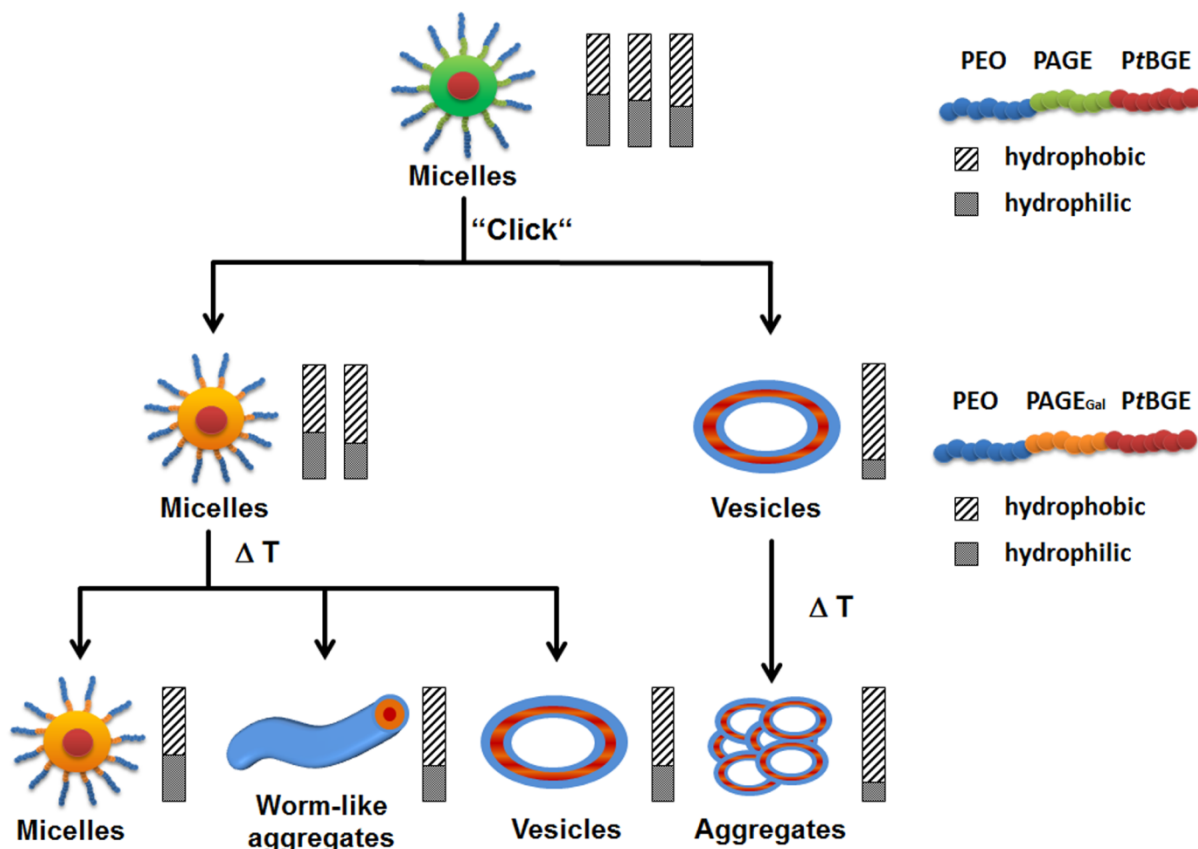


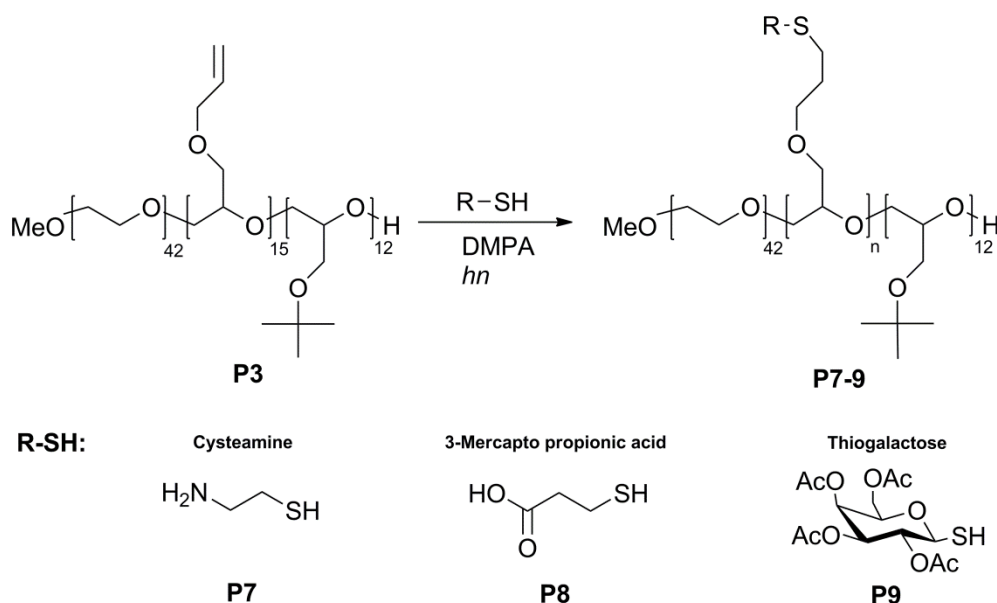
**Figure 2.4:** Schematic representation of the self-assembly behavior of the galactose-functionalized triblock terpolymers; color code: PEO (blue), PAGE (green), PAGE<sub>Gal</sub> (orange), and PtBGE (red); the ratio of hydrophilic / hydrophobic blocks is schematically shown by the corresponding bars (grey = hydrophilic, black/white stripes = hydrophobic).

An alternative approach for the advanced design of block copolymer micelles is mixing of diblock copolymers. As an example, AB and AC diblock copolymers – where A represents identical hydrophobic blocks – are mixed in non-selective solvents and are then transferred to a solvent or solvent mixture selective for B and C. It is generally believed that comparable degrees of polymerization (DP) for block A are beneficial. These materials revealed a high potential as drug carrier in delivery processes.<sup>52-55</sup>

Besides efforts to design structures of increased complexity for drug delivery applications, Kataoka *et al.* demonstrated that size does indeed matter and showed that micelles with diameters below 100 nm are highly interesting candidates in such approaches.<sup>56</sup> Commonly, nanostructures with diameters between 50 to 200 nm are used because endocytosis as predominant internalization process can be assumed, the interaction with the immune system is reduced, and renal clearance can be avoided.<sup>57, 58</sup> In contrast, polymeric micelles with sizes far below 100 nm are scarce in literature and, up to now, rarely studied with regard to interactions with biological matter.<sup>57</sup> In this context, spherical core-shell micellar structures of approximately 30 nm were found to effectively penetrate poorly permeable tumor

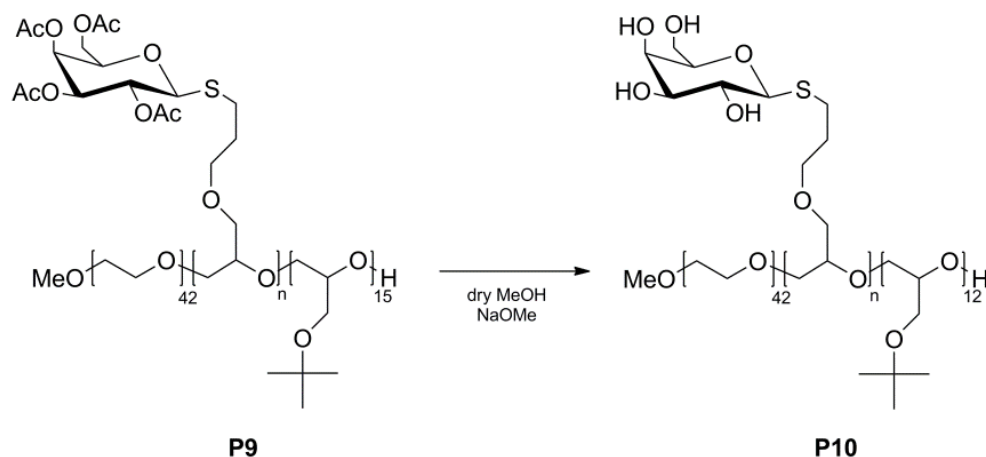
membranes.<sup>56</sup> Besides size, also charge significantly influences cell interactions of polymeric micelles, as well as their cytotoxicity and hemocompatibility. In general, the presence of cationic charges leads to increased interactions with the negatively charged cell membrane. Although this is advantageous for uptake, it also favors membrane destabilization and increases cytotoxicity. These side effects can be circumvented by using PEO as corona, but often at the cost of decreased cell interaction.<sup>59, 60</sup> As an alternative, the presence of negatively charged segments allows to decrease both the cytotoxicity and non-specific interactions with serum proteins.<sup>61</sup>

As for the presented PEO-*b*-PAGE-*b*-PtBGE triblock terpolymers very small self-assembled structures ( $\langle R_h \rangle_{n,app} < 10$  nm) could be obtained, these materials were applied in the described co-assembly process. For this purpose, a selected example (**P3**) was functionalized additionally to acetylated thiogalactose with cysteamine to introduce positive charges as well with 3-mercapto propionic acid to introduce negative charges (**Scheme 2.3**).



**Scheme 2.3:** Schematic representation of the thiol-ene click reaction of cysteamine, 3-mercapto propionic acid and acetylated thiogalactose on a PEO-*b*-PAGE-*b*-PtBGE triblock terpolymer.

For a targeted cellular uptake the acetylated thiogalactose has to be deprotected. As shown in **Scheme 2.4** one straight forward method is the treatment with sodium methanolate to cleave the acetyl groups. Therefore, the polymer was dissolved in dry methanol, an excess of sodium methanolate was added and the solution was stirred for 1 h.



**Scheme 2.4:** Schematic representation of the deprotection of acetylated thiogalactose attached to a PEO-*b*-PAGE-*b*-PtBGE triblock terpolymer.

Selected molecular characterization data for all materials can be found in **Table 2.4**.

**Table 2.4:** Characterization data of the synthesized polymers. The increment represent the degree of polymerization.

Entry	Sample	SEC		<sup>1</sup> H NMR	
		$M_n^a$ [g/mol]	PDI <sup>a</sup>	$M_n^b$ [g/mol]	$f$ [%] <sup>b</sup>
<b>P7</b>	PEO <sub>42</sub> - <i>b</i> -(PAGE <sub>8,NH2</sub> - <i>co</i> -PAGE <sub>7</sub> )- <i>b</i> -PtBGE <sub>12</sub>	3,500	1.06	5,750	53
<b>P8</b>	PEO <sub>42</sub> - <i>b</i> -PAGE <sub>15,COOH</sub> - <i>b</i> -PtBGE <sub>12</sub>	3,550	1.05	6,700	100
<b>P9</b>	PEO <sub>42</sub> - <i>b</i> -(PAGE <sub>10,AcGal</sub> - <i>co</i> -PAGE <sub>5</sub> )- <i>b</i> -PtBGE <sub>12</sub>	4,200	1.04	8,800	70
<b>P10</b>	PEO <sub>42</sub> - <i>b</i> -(PAGE <sub>10,Gal</sub> - <i>co</i> -PAGE <sub>5</sub> )- <i>b</i> -PtBGE <sub>12</sub>	10,400	1.10	7,100	70

<sup>a</sup> Obtained by SEC (CHCl<sub>3</sub>:*i*-Prop.:TEA 94:4:2, using PEO standards)

<sup>b</sup> Determined by <sup>1</sup>H NMR spectroscopy

For further applications and characterizations, Nile red, a hydrophobic red fluorescent dye, was encapsulated as model drug into the hydrophobic core of the micelles.

Subsequently, the solutions were analyzed by dynamic light scattering (DLS). In **Figure 2.5** the number weighted size distributions are depicted. For all samples, radii ( $\langle R_h \rangle_{n,app}$ ) in the range of 4 to 7 nm were detected in water.



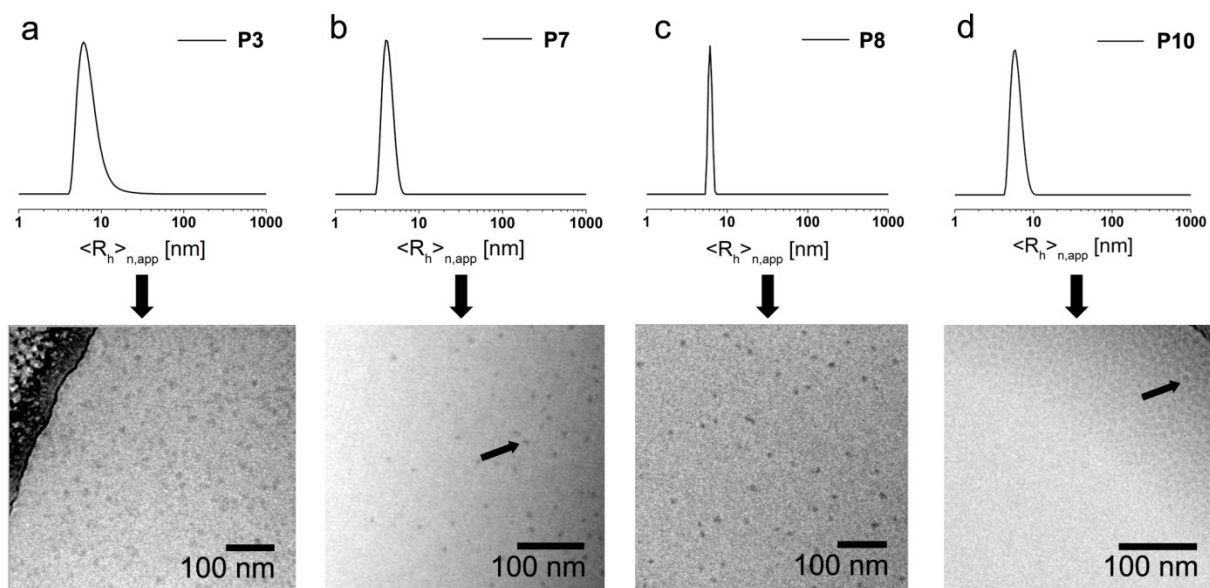


**Figure 2.5:** Number-weighted DLS CONTIN plots (upper section) for **P3** (a,  $\langle R_h \rangle_{n,app} = 7$  nm), **P7** (b,  $\langle R_h \rangle_{n,app} = 4$  nm), **P8** (c,  $\langle R_h \rangle_{n,app} = 6$  nm) and **P10** (d,  $\langle R_h \rangle_{n,app} = 6$  nm), as well as the corresponding cryo-TEM images (lower section) of the prepared self-assembled micelles. Due to the low contrast an arrow was introduced for **P7** (b) and **P10** (d) to highlight one micellar core.

For detailed assignment of the involved morphologies, cryo-TEM measurements were performed. As shown in **Figure 2.5**, micellar structures as main distribution could be detected for all prepared samples.

In comparison to the as-synthesized triblock terpolymer, the functionalized compounds should show an increased cell-uptake as for the application in biological systems, a combination of positive and negative charges would be desirable. These structures could mimic viral structures resulting in a synergistic effect for an enhanced cellular uptake.<sup>62</sup>

In the following approach, the synthesized triblock terpolymers **P7**, **P8** and **P10** were used as a platform for the preparation of co-assembled micelles by blending the polymeric precursors. For the co-assembled micelles, different ratios were prepared:

An excess of the positive charges (**P7/P8**)<sup>3.5:1</sup>, a slight excess of the positive charges (**P7/P8**)<sup>1.2:1</sup>, and an excess of the negative charges (**P7/P8**)<sup>1:2.6</sup>.

Subsequently, the prepared solutions were analyzed by DLS and cryo-TEM measurements (**Figure 2.6**).



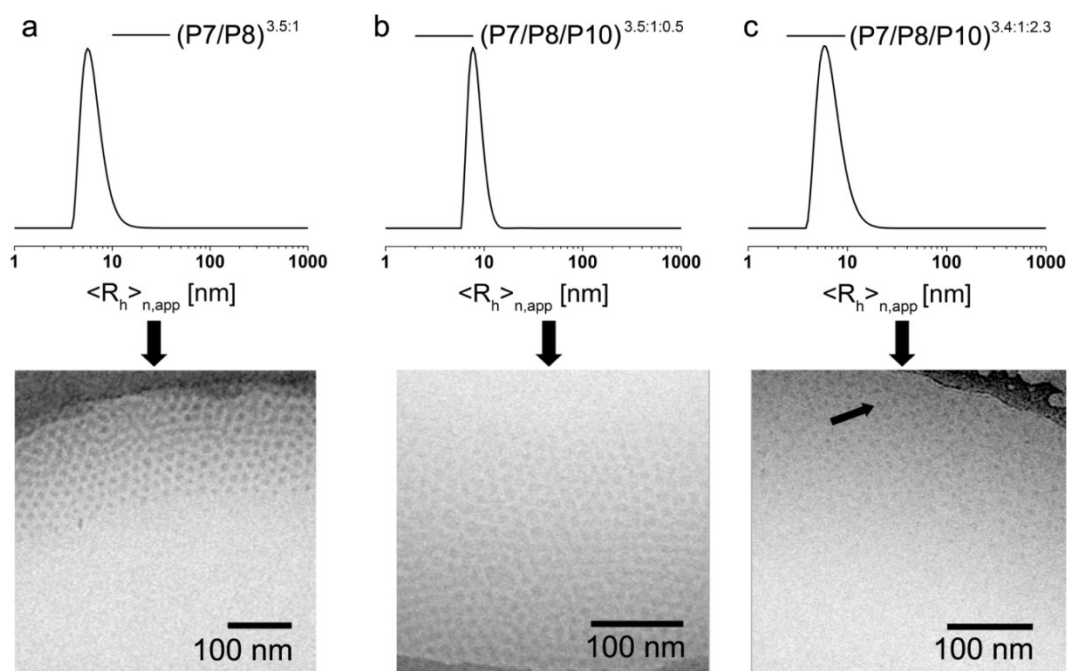


**Figure 2.6:** Number-weighted DLS CONTIN plots (upper section), as well as cryo-TEM images (lower section) of the prepared self-assembled mixed structures of  $(\mathbf{P7/P8})^{3.5:1}$  (a),  $(\mathbf{P7/P8/P10})^{3.5:1:0.5}$  (b), and  $(\mathbf{P7/P8/P10})^{3.4:1:2.3}$  (c).

In all cases micellar structures with sizes of  $\langle R_h \rangle_{n,app}$  of 4 to 6 nm in water could be obtained for the co-assembled triblock terpolymer. Additional to binary systems, also ternary systems of positively charged (**P7**), negatively charged (**P8**) and sugar-functionalized triblock terpolymers (**P10**) were prepared to enable a selective targeting of the cellular uptake, as the galactose moieties can act as a model ligand. For the preparation, two ratios of  $(\mathbf{P7/P8/P10})$  (3.5:1:0.5 and 3.4:1:2.3) were used and the solutions were characterized as described above. The obtained results can be found in **Figure 2.6 b** and **c**. In both cases, micellar structures with sizes of  $\langle R_h \rangle_{n,app} = 7$  nm for  $(\mathbf{P7/P8/P10})^{3.5:1:0.5}$  and 8 nm for  $(\mathbf{P7/P8/P10})^{3.4:1:2.3}$  could be detected.

Aiming at a later use of such triblock terpolymer micelles in targeting and/or delivery applications, their cytotoxicity was investigated using an Alamar blue assay. At first, triblock terpolymer micelles formed *via* the self-assembly of one single material were investigated. It could be demonstrated that **P3**, **P8** and **P10** did not show any cytotoxic effects for concentrations up to 0.5 mg/mL (cell viability was above 70 %). For **P7** ( $IC_{50} \approx 300$   $\mu\text{g/mL}$ ) a toxicity at higher concentrations was detectable (**Figure 2.7**).

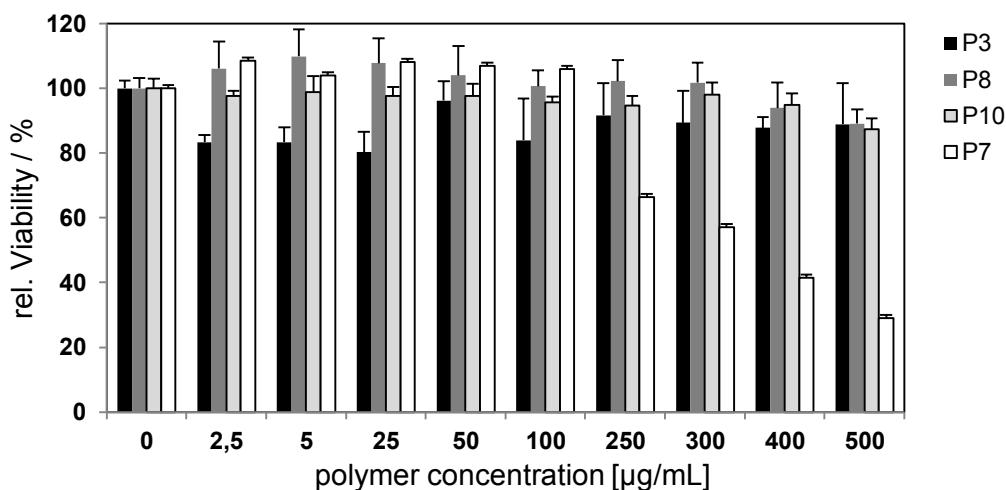


**Figure 2.7:** Cytotoxicity test of the micelles using L929 cells.

Subsequently, the internalization efficiency of micelles from **P3**, **P7**, **P8**, and **P10** into human embryonic kidney (HEK) cells, a model cell line for unspecific uptake studies under serum reduced and serum containing conditions was analyzed. Under serum reduced conditions the critical concentration, *i.e.* the concentration where **P3** shows nearly no uptake ( $1 \pm 1.1\%$ ), was determined to be  $10 \mu\text{g/mL}$  (**Figure 2.8**). From this data set, it becomes obvious that **P7** revealed the best uptake into  $79.7 \pm 4.5\%$  (at  $10 \mu\text{g/mL}$ ) of the cells. This can be attributed to the presence of positive charges in the shell and an increased interaction with the cell membrane. Compared to **P7**, the decreased uptake of **P8** and **P10** at a concentration of  $10 \mu\text{g/mL}$  with  $26.8 \pm 6.3\%$  and  $15.3 \pm 21.7\%$ , respectively, can be explained by the negative zeta potential of these particles, resulting in decreased interactions with cells. Nevertheless, **P8** and **P10** showed a significantly increased cellular uptake compared to the as-synthesized material **P3** at  $10 \mu\text{g/mL}$  ( $1 \pm 1.11\%$ ).

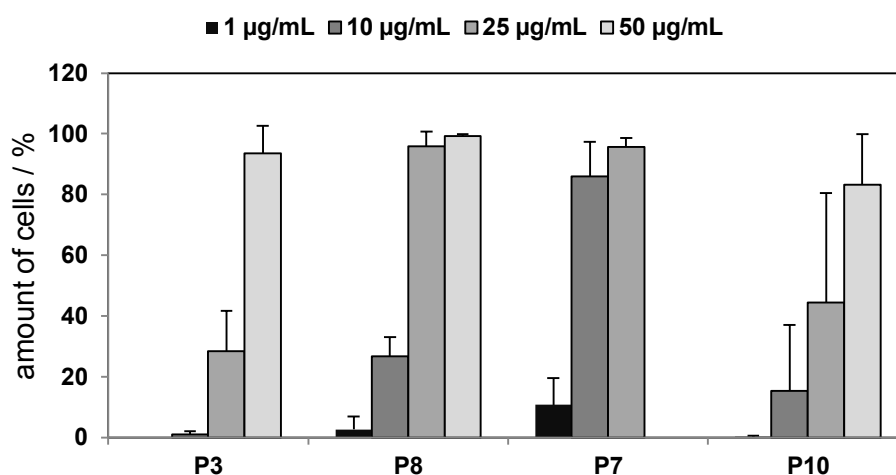


**Figure 2.8:** Cellular uptake of the micelles under serum reduced conditions in HEK cells.

In a second step the co-assembled structures were investigated regarding their internalization behavior. Here,  $(\text{P7/P8})^{3.5:1}$  demonstrated outstanding uptake compared to all other samples as already at a concentration of 10  $\mu\text{g/mL}$  under serum containing conditions  $75 \pm 11.5\%$  of the cells showed internalization (**Figure 2.9**). For  $(\text{P7/P8})^{1.2:1}$  and  $(\text{P7/P8})^{1:2.6}$ , a reduced uptake with 9% and 7% compared to  $(\text{P7/P8})^{3.5:1}$  could be observed. It could be, therefore, demonstrated that the charge ratio of the co-assembled micelles has a significant influence on the cellular uptake. In case of the ternary co-micelles  $(\text{P7/P8/P10})^{3.5:1:0.5}$ , a decreased uptake compared to  $(\text{P7/P8})^{3.5:1}$  was detected. This can be attributed to the presence of **P10** (**Figure 2.9**). Further increase of the galactose content leads to even lower values, which is in accordance with lower uptake of **P10** compared to **P9** and **P8**. Nevertheless, it should be noted that, in contrast to  $(\text{P7/P8})^{3.5:1}$ , both  $(\text{P7/P8/P10})^{3.5:1:0.5}$  and  $(\text{P7/P8/P10})^{3.4:1:2.3}$  did not show any detectable cytotoxicity.

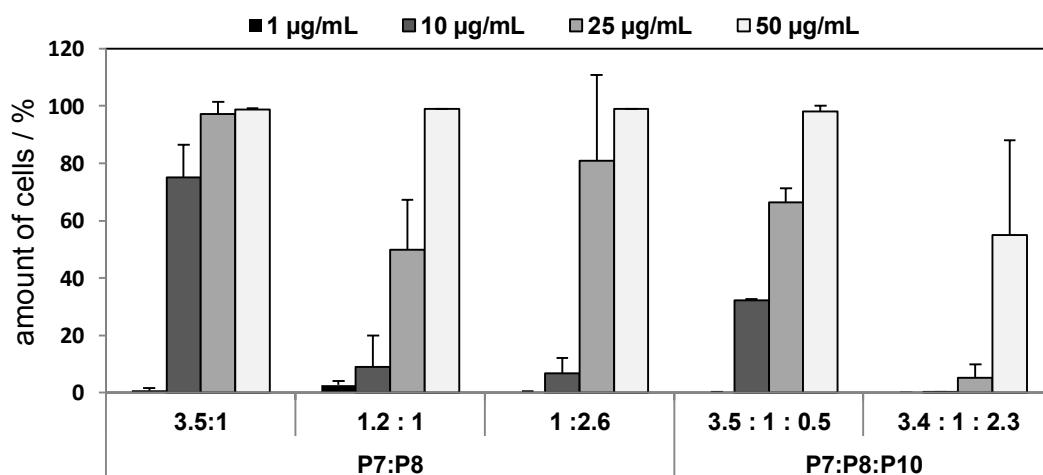


**Figure 2.9:** Cellular uptake of the co-assembled micellar structures in HEK cells. The values represent the mean  $\pm$  S.D.

In conclusion, it could be shown that functional polyether-based triblock terpolymers show a high potential for a possible application in the field of nanomedicine. Particularly the post-polymerization functionalization of the poly(allyl glycidyl ether) (PAGE) segment by thiol-ene chemistry represents a powerful tool for tuning the material properties. Nevertheless, these modifications are not limited to thiol-ene chemistry. The application of Diels-Alder reactions for this purpose will be demonstrated in **Chapter 3**.

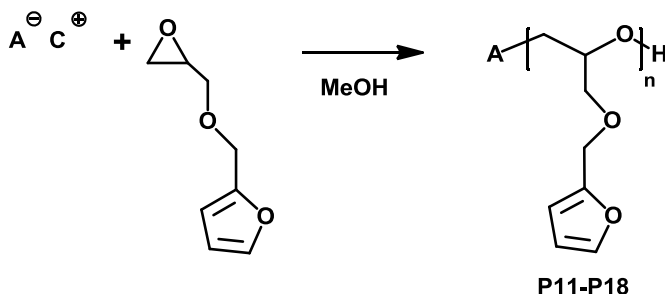


### 3 Furfuryl glycidyl ether – a new monomer for living anionic ring-opening polymerization

Parts of this chapter have been published: P4) M. J. Barthel, T. Rudolph, S. Crotty, F. H. Schacher, U. S. Schubert *J. Polym. Sci., Part A: Polym. Chem.* **2012**, *50*, 4958-4965.

Additionally to the introduction of pendent double bonds and the subsequent thiol-ene click chemistry as applied in **Chapter 2** a further possibility for a (reversible) post-polymerization functionalization is the introduction of furfuryl groups to the polymer chain. Kavita *et al.* used furfuryl methacrylate as a co-monomer in the polymerization of methacrylates.<sup>63</sup> After the polymerization, the furfuryl groups could be applied in a subsequent Diels-Alder reaction for, *e.g.*, cross-linking and network formation.<sup>64, 65</sup> Furthermore, heating above a certain temperature can be used to induce a retro-Diels-Alder reaction, resulting in cleavage of the network junctions. Subsequent cooling restores the network and the process was shown to be fully reversible. One possible application field for these systems are self-healing materials, as recently demonstrated for PEO-based networks.<sup>66, 67</sup> As an example for polyethers carrying furfuryl moieties in the side-chain, poly(furfuryl glycidyl ether) (PFGE) has been prepared using condensation reactions but with limited control over molar mass, molecular architecture, and PDI values.<sup>68</sup>

To provide an enhanced control over the polymerization mechanism the homopolymerization of furfuryl glycidyl ether by living anionic ring-opening polymerization (AROP) was performed. Hereby different initiators such as DPMK, sodium hydride (NaH), cesium hydroxide monohydrate (CsOH), and potassium *t*-butanolate (*t*-BuOK) were used (**Scheme 3.1**).



**Scheme 3.1:** Schematic representation of the homopolymerization of furfuryl glycidyl ether (FGE).

To investigate the influence of THF as solvent, the reactions were performed in solution as well as in the bulk. SEC measurements revealed (**Figure 3.1 a**, **Table 3.1**) that *t*-BuOK (**P14**, solid black line,  $M_{n,app} = 5,500$  g/mol) lead to (apparently) higher molar masses than DPMK

(**P13**, dashed black line,  $M_{n,app} = 3,100$  g/mol) under bulk conditions. CsOH (**P12**, dotted black line,  $M_{n,app} = 2,800$  g/mol), and NaH (**P11**, black line with alternating dots and dashes,  $M_{n,app} = 2,700$  g/mol) lead to even lower molar masses. However, coupling products were observed in case of *t*-BuOK (**P14**), DPMK (**P13**) and CsOH (**P12**) (bimodal distributions), as well as a broadening of the molar mass distribution using NaH as initiator.

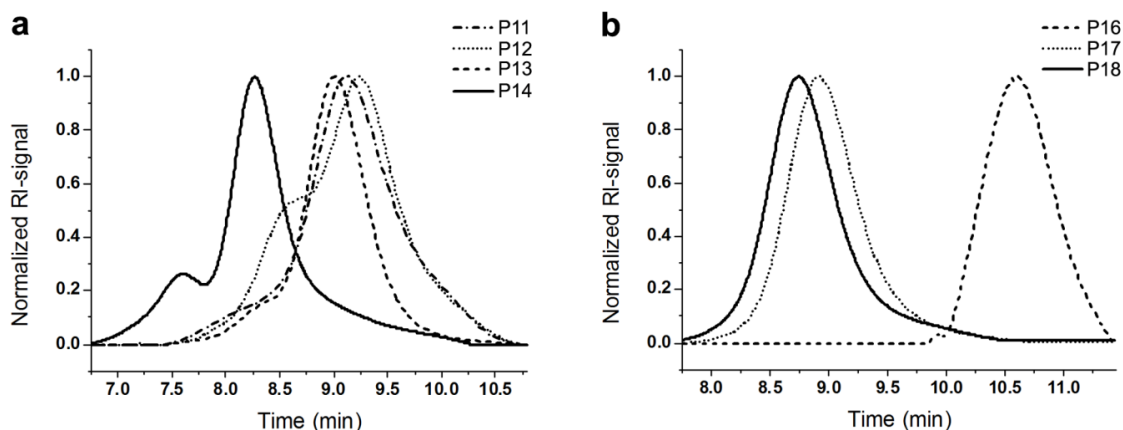


**Figure 3.1:** SEC traces for PFGE obtained by homopolymerization in the bulk (a) and in THF (b) using different initiators for living anionic ROP.

The results of the polymerization in THF are depicted in **Figure 3.1 b** and **Table 3.1**. The best results were obtained in case of *t*-BuOK (**P18**, solid black line,  $M_{n,app} = 2,900$  g/mol) yielding well-defined PFGE with higher molar masses as for DPMK (**P17**, dotted black line,  $M_{n,app} = 2,800$  g/mol). No product was obtained for NaH (**P15**), whereas for CsOH (**P16**, dashed black line,  $M_{n,app} = 865$  g/mol) lower molar masses were observed.

**Table 3.1:** Characterization data for the PFGE homopolymers initiated by different initiators in the bulk and in solution.

Entry	Initiator	in Bulk			Entry	in THF		
		$M_n^a$ [g/mol]	$M_w^a$ [g/mol]	PDI <sup>a</sup>		$M_n^a$ [g/mol]	$M_w^a$ [g/mol]	PDI <sup>a</sup>
<b>P11</b>	NaH	2,700	3,200	1.18	<b>P15</b>	---	---	---
<b>P12</b>	CsOH	2,800	3,300	1.18	<b>P16</b>	865	900	1.06
<b>P13</b>	DPMK	3,100	3,500	1.11	<b>P17</b>	2,800	3,150	1.09
<b>P14</b>	<i>t</i> -BuOK	5,500	7,000	1.28	<b>P18</b>	2,900	3,100	1.10

<sup>a</sup> Obtained by SEC (CHCl<sub>3</sub>:*i*-Prop.:TEA 94:4:2, using PEO standards)

To study the reaction kinetics for FGE, a polymerization using *t*-BuOK as initiator was performed in THF and monitored by a combination of SEC and  $^1\text{H}$  NMR measurements. The results are displayed in **Figure 3.2**.

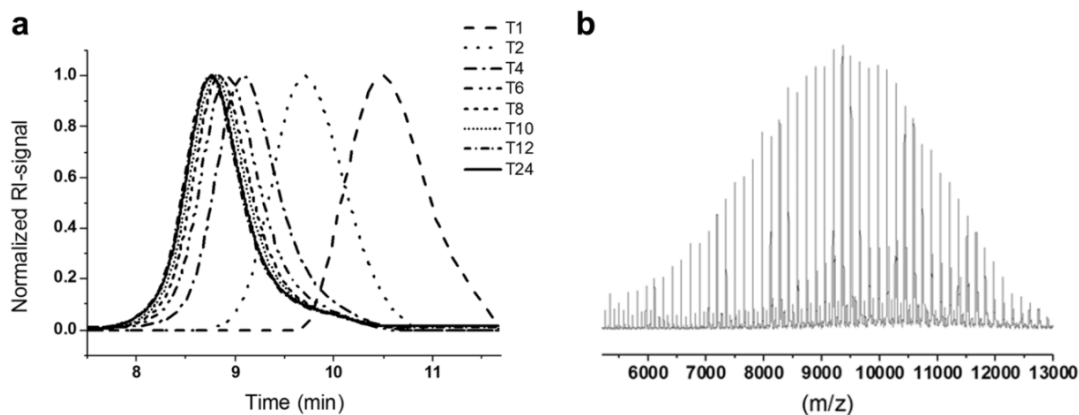
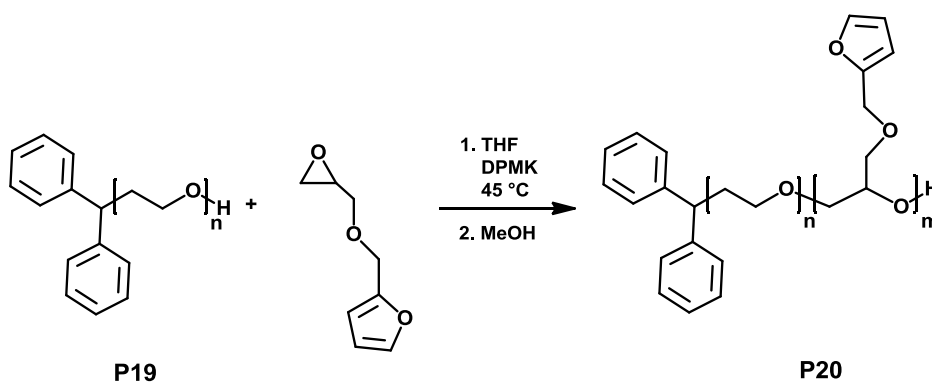


**Figure 3.2:** SEC traces of a kinetic study of the PFGE homopolymerization (a) and the corresponding MALDI-TOF MS spectrum of the final product (b,  $M_p = 9,400$  g/mol).

As shown in **Figure 3.2 a** in the SEC measurements, almost no increase in the molar mass could be observed after 12 h. The conversion of the monomer was simultaneously monitored by  $^1\text{H}$  NMR. After 24 h ( $M_n = 3,450$  g/mol) a monomer conversion of approximately 100% could be obtained, whereas T12 ( $M_n = 3,450$  g/mol) revealed 90% FGE consumption. As shown in **Figure 3.2 b**, a molar mass ( $M_p$ ) of 9,400 g/mol for the final product could be observed by MALDI-ToF MS measurements, being in good agreement with the targeted value of 10,000 g/mol.

Subsequently, an AB diblock copolymer (PEO-*b*-PFGE, **P20**) was prepared (**Scheme 3.2**, **Table 3.2**). The PEO precursor (**P19**) was prepared using DPMK as initiator for EO in THF. The corresponding macroinitiator, PEO-OH with a molar mass ( $M_n$ ) of 6,100 g/mol and a PDI value of 1.05, was subsequently re-activated using DPMK, followed by the addition of FGE.



**Scheme 3.2:** Synthesis of PEO-*b*-PFGE using sequential living anionic ROP.

**Table 3.2:** Characterization data for homopolymers and block copolymers.

Entry	Sample	$M_{n,theo}$ [g/mol]	$M_{n,SEC}^a$ [g/mol]	$M_{p,MALDI}$ [g/mol]	PDI <sup>a</sup>
<b>P19</b>	PEO	5,000	5,100	6,100	1.05
<b>P20</b>	PEO <sub>139</sub> - <i>b</i> -PFGE <sub>12</sub> <sup>b</sup>	10,000	6,000	8,050	1.06

<sup>a</sup> Obtained by SEC (CHCl<sub>3</sub>:*i*-Prop.:TEA 94:4:2, using PEO standards)

<sup>b</sup> Subscripts denote the degrees of polymerization of the corresponding block determined by <sup>1</sup>H-NMR spectroscopy

Due to its amphiphilic nature, **P20** forms micelles in aqueous solution, as demonstrated by DLS experiments. The structures presumably consist of a hydrophobic PFGE core and a hydrophilic PEO corona (**Figure 3.3 a**). The core-forming block, PFGE, can be crosslinked *via* Diels-Alder reactions using a bis-functional crosslinker, *e.g.*, a bis-maleimide (**Figure 3.3 a**). The controlled crosslinking of selected domains in micellar structures can be used to enhance their resistance against degradation, limit the diffusion of guest molecules into or out of the core domains, or ensure the stability within desired environments.<sup>69-71</sup>

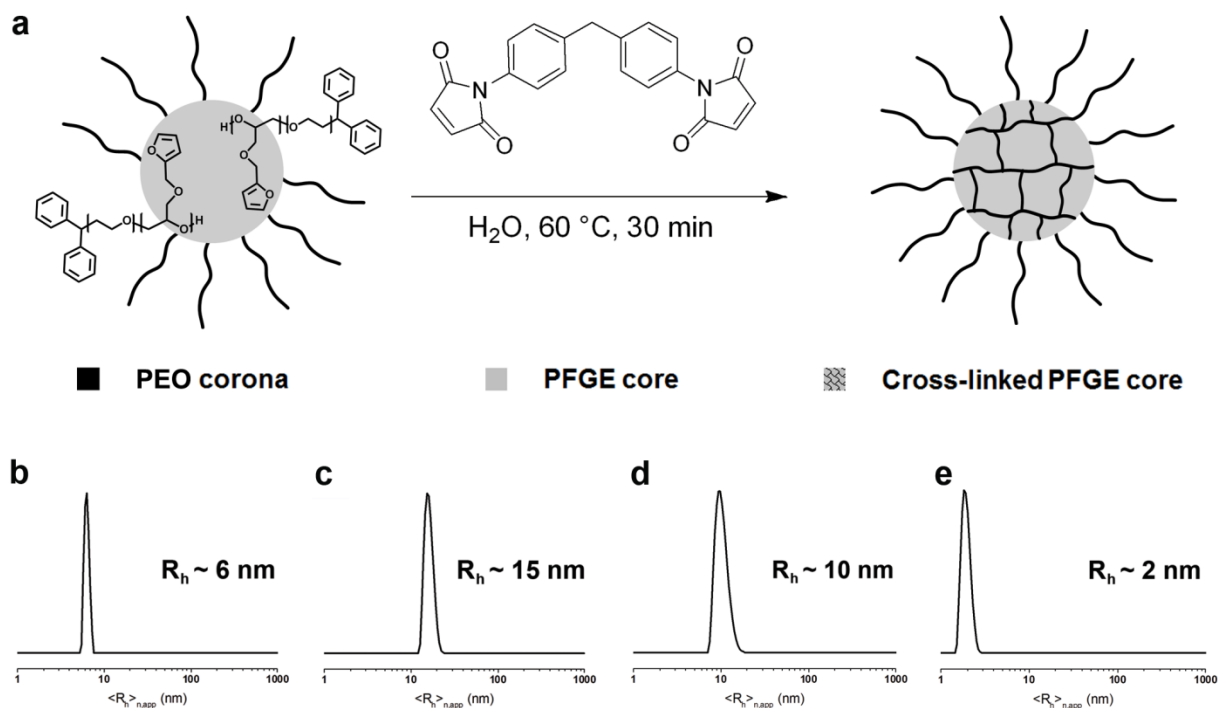


**Figure 3.3:** Cross-linking of the micellar core (a), number-weighted DLS CONTIN plots for PEO-*b*-PFGE micelles in water after crosslinking (b), in THF (c), and DMF (d), and after the retro-Diels-Alder reaction in DMF (e).

For this purpose, the BMI crosslinker was encapsulated in micelles formed of **P20** and the solution was subsequently heated to 60 °C for several hours. According to DLS, the micellar



size did not change significantly upon the crosslinking procedure (**Figure 3.3 b**). To prove the successful crosslinking of the PFGE core, the micelles were transferred to non-selective solvents for both blocks, THF. Here, micelles with a radius of  $\langle R_h \rangle_{n,app} = 15$  nm could be detected (**Figure 3.3 c**). The increase in size can be explained by a swelling of the crosslinked PFGE core in THF as a non-selective solvent. In a next step, the stability of the cross-linked structures was tested in DMF as an alternative non-selective solvent. Again, DLS studies revealed micelles with a solvent-swollen PFGE core and a radius of  $\langle R_h \rangle_{n,app} = 10$  nm even after several days (**Figure 3.3 d**). These results clearly indicate a successful crosslinking of the PFGE core. As the crosslinking *via* Diels-Alder chemistry should be reversible, the micellar solution was further heated to higher temperatures (150 °C) for 30 minutes. DLS measurements after 2 hours reveals that unimolecular block copolymer chains are present ( $\langle R_h \rangle_{n,app} = 2$  nm, **Figure 3.3 e**) indicating that the cross-linked network in the micellar core was cleaved resulting in a disassembly of the micelles.

Furthermore, a PFGE homopolymer (**P21**) was investigated by MALDI-ToF MS/MS.<sup>72</sup>

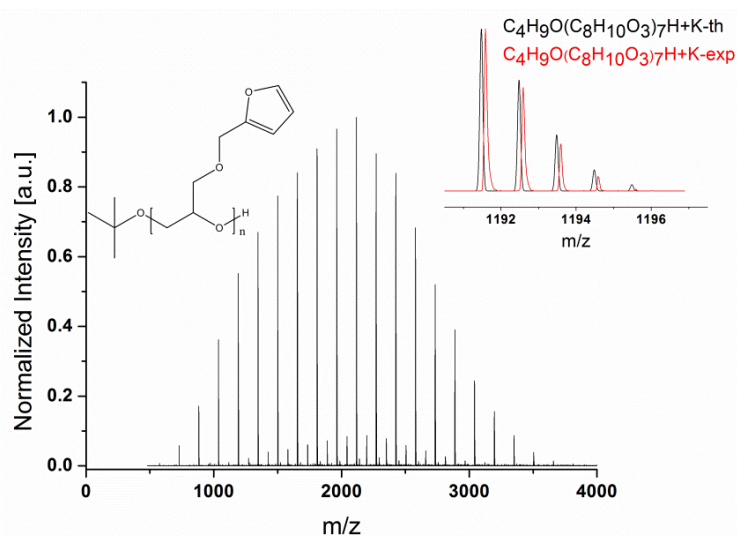


**Figure 3.4:** MALDI-ToF MS spectrum of the PFGE<sub>7</sub> homopolymer (**P21**).

The MALDI-ToF MS spectrum of **P21** shows one single major distribution and the calculated and observed isotopic pattern is in a good agreement (**Figure 3.4**).

Overall it could be demonstrated that furfuryl glycidyl ether can be polymerized by AROP in a living manner. Furthermore, the hydrophobic character of the resulting polymer and the versatility of the Diels-Alder reaction for a post-polymerization functionalization reaction open a wide range of potential applications for this monomer. Some examples are shown in **Chapter 4**.



## 4 Application of PFGE containing block copolymers

Parts of this chapter have been published: P5) M. J. Barthel, T. Rudolph, A. Teichler, R. M. Paulus, J. Vitz, S. Hoepfner, M. D. Hager, F. H. Schacher, U. S. Schubert, *Adv. Funct. Mater.* **2013**, *23*, 4921-4932. P6) T. Rudolph, M. J. Barthel, F. Kretschmer, U. Mansfeld, S. Hoepfner, U. S. Schubert, F. H. Schacher, *Macromol. Rapid Commun.* **2014**, DOI: 10.1002/marc201300875.

The capability to heal inflicted damage is ubiquitous in nature as, *e.g.*, shown *via* the merging of broken bones, the closure of injured blood vessels,<sup>73-75</sup> or the healing of byssal threads of marine mussels.<sup>76</sup> The present awareness that the availability of raw materials will decrease, accompanied by increasing material and production costs, renders self-healing approaches an attractive research field in polymer chemistry and materials science. Particular interest is devoted to the facile introduction of such features into mechanically robust polymeric systems whilst maintaining synthetic feasibility and, even more important, processability of the resulting materials.

Different methods have been reported to introduce self-healing properties to a polymeric material.<sup>77-79</sup> One possibility is the encapsulation of reactive ingredients (a polymerizable healing agent and an initiator) within the desired material. Scratching or crack formation leads to a release of the embedded substances (*e.g.*, by rupture of microcapsules), followed by mixing of both ingredients and resulting in a healing process of the damaged material.<sup>80</sup> This approach was also extended by the introduction of vascular networks containing a healing agent, which was released upon rupture.<sup>81</sup> As a consequence, multiple healing processes are possible. A second approach represents the utilization of intermolecular forces. For this purpose, reversible interactions (*i.e.* crosslinks) of polymer chains with, *e.g.*, hydrogen bonds represent a widely used strategy. After being damaged, these bonds enable a healing due to the reformation of bonds without any external stimuli such as heating or irradiation being necessary. This has been realized using highly specific donor-acceptor systems,<sup>82-87</sup> and could recently be also applied for “hard” epoxy networks.<sup>88</sup>

The temperature-dependent reversible covalent crosslinking of polymers or block copolymers represents another interesting concept for the implementation of intrinsic self-healing into a material. Hereby, the Diels-Alder reaction represents a powerful tool.<sup>89-95</sup> One well-known example is the combination of furan and maleimide functionalities.<sup>55, 96, 97</sup> As shown in **Chapter 3** the furan units of self-assembled poly(ethylene oxide)-*b*-poly(furfuryl glycidyl ether) (PEO-*b*-PFGE) block copolymers can be used for the reversible crosslinking of the micellar cores formed from these block copolymers in selective solvents. The application of polymer networks bearing free furan groups with a suitable linker (*e.g.*, bismaleimides) in

reversible Diels-Alder reactions represents a powerful system for potential self-healing applications.<sup>55, 89-92, 96-100</sup> This has been reported in case of furfuryl glycidyl ether<sup>68, 101</sup> where the epoxy-ring was used in a condensation reaction with amino groups to create polymeric materials. These polymers can be turned into a network structure by reacting them with a bismaleimide compound.

Now the features of PEO-*b*-PFGE block copolymers for the generation of self-healing materials, in particular of nanostructured polymer films shall be exploited.

For this purpose, a *t*-BuOK initiated PFGE homopolymer (**P22**) as well as a PEO-*b*-PFGE diblock copolymer (**P24**) were synthesized using the investigated reaction conditions explained in **Chapter 3**. The molecular characterization data can be found in **Table 4.1**.

**Table 4.1:** Characterization data of the used homo- and block copolymers.

Entry	Sample	$M_{n,theo}$ [g/mol]	$M_{n,SEC}$ [g/mol] <sup>b)</sup>	$M_{p,MALDI}$ [g/mol]	PDI <sup>b)</sup>
<b>P22</b>	PFGE <sub>55</sub>	10,000	2,900	8,400	1.07
<b>P23</b>	PEO <sub>330</sub> <sup>a)</sup>	14,000	14,800	14,500	1.05
<b>P24</b>	PEO <sub>330</sub> - <i>b</i> -PFGE <sub>20</sub> <sup>c)</sup>	17,600	17,400	17,000	1.04

<sup>a)</sup> Precursor

<sup>b)</sup> Obtained by SEC (CHCl<sub>3</sub>:*i*-Prop.:TEA 94:4:2, using PEO standards)

<sup>c)</sup> Subscripts denote the degrees of polymerization of the corresponding block determined by <sup>1</sup>H NMR spectroscopy

Both **P22** and **P24** were analyzed using differential scanning calorimetry (DSC). It could be observed that the homopolymer **P22** exhibits a  $T_g$  at approximately  $-40$  °C. **P24** shows a strong melting peak at  $T_m = 59$  °C, which can be attributed to the PEO segments and reveals two separated glass transition temperatures at  $-79$  and  $-40$  °C, respectively. The first value can be assigned to PEO,<sup>102</sup> whereas  $-40$  °C reflects the PFGE segments. The presence of two separated  $T_g$ 's hints towards phase separation although the overall molar mass of **P24** is rather low. To confirm this assumption, additional SAXS experiments were performed on films which were annealed at  $70$  °C for 30 min and afterwards cooled to room temperature (**Figure 4.1 a**).

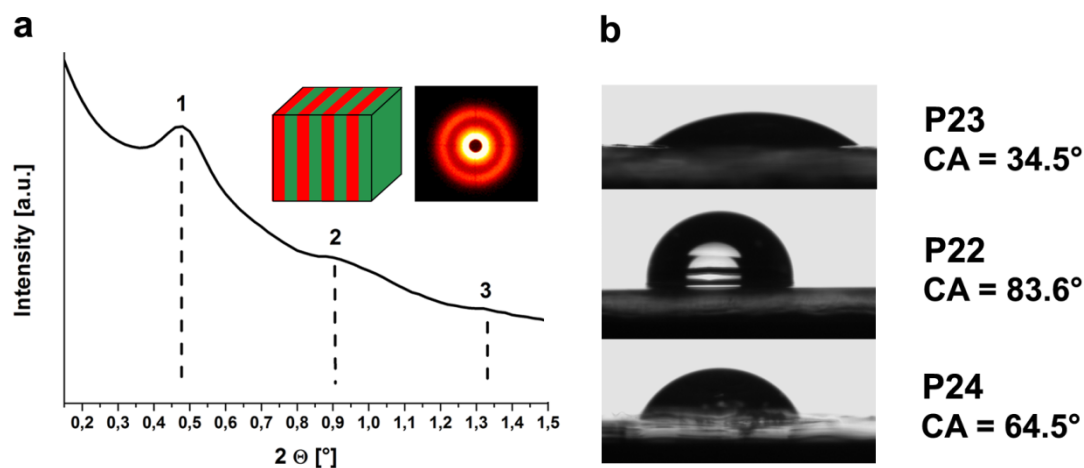


**Figure 4.1:** SAXS measurements of PEO<sub>330</sub>-*b*-PFGE<sub>20</sub> (**P24**) and schematic representation of the proposed block copolymer bulk morphology (a). b: Contact angle measurements for PEO<sub>330</sub> (**P23**), PFGE<sub>55</sub> (**P22**) and PEO<sub>330</sub>-*b*-PFGE<sub>20</sub> (**P24**).

For **P24** reflections for 0.46°, 0.92°, and 1.36° could be observed, corresponding to the [100] : [200] : [300] positions of a potential lamellar pattern, and the most intense [100] signal corresponds to a domain size of  $d_{\text{lam}} = 19 \pm 2$  nm. The formation of lamellae is rather surprising, as the volume fraction of PFGE in the diblock copolymer **P24** is about 17.5 wt%, rather hinting towards the formation of cylindrical domains. To probe the surface properties of the investigated films, contact angle measurements were performed on PEO<sub>330</sub> (**P23**), PFGE<sub>55</sub> (**P22**), and PEO<sub>330</sub>-*b*-PFGE<sub>20</sub> (**P24**) surfaces (**Figure 4.1 b**). As expected, **P23** shows a contact angle of 34.5°, being characteristic for a hydrophilic surface, whereas this increases to 83.6° for **P22**. In case of **P24**, a value of 64.5° was obtained, revealing surface characteristics in between the two corresponding homopolymers. At this point, the formation of a lamellar bulk morphology in case of **P24** is assumed.

For self-healing studies, films were prepared from a mixture of the respective polymer and the 1,1-diphenylmethyl bismaleimide (BMA) crosslinker in dichloromethane. For crosslinking, the polymer films were heated to 65 °C. Subsequent network formation *via* crosslinking of the furan groups led to a significant change in the material properties and, in both cases, an increase of the film hardness was observed during crosslinking using depth sensing indentation measurements (**Figure 4.2**).

First, the mechanical properties of PFGE-based films prior to and after crosslinking with BMA were investigated. As pristine films from homopolymer **P22** were liquid (highly viscous) at room-temperature, no indentation measurements were possible. The diblock copolymer **P24** shows a hardness ( $H_i$ , defined as load/indentation area) of 0.038 GPa and a stiffness ( $E_i$ , Young modulus) of 0.46 GPa. All  $H_i$  values provided refer to a displacement of 150 nm. The  $E_i$  values represent average values of the obtained data in the linear range. After

crosslinking, **P22** shows a hardness of 0.6 GPa and a stiffness of  $E_i = 5.13$  GPa (**Figure 4.2 a, c**), the values being slightly higher as reported for “hard” polymers, like poly(methyl methacrylate) (PMMA, 0.32 GPa, 4.8 GPa) as well as polystyrene (PS, 0.34 GPa, 4.8 GPa).<sup>103</sup> This can be explained by a rather high degree of crosslinking, as each monomer unit carries a furan group in the side chain. For **P24**, significantly lower values of  $H = 0.071$  GPa and  $E_i = 0.91$  GPa compared to **P22**, but increased by a factor of two compared to the non-crosslinked state were obtained (**Figure 4.2 b, d**). This can be rationalized by the presence of only 17.5 wt% PFGE and, hence, a lower overall degree of crosslinking.

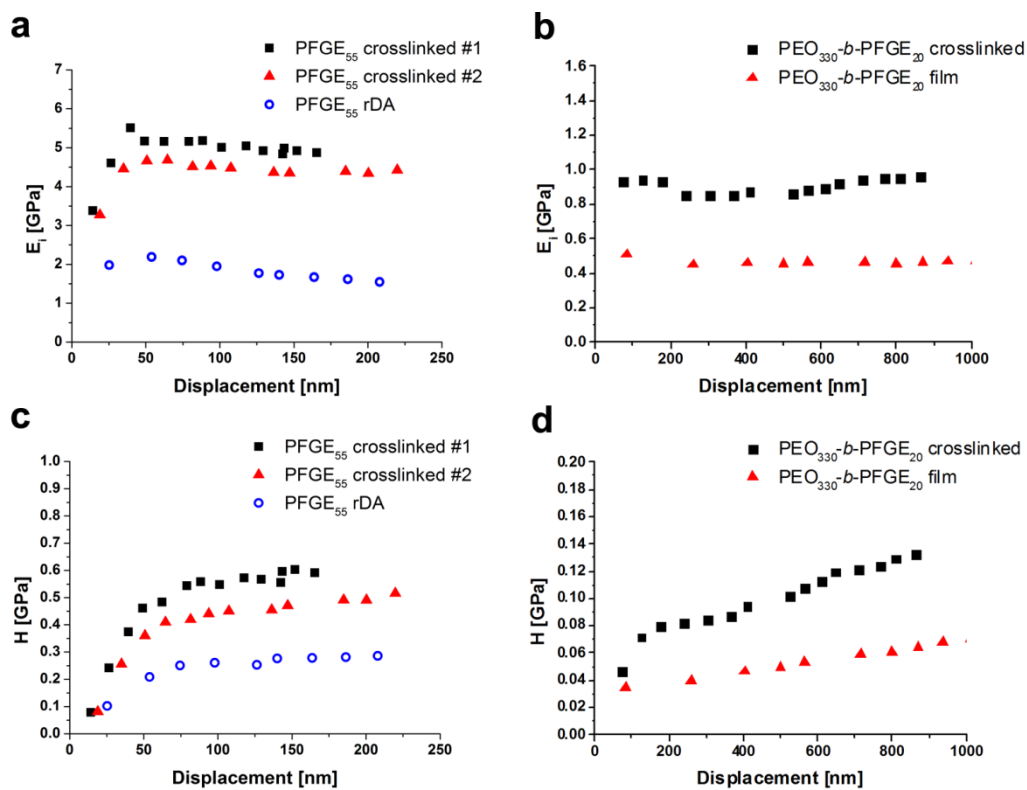


**Figure 4.2:** Depth-sensing indentation measurements for PFGE<sub>55</sub> (**P22**, a,c) and PEO<sub>330</sub>-b-PFGE<sub>20</sub> films (**P24**, b,d) before and after crosslinking.

The demonstrated increase of both hardness and stiffness can be attributed to the crosslinking of **P22** and **P24** and, therefore, the rDA reaction is expected to invert this process. The films were therefore heated to 155 °C for 3 h and subjected to additional depth-sensing-indentation measurements at RT.

As expected, after the treatment at 155 °C the  $E_i$ -modulus decreased to 1.76 GPa and the hardness was reduced to 0.26 GPa for **P22** (**Figure 4.2 b, d**). Subsequent re-crosslinking by heating to 65 °C for 14 h led to an increase to 4.51 GPa ( $E_i$ -modulus) and 0.45 GPa (hardness), although the values are slightly lower than after the first crosslinking procedure. This can be attributed to an incomplete DA reaction. For the **P24** block copolymer film, no

significant changes after the rDA reaction were observed, which can be attributed to the rather low weight fraction of the PFGE segment.

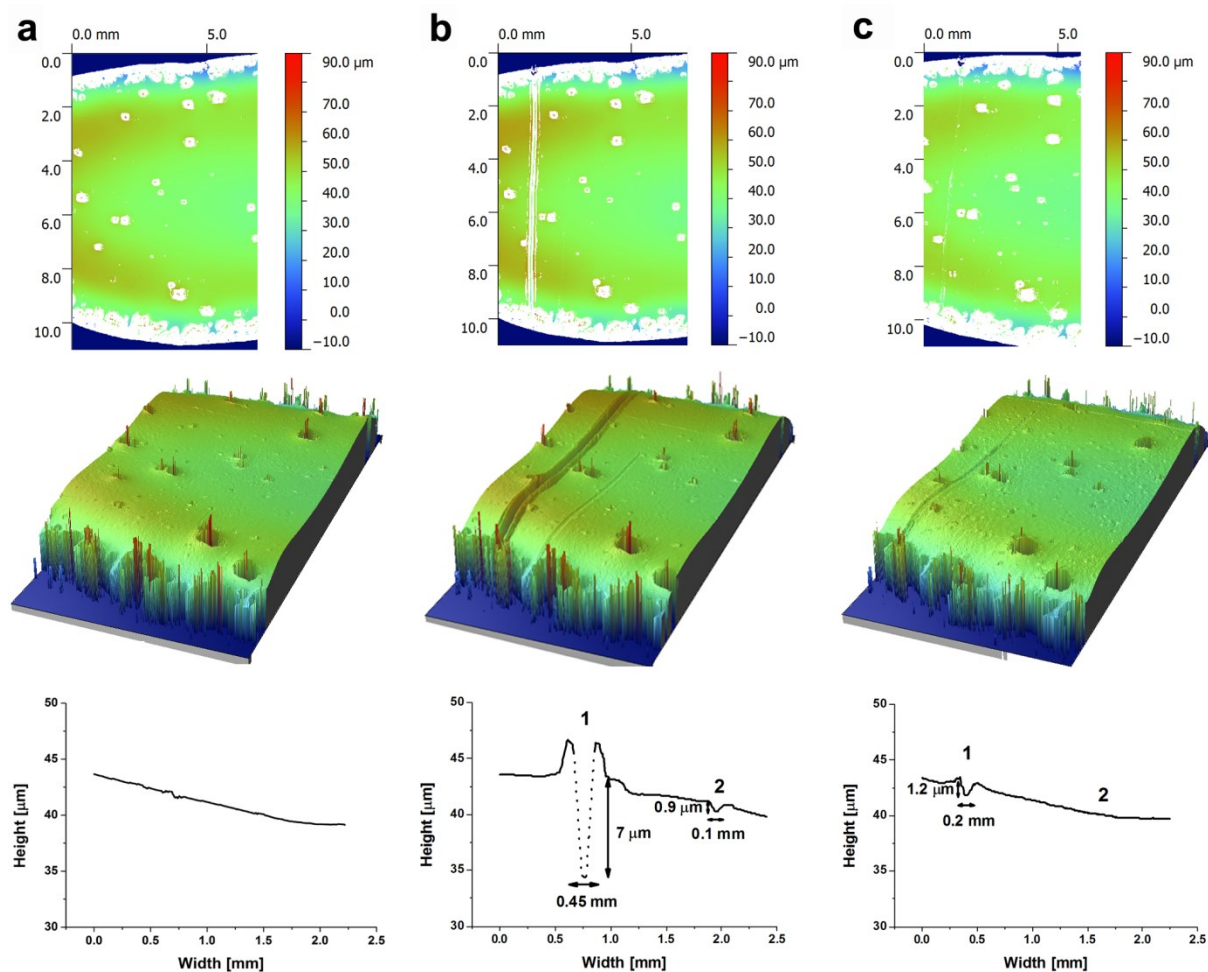


**Figure 4.3:** Profilometry measurements of PEO<sub>330</sub>-*b*-PFGE<sub>20</sub> (**P24**) block copolymer films after crosslinking (a), scratching with a spatula (b), and the healing process at 155 °C (c).

Subsequently, films containing **P24** and the BMA crosslinker (molar ratio was 1:1) were prepared and crosslinked at 65 °C for 14 h. After crosslinking, the film surface was analyzed using an optical profilometer (**Figure 4.3**) and scratched with a spatula. As it can be seen, defined scratches (Scratch 1: 7 μm depth, 0.45 mm width, length 8 mm; Scratch 2: 0.9 μm depth, 0.1 mm width, length of 3.5 mm) were created (**Figure 4.3 b**, the dashed lines are a guide to the eye as the instrument is not able to resolve the steep walls of this particular scratch). Afterwards, the block copolymer film was heated for 3 h at 155 °C, allowed to cool down slowly to 65 °C, and re-crosslinked for 14 h at 65 °C. After the rDA reaction at 155 °C and subsequent crosslinking at 65 °C, profilometry revealed that Scratch 2 disappeared completely and Scratch 1 decreased to 1.2 μm depth and 0.2 mm width (**Figure 4.3 c**). Repetition of the heating process and increasing of the heating time did not lead to a further reduction of the scratch size. During all steps of this process, the overall thickness of the film



was monitored and shown to be constant (height  $\sim 54 \mu\text{m}$ ). Furthermore, defects within the block copolymer film remained unchanged, which would not be the case if the sample would undergo melting.

Also complex scratch patterns were applied to crosslinked block copolymer films (**Figure 4.4**). As shown in **Figure 4.4 b**, small scratches with, *e.g.*, a depth of  $1.2 \mu\text{m}$  and a width of  $0.16 \text{ mm}$  disappeared completely, whereas deeper scratches with a depth of  $6.2$  or  $9.8 \mu\text{m}$  and widths of  $0.45$  and  $0.5 \text{ mm}$  only decreased in size. The depths could be reduced to  $0.8$  and  $3.8 \mu\text{m}$ , respectively, as well as the scratch width to  $0.23$  and  $0.3 \text{ mm}$ .

**Figure 4.4 c** depicts a rather challenging scratch pattern, two ‘‘Santa’s houses’’ with depths of approximately  $1.8$  to  $6.8 \mu\text{m}$  and  $4.2$  to  $16 \mu\text{m}$ . As shown in **Figure 4.4 d**, the left (less deep) pattern vanished nearly completely. Only in case of the deeper scratch ( $6.5 \mu\text{m}$ ), the depth was reduced to  $1.8 \mu\text{m}$ , whereas the right-hand pattern comprising deeper scratches ( $12$  to  $16 \mu\text{m}$ ) can still be seen afterwards (remaining scratches with  $7.1$  and  $8.7 \mu\text{m}$  depth).

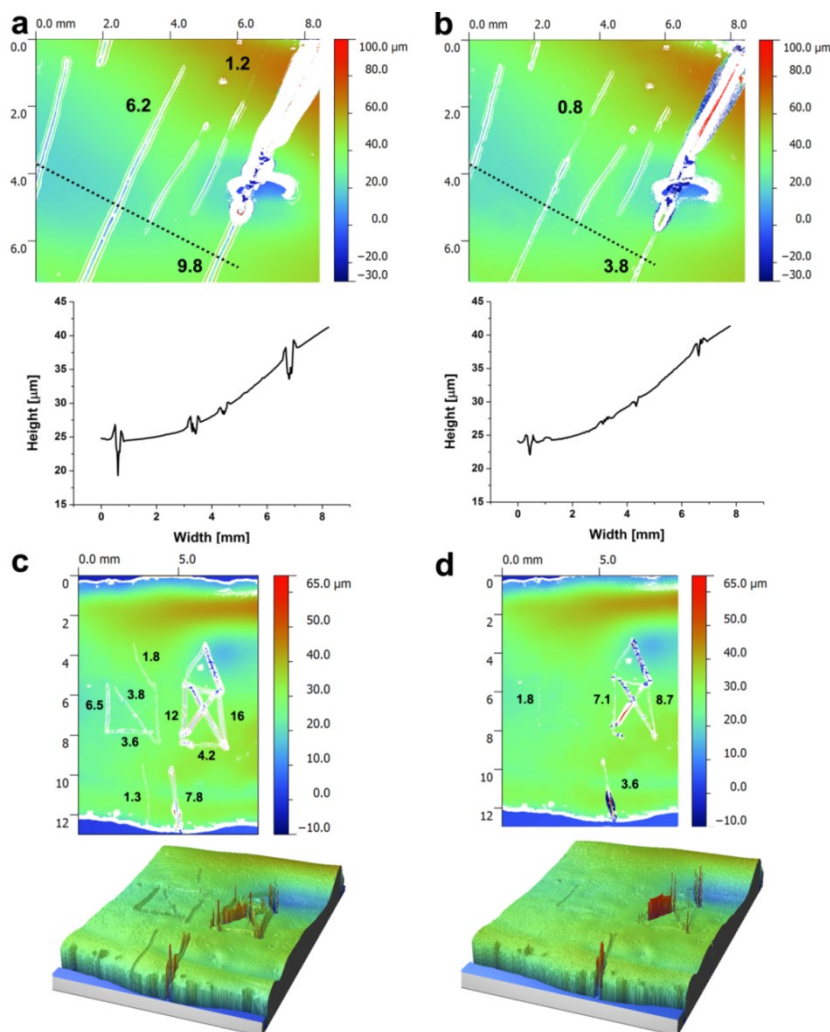
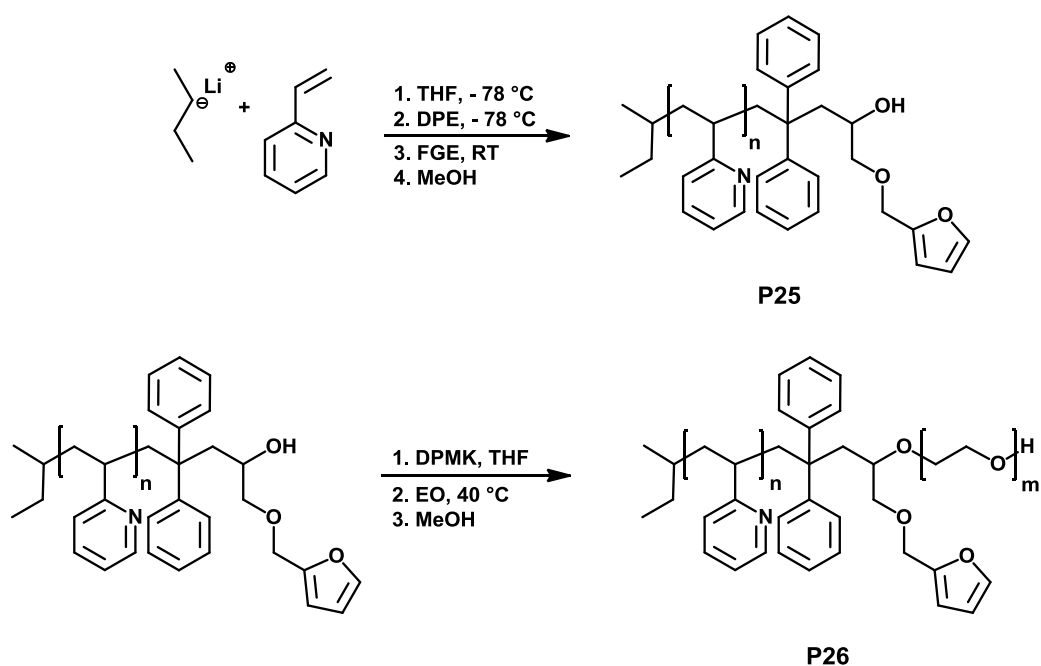


**Figure 4.4:** Self-healing process of a multi-scratch pattern (before a, and after b) as well as a complex pattern within a crosslinked PEO<sub>330</sub>-*b*-PFGE<sub>20</sub> (P24) block copolymer film (before c, and after heating to  $155 \text{ }^\circ\text{C}$  d).

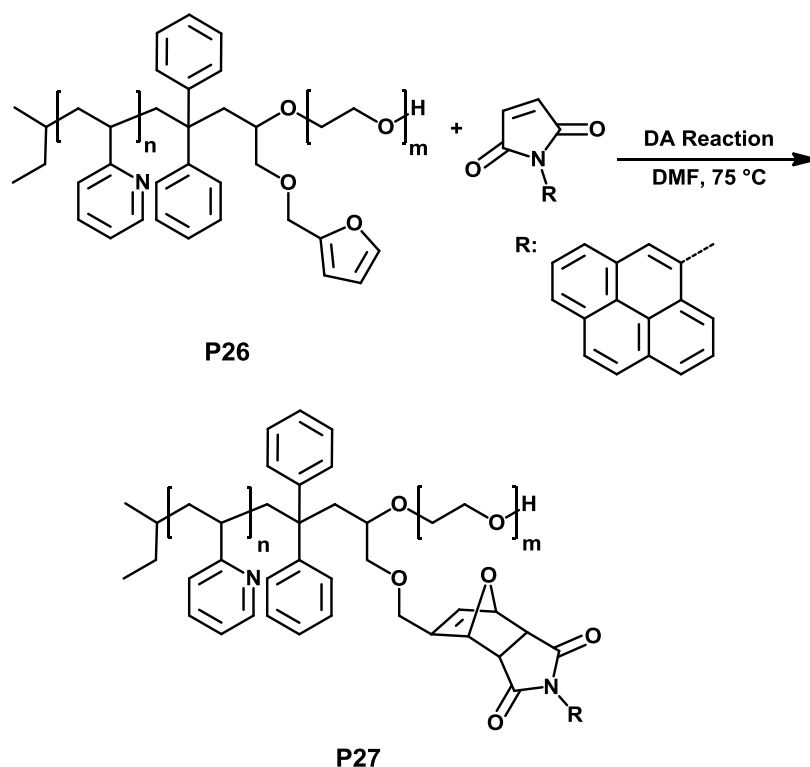


Despite of the application as self-healing coatings FGE containing materials can be used in a wide range of application, due to the versatility of the Diels-Alder reaction. As reported in the literature, ethylene oxide and related glycidyl ethers can be used as efficient end-capping agents for living anionic polymerizations initiated with a lithium compound.<sup>104, 105</sup> After addition of one epoxy unit further ring-opening polymerization is prevented by the formation of a strong lithium-oxygen ion pair. In the present case, furfuryl glycidyl ether was used for the efficient end-capping of a living poly(2-vinyl pyridine) chain carrying a lithium counterion. Subsequently, the terminal hydroxy group was re-activated for the polymerization of ethylene oxide, resulting in a P2VP-*b*-PEO block copolymer, carrying a furfuryl group at the block junction (**Scheme 4.1**).



**Scheme 4.1:** Schematic representation of the synthesis of poly(2-vinyl pyridine)-*block*-poly(ethylene oxide) (P2VP-*b*-PEO) carrying a furfuryl glycidyl ether moiety at the block junction.

As shown above the pendant furan unit can be used in post-polymerization functionalization reactions for, *e.g.*, the attachment of a fluorescent dye to the polymer. For this purpose the maleimide group of pyrenyl maleimide was reacted in a Diels-Alder reaction as shown in **Scheme 4.2**. Selected characterization data for **P25-P27** can be found in **Table 4.2**.



**Scheme 4.2:** Schematic representation of the Diels-Alder reaction of pyrenyl maleimide and the pendant furan unit at the chain junction of a P2VP-*b*-PEO block copolymer.

**Table 4.2:** Characterization of the homopolymer (P2VP<sub>68</sub>-FGE-OH), block copolymer (P2VP<sub>68</sub>-FGE-*b*-PEO<sub>390</sub>) and the pyrenyl functionalized P2VP<sub>68</sub>-FGE-*b*-PEO<sub>390</sub>.

Entry	Polymer	$M_{n, SEC}^a$ [g/mol]	PDI <sup>a</sup>	$M_{p, MALDI}$ [g/mol]
<b>P25</b>	P2VP <sub>68</sub> -FGE-OH <sup>b</sup>	8,700	1.08	7,200
<b>P26</b>	P2VP <sub>68</sub> -FGE- <i>b</i> -PEO <sub>390</sub> <sup>b</sup>	19,000	1.11	24,500
<b>P27</b>	P2VP <sub>68</sub> -pyr- <i>b</i> -PEO <sub>390</sub>	17,000	1.22	-

a) Obtained by SEC (CHCl<sub>3</sub>:*i*-Prop.:TEA 94:4:2, using PS standards)

b) Determination by a combination of <sup>1</sup>H-NMR and MALDI-TOF MS

An interesting feature is that pyrenyl maleimide reveals a non-fluorescent character in the pristine state. If this moiety is attached to the polymer chain *via* the Diels-Alder reaction, a strong increase of the fluorescence can be monitored due to the change in the electronic structure of the molecule (**Figure 4.5**).

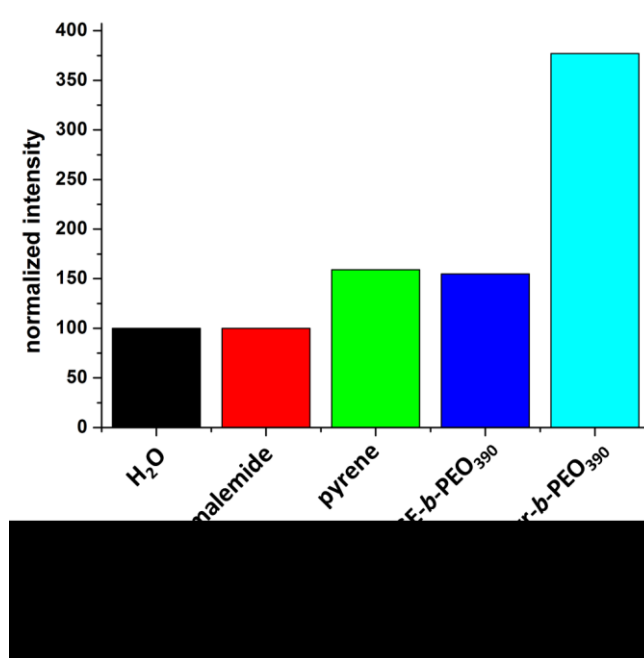


**Figure 4.5:** Comparison of the fluorescence measurements normalized in comparison to H<sub>2</sub>O (black) for *N*-(1-pyrenyl)-maleimide (red), pyrene (green), P2VP<sub>68</sub>-FGE-*b*-PEO<sub>390</sub> (**P26**, blue, 5 mg/mL) and P2VP<sub>68</sub>-pyr-*b*-PEO<sub>390</sub> (**P27**, cyan, 5 mg/mL) in water (at pH 7) under comparable conditions.

The synthesized block copolymer **P26** can be further used for the covalent coating of functional gold nanoparticles. For this purpose, the surface of the nanoparticles were functionalized in a first step with maleimide groups and reacted subsequently with the furane unit of the polymer by heating to 75 °C. To ensure the covalent attachment of the polymer on the particle surface the gold particles were washed several times with dimethylformamide (DMF) to remove remaining unbound polymer and the samples were analyzed by transmission electron microscopy (TEM). In contrast to the pristine gold nanoparticles (**Figure 4.6 a**) a polymeric shell could be detected for the functionalized nanoparticles (**Figure 4.6 b**) indicating a successful coating reaction.

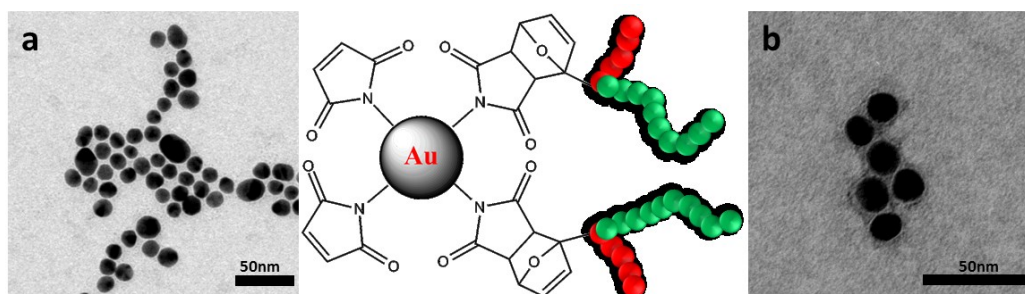


**Figure 4.6:** Schematic representation of the surface coating of gold nano particles by Diels-Alder chemistry. TEM images of the pristine gold nano particles (a) and the coated particles with a polymer shell (b).

It could be, therefore, demonstrated that furfuryl glycidyl containing polymers represent a powerful tool which can be applied in the bulk as well as in solution. Apart from examples as self-healing or particle coating involving mainly material science, the possible functionalization with bioactive moieties as biotin maleimide or maleimide functionalized dyes would lead to promising examples for such application in the field of, *e.g.*, nano-medicine.

## 5 Summary

In the last decades a significant scientific effort was invested on the synthesis of well-defined diblock copolymers and triblock terpolymers due to the broad field of potential applications and the high versatility of these materials. Depending on the application area (*e.g.*, material science or nanomedicine) the polymers can be used in the bulk as well as in solution. Classical applications are phase-separated coatings for, *e.g.*, specific patterning of metal nanoparticles or anti-fouling approaches. In solution drug-delivery approaches represents an emerging research area where well-defined block copolymers reveal a high potential as efficient drug-carriers. A widely used material as hydrophilic, non-toxic segment in a block copolymer is poly(ethylene oxide) (PEO) due to its outstanding physical and chemical properties. PEO is soluble in a wide range of solvents, is chemically inert, non-toxic and, thus, a predestined candidate for biomedical applications.

A powerful tool for the controlled synthesis of PEO containing polymers represents the living anionic ring-opening polymerization (AROP). With help of this technique well-defined block structures, predictable molar masses and selected end-group functionalization of the materials can be obtained.

In this thesis, samples of poly(ethylene oxide)-*block*-poly(allyl glycidyl ether)-*block*-poly(*t*-butyl glycidyl ether) (PEO-*b*-PAGE-*b*-PtBGE) triblock terpolymers with varying degrees of polymerization for the PAGE segment were prepared by living AROP and used to screen the formation of different morphologies of self-assembled structures in aqueous solution. Furthermore, acetylated thiogalactose was attached to the PAGE domains by thiol-ene chemistry to increase the weight fraction of the hydrophobic segments. To analyze the self-assembly of these materials dynamic light scattering (DLS) and cryo-TEM measurements were used. With the help of these methods spherical micelles as well as vesicular structures could be observed. Additionally to the self-assembly at room temperature heat-induced transformations from spherical micelles to worm-like and vesicular structures as well as aggregates of them were found.

PEO-*b*-PAGE-*b*-PtBGE micelles (as well as vesicles) are of particular interest for biomedical applications, where combinations of a hydrophobic core, a biocompatible corona, and a shell, which can be potentially functionalized, are targeted. Therefore, the most promising candidate of the previous prepared samples for a possible application in nanomedicine, PEO<sub>42</sub>-*b*-PAGE<sub>15</sub>-*b*-PtBGE<sub>12</sub>, was further modified by the attachment of cysteamine and 3-mercaptopropionic acid to introduce charges to the triblock terpolymer. Furthermore, the

acetylated thiolgalactose was deprotected as galactose moieties reveal a cell-specific uptake for, *e.g.*, hepatocyte cells. The functionalized triblock terpolymers were used subsequently as a platform for the formation of functional sub-30 nm micelles. Blending these materials and subsequent nano-precipitation leads to the formation of binary or ternary mixed micellar structures. Here, different charge ratios of the PAGE shell and the introduction of galactose as target moiety could be achieved. For a detailed characterization, DLS and cryo-TEM measurements were performed. Furthermore, the prepared nano-structures were tested regarding their toxicity and a possible cellular uptake focusing on the influence of different charges of the PAGE shell. It could be demonstrated that different charge ratios of the shell lead to an increased cell uptake of adherent HEK cells in comparison to the purely positively or negatively charged micelles.

Additionally to the thiol-ene chemistry, Diels-Alder reactions represent a powerful tool for a possible post-polymerization functionalization. A promising candidate for this type of reaction is furfuryl glycidyl ether (FGE) due to the pendant furan ring which can be reacted with, *e.g.*, a maleimide. As for FGE no living or controlled polymerization method was reported so far the compound was investigated as monomer for the living anionic ring-opening polymerization. With the help of this polymerization technique the synthesis of well-defined homo- and diblock copolymers containing furfuryl glycidyl ether with a narrow molar mass distribution was achieved. For this purpose, different initiators as diphenylmethyl potassium (DPMK), sodium hydride, cesium hydride and potassium *t*-butanolate in the bulk and solution as well as the reaction kinetics were investigated in detail. For the controlled synthesis of poly(furfuryl glycidyl ether) (PFGE) homopolymers potassium *t*-butanolate was identified as most efficient initiator. As PFGE revealed a highly hydrophobic character, the self-assembly of poly(ethylene oxide)-*block*-poly(furfuryl glycidyl ether) (PEO-*b*-PFGE) in aqueous solution resulted in the formation of well-defined spherical micelles with a PFGE core and a PEO corona. Subsequently, the PFGE core was reversibly crosslinked using Diels-Alder chemistry leading to stable particles in non-selective solvents like THF or DMF. Inducing the retro-DA process at elevated temperatures led to a disassembly of the micelles into unimolecular chains. As this reversible crosslinking shows a high potential for self-healing surfaces PFGE and PEO-*b*-PFGE were analyzed regarding the application as coating materials. For polymer films of PEO-*b*-PFGE a lamellar bulk morphology with a domain size of approximately 19 nm was detected by small angle light x-ray scattering measurements (SAXS). For both materials the reversible crosslinking/de-crosslinking could be demonstrated, resulting in a change of the hardness of the coating. The differences in the

hardness were investigated in detail by depth-sensing indentation measurements. With help of optical profilometry it could be shown that PEO-*b*-PFGE block copolymers are promising candidates for self-healing surfaces as a healing of scratches of up to 6  $\mu\text{m}$  depth and 1.7 mm width were observed.

In an additional approach FGE was used as efficient termination agent for a living anionic polymerization initiated by a lithium containing compound. Subsequently, the hydroxyl group was re-activated for the polymerization of ethylene oxide. With this method a well-defined poly(2-vinyl pyridine)-*block*-poly(ethylene oxide) (P2VP-*b*-PEO) polymer containing a single FGE unit at the chain junction could be obtained. The pendant furan group was used afterwards for the attachment of a fluorescent dye or the covalent surface coating of gold nanoparticles by Diels-Alder reactions.

In summary well-defined polyether-based materials were synthesized by living AROP. Due to the application of functional monomers as allyl glycidyl ether and furfuryl glycidyl ether possible post-polymerization functionalizations by thiol-ene chemistry and Diels-Alder reactions, respectively, were enabled (**Figure 5.1**). The synthesized materials were used for self-assembly studies and the high potential for drug-delivery approaches could be demonstrated. The reversible Diels-Alder reaction was applied to prepare self-healing surface coatings as well as the covalent coating of gold nanoparticles.

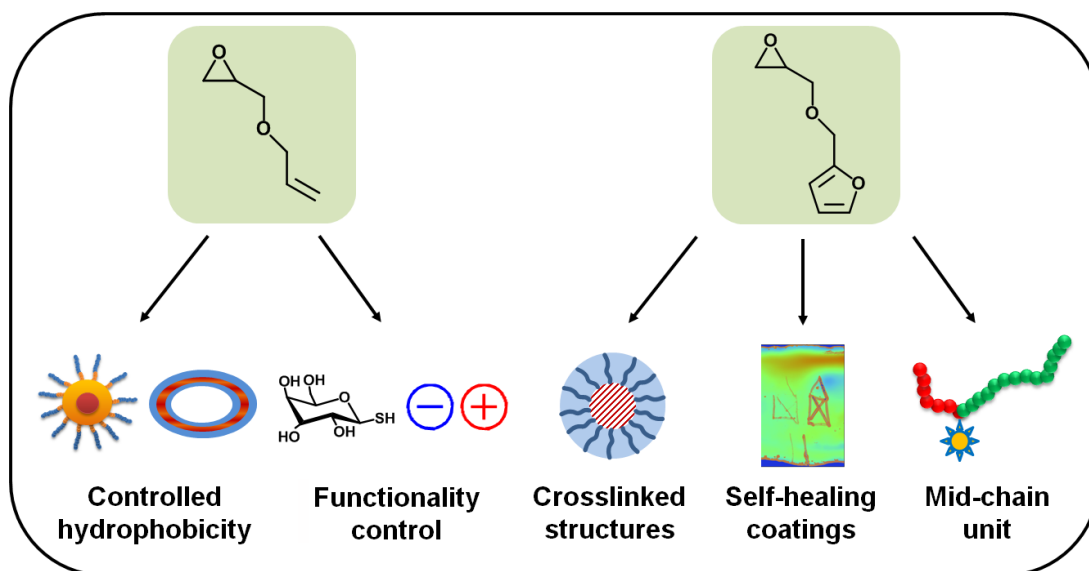


**Figure 5.1:** Overview of possible application fields of glycidyl ethers shown in this thesis.





## 6 Zusammenfassung

Durch das breite potentielle Anwendungsfeld und die hohe Vielfältigkeit von definierten Diblock-Copolymeren und Triblock-Terpolymeren stand die Synthese dieser Materialien in den vergangenen Jahrzehnten im Fokus der Polymerchemie. Je nach Anwendungsbereich (z.B. Materialwissenschaften oder Nanomedizin) können diese Materialien entweder im Bulk oder in Lösung verwendet werden. Klassische Anwendungsbereiche sind phasenseparierte Filme zur spezifischen Anordnung von metallischen Nanopartikeln oder so genannte „Anti-fouling“-Beschichtungen. In Lösung repräsentieren gezielte Wirkstofftransporte in der Pharmakotherapie einen aufstrebenden Forschungsbereich in dem definierte Block-Copolymer ein hohes Anwendungspotential als Wirkstoffträger aufweisen. Durch seine herausragenden chemischen und physikalischen Eigenschaften ist Poly(ethylen oxid) (PEO) ein weit verbreitetes Material für hydrophile Segmente in Block-Copolymeren. PEO ist in einer großen Auswahl an Lösungsmitteln löslich, chemisch inert, nicht toxisch und dadurch für biomedizinische Anwendungen prädestiniert.

Ein herausragendes Werkzeug für die Synthese von PEO basierten Polymeren ist die lebende anionische Ringöffnungspolymerisation (im Englischen „living anionic ring-opening polymerization“ AROP). Mit Hilfe dieser Technik sind die Herstellung definierter Blockstrukturen, vorhersagbare molare Massen und selektive Endgruppenfunktionalisation der Materialien möglich.

In dieser Dissertation wurden Poly(ethylenoxid)-*block*-Poly(allylglycidylether)-*block*-Poly(*t*-butylglycidylether) (PEO-*b*-PAGE-*b*-PtBGE) Triblock-Terpolymere mit variierenden Polymerisationsgraden des PAGE Segments durch lebende AROP hergestellt und für die Untersuchung verschiedener Morphologien der selbst-assemblierten Strukturen der Materialien in wässriger Lösung genutzt. Weiterhin wurden die PAGE Segmente durch thiole-ene Chemie mit acetylierter Thiogalaktose funktionalisiert, um den Massenanteil der hydrophoben Segmente zu erhöhen. Um die Selbstassemblierung dieser Materialien zu studieren wurden dynamische Lichtstreuungs- (DLS) und cryo-TEM Messungen durchgeführt. Mit diesen Methoden konnten sphärische Mizellen und vesikuläre Strukturen identifiziert werden. Zusätzlich zur Selbstassemblierung bei Raumtemperatur konnten temperaturinduzierte Transformationen von Mizellen zu wurmartigen und vesikulären Strukturen sowie Aggregaten derer beobachtet werden.

PEO-*b*-PAGE-*b*-PtBGE Mizellen (sowie Vesikel) sind für biomedizinische Anwendungen von besonderem Interesse, bei denen Kombinationen eines hydrophoben Kern, einer

biokompatiblen Korona und einer funktionalisierbaren Schale notwendig sind. Darum wurde der vielversprechendste Kandidat für eine mögliche Anwendung in der Nanomedizin, PEO<sub>42</sub>-*b*-PAGE<sub>15</sub>-*b*-PtBGE<sub>12</sub>, der vorher hergestellten Substanzen ausgewählt und weiterhin mit Cysteamin und 3-Mercaptopropionsäure funktionalisiert, um Ladungen in das Triblock-Terpolymer einzuführen. Darüber hinaus wurde die acetylierte Thiogalaktose entschützt, da Galaktoseeinheiten eine zellspezifische Aufnahme in beispielsweise Hepatocytenzellen ermöglicht. Die funktionalisierten Triblock-Terpolymere wurden danach als Plattform für die Herstellung von funktionalen sub-30 nm Mizellen genutzt. Mischen dieser Materialien führte zur Bildung binär oder tertiär gemischter mizellarer Strukturen. Dabei wurden verschiedene Ladungsverhältnisse sowie Galaktosegruppen als Targeting-Einheit in die PAGE Schale eingeführt. Für eine detaillierte Strukturaufklärung wurden DLS und cryo-TEM Messungen durchgeführt. Zusätzlich wurden die hergestellten Nanostrukturen in Bezug auf ihre Zelltoxizität und eine mögliche Zellaufnahme getestet. Dabei wurde sich auf den Einfluss der verschiedenen Ladungen der PAGE Schale konzentriert. Es konnte gezeigt werden, dass im Vergleich zu den reinen positiv oder negativ geladenen Mizellen, verschiedene Ladungsverhältnisse zu einer erhöhten Zellaufnahme in adherenten HEK Zellen führte.

Zusätzlich zur thiol-ene Chemie repräsentieren Diels-Alder Reaktionen ein vielseitiges Werkzeug für Post-Polymerisationsfunktionalisationen. Durch die freie Furaneinheit in der Seitenkette ist Furfurylglycidylether (FGE) ein vielversprechender Kandidat für diese Art von Reaktion, da diese Einheit z.B. mit einem Maleimid reagieren kann. Da für FGE keine kontrollierte Polymerisationsmethode bekannt war, wurde die Eignung dieser Substanz für die lebende anionische Ringöffnungspolymerisation getestet. Mit Hilfe dieser Polymerisationsmethode konnten definierte, FGE-enthaltende, Homo- und Blockcopolymere mit einer engen Massenverteilung erhalten werden. Zu diesem Zweck wurden verschiedene Initiatoren wie Diphenylmethyl-Kalium (DPMK), Natriumhydrid, Cäsiumhydrid und Kalium-*t*-Butanolat im Bulk sowie in Lösung getestet und die Reaktionskinetik untersucht. Für die kontrollierte Synthese von PFGE Homopolymeren wurde Kalium-*t*-Butanolat als effektivster Initiator identifiziert. Da PFGE einen stark hydrophoben Charakter aufweist, führte die Selbstassemblierung von Poly(ethylenoxid)-*block*-Poly(furfurylglycidylether) (PEO-*b*-PFGE) in wässriger Lösung zu definierten, sphärischen Mizellen, bestehend aus einem PFGE Kern und einer PEO Korona. Im Anschluss daran wurde der Kern durch eine Diels-Alder Reaktion reversibel verlinkt und stabile Partikel in nicht selektiven Lösungsmitteln (THF oder DMF) konnten erhalten werden. Induziert man die retro-Diels Alder Reaktion bei hohen

Temperaturen kann die Disassemblierung der Mizellen in einzelne Polymerketten beobachtet werden.

Da ein reversibles Vernetzen des Materials ein hohes Potential für selbstheilende Beschichtungen bietet, wurden PFGE und PEO-*b*-PFGE als Beschichtungsmaterial untersucht. Für Filme bestehend aus PEO-*b*-PFGE konnte eine lamellare Morphologie im Bulk mit einer Domänengröße von circa 19 nm mit Hilfe von Kleinwinkelröntgenstreuung (im Englischen „small angle x-ray scattering“, SAXS) Messungen bestimmt werden. Für beide Materialien konnte das reversible vernetzen/entnetzen demonstriert werden, welches in eine Änderung der Materialhärte resultierte. Diese Härteänderungen wurden mit Hilfe von Nanoindentierung untersucht. Durch optische Profilometrie konnte gezeigt werden, dass PEO-*b*-PFGE Blockcopolymerer vielversprechende Materialien für selbstheilende Oberflächen repräsentieren, da Kratzer mit einer Tiefe von bis zu 6 µm und einer Breite von 1.7 mm geheilt werden konnten.

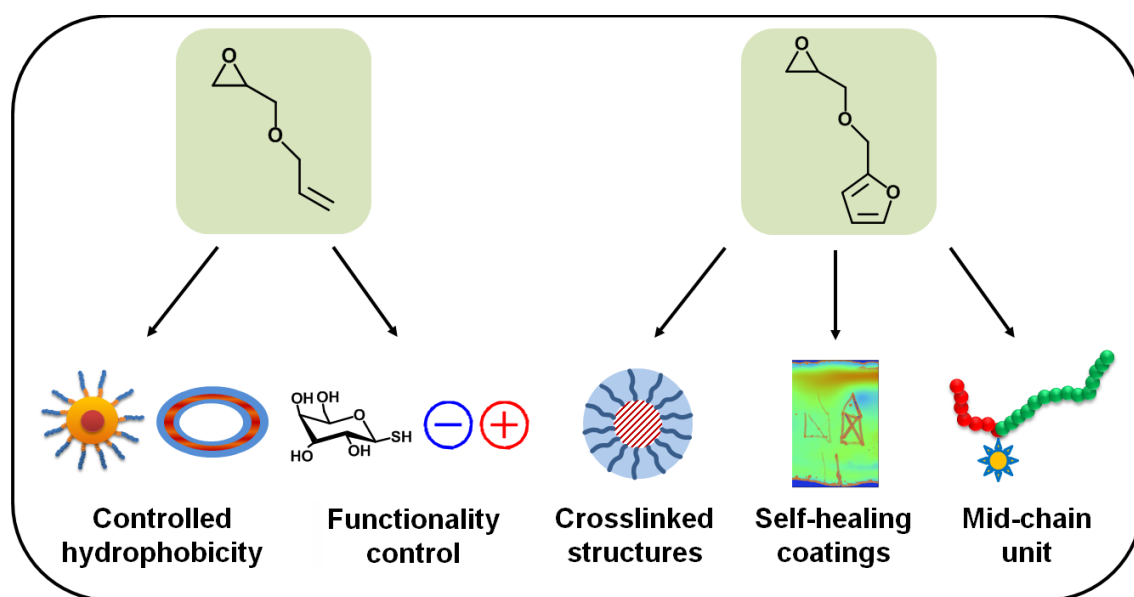


**Abbildung 6.1:** Übersicht über in dieser Arbeit demonstrierte Anwendungsgebiete für Glycidyl Ether.

In einer weiteren Anwendung konnte FGE als effizientes Terminierungsreagenz für eine lebende anionische Polymerisation genutzt werden, welche mit einer lithiumhaltigen Verbindung initiiert wurde. Anschließend wurde die Hydroxylgruppe für die Polymerisation von Ethylenoxid reaktiviert. Mit Hilfe dieser Methode konnte ein definiertes Poly(2-vinylpyridin)-*block*-Poly(ethylenoxid) (P2VP-*b*-PEO) Blockcopolymer mit einer einzelnen FGE-Einheit an der Blockgrenze hergestellt werden. Die freie Furan-Gruppe wurde danach zur Anbindung eines fluoreszierenden Farbstoffs sowie für die kovalente Beschichtung von Gold-Nanopartikeln durch Diels-Alder Reaktionen genutzt.

Zusammenfassend konnten definierte Polyether-basierte Materialien durch lebende AROP hergestellt werden. Durch die Anwendung funktioneller Monomere wie Allylglycidylether und Furfurylglycidylether waren Post-Polymerisationsfunktionalisierungen durch thiol-ene Chemie und Diels-Alder Reaktionen möglich (**Abbildung 6.1**). Die hergestellten Materialien wurden zu Selbstassemblierungsstudien genutzt und das große Potential als Wirkstofftransporter konnte demonstriert werden. Die reversible Diels-Alder Reaktion wurde für die Herstellung selbstheilender Oberflächenbeschichtungen sowie die kovalente Beschichtung von Gold-Nanopartikeln genutzt.

## 7 References

1. A. Blanazs, S. P. Armes, A. J. Ryan, *Macromol. Rapid Commun.*, **2009**, *30*, 267-277.
2. S. B. Darling, *Prog. Polym. Sci.*, **2007**, *32*, 1152-1204.
3. F. H. Schacher, P. A. Rugar, I. Manners, *Angew. Chem. Int. Ed.*, **2012**, *51*, 7898-7921.
4. Y. Y. Mai, A. Eisenberg, *Chem. Soc. Rev.*, **2012**, *41*, 5969-5985.
5. C. T. Black, R. Ruiz, G. Breyta, J. Y. Cheng, M. E. Colburn, K. W. Guarini, H. C. Kim, Y. Zhang, *IBM J. Res. Dev.*, **2007**, *51*, 605-633.
6. K. Knoll, N. Niessner, *Macromol. Symp.*, **1998**, *132*, 231-243.
7. T. Sakai, P. Alexandridis, *Langmuir*, **2004**, *20*, 8426-8430.
8. K. Knop, R. Hoogenboom, D. Fischer, U. S. Schubert, *Angew. Chem. Int. Ed.*, **2010**, *49*, 6288-6308.
9. C. Monfardini, F. M. Veronese, *Bioconjugate Chem.*, **1998**, *9*, 418-450.
10. M. Szwarc, *Nature*, **1956**, *178*, 1168-1169.
11. D. Baskaran, A. H. E. Müller, *Prog. Polym. Sci.*, **2007**, *32*, 173-219.
12. D. H. Richards, M. Szwarc, *T. Faraday Soc.*, **1959**, *55*, 1644-1650.
13. H. Normant, B. Angelo, *B. Soc. Chim. Fr.*, **1960**, 354-359.
14. M. Hruby, C. Konak, K. Ulbrich, *J. Appl. Polym. Sci.*, **2005**, *95*, 201-211.
15. P. Dimitrov, S. Rangelov, A. Dworak, N. Haraguchi, A. Hirao, C. B. Tsvetanov, *Macromol. Symp.*, **2004**, *215*, 127-139.
16. M. J. Barthel, T. Rudolph, S. Crotty, F. H. Schacher, U. S. Schubert, *J. Polym. Sci., Part A: Polym. Chem.*, **2012**, *50*, 4958-4965.
17. B. Obermeier, H. Frey, *Bioconjugate Chem.*, **2011**, *22*, 436-444.
18. V. Abetz, P. F. W. Simon, *Adv. Polym. Sci.*, **2005**, *189*, 125-212.
19. D. Leckband, S. Sheth, A. Halperin, *J. Biomat. Sci., Polym. Ed.*, **1999**, *10*, 1125-1147.
20. C. Allen, D. Maysinger, A. Eisenberg, *Colloid Surf., B*, **1999**, *16*, 3-27.
21. M. Hruby, C. Konak, K. Ulbrich, *J. Control. Release*, **2005**, *103*, 137-148.
22. C. Price, T. P. Lally, Stubbers.R, *Polymer*, **1974**, *15*, 541-543.
23. K. Arai, T. Kotaka, Y. Kitano, K. Yoshimura, *Macromolecules*, **1980**, *13*, 455-457.
24. Y. Mogi, H. Kotsuji, Y. Kaneko, K. Mori, Y. Matsushita, I. Noda, *Macromolecules*, **1992**, *25*, 5408-5411.
25. C. Auschra, R. Stadler, *Macromolecules*, **1993**, *26*, 2171-2174.
26. J. Beckmann, C. Auschra, R. Stadler, *Macromol. Rapid Commun.*, **1994**, *15*, 67-72.
27. Y. Mogi, M. Nomura, H. Kotsuji, K. Ohnishi, Y. Matsushita, I. Noda, *Macromolecules*, **1994**, *27*, 6755-6760.
28. J. L. Huang, X. Y. Huang, W. B. Hu, W. K. Lou, *Sci. China, Ser. B: Chem.*, **1997**, *40*, 663-669.
29. X. Y. Huang, S. Chen, J. L. Huang, *J. Polym. Sci., Part A: Polym. Chem.*, **1999**, *37*, 825-833.
30. S. Grund, M. Bauer, D. Fischer, *Adv. Eng. Mater.*, **2011**, *13*, B61-B87.
31. G. Riess, *Prog. Polym. Sci.*, **2003**, *28*, 1107-1170.
32. G. S. Kwon, K. Kataoka, *Adv. Drug. Deliver. Rev.*, **1995**, *16*, 295-309.
33. D. E. Discher, A. Eisenberg, *Science*, **2002**, *297*, 967-973.
34. G. Gaucher, M. H. Dufresne, V. P. Sant, N. Kang, D. Maysinger, J. C. Leroux, *J. Control. Release*, **2005**, *109*, 169-188.
35. A. O. Moughton, M. A. Hillmyer, T. P. Lodge, *Macromolecules*, **2011**, *45*, 2-19.
36. F. Schacher, A. Walther, M. Ruppel, M. Drechsler, A. H. E. Müller, *Macromolecules*, **2009**, *42*, 3540-3548.

37. E. Betthausen, M. Drechsler, M. Förtsch, F. H. Schacher, A. H. E. Müller, *Soft Matter*, **2011**, *7*, 8880-8891.
38. C. Mangold, F. Wurm, H. Frey, *Polym. Chem.*, **2012**, *3*, 1714-1721.
39. P. Dimitrov, S. Rangelov, A. Dworak, C. B. Tsvetanov, *Macromolecules*, **2004**, *37*, 1000-1008.
40. M. Backes, L. Messenger, A. Mourran, H. Keul, M. Möller, *Macromolecules*, **2010**, *43*, 3238-3248.
41. B. F. Lee, M. J. Kade, J. A. Chute, N. Gupta, L. M. Campos, G. H. Fredrickson, E. J. Kramer, N. A. Lynd, C. J. Hawker, *J. Polym. Sci., Part A: Polym. Chem.*, **2011**, *49*, 4498-4504.
42. A. A. Toy, S. Reinicke, A. H. E. Müller, H. Schmalz, *Macromolecules*, **2007**, *40*, 5241-5244.
43. J. C. Persson, P. Jannasch, *Chem. Mater.*, **2006**, *18*, 3096-3102.
44. J. N. Hunt, K. E. Feldman, N. A. Lynd, J. Deek, L. M. Campos, J. M. Spruell, B. M. Hernandez, E. J. Kramer, C. J. Hawker, *Adv. Mater.*, **2011**, *23*, 2327-2331.
45. F. Özdemir, H. Keul, A. Mourran, M. Möller, *Macromol. Rapid. Commun.*, **2011**, *32*, 1007-1013.
46. Y. Koyama, M. Umehara, A. Mizuno, M. Itaba, T. Yasukouchi, K. Natsume, A. Suginata, K. Watanabe, *Bioconjugate Chem.*, **1996**, *7*, 298-301.
47. M. J. Barthel, K. Babiuch, T. Rudolph, J. Vitz, S. Hoepfener, M. Gottschaldt, M. D. Hager, F. H. Schacher, U. S. Schubert, *J. Polym. Sci., Part A: Polym. Chem.*, **2012**, *50*, 2914-2923.
48. K. Kempe, C. Weber, K. Babiuch, M. Gottschaldt, R. Hoogenboom, U. S. Schubert, *Biomacromolecules*, **2011**, *12*, 2591-2600.
49. H. Cui, T. K. Hodgdon, E. W. Kaler, L. Abezgauz, D. Danino, M. Lubovsky, Y. Talmon, D. J. Pochan, *Soft Matter*, **2007**, *3*, 945-955.
50. S. J. Holder, N. A. J. M. Sommerdijk, *Polym. Chem.*, **2011**, *2*, 1018-1028.
51. S. Zhong, D. J. Pochan, *Polym. Rev.*, **2010**, *50*, 287-320.
52. C. L. Wu, R. J. Ma, H. He, L. Z. Zhao, H. J. Gao, Y. L. An, L. Q. Shi, *Macromol. Biosci.*, **2009**, *9*, 1185-1193.
53. A. B. E. Attia, Z. Y. Ong, J. L. Hedrick, P. P. Lee, P. L. R. Ee, P. T. Hammond, Y. Y. Yang, *Curr. Opin. Colloid Interface Sci.*, **2011**, *16*, 182-194.
54. X. Liu, Y. Liu, Z. K. Zhang, F. Huang, Q. Tao, R. J. Ma, Y. L. An, L. Q. Shi, *Chem. Eur. J.*, **2013**, *19*, 7437-7442.
55. J. P. Lin, J. Q. Zhu, T. Chen, S. L. Lin, C. H. Cai, L. S. Zhang, Y. Zhuang, X. S. Wang, *Biomaterials*, **2009**, *30*, 108-117.
56. H. Cabral, Y. Matsumoto, K. Mizuno, Q. Chen, M. Murakami, M. Kimura, Y. Terada, M. R. Kano, K. Miyazono, M. Uesaka, N. Nishiyama, K. Kataoka, *Nat. Nanotechnol.*, **2011**, *6*, 815-823.
57. H. Dong, N. Dube, J. Y. Shu, J. W. Seo, L. M. Mahakian, K. W. Ferrara, T. Xu, *ACS Nano*, **2012**, *6*, 5320-5329.
58. F. Alexis, E. Pridgen, L. K. Molnar, O. C. Farokhzad, *Mol. Pharm.*, **2008**, *5*, 505-515.
59. J. Nguyen, X. Xie, M. Neu, R. Dumitrascu, R. Reul, J. Sitterberg, U. Bakowsky, R. Schermuly, L. Fink, T. Schmehl, T. Gessler, W. Seeger, T. Kissel, *J. Gene. Med.*, **2008**, *10*, 1236-1246.
60. S. Mishra, P. Webster, M. E. Davis, *Eur. J. Cell. Biol.*, **2004**, *83*, 97-111.
61. J. Sun, F. Zeng, H. Jian, S. Wu, *Biomacromolecules*, **2013**, *14*, 728-736.
62. A. C. Rinkenauer, A. Schallon, U. Günther, M. Wagner, E. Betthausen, U. S. Schubert, F. H. Schacher, *ACS Nano*, **2013**, *7*, 9621-9631.
63. A. A. Kavitha, N. K. Singha, *J. Polym. Sci., Part A: Polym. Chem.*, **2007**, *45*, 4441-4449.

64. A. A. Kavitha, N. K. Singha, *Macromolecules*, **2010**, *43*, 3193-3205.
65. S. D. Bergman, F. Wudl, *J. Mater. Chem.*, **2008**, *18*, 41-62.
66. P. M. Imbesi, C. Fidge, J. E. Raymond, S. I. Cauet, K. L. Wooley, *ACS Macro Lett.*, **2012**, *1*, 473-477.
67. Q. A. Tian, M. Z. Rong, M. Q. Zhang, Y. C. Yuan, *Polym. Int.*, **2010**, *59*, 1339-1345.
68. P. A. Pratama, A. M. Peterson, G. R. Palmese, *Macromol. Chem. Phys.*, **2012**, *213*, 173-181.
69. Y. Kim, M. H. Pourgholami, D. L. Morris, M. H. Stenzel, *Biomacromolecules*, **2012**, *13*, 814-825.
70. F. H. Schacher, A. Walther, M. Ruppel, M. Drechsler, A. H. E. Müller, *Macromolecules*, **2009**, *42*, 3540-3548.
71. R. K. O'Reilly, C. J. Hawker, K. L. Wooley, *Chem. Soc. Rev.*, **2006**, *35*, 1068-1083.
72. S. Crotty, M. J. Barthel, F. H. Schacher, U. S. Schubert, *unpublished results (2013)*.
73. M. D. Hager, P. Greil, C. Leyens, S. van der Zwaag, U. S. Schubert, *Adv. Mater.*, **2010**, *22*, 5424-5430.
74. R. S. Trask, H. R. Williams, I. P. Bond, *Bioinspir. Biomim.*, **2007**, *2*, P1-P9.
75. E. W. Davie, O. D. Ratnoff, *Science*, **1964**, *145*, 1310-1312.
76. E. Vaccaro, J. H. Waite, *Biomacromolecules*, **2001**, *2*, 906-911.
77. B. J. Blaiszik, S. L. B. Kramer, S. C. Olugebefola, J. S. Moore, N. R. Sottos, S. R. White, *Annu. Rev. Mater. Res.*, **2010**, *40*, 179-211.
78. N. K. Guimard, K. K. Oehlenschlaeger, J. W. Zhou, S. Hilf, F. G. Schmidt, C. Barner-Kowollik, *Macromol. Chem. Phys.*, **2012**, *213*, 131-143.
79. B. Sandmann, S. Bode, M. D. Hager, U. S. Schubert, *Polym. Chem.*, **2013**, *4*, 4966-4973.
80. S. R. White, N. R. Sottos, P. H. Geubelle, J. S. Moore, M. R. Kessler, S. R. Sriram, E. N. Brown, S. Viswanathan, *Nature*, **2001**, *409*, 794-797.
81. H. R. Williams, R. S. Trask, P. M. Weaver, I. P. Bond, *J. R. Soc. Interface*, **2008**, *5*, 55-65.
82. V. Berl, M. Schmutz, M. J. Krische, R. G. Khoury, J. M. Lehn, *Chem. Eur. J.*, **2002**, *8*, 1227-1244.
83. J. L. Wietor, A. Dimopoulos, L. E. Govaert, R. A. T. M. van Benthem, G. de With, R. P. Sijbesma, *Macromolecules*, **2009**, *42*, 6640-6646.
84. R. P. Sijbesma, F. H. Beijer, L. Brunsveld, B. J. B. Folmer, J. H. K. K. Hirschberg, R. F. M. Lange, J. K. L. Lowe, E. W. Meijer, *Science*, **1997**, *278*, 1601-1604.
85. O. A. Scherman, G. B. W. L. Ligthart, R. P. Sijbesma, E. W. Meijer, *Angew. Chem. Int. Ed.*, **2006**, *45*, 2072-2076.
86. H. Ohkawa, G. B. W. L. Ligthart, R. P. Sijbesma, E. W. Meijer, *Macromolecules*, **2007**, *40*, 1453-1459.
87. P. Cordier, F. Tournilhac, C. Soulie-Ziakovic, L. Leibler, *Nature*, **2008**, *451*, 977-980.
88. D. Montarnal, M. Capelot, F. Tournilhac, L. Leibler, *Science*, **2011**, *334*, 965-968.
89. X. X. Chen, M. A. Dam, K. Ono, A. Mal, H. B. Shen, S. R. Nutt, K. Sheran, F. Wudl, *Science*, **2002**, *295*, 1698-1702.
90. X. X. Chen, F. Wudl, A. K. Mal, H. B. Shen, S. R. Nutt, *Macromolecules*, **2003**, *36*, 1802-1807.
91. Y. L. Liu, C. Y. Hsieh, *J. Polym. Sci., Part A: Polym. Chem.*, **2006**, *44*, 905-913.
92. M. Wouters, E. Craenmehr, K. Tempelaars, H. Fischer, N. Stroeks, J. van Zanten, *Prog. Org. Coat.*, **2009**, *64*, 156-162.
93. J. Zhou, N. K. Guimard, A. J. Inglis, M. Namazian, C. Y. Lin, M. L. Coote, E. Spyrou, S. Hilf, F. G. Schmidt, C. Barner-Kowollik, *Polym. Chem.*, **2012**, *3*, 628-639.
94. A. J. Inglis, L. Nebhani, O. Altintas, F. G. Schmidt, C. Barner-Kowollik, *Macromolecules*, **2010**, *43*, 5515-5520.

95. J. Kötteritzsch, S. Stumpf, S. Hoepfner, J. Vitz, M. D. Hager, U. S. Schubert, *Macromol. Chem. Phys.*, **2013**, *214*, 1636-1649.
96. A. Gandini, *Prog. Polym. Sci.*, **2013**, *38*, 1-29.
97. J. A. Syrett, C. R. Becer, D. M. Haddleton, *Polym. Chem.*, **2010**, *1*, 978-987.
98. R. Gheneim, C. Perez-Berumen, A. Gandini, *Macromolecules*, **2002**, *35*, 7246-7253.
99. Q. Tian, Y. C. Yuan, M. Z. Rong, M. Q. Zhang, *J. Mater. Chem.*, **2009**, *19*, 1289-1296.
100. C. Gousse, A. Gandini, P. Hodge, *Macromolecules*, **1998**, *31*, 314-321.
101. A. M. Peterson, R. E. Jensen, G. R. Palmese, *ACS Appl. Mater. Inter.*, **2010**, *2*, 1141-1149.
102. E. Araneda, A. Leiva, L. Gargallo, N. Hadjichristidis, I. Mondragon, D. Radic, *Polym. Eng. Sci.*, **2012**, *52*, 1128-1136.
103. B. J. Briscoe, L. Fiori, E. Pelillo, *J. Phys. D. Appl. Phys.*, **1998**, *31*, 2395-2405.
104. N. Hadjichristidis, M. Pitsikalis, S. Pispas, H. Iatrou, *Chem. Rev.*, **2001**, *101*, 3747-3792.
105. A. Natalello, C. Tonhauser, E. Berger-Nicoletti, H. Frey, *Macromolecules*, **2011**, *44*, 9887-9890.



**List of abbreviations**

AGE	Allyl glycidyl ether
AROP	Anionic ring-opening polymerization
BMI	Bismaleimide
c	Concentration
CsOH	Cesium hydride
Cryo-TEM	Cryogenic transmission electron microscopy
$\delta$	Chemical shift
DA	Diels-Alder
DLS	Dynamic light scattering
DMF	Dimethylformamid
DMPA	2,2-Dimethoxy-2-phenylacetophenone
DPMK	Diphenylmethyl potassium
DSC	Differential scanning calorimetry
$E_i$	Young modulus
EO	Ethylene oxide
FGE	Furfuryl glycidyl ether
H	Hardness
LCST	Lower critical solution temperature
M	Molar mass
MALDI-ToF	Matrix assisted laser desorption ionization – time of flight
MeOH	Methanol
NaH	Sodium hydride
NaOMe	Sodium methanolate
NMR	Nuclear magnetic resonance
P2/4VP	Poly(2/4-vinyl pyridine)
PAA	Poly(acrylic acid)
PAGE	Poly(allyl glycidyl ether)
PB	Polybutadiene
PCL	Poly( $\epsilon$ -caprolactone)
PDI	Polydispersity index
PEG	Poly(ethylene glycol)

## List of abbreviations

---

PEO	Poly(ethylene oxide)
PFGE	Poly(furfuryl glycidyl ether)
PI	Polyisoprene
PLUMS	Polymer labeling using mass spectrometry
PMMA	Poly(methyl methacrylate)
PNIPAM	Poly( <i>n</i> -isopropylacrylamide)
PS	Polystyrene
P <i>t</i> BGE	Poly( <i>t</i> -butyl glycidyl ether)
rDA	Retro-Diels Alder
$\langle R_h \rangle_{n,app}$	Number weight hydrodynamic radius
SEC	Size exclusion chromatography
T	Temperature
<i>t</i> BGE	<i>t</i> -butyl glycidyl ether
<i>t</i> BuOK	Potassium <i>t</i> -butanolate
THF	Tetrahydrofuran

## Curriculum vitae

### Personal information:

Last name: Barthel  
First name: Markus J.  
Date of birth: 12<sup>th</sup> July 1985  
Place of birth: Zwickau, Germany  
Citizenship: German  
Marital status: Married



### Education:

- Since 11/2010      PhD-Student in macromolecular chemistry  
Title “Synthesis and applications of polyether-based block copolymers”  
*Friedrich Schiller University Jena*  
*Supervisor: Prof. Dr. U. S. Schubert,*  
*Funding by Dutch Polymer Institute (DPI) – Industrial partners:*  
*Michelin, Evonik, Chemspeed*  
*Cooperation with Prof. P. J. Lutz, ICS Strasbourg*
- 12/2009-10/2010      Diploma thesis (corresponds M. Sc. thesis)  
Title: “Living anionic polymerization of reactive monomers”  
*Friedrich Schiller University Jena (Prof. Dr. U. S. Schubert)*  
*Cooperation with Prof. Dr. P. J. Lutz, ICS Strasbourg*
- 10/2005-10/2010      Diploma-studies in chemistry (corresponds B. Sc + M. Sc.)  
Specialization on macromolecular chemistry and metal-organic  
chemistry  
*Friedrich Schiller University Jena*
- 1996-2004              Abitur (corresponds A-Level)  
*Käthe-Kollwitz-Gymnasium Zwickau*

Jena, 31.01.2014

---

Markus J. Barthel



## Publication list

### *Peer-reviewed publications:*

1. **M. J. Barthel**, K. Babiuch, T. Rudolph, J. Vitz, S. Hoepfener, M. Gottschaldt, M. D. Hager, F. H. Schacher, U. S. Schubert  
 “Bis-hydrophilic and functional triblock terpolymers based on polyethers: Synthesis and self-assembly in solution”  
*J. Polym. Sci., Part A: Polym. Chem.* **2012**, *50*, 2914–2923.
2. **M. J. Barthel**<sup>#</sup>, T. Rudolph<sup>#</sup>, S. Crotty, F. H. Schacher, U. S. Schubert  
 “Homo- and block copolymers of poly(furfuryl glycidyl ether) by living anionic polymerization: Towards reversibly core-crosslinked micelles”  
*J. Polym. Sci., Part A: Polym. Chem.* **2012**, *50*, 4958–4965.
3. G. M.-E. Pozza, H. Harris, **M. J. Barthel**, J. Vitz, U. S. Schubert, P. J. Lutz  
 “Macromonomers as well-defined building blocks in the synthesis of hybrid octafunctional star-shaped poly(ethylene oxide)s”  
*Macromol. Chem. Phys.* **2012**, *213*, 2181–2191.
4. **M. J. Barthel**, U. Mansfeld, S. Hoepfener, J. A. Czaplewska, F. H. Schacher, U. S. Schubert  
 “Understanding and tuning the self-assembly of polyether-based triblock terpolymers in aqueous solution”  
*Soft Matter* **2013**, *9*, 3509–3520.
5. **M. J. Barthel**<sup>#</sup>, T. Rudolph<sup>#</sup>, A. Teichler, R. M. Paulus, J. Vitz, S. Hoepfener, M. D. Hager, F. H. Schacher, U. S. Schubert  
 “Self-healing materials *via* reversible crosslinking of poly(ethylene oxide)-*block*-poly(furfuryl glycidyl ether) (PEO-*b*-PFGE) block copolymer films”  
*Adv. Funct. Mater.* **2013**, *23*, 4921-4932.

<sup>#</sup>Both authors contributed equally to this work.

6. T. Rudolph<sup>#</sup>, **M. J. Barthel**<sup>#</sup>, F. Kretschmer, U. Mansfeld, S. Hoepfener, M. D. Hager, U. S. Schubert, F. H. Schacher  
“Poly(2-vinyl pyridine)-*block*-poly(ethylene oxide) featuring a furan group at the block junction – Synthesis and functionalization”  
*Macromol. Rapid. Commun.* **2014**, DOI: 10.1002/marc201300875.
7. **M. J. Barthel**, F. H. Schacher, U. S. Schubert  
“Poly(ethylene oxide) (PEO)-based ABC triblock terpolymers – Synthetic complexity vs. application benefits”  
*Polym. Chem.* **2014**, DOI: 10.1039/C3PY01666H.

***Submitted publications:***

1. **M. J. Barthel**<sup>#</sup>, A. C. Rinkenauer<sup>#</sup>, M. Wagner, U. Mansfeld, S. Hoepfener, J. A. Czaplewska, M. Gottschaldt, A. Schallon, F. H. Schacher, U. S. Schubert  
*submitted to Adv. Funct. Mater.*  
“Small but powerful: Co-assembly of polyether-based triblock terpolymers into sub-30 nm micelles and synergistic effects on cellular interactions”

***Manuscripts in preparation:***

1. S. Crotty, **M. J. Barthel**, F. H. Schacher, U. S. Schubert  
“MALDI-ToF MS/MS of polyether-based homo and diblock copolymers using software-based data analysis”  
*in preparation.*
2. G. M.-E. Pozza, **M. J. Barthel**, S. Crotty, A. Baumgaertel, J. Vitz, F. H. Schacher, P. J. Lutz, U. S. Schubert  
“Precise Synthesis of Undecenyl Poly(ethylene oxide) Macromonomers as Heterofunctional Building Blocks for the synthesis of branched materials”  
*in preparation.*

<sup>#</sup>Both authors contributed equally to this work.

***Oral presentations:***

1. M. J. Barthel, A. Can, M. D. Hager, “Synthesis *via* living anionic polymerization”, **High-Throughput Experimentation Review Meeting of the Dutch Polymer Institute (DPI)**, *Eindhoven*, The Netherlands, **04/22/2010**.
2. M. J. Barthel, J. Vitz, “Designer polyethers and water soluble polymers – from living anionic polymerization to online analysis”, **High-Throughput Experimentation Review Meeting of the Dutch Polymer Institute (DPI)**, *Jena*, Germany, **09/12/2010**.
3. M. J. Barthel, “Designer polyether *via* living anionic polymerization and post-polymerization functionalization”, **High-Throughput Experimentation Review Meeting of the Dutch Polymer Institute (DPI)**, *Darmstadt*, Germany, **06/05/2011**.
4. M. J. Barthel, “Designer polyether *via* living anionic polymerization of EO and post-polymerization functionalization”, **High-Throughput Experimentation Review Meeting of the Dutch Polymer Institute (DPI)**, *Jena*, Germany, **12/05/2011**.
5. M. J. Barthel, “Libraries of designer polyethers: Synthesis and application - DPI project #690”, **High-Throughput Experimentation Review Meeting of the Dutch Polymer Institute (DPI)**, *Darmstadt*, Germany, **06/06/2012**.
6. M. J. Barthel, “Designer polymers by living anionic polymerization - DPI project #690”, **High-Throughput Experimentation Review Meeting of the Dutch Polymer Institute (DPI)**, *Jena*, Germany, **12/03/2012**.
7. M. J. Barthel, T. Rudolph, A. Teichler, R. M. Paulus, J. Vitz, S. Hoepfener, M. D. Hager, F. H. Schacher, U. S. Schubert “Self-healing materials *via* reversible crosslinking of poly(ethylene oxide)-*block*-poly(furfuryl glycidyl ether) (PEO-*b*-PFGE) block copolymer films”, **EPF conference**, *Pisa*, Italy, **06/18/2013**.
8. G. Pozza, M. J. Barthel, “DPI project #690”, **High-Throughput Experimentation Review Meeting of the Dutch Polymer Institute (DPI)**, *Darmstadt*, Germany, **07/04/2013**.

9. M. J. Barthel, “Tailor-made poly(ethylene oxide) libraries - DPI project #690”, **High-Throughput Experimentation Review Meeting of the Dutch Polymer Institute (DPI)**, *Arnhem*, The Netherlands, **11/05/2013**.

***Poster presentations:***

1. M. J. Barthel, J. Vitz, A. Can, M. D. Hager, P. Lutz, U. S. Schubert, “Living anionic polymerization: Poly(isoprene) and designer polyether”, **DPI Annual Meeting**, *Bergen op Zoom*, The Netherlands, **11/17/2010**.
2. M. J. Barthel, J. Vitz, G. Pozza, M. D. Hager, P. Lutz, U. S. Schubert, “Designer polyether *via* living anionic polymerization”, **Thüringer Werkstofftag**, *Jena*, Germany, **03/30/2011**.
3. M. J. Barthel, J. Vitz, M. D. Hager, P. Lutz, U. S. Schubert, “Designer polyether *via* living anionic polymerization”, **DPI Annual Meeting**, *Zeist*, The Netherlands, **11/15/2011**.
4. M. J. Barthel, T. Rudolph, S. Crotty, F. H. Schacher, U. S. Schubert, “Furfuryl glycidyl ether – a new tool in the field of living anionic polymerization”, **DPI Annual Meeting**, *Zeist*, The Netherlands, **11/13/2012**.
5. M. J. Barthel, U. Mansfeld, S. Hoepfner, J. A. Czaplewska, F. H. Schacher, U. S. Schubert, “Understanding and tuning the self-assembly of polyether-based triblock terpolymers in aqueous solution”, **EPF conference**, *Pisa*, Italy, **06/18/2013**.



## Acknowledgements / Danksagung

Da eine Arbeit wie diese unmöglich allein anzufertigen ist, möchte ich die folgenden Zeilen nutzen, um mich bei den Menschen zu bedanken, die mir auf meinem Weg zur Seite standen und mich bei meiner Forschung unterstützt haben.

Als Erstes möchte ich mich bei meinem wissenschaftlichen Betreuer, Prof. Dr. Ulrich S. Schubert, für die Möglichkeit bedanken, auf einem interessanten und gleichzeitig wissenschaftlich sowie technisch anspruchsvollem Thema wie die Synthese PEO-basierter Systeme zu forschen. Durch die perfekte Laborausstattung und den gegebenen Freiraum für eigene Ideen haben Sie die in dieser Arbeit enthaltenen Ergebnisse möglich gemacht. Weiterhin möchte ich mich bei Ihnen für die Einbindungen in die Kooperation mit dem Institut Charles Sadron (ICS) Straßburg sowie in weitere interessante Projekte wie PeTra oder BASIS bedanken. Ein besonderer Dank gilt dabei Prof. Dr. Pierre J. Lutz für die Einführung in die Grundlagen der PEO-Synthese und die erfolgreiche Kooperation. Weiterhin möchte ich Ihnen für die Möglichkeit der regelmäßigen Forschungsaufenthalte in Straßburg danken. Verbunden mit dieser Kooperation danke ich dem Dutch Polymer Institute (DPI) im Rahmen des Projekts #690 für die finanzielle Unterstützung.

Für die finanzielle Förderung der Kooperationsbesuche in Strasbourg und meiner Konferenzreise zur EPF Konferenz 2013 in Pisa, danke ich dem Deutschen Akademischen Austauschdienst (DAAD).

Besonders hervorheben möchte ich meinen Co-Betreuer Jun.-Prof. Dr. Felix H. Schacher. Felix, ich danke dir von ganzem Herzen für die permanente Unterstützung während meiner Zeit als Doktorand. Du hast die Ideen gebündelt, in die richtigen Bahnen gelenkt und standst mir immer mit einem offenen Ohr zur Seite. Ohne dich hätte ich diese Arbeit nicht so erfolgreich abschließen können.

Für die technische Unterstützung im EO-Labor möchte ich mich bei Dr. Jürgen Vitz und Alexander Meier bedanken. Es war ein harter Weg den Reaktor und die Glovebox aufzubauen, aber ich glaube, dass ich für uns sprechen und sagen kann: Es hat sich gelohnt! Viel Erfolg weiterhin mit all den Robotern, Reaktoren und unzähligen Geräten.

I would like to acknowledge Renzo Paulus for TGA and DSC measurements as well as the IT support in all these years.

I want to thank Sarah Crotty for the MALDI measurements and in particular for all the highly urgent, priority samples you measured for me. Besides from the scientific part I want to thank

you for being a friend I could always count on. I wish you all the best for your future – wherever it will be! Stay as you are!

Für die AFM, TEM und cryo-TEM Messungen möchte ich mich herzlich bei Dr. Stephanie Höppener und Ulrich Mansfeld bedanken.

Besonders wichtig für einen Polymerchemiker ist die SEC. Hier möchte ich Dr. Grit Festag und Nicole Fritz erwähnen, die mit ihrem ausdauernden Einsatz all die Systeme tagtäglich am Laufen gehalten haben. Grit, ich möchte mich noch einmal direkt für die Messungen meiner Proben bedanken, die einfach nie so wollten, wie ich es wollte.

Unseren NMR-Spezialisten Dr. Günther und Frau Sentis möchte ich für eine Vielzahl an Messungen und das Unterhalten der Geräte danken.

I would like to thank Dr. Michael Gottschald and Dr. Justyna Czaplewska for the cooperation regarding the “sugar chemistry”. Justyna for the provided thiosugars shown in this thesis I’m very grateful.

Furthermore, I would acknowledge Gladys Pozza for the great cooperation within the PEO project.

Florian Kretschmer danke ich für die Herstellung der funktionalisierten Nanopartikel.

Dr. Uwe Köhn, Sandra Köhn, Sylvia Braunsdorf, Simone Burchardt und Doreen Kuchler möchte ich für die Hilfe bei Bestellungen, organisatorischen Schwierigkeiten und Abrechnungen danken. Ohne euch würde die Schubert Group nicht funktionieren!

An dieser Stelle möchte ich noch einige private Worte des Dankes an Personen richten, die mir in meiner Zeit als Doktorand besonders ans Herz gewachsen sind.

Als Erstes ist da natürlich Tobias R. zu nennen: Ich danke dir für die schöne Zeit und werde unsere Zusammenarbeit wirklich vermissen. Es reicht ja ein Blick auf unsere Publikationen, um zu erkennen, dass wir ein großartiges Gespann waren. Ich sag es dir, irgendwann stellen wir unsere eigene Gruppe wirklich noch auf die Beine.

Ein herzlicher Gruß und großes Dankeschön geht an meine alten TO-Bürokollegen Christian, Anke und Andreas (der später würdig von Tobi M. ersetzt wurde). Was haben wir in all der Zeit alles erlebt und gelacht. Es war wirklich eine tolle Zeit mit euch und ich werde euch alle sehr vermissen. Ich denke dabei an Pietschers Feuerball (den Sarah dann nochmal fabriziert hat), an Pietschers Spruch „Ich habe gerade nicht zugehört“, unsere musikalischen Freitage ;-), Andreas unnützes (aber unheimlich erheiterndes) Wissen, Anke, die uns immer mit Schoki versorgt hat,... Tobi, es war mir eine Freude dich als meinen ersten Diplomanden zu betreuen. Auch wenn du mir als erste Amtshandlung einen Dewar in Feinstaub verwandelt

hast ;-). Wir haben unzählige Geschichten erlebt, die ich immer im Herzen tragen werde. Christian, dir danke ich besonders für die nun fast zwei Jahre, die wir zusammen beim Klimpern mit der Gitarre verbrachten. Alex wird froh sein, dass dies nun vorbei ist ;-)

Ich freue mich besonders, dass wir es noch gegen Ende geschafft haben, ein Bio-Projekt auf die Beine zu stellen und ich dadurch die Chance hatte, Anja, Alex und Micha wirklich kennenzulernen. Schade, dass es erst so spät war, denn ihr seid wirklich drei tolle Personen. Ihr und unser Dienstagmittag werdet mir fehlen!

Einen festen Platz in meinen Erinnerungen wird unsere tolle TO-Gruppe (samt historischen Mitgliedern wie BAnja, Flummi Antje, Sofia, Katrin, Mirko, Torsten + TO-Fremde wie Gottsche, Uwe, Martin, Christine und Christoph) haben. Die gefeierten Geburtstage, Grill- und Spieleabende und das super Klima untereinander ist einer der wesentlichen Gründe, warum ich mit Freude an meine Zeit in der AG Schubert zurückdenke.

Ein besonderer Dank geht auch an meine zweite Heimat im TO – das Büro der AG Schacher. Ich danke euch, dass ihr trotz akuten Platzmangels immer ein Fleckchen und einen Kaffee für mich hattet.

Sono stato anche molto fortunato ad aver conosciuto due fantastiche persone che hanno fatto parte del nostro gruppo scientifico: Daniela e Guido. Siete arrivati come sconosciuti, siete andati via come amici e spero che ci rivedremo presto.

Ein besonderer Dank gilt auch all meinen Freunden in Jena, die mich all die Jahre begleitet haben. Besonders Thomas und Martin sowie der italienische Stammtisch waren immer ein sicherer Rückhalt, auch in schweren Zeiten. Danke!

Zu guter Letzt möchte ich noch den wichtigsten Menschen in meinem Leben danken.

Liebe Familie, ohne eure Unterstützung und all die Mühen, die ihr auf euch genommen habt, hätte ich nicht die Chance gehabt, meinen Weg zu gehen und eine weitere Etappe mit dieser Doktorarbeit zu erreichen. Ich bin glücklich, Eltern wie euch zu haben!

Poi, qualcuno lo chiama destino, ho avuto la fortuna di trovare un'altra famiglia: la mia famiglia italiana. All'inizio non parlavo la vostra lingua, ma sin dal primo minuto mi sono sentito con voi a casa. Vi ringrazio di cuore per la vostra fiducia e il vostro sostegno! Sono contento che facciate parte della mia famiglia!

Claudia, mia moglie, manchi solo tu... Ti ringrazio per tutto quello che hai fatto per me. Mi hai dato sempre la forza di andare avanti, hai avuto fiducia in me e mi sei stata sempre vicina. Non ci sono parole per dirti grazie per tutto quello che sei e che hai fatto per me – solo *ti amo!*



## **Declaration of authorship / Selbstständigkeitserklärung**

Ich erkläre, dass ich die vorliegende Arbeit selbständig und unter Verwendung der angegebenen Hilfsmittel, persönlichen Mitteilungen und Quellen angefertigt habe.

I certify that the work presented here is, to the best of my knowledge and belief, original and the result of my own investigations, except as acknowledged, and has not been submitted, either in part or whole, for a degree at this or any other university.

Jena, 31.01.2014



---

Markus J. Barthel



## Publication P1 – P6

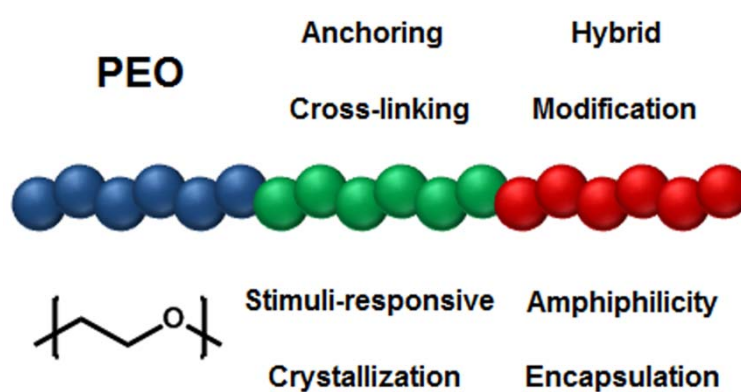
- P1:** *Polym. Chem.* **2014**, DOI: 10.1039/C3PY01666H. Reproduced by permission of The Royal Society of Chemistry.
- P2:** *Soft Matter* **2013**, *9*, 3509-3520. Reproduced by permission of The Royal Society of Chemistry.
- P3:** Manuscript submitted to *Adv. Funct. Mater.*
- P4:** *J. Polym. Sci., Part A: Polym. Chem.* **2012**, *50*, 4958-4965. Reproduced with permission. Copyright © 2012 Wiley Periodicals, Inc.
- P5:** *Adv. Funct. Mater.* **2013**, *23*, 4921-4932. Reproduced with permission. Copyright © 2013 WILEY-VCH Verlag GmbH & Co. KGaA, Weinheim.
- P6:** *Macromol. Rapid. Commun.* **2014**, DOI: 10.1002/marc201300875. Reproduced with permission. Copyright © 2014 WILEY-VCH Verlag GmbH & Co. KGaA, Weinheim.

## Publication P1

### Poly(ethylene oxide) (PEO)-based ABC triblock terpolymers – Synthetic complexity vs. application benefits

Markus J. Barthel, Felix H. Schacher, Ulrich S. Schubert

*Polym. Chem.* **2014**, DOI: 10.1039/C3PY01666H.





# Poly(ethylene oxide) (PEO)-based ABC triblock terpolymers – synthetic complexity vs. application benefits

Cite this: DOI: 10.1039/c3py01666h

Markus J. Barthel,<sup>abc</sup> Felix H. Schacher<sup>\*ab</sup> and Ulrich S. Schubert<sup>\*abc</sup>

Received 30th November 2013  
Accepted 7th January 2014

DOI: 10.1039/c3py01666h

[www.rsc.org/polymers](http://www.rsc.org/polymers)

During the last few decades considerable scientific effort has been devoted to the synthesis, self-assembly, and application of ABC triblock terpolymers with various building blocks. Such materials show high potential in the fields of materials science and life sciences. In particular, poly(ethylene oxide) (PEO) is a versatile building block and related materials featuring PEO segments are often exploited due to its solubility in a wide range of solvents, its non-toxicity, biocompatibility, and the so called "stealth effect". This review presents a short summary of possible synthetic routes for the synthesis of PEO-containing triblock terpolymers, as well as different applications in the bulk and in solution – including the preparation of porous materials, hybrid systems, and carriers for controlled drug delivery.

## 1. Introduction and state of the art

Nowadays, block copolymers are of broad interest regarding a variety of applications within the fields of materials science, nanotechnology, and life sciences. In general, a combination of monomers with different chemical and physical properties is used to prepare such materials, in most cases of AB (diblock copolymers) or ABA (triblock copolymers) type. Both the combination of different properties of the constituting building

<sup>a</sup>Laboratory of Organic and Macromolecular Chemistry (IOMC), Friedrich Schiller University Jena, Humboldtstr. 10, 07743 Jena, Germany. E-mail: [ulrich.schubert@uni-jena.de](mailto:ulrich.schubert@uni-jena.de); [felix.schacher@uni-jena.de](mailto:felix.schacher@uni-jena.de)

<sup>b</sup>Jena Center for Soft Matter (JCSM), Friedrich Schiller University Jena, Philosophenweg 7, 07743 Jena, Germany

<sup>c</sup>Dutch Polymer Institute (DPI), P.O. Box 902, 5600 AX Eindhoven, The Netherlands



Markus J. Barthel was born in 1985 in Zwickau (Germany) and studied chemistry at the Friedrich Schiller University Jena (Germany, 2005–2010). In 2010 he obtained his MSc degree in Chemistry. Since 2010 he has been performing his PhD studies in Jena under the supervision of Prof. Ulrich S. Schubert. His research focuses on the synthesis and application of functional polyether-based materials via living anionic ring-opening polymerization.



Felix H. Schacher was born in Lichtenfels, Germany, in 1980. After finishing his graduate studies in chemistry at the University of Bayreuth, Germany, in 2006, he completed his doctoral work under the supervision of Prof. Axel H. E. Müller in 2009. His thesis focused on living anionic polymerization techniques and functional nanostructured systems based on block co- and terpolymers in

the bulk and in solution. Afterwards, he joined the group of Prof. Ian Manners as a DAAD postdoctoral fellow, working on the synthesis and self-assembly of organometallic block copolymers. Since 2010, he has been a junior professor at the Friedrich Schiller University Jena, Germany. His research interests are polymer synthesis, self-assembly of polymer-based materials, and different characterization techniques related to block copolymer nanostructures.

blocks as well as the immiscibility of unlike polymer segments are exploited, leading to self-assembly in the bulk, in thin-films, and in solution.<sup>1–3</sup> If a hydrophilic block A and a hydrophobic block B are combined, amphiphilic block copolymers are obtained.<sup>4</sup> Commercially established examples of block copolymers are polystyrene-*block*-polybutadiene-*block*-polystyrene (SBS) rubbers and polystyrene-*block*-poly(methyl methacrylate) (PS-*b*-PMMA) thin-films in lithography strategies by *e.g.*, IBM to pattern integrated circuit elements on length scales which cannot be reached by classical approaches.<sup>5,6</sup>

One widely used building block in various application fields as a hydrophilic, non-toxic segment is poly(ethylene oxide) (PEO) or poly(ethylene glycol) (PEG), the nomenclature typically depends on the molar mass of the polymer. The most versatile technique for the synthesis of PEO materials with precisely controlled chain length, narrow dispersity, and different functional groups is living anionic ring-opening polymerization.<sup>7</sup> This is also the basis for pluronics, a class of commercially available ABA triblock copolymers of poly(ethylene oxide)-*block*-poly(propylene oxide)-*block*-poly(ethylene oxide) (PEO-*b*-PPO-*b*-PEO). These materials are mostly used as stabilizers for, *e.g.*, the synthesis of inorganic nanoparticles (Au and Ti).<sup>8</sup> The versatility of PEO and related materials can be explained by its outstanding physical and chemical properties. PEO is chemically inert, non-toxic, and thus a predestined candidate for biomedical applications.<sup>9</sup> PEO ensures good solubility in common organic solvents as well as water and, furthermore, is capable of preventing undesired interactions with the human immune system – the so called “stealth effect”.<sup>10</sup> Nevertheless, there is a growing interest in the incorporation of functional groups into PEO-related materials. This can be achieved *via* the preparation of block copolymers with segments containing functional monomers like butadiene, isoprene, vinylpyridine, or suitable glycidyl ethers featuring essentially the same poly-ether backbone. Traditionally used glycidyl ethers are allyl glycidyl ether (AGE, free double bond), ethoxy ethyl glycidyl ether (EEGE, protected hydroxyl groups), furfuryl glycidyl ether (FGE,

furan moieties), and *N,N'*-dibenzyl amino glycidol (DBAG, protected amines).<sup>11–14</sup>

In general, applications involving PEO-based block copolymers can be divided according to examples in the bulk or in solution. In both cases, mainly the phase separation of such systems is used to design nanostructured materials. Typically, applications in the bulk use PEO as a soft segment within block copolymer films of different composition, thickness, and morphology.<sup>15</sup> Further, PEO containing block copolymer films have been employed for the coating of surfaces, exploiting its anti-fouling properties to prevent uncontrolled adhesion and adsorption of proteins, cells, bacteria, and other microorganisms.<sup>16</sup>

In solution, PEO most often serves as the hydrophilic part of amphiphilic or double hydrophilic block copolymers. Regarding amphiphilic systems, classical examples contain PS, PI or PB as hydrophobic segments. In aqueous media, such materials undergo self-assembly into micellar structures where the hydrophobic block forms the core. Many recent examples then load these aggregates with hydrophobic compounds such as dyes or drugs (into the core). The PEO corona, on the other hand, provides solubility in aqueous media and, additionally, the stealth-effect attributed to PEO prevents undesired interactions with proteins and makes such particles attractive for potential biomedical applications.<sup>9</sup> One example is PEO-*b*-poly( $\epsilon$ -caprolactone) (PEO-*b*-PCL), where the PCL block forms a biodegradable core.<sup>17</sup> Also, the use of poly(ethylene oxide)-*block*-poly(allyl glycidyl ether) (PEO-*b*-PAGE) block copolymers in drug-delivery approaches has been reported by Hruby.<sup>18</sup> Here, micelles with a hydrophobic PAGE core and a PEO corona were formed in aqueous solution and the pendant double bonds within the PAGE side chain were used to covalently attach doxorubicin (anti-cancer drug) *via* a pH-labile linker. As the pH value in cells is distinctly lower than in the blood stream, the linker was cleaved upon cell uptake and the drug is released selectively at the desired site.

Despite this broad field of applications, it is of great interest to introduce further segments into block copolymers, *e.g.*, when dealing with ABC triblock terpolymers. This significantly increases the morphological variety as well as the range of functional groups or stimuli with which such materials can be addressed externally. In the last 15 years, a lot of scientific effort was invested to realize the synthesis of well-defined ABC triblock terpolymers although the first examples were already reported in the 1970s and 80s.<sup>19</sup> In these cases, the phase diagram of polystyrene-*block*-polybutadiene-*block*-poly(4-vinyl pyridine) (PS-*b*-PB-*b*-P4VP) or polystyrene-*block*-polyisoprene-*block*-poly(4-vinyl pyridine) (PS-*b*-PI-*b*-P4VP) was intensively studied.<sup>20</sup> However, this field intensified during the early 1990s, *e.g.*, through pioneering work on polystyrene-*block*-polybutadiene-*block*-poly(methyl methacrylate) (PS-*b*-PB-*b*-PMMA) by Stadler and coworkers.<sup>21–24</sup> The first examples of ABC triblock terpolymers containing a PEO segment were reported by Huang *et al.* in the late 1990s for poly(ethylene oxide)-*block*-polystyrene-*block*-poly(methyl methacrylate) (PEO-*b*-PS-*b*-PMMA) or (PS-*b*-PEO-*b*-PMMA) systems.<sup>25,26</sup> The use of PEO within ternary systems can significantly broaden the range of possible



*Prof. Ulrich S. Schubert studied chemistry at the Universities of Frankfurt and Bayreuth (both in Germany) and the Virginia Commonwealth University, Richmond (USA). His PhD thesis was executed at the University of Bayreuth and the University of South Florida/Tampa. After postdoctoral training with Professor Lehn at the Université Strasbourg (France) he moved to the Technische Universität*

*München (Germany) to obtain his Habilitation in 1999, followed by a temporal position as professor at the Center for Nanoscience, Universität München (Germany). From 2000 to 2007 he was a Full-Professor at the Eindhoven University of Technology. Currently he holds a chair at the Friedrich Schiller University Jena.*

applications and lead to fascinating materials. To be more specific, the following benefits can be identified:

- (1) Introduction of a crystallizable segment and, therefore, an additional driving force to improve control over and the variety of volume morphologies;
- (2) The possibility to tune block interactions, as well as the formation of organic–inorganic hybrid structures;
- (3) Control over cell-adhesion onto nanostructured block copolymer coatings;
- (4) Morphology control of solution structures;
- (5) Formation and solubility of stimuli-responsive nanostructured materials (pH, temperature, light); and
- (6) Versatile materials for drug-delivery approaches.

Within the course of this review, we focus on linear ABC triblock terpolymers containing PEO segments. In the following paragraphs we want to summarize recent developments in the fields of synthesis and application of such materials.

## 2. Synthetic strategies for the synthesis of PEO-based triblock terpolymers

We will only shortly discuss recent achievements concerning the synthesis of ABC triblock terpolymers as this topic is well-described in the literature.<sup>27</sup> One general and important requirement is a defined block sequence and a narrow polydispersity index, usually provided by living or controlled polymerization techniques. Despite the sequential polymerization of monomers also post-polymerization modification reactions such as click chemistry can be used to engineer ABC sequences.<sup>28</sup>

In the case of ethylene oxide, living anionic ring-opening polymerization (AROP) is typically the method of choice regarding control over molar masses and very narrow molar mass distributions. Using sequential monomer addition of glycidyl ethers, polyether-based ABC triblock terpolymers can be synthesized. A schematic representation of possible synthetic routes for the synthesis of ABC triblock terpolymers is depicted in Scheme 1. One example is poly(ethylene oxide)-*block*-poly(allyl glycidyl ether)-*block*-poly(*t*-butyl glycidyl ether) (PEO-*b*-PAGE-*b*-P(*t*-BGE)).<sup>29,30</sup> For the polymerization of glycidyl ethers, sometimes also the molar mass which can be achieved is limited or upon reaching a critical chain length more side reactions are observed. This can in parts be improved by using special initiator systems, solvent mixtures or suitable additives – one example being tetraoctylammonium bromide as initiator and triisobutylaluminum as activator for the preparation of high molar mass P(*t*-BGE).<sup>31</sup> Nevertheless, often combinations of different polymerization techniques have to be used. In the case of polystyrene-*block*-poly(ethylene oxide)-*block*-poly( $\epsilon$ -caprolactone) (PS-*b*-PEO-*b*-PCL), living anionic polymerization of polystyrene is carried out, followed by termination with ethylene oxide and subsequent AROP using a different counterion. The terminal OH functionality at the chain end can then be used for the Sn(Oct)<sub>2</sub> catalyzed ring-opening polymerization of  $\epsilon$ -caprolactone.<sup>32,33</sup> It is also possible to transform the OH

end-group of PEO with, *e.g.*, 2-bromoisobutryl bromide to obtain a macroinitiator for atom transfer radical polymerization (ATRP).<sup>34</sup> This has already enabled the synthesis of poly(ethylene oxide)-*block*-poly(2-hydroxyethyl methacrylate)-*block*-poly(*tert*-butyl acrylate) (PEO-*b*-PHEMA-*b*-PtBA) triblock terpolymers.<sup>35</sup> As an alternative, also a functional initiator can be used for the synthesis of the PEO block and used as a macroinitiator for, *e.g.*, single-electron transfer living radical polymerization (SET-LRP) afterwards.<sup>36</sup> Also, the functionalization of PEO with an alkyne moiety for the use in copper mediated 1,3-cycloaddition reactions with an azide functionalized PtBA counterpart has been demonstrated.<sup>37</sup> In addition, supramolecular approaches have been reported as well. [4 + 2] cycloadditions (Diels–Alder reactions) can be used, *e.g.*, to form ABC triblock terpolymers (Scheme 2).<sup>38,39</sup> Another possibility is the functionalization of the chain ends with metal complexing ligands and, if terpyridine units are used, block formation *via* the addition of Ru<sup>2+</sup> ions.<sup>40</sup>

Nevertheless, the presence of three distinct segments during the polymerization (at least of the third block) often poses great challenges regarding the choice of solvent or the overall polymerization conditions.

## 3. Applications in the bulk

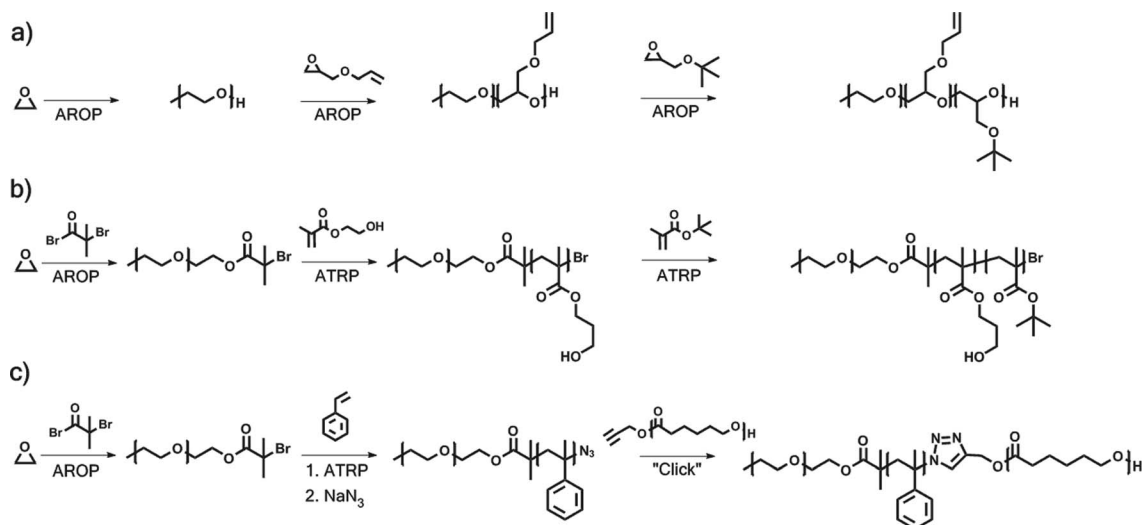
Bulk applications of block copolymers often involve patterning processes, their utilization as structure directing agents, or creating structured surfaces with tunable hydrophobicity/hydrophilicity. In comparison to the intensely studied AB systems, the introduction of a third block here allows further fine tuning of the parameters, incorporating functional groups, or an additional response to external stimuli. In the following paragraph we want to provide a brief overview of systems reported in the field featuring PEO segments.

### 3.1. Tuneable material properties

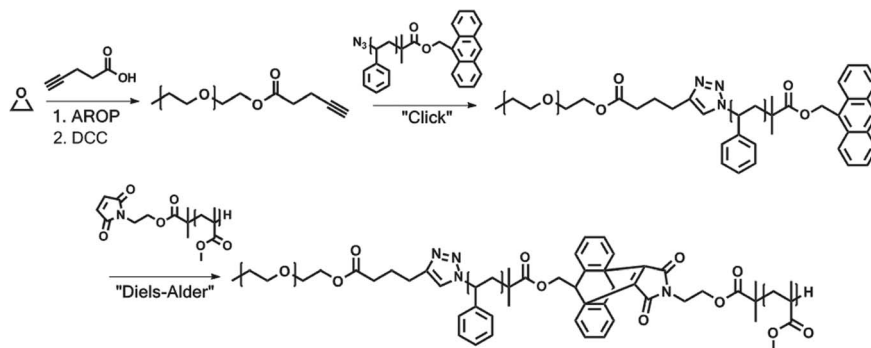
The introduction of a third block opens up a wide range of accessible bulk morphologies. As an example, polystyrene-*block*-polyisoprene-*block*-poly(ethylene oxide) (PS-*b*-PI-*b*-PEO) triblock terpolymer films show, depending on the used volume fractions, the formation of lamellae, gyroids, core–shell cylinders, and 3-domain lamellae.<sup>41</sup> This process can also be controlled by variation of the block sequence, *e.g.*, from PS-*b*-PI-*b*-PEO to PI-*b*-PS-*b*-PEO. The resulting film morphologies could also be influenced by the incorporation of inorganic compounds such as lithium perchlorate<sup>42</sup> or by varying the polydispersity index (PDI) of the PEO segment.<sup>43</sup>

### 3.2. Crystallization of triblock terpolymers

Besides polymer–polymer de-mixing due to the immiscibility of unlike segments, the crystallization of suitable building blocks represents an additional unique driving force. One example for triblock terpolymers containing two crystallizable segments is polyethylene-*block*-poly(ethylene propylene)-*block*-poly(ethylene oxide) (PE-*b*-PEP-*b*-PEO) which can be synthesized by the catalytic hydrogenation of a polybutadiene-*block*-polyisoprene-*block*-



**Scheme 1** Schematic representation of possible synthesis pathways for ABC triblock terpolymers: synthesis of PEO-*b*-PAGE-*b*-PtBGE via sequential AROP (a, [ref. 30]), synthesis of PEO-*b*-PHEMA-*b*-PtBA via a combination of AROP and ATRP (b, [ref. 35]) and synthesis of PEO-*b*-PS-*b*-PCL via a combination of AROP, ATRP and click-chemistry (c, [ref. 34]).



**Scheme 2** Schematic representation of a possible synthesis pathway for the synthesis of PEO-*b*-PS-*b*-PMMA via a combination of AROP, click chemistry and Diels-Alder chemistry [ref. 38].

poly(ethylene oxide) (PB-*b*-PI-*b*-PEO) precursor. The precursor itself was synthesized by sequential living anionic polymerization and the crystallization of both the PE and the PEO block was studied depending on the formed PEO microdomains (spherical or cylindrical). Selected examples are shown in Fig. 1.<sup>44–46</sup> Another example is polyethylene-*block*-polystyrene-*block*-poly(ethylene oxide) (PE-*b*-PS-*b*-PEO) obtained via hydrogenation of polybutadiene-*block*-polystyrene-*block*-poly(ethylene oxide) (PB-*b*-PS-*b*-PEO).<sup>47</sup> Here a triblock terpolymer containing two crystallizable segments (PB and PEO) and a glassy middle block (PS) revealed a templating effect of the PEO segment on the microdomain formation as the morphologies are determined by the crystallization of the PE segment and the segregation of PEO. Moreover, the synthesis of materials with three potentially crystallizable blocks yielded polyethylene-*block*-poly(ethylene oxide)-*block*-poly( $\epsilon$ -caprolactone) (PE-*b*-PEO-*b*-PCL).<sup>48</sup> The preparation of polymer single crystals can be achieved by the selective crystallization of the PEO middle block in polystyrene-*block*-poly(ethylene oxide)-*block*-poly(1-butene oxide) (PS-*b*-PEO-*b*-PBO)

or polystyrene-*block*-poly(ethylene oxide)-*block*-poly(dimethyl siloxane) (PS-*b*-PEO-*b*-PDMS). The microphase separation of the outer A and C blocks leads to unbalanced surface stress and the formation of large scrolled single crystals.<sup>49</sup>

### 3.3. Structural control: synthesis of porous systems and patterning

In addition to the superior control and the variety of morphologies accessible in films, the use of ABC triblock terpolymers as templates for inorganic materials is highly interesting. In that way, the controlled synthesis of porous systems is possible as shown for polyethylene-*block*-poly(ethylene oxide)-*block*-poly( $\epsilon$ -caprolactone) (PE-*b*-PEO-*b*-PCL) as a structure directing agent for the formation of mesoporous silica via sol-gel processes. The triblock terpolymer and tetraethyl orthosilicate as a silica precursor were dissolved in THF. Due to subsequent evaporation induced self-assembly (EISA), mesoporous silica is formed. The PE block hereby leads to the formation of spherical pores



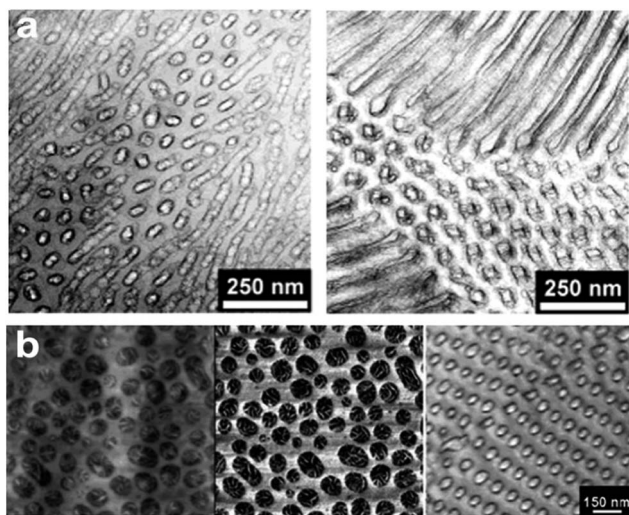


Fig. 1 TEM micrographs of a PE-*b*-PEP-*b*-PEO triblock terpolymer film containing two crystallizable blocks revealing cylindrical structures of the crystallized PEO segment (a, reprinted with permission from ref. 44, Copyright © 2002 American Chemical Society); AFM image (left and middle image) and TEM micrograph (right image) of a PE-*b*-PS-*b*-PEO film showing spherical domains filled with crystalline PEO lamellae (b, reprinted with permission from ref. 46, Copyright © 2007 American Chemical Society). New scale bars have been added to the figures.

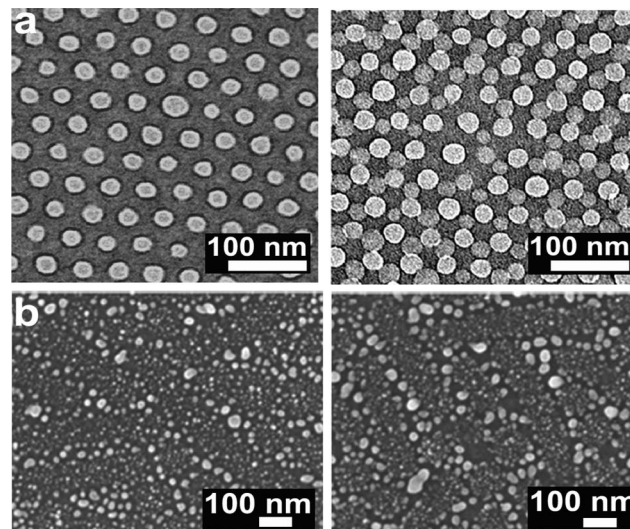


Fig. 2 Bright field TEM plan-view images of PEO-*b*-PMMA-*b*-PS thin films after solvent annealing, UV degradation, and acid washing. Variation of the film thickness (43 nm for the left image, 73 nm for the right image) leads to the formation of porous systems with different structures (a, reprinted with permission from ref. 54, Copyright © 2006 American Chemical Society); SEM images of Au/Ag nanostructures with an Au core and Ag shell on SiO<sub>x</sub>-capped silicon wafer shards after removal of the triblock terpolymer template (b, reprinted with permission from ref. 57, Copyright © 2006 American Chemical Society). New scale bars have been added to the figures.

with pore sizes of about 5 nm, the PCL block forms tetragonal cylindrical pores with sizes from 5 to 16 nm (depending on the block length) after calcination.<sup>50</sup> In another approach, embedding of poly(ethylene oxide)-*block*-poly( $\epsilon$ -caprolactone)-*block*-polystyrene (PEO-*b*-PCL-*b*-PS) within an epoxy resin led to spherical phases with diameters of 20 to 30 nm or lamellar morphologies with domain sizes of 40 nm. The morphologies could further be influenced by using different hardeners.<sup>51</sup> Highly regular, porous structures were also obtained by the self-assembly of poly(ethylene oxide)-*block*-poly(methyl methacrylate)-*block*-polystyrene (PEO-*b*-PMMA-*b*-PS) and subsequent photodegradation of the PMMA segments. In this case the pore sizes could be varied from 23 to 59 nm depending on the block length of the PS and the PMMA segment. The benefit of this approach is that the high lateral ordering as often observed for PS-*b*-PEO block copolymers and the good photodegradation of the PMMA part can be combined. An example for a porous system obtained by this triblock terpolymer is shown in Fig. 2a. Moreover, the frequently reported lack of long-range ordering for PS-*b*-PMMA samples can be avoided.<sup>52</sup> One additional trigger regarding film applications of PEO-containing materials is its inherent sensitivity to moisture. This allows tuning of the morphology simply by a selective swelling of the PEO phase.<sup>53,54</sup> Such triblock terpolymers can be also used for the synthesis of mesoporous carbons (pore size up to 55 nm) with a good long-range order.<sup>55</sup>

Another approach for the fabrication of porous systems is the formation of poly(ethylene oxide)-*block*-polystyrene-*block*-poly(divinyl benzene-*co*-styrene) (PEO-*b*-PS-*b*-P(DVB/S)) micelles, followed by subsequent crosslinking of the micellar core and embedding in an epoxy resin. The formed spherical

nanodomains can be selectively etched by THF treatment and materials with narrowly dispersed pores (pore sizes from 29 to 32 nm) are formed.<sup>56</sup>

If materials are used which contain at least one segment featuring nitrogen atoms, specific interactions with metal ions can be exploited. This phenomenon can be used for the patterning of, *e.g.*, Au or Ag on nanostructured block copolymer films. One example is the specific location of Au<sup>III</sup> and Ag<sup>I</sup> within polystyrene-*block*-poly(2-vinyl pyridine)-*block*-poly(ethylene oxide) (PS-*b*-P2VP-*b*-PEO) films as depicted in Fig. 2b. The Au particles are specifically located within the P2VP domains whereas Ag can be found in the PEO phase.<sup>57</sup> Also here, the obtained morphologies after film preparation *via* spin-coating can be tuned by different parameters, including the crystallization of the PEO domain, different solvents being used, the underlying substrate, concentration, and the casting speed.<sup>58</sup> Another application of PS-*b*-P2VP-*b*-PEO films with a lamellar morphology is as templates for tethered diblock copolymer chains. Traces of water in the solvent have a drastic influence on the final microstructure due to interactions with the hydrophilic PEO block. The triblock terpolymer forms micellar structures in toluene during the early stage. Due to hydrogen bonding occurring between the water molecules and the PEO segments the micellar structures change into lamellar platelets.<sup>59</sup> Furthermore, this particular system can be used in blends with poly(vinylidene fluoride)-*ter*-poly(hexafluoropropylene)-*ter*-poly(trifluoromethacrylic acid) P(VDF-*ter*-HFP-*ter*-TFMA) terpolymers to form multicompart ment micelles in DMF.<sup>60</sup> The blending leads to the formation of a

micellar core with P(VDF-*ter*-HFP) segments and TFMA/2VP complexes. The PS and PEO block form the corona. Depending on the VDF content separated nanodomains within the core could be visualized.

### 3.4. Controlled cell-adhesion and binding

In addition to templating approaches, PEO containing triblock terpolymers can be used in the bulk for biomedical applications. It is known that PEO exhibits antifouling properties and, therefore, inhibits non-desired cell attachment on surfaces. In contrast, poly(L-lysine) (PLL) increases and favors cell adhesion. The combination of both materials now allows for a selective adjustment of cell adhesion. In that way, poly(ethylene oxide)-*block*-poly(L-lactide)-*block*-poly(L-lysine) (PEO-*b*-PLLA-*b*-PLL) triblock terpolymers were able to adjust the cell affinity of different surface coatings.<sup>61</sup> Moreover, the incorporation of functionalized PEO segments enabled the modification with fluorinated compounds to further decrease the tendency for cell adhesion. As a consequence, highly effective anti-fouling coatings could be obtained.<sup>62</sup>

## 4. Application in solution

### 4.1. Morphology control

Apart from applications in the bulk, the use of block copolymers in solution represents a highly interesting research area with various possibilities. Typically, each segment within ABC triblock terpolymers represents a specific function or functionality. One segment (block A, exemplarily) ensures the solubility of the material. In aqueous environments often PEO segments are used for this task due to their broad solubility range and chemical stability. Furthermore, polyoxazolines or poly(*n*-isopropylacrylamide)s can be used as well.<sup>9,63,64</sup> Another segment (B, exemplarily) carries functional groups and allows for post-polymerization functionalizations (*e.g.*, due to a free double bond) or can be addressed by physical stimuli (*e.g.*, changes of the pH value or temperature). The third block (*e.g.*, C) is often hydrophobic (or, more generally, solvophobic) and ensures that such particular materials undergo self-assembly within selective solvents.<sup>65</sup> As already shown for the bulk state, also in solution different morphologies can be observed, typically including spherical micelles, worm-like structures, and vesicles.<sup>1</sup> Additionally, more complex architectures such as multilamellar vesicles, cylinder containing vesicles, or entrapped vesicles have been reported by variation of the hydrophilic/hydrophobic balance of, *e.g.*, poly(ethylene oxide)-*block*-polystyrene-*block*-poly( $\epsilon$ -caprolactone) (PEO-*b*-PS-*b*-PCL).<sup>66</sup> Further set screws to be exploited are monomer variations or the block sequence. It could be shown that polystyrene-*block*-poly(ethylene oxide)-*block*-poly(acrylic acid) (PS-*b*-PEO-*b*-PAA) has a higher critical water content (CWC) and forms large vesicles in selective solvents in comparison to poly(ethylene oxide)-*block*-polystyrene-*block*-poly(acrylic acid) (PEO-*b*-PS-*b*-PAA).<sup>67</sup> Furthermore, the preparation pathway (direct dissolution, dialysis, or the use of additional surfactants) has a significant influence.<sup>68-70</sup> One example for the use of surfactants are

poly(ethylene oxide)-*block*-poly(sodium 2-acrylamido-2-methylpropanesulfonate)-*block*-poly(methacrylic acid) (PEO-*b*-PMAPS-*b*-PMAA) micelles after addition of cetyltrimethylammonium chloride.<sup>71</sup>

Apart from covalently bound triblock terpolymers, also metal-ligand interactions can be used for the incorporation of additional segments. This has been shown for polystyrene-*block*-poly(*p*-trifluoromethylstyrene)-[Ru]-poly(ethylene oxide) PS-*b*-PTFMS-[Ru]-PEO. Here, changes in the solubility of the PTFMS block in different alcohols allowed for directing the self-assembly process.<sup>40</sup> In a similar approach the PTFMS segment is replaced by poly(2-vinyl pyridine) resulting in polystyrene-*block*-poly(2-vinyl pyridine)-[Ru]-poly(ethylene oxide) (PS-*b*-P2VP-[Ru]-PEO) where the P2VP segments induce pH responsive behavior.<sup>72</sup> For this approach also iron can be applied as shown for polystyrene-*block*-poly(*tert*-butyl acrylate)-[Fe]-poly(ethylene oxide) (PS-*b*-PtBA-[Fe]-PEO). This material forms large micellar structures in ethanol and after changing the solvent to water a decrease in size of the micelles could be detected.<sup>73</sup>

In the following paragraphs, we will point out the benefits obtained by the introduction of a third block regarding solution behavior, accessing individual domains, stimuli-response, or towards specific applications.

### 4.2. Crosslinkable nanostructures in solution

Controlled crosslinking of individual domains in block copolymer nanostructures in solution is a straightforward approach towards increasing their stability or the range of solvents that can be used. Covalent crosslinking is widely used also for AB diblock copolymer micelles.<sup>74</sup> In this case either the core or the shell can be addressed and the introduction of a third block enables, *e.g.*, equipping such structures with an additional responsive segment.

Triblock terpolymers, *e.g.* poly(ethylene oxide)-*block*-poly([(n,n-dimethylacrylamide)-*stat*-(N-acryloxysuccinimide)]-*block*-poly(*n*-isopropylacrylamide) (PEO-*b*-(DMA-*s*-NAS)-*b*-NIPAM) or poly(ethylene oxide)-*block*-poly(*n*-3-aminopropyl methacrylamide)-*block*-poly(2-(diisopropylamino) ethyl methacrylate) (PEO-*b*-PAPMA-*b*-PDPAEMA), form micellar structures with a crosslinkable shell – the latter can be selectively crosslinked by the addition of a suitable diamine in the case of *N*-acryloxysuccinimide units or polymeric NHS linker for the PAPMA shell. The crosslinking leads to stabilized particles showing a swelling/shrinking after addressing the micellar core by changing the pH value for (PEO-*b*-PAPMA-*b*-PDPAEMA) or heating above the LCST for (PEO-*b*-(DMA-*s*-NAS)-*b*-NIPAM).<sup>75,76</sup> Also the PAEMA shell of poly(ethylene oxide)-*block*-poly(2-aminoethyl methacrylate hydrochloride)-*block*-poly(heptadeca-fluorodecyl acrylate) (PEO-*b*-PAEMA-*b*-PHFDA) micelles can be crosslinked by glutaraldehyde to form stable liquid-filled structures.<sup>77</sup> This principle can be also used in drug-delivery approaches which will be discussed later on.

### 4.3. Stimuli responsive materials

**4.3.1. pH value.** There is still a growing interest in polymeric materials and micellar structures which are capable of

undergoing distinct changes in size, shape, or solubility upon exposure to external triggers. One very elegant way, of course, is the introduction of a stimuli-sensitive block within binary or ternary block copolymer materials. In the latter case (ABC systems), solubility can be maintained even upon collapse of one segment (*e.g.*, with A being the corona and C being the core-forming block) whereas solubility changes in AB-based nanostructures often lead to aggregation, sometimes unwanted and, even worse, irreversible. One possibility for an external trigger is the change of the pH value of the surrounding medium (typically water). For example, a pH-sensitive triblock terpolymer, poly(ethylene oxide)-*block*-poly(acrylic acid)-*block*-polystyrene (PEO-*b*-PAA-*b*-PS) forms micellar structures consisting of a PS core, a PAA shell and a PEO corona. While changing the pH value, the PAA shell can be (de)protonated and, therefore, electrostatical interactions can be induced. These forces lead to stretching or shrinkage of the PAA shell.<sup>78</sup>

Another interesting example is poly(ethylene oxide)-*block*-poly(2-(diethylamino)ethyl methacrylate)-*block*-poly(succinic ester methacrylate) (PEO-*b*-PDEA-*b*-PSEMA), forming zwitterionic micellar structures in aqueous solution. By adjusting the pH value and, therefore, the charge density within both the PDEA and the PSEMA block, the composition of the resulting micelles can be adjusted as shown in Fig. 3a.<sup>79</sup> This process can be observed also for a poly(ethylene oxide)-*block*-polystyrene-*block*-poly(2-(diethylamino)ethyl methacrylate) (PEO-*b*-PS-*b*-PDEA) triblock terpolymer dissolved in aqueous solution at pH 10.4. As depicted in Fig. 4b a decrease of the pH value leads to a swelling of the vesicle due to protonation of the PDEA layer. As the process is reversible a kind of “breathing vesicles” are obtained.<sup>80</sup> In a similar approach, poly(ethylene oxide)-*block*-poly(glycidyl methacrylate)-*block*-poly(2-(diethylamino)ethyl methacrylate) (PEO-*b*-PGMA-*b*-PDEA) forms micellar structures with a PDEA core, a PGMA shell which can be additionally crosslinked by divinyl sulfone, and a PEO corona. The pH-sensitive PDEA core shows swelling/deswelling upon changes in the pH value. One possible application of such structures is as nanoreactors for the synthesis of gold nanoparticles.<sup>81,82</sup> This swelling/deswelling process can also be observed for poly(ethylene oxide)-*block*-poly(glycidyl methacrylate)-*block*-poly(2-(diisopropylamino)ethyl methacrylate) (PEO-*b*-PGMA-*b*-PDPA).<sup>83</sup>

In addition to the ability of poly(vinyl pyridine)s to interact with metal ions, this class of materials can also be used in pH-responsive structures as shown by Pispas and Hadjichristidis for P2VP.<sup>84</sup> Here, the micellar size of polyisoprene-*block*-poly(2-vinyl pyridine)-*block*-poly(ethylene oxide) (PI-*b*-P2VP-*b*-PEO) consisting of a PI core, a P2VP shell and a PEO corona can be varied. Decreasing the pH value from neutral to acidic conditions leads to a protonation of the P2VP shell and the electrostatic repulsion of the positive charges causes an increase in the particle size. Also PLGA can be introduced as a pH-sensitive (degradable) segment: one class of examples are poly(ethylene oxide)-*block*-poly(L-lactide)-*block*-poly(lactic-co-glycolic acid) (PEO-*b*-PLLA-*b*-PLGA) triblock terpolymers.<sup>85</sup>

Another strategy involves pH-labile crosslinkers, as shown for poly(ethylene oxide)-*block*-poly(*N*-acryloxysuccinimide)-*block*-polystyrene (PEO-*b*-PNAS-*b*-PS). Here, the triblock terpolymer

forms multicompartiment micelles in aqueous solution which can be crosslinked depending on the pH value by the reaction of the *N*-acryloxysuccinimide block with a pyrazine-based diamino crosslinker.<sup>86</sup>

**4.3.2. Temperature.** Another frequently employed external stimulus is the temperature. Hereby, the “workhorses” are materials featuring a lower critical solution temperature (LCST) with poly(*n*-isopropylacrylamide) (PNIPAm) being most prominent. Similar as in the case of pH-responsive systems, triggering the LCST in amphiphilic AB-based micellar structures often leads to agglomeration or even precipitation. The use of ABC triblock terpolymers enables studying structural changes within single particles. An interesting influence can be observed for poly(ethylene-*alt*-propylen)-*block*-poly(ethylene oxide)-*block*-poly(*n*-isopropylacrylamide) (PEP-*b*-PEO-*b*-PNIPAm) materials, which form flower-like micellar structures in aqueous solution upon heating above the LCST of the PNIPAm block (Fig. 3b). Upon further heating these micellar structures associate to form larger aggregated structures.<sup>87</sup> The temperature response can also be implemented into organic-inorganic hybrid systems such as poly(ethylene oxide)-*block*-poly(methacrylisobutyl polyhedral oligomeric silsesquioxane)-*block*-poly(*n*-isopropylacrylamide) PEO-*b*-P(MA-POSS)-*b*-PNIPAm.<sup>88</sup> Also micelles of poly(ethylene oxide)-*block*-poly(*n*-isopropylacrylamide)-*block*-polystyrene PEO-*b*-PNIPAm-*b*-PS show thermo-responsive behavior due to swelling or shrinking of the PNIPAm segment.<sup>89</sup> A detailed study of the self-assembly behavior of thermo-responsive bis-hydrophilic triblock terpolymers was carried out for poly(ethylene oxide)-*block*-poly(*n*-butyl acrylate)-*block*-poly(*n*-isopropylacrylamide) (PEO-*b*-PnBuA-*b*-PNIPAm) – these materials showed a wide range of morphologies, including spherical micelles, multicompartiment structures, and partial “Janus” micelles (Fig. 4a).<sup>90</sup>

**4.3.3. Light.** Another interesting approach is the introduction of photoactive blocks into block copolymer nanostructures. Hereby, micelles formed from poly(ethylene oxide)-*b*-polystyrene-*b*-poly(poly[6-(4-methoxy-azobenzene-4'-oxy) hexyl methacrylate]) (PEO-*b*-PS-*b*-PMMAZO), containing an azo-functionalized PMMA block, show a distinct deformation after UV irradiation due to the switching in between the *cis/trans* conformation of the azo moiety.<sup>91</sup> As for poly(ethylene oxide)-(*o*-nitrobenzene)-poly(2-(perfluorooctyl)ethyl methacrylate)-*block*-poly(2-cinnamoloxyethyl methacrylate) (PEO-ONB-PFOEMA-*b*-PCEMA), a photocleavable unit (*o*-nitrobenzene) has been introduced in between blocks A and B and, additionally, a photo-crosslinkable block (PCEMA) is present. Therefore, a dual light responsive triblock terpolymer can be obtained (Fig. 4c).<sup>92</sup> Furthermore, the overall hydrophilic/hydrophobic balance of a system can be controlled by using UV active building blocks. As shown in Fig. 3c, hydrophobic pyrene units can be cleaved off by irradiation from the poly(pyrenylmethyl methacrylate) (PPy) block of poly(pyrenylmethyl methacrylate)-*block*-polystyrene-*block*-poly(ethylene oxide) (PPy-*b*-PS-*b*-PEO), resulting in a significant change in solubility and the disassembly of priorly formed micelles. This process can be used to release encapsulated substances. In the depicted example the hydrophobic dye Nile red is released due to the disassembly of the nanostructures.<sup>93</sup> UV



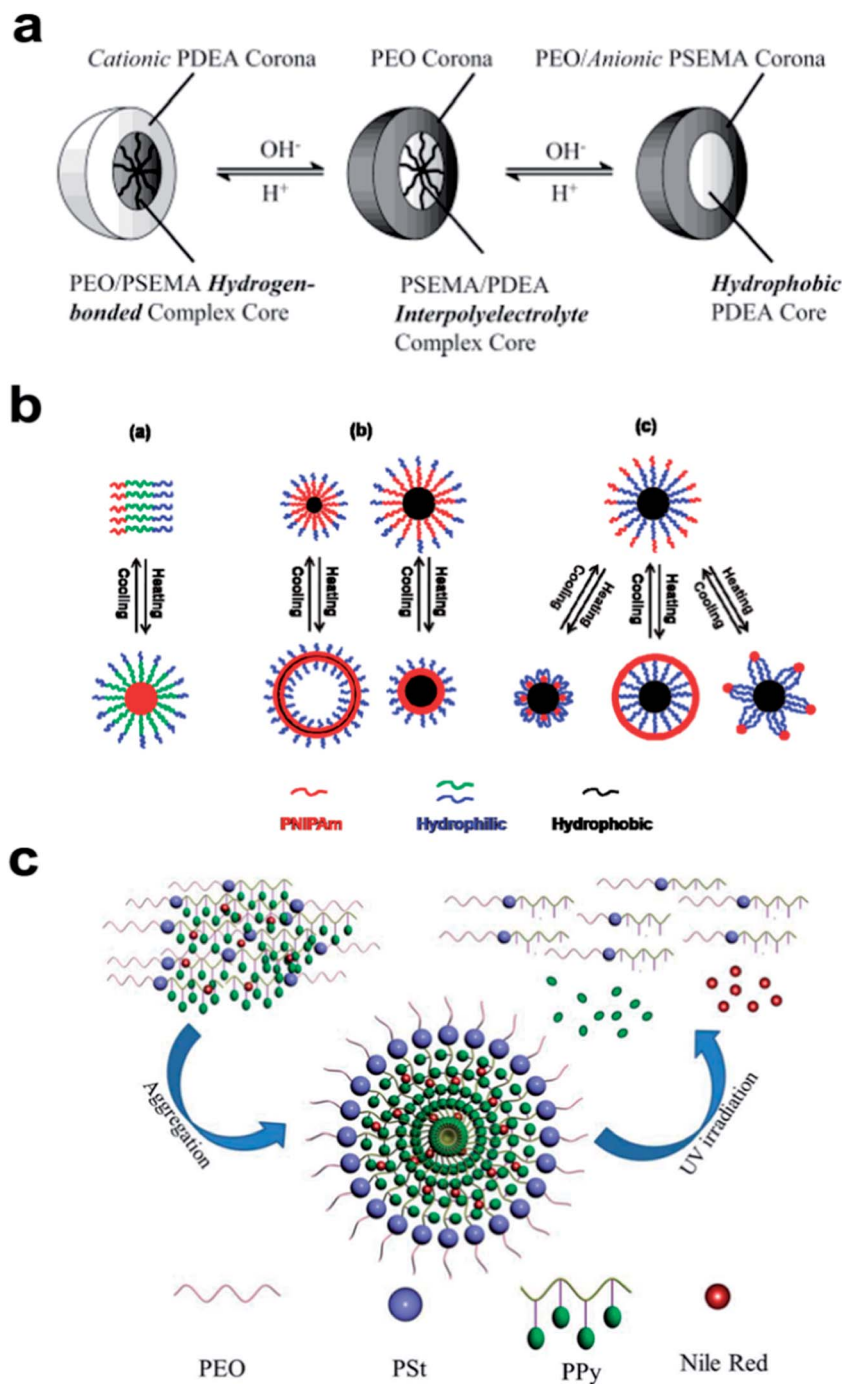


Fig. 3 Schematic representation of the stimuli response of triblock terpolymers in solution: micellar aggregates formed by the zwitterionic triblock terpolymer PEO-*b*-PDEA-*b*-PSEMA in aqueous solution by adjusting the solution pH (a, reprinted with permission from ref. 79, Copyright © 2004 American Chemical Society); temperature-induced structural changes of PNIPAm-containing triblock terpolymer micelles (b, reprinted with permission from ref. 87, Copyright © 2011 American Chemical Society); encapsulation of Nile Red within the hydrophobic core of aggregates and its release upon disruption of the structures by UV light (c, reprinted with permission from ref. 93, Copyright © 2011 Wiley Periodicals, Inc.).

irradiation can be also used for the crosslinking of the shell of poly(ethylene oxide)-*block*-poly(glycerol monomethacrylate)-*block*-poly(2-(diethylamino)ethyl methacrylate) (PEO-*b*-(PCGMA-co-PGMA)-*b*-PDEA) micelles. Furthermore, the structures are pH-responsive due to the PDEA core.<sup>94</sup> Related to this approach are poly(ethylene oxide)-*block*-poly(2-cinnamoyloxyethyl methacrylate)-*block*-poly(methyl methacrylate) (PEO-*b*-PCEMA-*b*-PMMA)

materials, synthesized by the post-polymerization functionalization of poly(ethylene oxide)-*block*-poly(2-hydroxyethyl methacrylate)-*block*-poly(methyl methacrylate) PEO-*b*-PHEMA-*b*-PMMA using cinnamoyl chloride. The resulting material was used to encapsulate gold nanoparticles or pyrene and the PCEMA was crosslinked by UV-irradiation and, therefore, stabilized.<sup>95</sup>



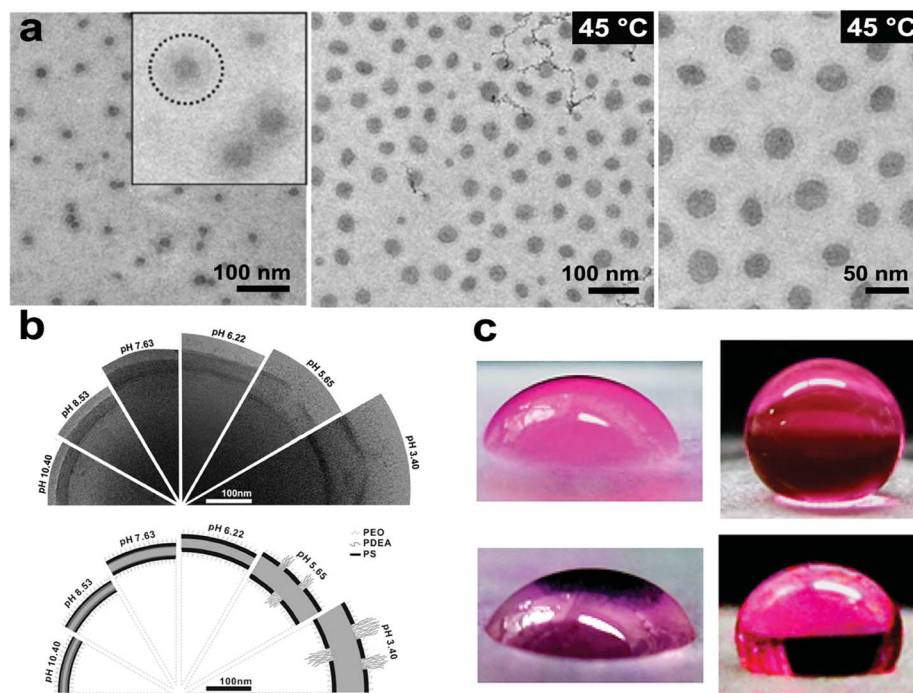


Fig. 4 Applications of stimuli-responsive triblock terpolymers: cryo-TEM images of self-assembled structures of PEO-*b*-PnBuA-*b*-PNIPAm triblock terpolymers before and after heating (a, reprinted with permission from ref. 90, Copyright © 2010 American Chemical Society); representation of a PEO-*b*-PS-*b*-PDEA "breathing" vesicle at different pH values (b, reprinted with permission from ref. 80, Copyright © 2009 American Chemical Society); photographs of H<sub>2</sub>O droplets on films of photoactive and photolyzed micelles (c, reprinted with permission from ref. 92, Copyright © 2012 American Chemical Society). New scale bars have been added to Fig. 4a.

**4.3.4. Dual responsive materials.** One further outstanding advantage of triblock terpolymers is the possibility to introduce multiple stimuli. For example, the P2VP block of poly(2-vinyl pyridine)-*block*-poly(ethylene oxide)-*block*-poly(oligo(ethylene glycol) methyl ether methacrylate) (P2VP-*b*-PEO-*b*-POEGMA) is pH-responsive, whereas the POEGMA block can be thermally addressed by heating above the cloud point temperature.<sup>96</sup> Another example for a dual-responsive material is poly(ethylene oxide)-*block*-poly(*n*-butyl methacrylate)-*block*-poly(dimethylaminoethyl methacrylate) (PEO-*b*-PnBMA-*b*-PDMAEMA), which forms spherical micelles under acidic conditions and cylindrical structures at high pH values. Furthermore, the re-assembly from a cylinder to a toroid or a vesicle can be tuned by variations in temperature and the pH value.<sup>97</sup> *Via* the combination of different monomers within one block also multi-stimuli sensitive examples can be created, as shown for poly(ethylene-*alt*-propylene)-*block*-poly(ethylene oxide)-*block*-poly(*n*-isopropylacrylamide-*co*-acrylic acid) (PEP-*b*-PEO-*b*-P(NIPAm-*co*-AA)). This material forms micellar structures in aqueous solution which simultaneously respond to changes in temperature and/or the pH value.<sup>98</sup>

#### 4.4. Smart hydrogels

The herein shown stimuli responsive building blocks can also be used for the formation of hydrogels with controlled architecture and internal fine structure. Thereby, it is possible to adjust the structures of the resulting hydrogel by varying the block sequences of terpolymers consisting of polybutadiene,

poly(ethylene oxide), and poly(perfluoropropylene oxide).<sup>99</sup> Also the formation of "smart" hydrogels using poly(2-vinyl pyridine)-*block*-poly(ethylene oxide)-*block*-poly(glycidyl methyl ether-*co*-ethyl glycidyl ether) (P2VP-*b*-PEO-*b*-P(GME-*co*-EGE)) is possible.<sup>100</sup> For this compound a flow-induced ordering into cubic gels has been observed.<sup>101</sup> Furthermore, a magneto-responsive hydrogel of this material could be obtained by encapsulation of superparamagnetic maghemite into the P2VP domains. Subsequent heating above the LCST of the GME/EGE led to the formation of a hydrogel and the magnetic character enabled discrete heating by applying magnetic fields.<sup>102</sup>

#### 4.5. Drug-delivery systems

In particular in the field of drug-delivery approaches often AB diblock copolymers are used as efficient drug carriers.<sup>103</sup> Nevertheless, the introduction of an additional segment can be beneficial regarding the efficiency, addressability, or applicability of such materials. In addition to providing excellent solubility in aqueous media as shown in section 4.1, PEO can be used to effectively shield polymer-based particles. For this purpose, the so-called stealth effect is exploited – the inhibition of non-desired interactions with the human immune system. For materials to be used in drug delivery different requirements must be fulfilled. They should be able to encapsulate a certain payload, be non-toxic, chemically stable, biocompatible, and preferably biodegradable. Poly(ethylene oxide) shows the limitation that it is only poorly biodegradable and accumulates in the human body, in particular in muscles, skin, bones and liver

if the molar mass exceeds  $20\,000\text{ g mol}^{-1}$ .<sup>9,104</sup> This problem can be partially solved by the introduction of a biodegradable block. After degradation, shorter fragments of the former block copolymers remain and can be released from the body. One example is poly(ethylene oxide)-*block*-poly( $\epsilon$ -caprolactone)-*block*-poly(lactic acid) (PEO-*b*-PCL-*b*-PLA), which has been shown to form micelles in aqueous solution. Doxorubicin as an anti-cancer drug could be successfully encapsulated and both the PCL and the PLA block ensure biodegradability.<sup>105</sup> In addition to degradable PEO-*b*-PCL structures the introduction of a short third block such as poly(benzobisoxazole) (PBO), resulting in poly(ethylene oxide)-*block*-polybenzobisoxazole-*b*-poly( $\epsilon$ -caprolactone) (PEO-*b*-PBO-*b*-PCL), provides an increased protection from hydrolysis of the ester group and, therefore, an increased stability of the self-assembled structures.<sup>106</sup> Another system used in doxorubicin delivery is poly(ethylene oxide)-*block*-poly(*t*-butyl acrylate)-*block*-poly(2-hydroxyethyl methacrylate) (PEO-*b*-PtBA-*b*-PHEMA).<sup>107</sup>

Biodegradable amphiphilic poly(ethylene oxide)-*block*-poly(*l*-lysine)-*block*-poly(lactic acid) (PEO-*b*-PLL-*b*-PLA) or poly(ethylene oxide)-*block*-poly(*l*-lactide)-*block*-poly( $\epsilon$ -caprolactone) (PEO-*b*-PLLA-*b*-PCL) triblock terpolymers form multilayered micelles where paclitaxel could be successfully encapsulated.<sup>108,109</sup> Another system which is closely related to drug delivery approaches is poly(ethylene oxide)-*block*-poly(propylene oxide)-*block*-poly( $\epsilon$ -caprolactone) (PEO-*b*-PPO-*b*-PCL). Depending on the block length of the PCL segment spherical micelles or worm-like structures can be observed and used to encapsulate hydrophobic compounds such as pyrene.<sup>110</sup> Poly(ethylene oxide)-*block*-poly( $\epsilon$ -caprolactone)-*block*-poly(2-(diethylamino)-ethyl methacrylate) (PEO-*b*-PCL-*b*-PDEA) has been used as a biodegradable chimaeric polymersome for exogenous proteins. Polymersomes are vesicular structures based on amphiphilic polymers. In this case the PEO segments should be located at the polymersome outlayer, whereas the shorter PDEA segment should be orientated to the inside. This will facilitate the encapsulation of proteins and should assist the release by the "proton sponge effect". The biodegradable PCL block can be furthermore used for the encapsulation of drugs such as doxorubicin.<sup>111</sup> The introduction of a polyglycidol segment by deprotection of poly(ethoxyethyl glycidol) in the case of poly(ethylene oxide)-*block*-polyglycidol-*block*-poly(*l*-lactide) (PEO-*b*-PGly-*b*-PLLA) led to materials featuring both biocompatibility and biodegradability.<sup>112</sup> The combination of both a biodegradable and a functional block which enables post-polymerization functionalization is highly attractive. An example is poly(ethylene oxide)-*block*-poly(allyl glycidyl ether)-*block*-poly(lactic acid) (PEO-*b*-PAGE-*b*-PLA), where the PAGE block can be functionalized with a luteinizing hormone-releasing hormone (LHRH). Dissolving the compound in water leads to the formation of micellar structures.<sup>113</sup>

One possible payload to be transported by potentially biodegradable, PEO-containing materials is si-RNA. "Loading" can be achieved by using an amine containing segment for polyplex formation with si-RNA in addition to a hydrophobic and biodegradable core (*e.g.*, PCL) and a hydrophilic shell (PEO). This has been demonstrated for poly(ethylene oxide)-

*block*-poly(ethylene imine)-*block*-poly( $\epsilon$ -caprolactone) (PEO-*b*-PEI-*b*-PCL) triblock terpolymers.<sup>114,115</sup> In another example, methoxy-poly(3-hydroxybutyrate-*co*-4-hydroxybutyrate)-*block*-poly(ethylene oxide)-*block*-poly(ethylene imine) (mP3/4HB-*b*-PEO-*b*-PEI) could be used to successfully transport si-RNA.<sup>116</sup> Apart from PEI, also other amine-containing materials can be applied, *e.g.*, poly(ethylene oxide)-*block*-poly( $\epsilon$ -caprolactone)-*block*-poly(2-(2-aminoethyl amino) ethyl methacrylate) (PEO-*b*-PCL-*b*-PAEAEMA), poly(ethylene oxide)-*block*-poly( $\epsilon$ -caprolactone)-*block*-poly(2-(*N,N*-dimethylamino)ethyl methacrylate) (PEO-*b*-PCL-*b*-PAMA), or poly(ethylene oxide)-*block*-poly(*n*-butyl acrylate)-*block*-poly(*N,N'*-dimethylaminoethyl methacrylate) (PEO-*b*-PnBA-*b*-PDMAEMA).<sup>117-119</sup>

One very intriguing aspect regarding micellar structures based on triblock terpolymers is that they can be loaded with two different drugs. In that way, micelles from poly(ethylene oxide)-*block*-poly( $\epsilon$ -caprolactone)-*block*-poly(acrylic acid) (PEO-*b*-PCL-*b*-PAA) could be loaded with doxorubicin (PCL core) and additionally enriched with *cis*-platin in the PAA shell.<sup>120</sup>

Again, particle stability in various environments can be increased *via* crosslinking as demonstrated for poly(ethylene oxide)-*block*-poly(2-hydroxyethyl methacrylate)-*block*-poly(methyl methacrylate) (PEO-*b*-PHEMA-*b*-PMMA) after UV irradiation in the presence of a suitable crosslinker (di(4-hydroxybenzophenone) dodecanedioate) for the PHEMA shell.<sup>121,122</sup> In addition, the use of poly(ethylene oxide)-*block*-poly(*l*-lysine)-*block*-poly(*l*-leucine) (PEO-*b*-PLL-*b*-PLeu) has been demonstrated for glutathione mediated drug delivery. Here, the PEO block is attached to the PLL segments *via* a disulfide linker. The triblock terpolymer forms micellar structures consisting of a PEO corona, a PLL shell which can be crosslinked by addition of 3,3'-dithiodipropionic acid, and a PLeu core where the drug camptothecin can be encapsulated. In an intracellular environment the disulfide bonding is cleaved which results in the release of the PEO segment, the de-crosslinking of the shell and, finally, the release of the encapsulated drug.<sup>123</sup> Furthermore, poly(ethylene oxide)-*block*-poly(2,4,6-trimethoxybenzylidene-1,1,1-tris(hydroxyl methyl)ethane methacrylate)-*block*-poly(acrylic acid) (PEO-*b*-PTTMA-*b*-PAA) has been employed for the pH-dependent delivery of doxorubicin hydrochloride.<sup>124</sup>

#### 4.6. Controlled release using external stimuli

**4.6.1. pH value.** It is not only of interest to load polymeric carriers with drugs, also the release should occur at the desired location and under controlled conditions. A schematic representation for a possible stimuli responsive micellar structure for drug-delivery approaches is depicted in Fig. 5. Most frequently employed is the targeted release due to changes in the pH value. The physiological pH value of blood is 7.4 and, in comparison, the pH value inside cells can be more acidic (pH  $\sim$ 5). This difference can be exploited using pH-sensitive blocks such as poly(2-vinyl pyridine). Biotinylated poly( $\epsilon$ -caprolactone)-*block*-poly(ethylene oxide)-*block*-poly(2-vinyl pyridine) (PCL-*b*-PEO-*b*-P2VP) forms flower-like micelles at pH  $\sim$ 7 in aqueous solution. Upon a decrease in the pH value a transition can be observed and the biotin moieties are exposed at the micellar surface.<sup>125,126</sup>

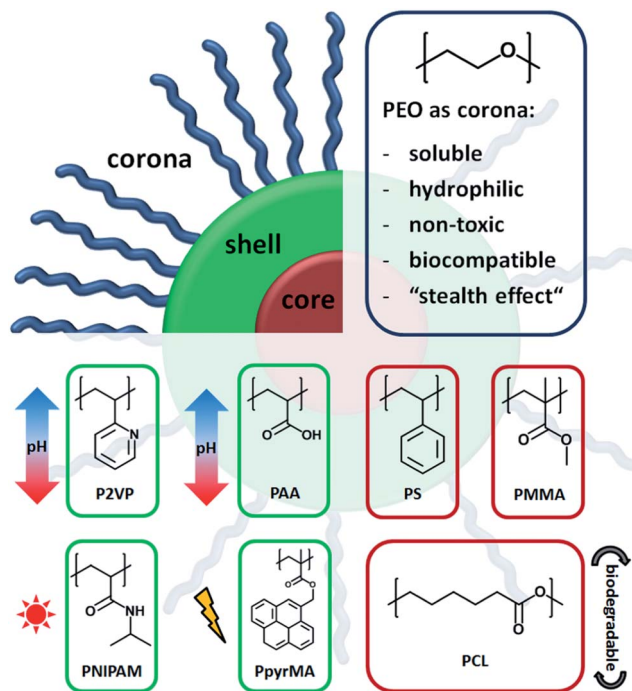


Fig. 5 Schematic representation of a micellar structure for drug-delivery approaches showing selected examples for stimuli responsive building blocks for the shell or core segment. Poly(2-vinyl pyridine) (P2VP, [ref. 125]) and poly(acrylic acid) (PAA, [ref. 78]) are depicted as pH sensitive building blocks. Poly(*n*-isopropylacrylamide) (PNIPAm, [ref. 131]) represents a thermo responsive unit whereas poly-(pyrenylmethyl methacrylate) (PpyrMA, [ref. 93]) acts as a light sensitive moiety. Possible hydrophobic core-forming blocks are polystyrene (PS, [ref. 66]) or poly(methyl methacrylate) (PMMA, [ref. 135]). PCL represents a biodegradable hydrophobic segment.

Another promising candidate for pH-sensitive drug-release are poly(ethylene oxide)-*block*-polyhistidine-*block*-poly(L-lactic acid) (PEO-*b*-PH-*b*-PLLA) triblock terpolymers. Micellar structures are formed in aqueous solution featuring a biodegradable PLLA core, a pH-sensitive polyhistidine shell, and a PEO corona. After loading with doxorubicin the system showed an increased drug release at lower pH values, making this combination promising for *in vitro* applications.<sup>127</sup> Another example employs poly(ethylene oxide)-*block*-poly(dimethyl acrylamide)-*b*-poly( $\epsilon$ -caprolactone) (PEO-*b*-PDMA-*b*-PCL) for this approach.<sup>128</sup> Also the use of pH-labile linkers is very attractive, as demonstrated for the shell of doxorubicin loaded poly(ethylene oxide)-*block*-poly(L-aspartic acid)-*block*-poly(L-phenylalanine) (PEO-*b*-PAsp-*b*-PPhe) micelles after reversible crosslinking using a ketal moiety. This crosslinker is cleaved under acidic conditions enabling the release of the encapsulated drug.<sup>129</sup> This strategy in combination with more complex polymeric architectures can lead to powerful new combinations of the carrier and active "guest". In another example, vesicular structures based on poly(ethylene oxide)-*block*-polylysine-*b*-poly( $\epsilon$ -caprolactone) (PEO-*b*-PLys-*b*-PCL) triblock terpolymers were used for the encapsulation of the hydrophobic drug camptothecin in the hydrophobic membrane and doxorubicin hydrochloride within

the aqueous core, increasing the cytotoxicity of these particles towards cancer cells.<sup>130</sup>

**4.6.2. Temperature.** Changes in temperature can also be used to release encapsulated cargo. Exemplarily, a PNIPAm block can be introduced as shown for poly( $\epsilon$ -caprolactone)-*block*-poly(ethylene oxide)-*block*-poly(*n*-isopropylacrylamide) (PCL-*b*-PEO-*b*-PNIPAm). Micelles with a PCL core and a PEO-*b*-PNIPAm shell are formed in aqueous media and can be loaded with doxorubicin. Upon heating to 42 °C above the LCST temperature, the PNIPAm block collapses which, in turn, induces a shrinkage of the PCL core, leading to an increased release of the drug.<sup>131</sup> A similar approach can be used to thermally control the release of ibuprofen from poly( $\epsilon$ -caprolactone)-*block*-poly(ethylene oxide)-*block*-poly(*n*-isopropylacrylamide) (PCL-*b*-PEO-*b*-PNIPAm) microspheres.<sup>132</sup> Also reversibly crosslinked PEO-*b*-PAA-*b*-PNIPAm can be used for this approach. Here, the triblock terpolymer forms polymersomes upon heating above the LCST. The PAA segment can be cross-linked using cysteamine by carbodiimide chemistry resulting in stabilized vesicular structures against temperature, dilution or organic solvents. Mimicking an intracellular environment by reductive conditions leads to a fast dissociation of the structures.<sup>133</sup> The same block sequence could also be used for the synthesis of dual-responsive crosslinked polymersomes for targeted intracellular protein delivery.<sup>134</sup>

The use of labels or targeting moieties is another set screw to increase specificity in polymeric delivery approaches. Biotin labeled poly(ethylene oxide)-*block*-poly(*n*-isopropylacrylamide)-*co*-poly(*N*-hydroxymethylacrylamide)-*block*-poly(methyl methacrylate) (Biotin-PEO-*b*-PNIPAm-*co*-PHMAAm-*b*-PMMA) triblock quaterpolymers form bioactive micelles featuring a thermo-responsive PNIPAm-*co*-HMAAm shell which enables the release of the anti-cancer drug methotrexate (MTX) by temperature changes. Here, the biotin moiety is used for pretargeting in tumor chemotherapy due to the formation of biotin-avidin systems (BAS).<sup>135</sup>

#### 4.7. Synthesis of hybrid materials

Hybrid materials are of broad scientific interest as they combine the properties of both organic and inorganic materials (in the case of organic-inorganic hybrids) and show a wide range of applications such as in photonic band gap materials or catalysis.<sup>136</sup> The use of triblock terpolymers in this context is of high interest, depending on the monomer choice, block sequence, and surrounding conditions the interactions of the inorganic precursors with any segment can be precisely tuned. One example is to control the crystallization of inorganic compounds: in this case, both the crystallization and the morphology of CaCO<sub>3</sub> particles could be directed using poly(ethylene oxide)-*block*-poly(acrylic acid)-*block*-polystyrene (PEO-*b*-PAA-*b*-PS) triblock terpolymers. The interaction of the inorganic compound with the polymeric additive strongly depends on the amount of PAA (as well as the solution pH value) and can, therefore, be tuned by using different block lengths.<sup>137</sup> A similar approach was used in the case of poly(ethylene oxide)-*block*-poly(acrylic acid)-*block*-poly(*n*-butyl acrylate) (PEO-*b*-PAA-*b*-



*PnBA*) for the preparation of calcite crystals which, at the *c*-axes, were capped by rhombohedral facets (Fig. 6a).<sup>138</sup> One further example are silica-containing hybrid materials synthesized by (3-glycidioxypropyl) trimethoxy silane and aluminum *sec*-butoxide in combination with polystyrene-*block*-poly(ethylene oxide)-*block*-poly( $\epsilon$ -caprolactone) (PS-*b*-PEO-*b*-PCL). The silica particles are located at the PS-PEO interface, whereas the PCL block is allowed to crystallize.<sup>139</sup> As shown in Fig. 6b, polypropylene-*block*-poly(ethylene oxide)-*block*-poly(hexyl methacrylate) (PEP-*b*-PEO-*b*-PHMA) was used for the formation of hybrid compounds with hexagonally patterned lamellar morphologies. In this case aluminosilicates could be incorporated into the PEO phase, resulting in the formation of highly ordered nanocomposites.<sup>140</sup> Variations of the volume ratios of the constituting building blocks led to even more complex structures such as a four layered woodpile zigzag morphology.<sup>141</sup>

Another application is the formation of CdTe nanowires. Here a mixture of poly(ethylene oxide)-*block*-polystyrene-*block*-poly(acrylic acid) (PEO-*b*-PS-*b*-PAA) and Cd<sup>2+</sup> ions, which forms micellar structures in a dioxane/water mixture with Cd<sup>2+</sup> polychelate PAA cores, can be used. After the addition of NaHTe the formation of CdTe nanocrystals was observed. The PS block forms a densely packed shell around the nanowires and the PEO corona ensures solubility.<sup>142</sup> With the same polymer and fabrication technique CdS quantum dots could also be obtained.<sup>143</sup>

Directly connected to the controlled synthesis of nanoparticles, such triblock terpolymers can be used in “so-called”

place-exchange reactions. It is well-known that gold or palladium nanoparticles can be prepared using a tetraoctylammonium bromide stabilizer. This molecule can be replaced by a poly(ethylene oxide)-*block*-polystyrene-*block*-poly(4-vinyl pyridine) (PEO-*b*-PS-*b*-P4VP) triblock terpolymer where the P4VP block strongly interacts with the metals (Fig. 6c).<sup>144</sup> In another example, polystyrene-*block*-poly(2-vinyl pyridine)-*block*-poly(ethylene oxide) (PS-*b*-P2VP-*b*-PEO) was used to form organic-inorganic tungstate nano-complexes.<sup>145</sup> Additionally, ultra-small single gold nano-particles can be prepared by the application of poly(ethylene oxide)-*block*-poly(lipoic acid 2-hydroxy-3-(methacryloyloxy)-propyl ester-*co*-glycidyl methacrylate)-*block*-polystyrene (PEO-*b*-P(LAMP-*co*-GMA)-*b*-PS) where one individual gold particle is anchored to one terpolymer chain.<sup>146</sup> Furthermore, hollow silica nano-particles can be produced by using polystyrene-*block*-poly(2-vinyl pyridine)-*block*-poly(ethylene oxide) (PS-*b*-P2VP-*b*-PEO) as a template in aqueous solution where the P2VP shell was loaded with a tetramethoxysilane precursor and the composite was subsequently calcinated.<sup>147</sup> The obtained hollow particles are of interest regarding their use in rechargeable lithium batteries.<sup>148</sup> As shown in Fig. 6d, polystyrene-*block*-poly(acrylic acid)-*block*-poly(ethylene oxide) (PS-*b*-PAA-*b*-PEO) can be used in a comparable approach for the formation of hollow LaBO<sub>3</sub>, CaCO<sub>3</sub>, or BaSO<sub>4</sub> nanoparticles.<sup>149-151</sup> Furthermore, poly(ethylene oxide)-*block*-poly(acrylic acid)-*block*-poly( $\epsilon$ -caprolactone) (PEO-*b*-PAA-*b*-PCL) was applied in tuning the mineralization of hydroxyapatite.<sup>152</sup>

One well-known commercial application of nanoparticulate systems is sun screen agents. The drawback of TiO<sub>2</sub> nanoparticles is the accelerated photodamage of the skin due to their photocatalytic degradation activity. To avoid this problem the nanoparticles can be encapsulated within a triblock terpolymer, PEO-*b*-PDMA-*b*-PS. More specifically, tetrabutyl titanate (TBT) can be loaded into the PDMA shell in polar solvents where a thin protective TiO<sub>2</sub> layer is formed. Hereby, the PEO corona prevents direct skin-contact of the hybrid nanoparticles.<sup>153</sup>

## 5. Concluding remarks

The evolution of triblock terpolymers regarding synthetic feasibility, building block diversity, and monomer combinations enabling multiple and combined stimuli-response is remarkable. Alongside, it could be shown in a multitude of approaches that materials containing PEO segments offer high potential for many applications in the fields of chemistry, materials science, and life sciences. Nevertheless, these materials still require multi-step synthesis, high purity monomers or solvents, and sometimes even changes of the polymerization technique during polymerization, which make them rather cost-intensive. Any application exploiting the benefits of using ternary systems, either as nanostructured films or solution structures, will have to cope with that and we believe that amongst the possibilities listed here, the field of life sciences (often also called “nanomedicine”) sounds most promising.

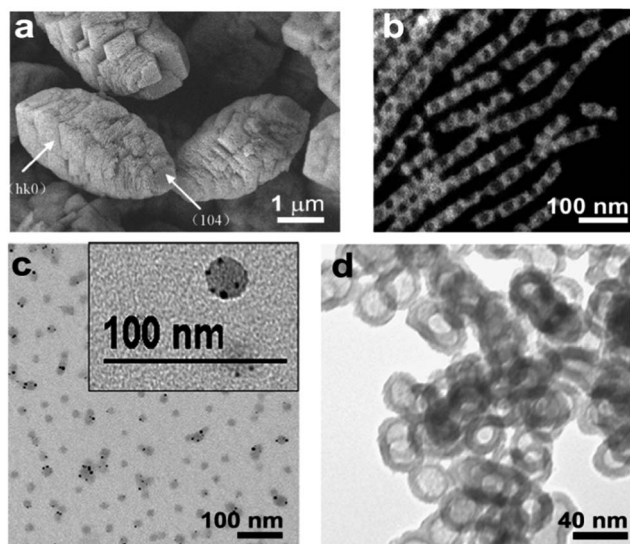


Fig. 6 SEM images of CaCO<sub>3</sub> crystals obtained in the presence of PEG-*b*-PAA-*b*-*PnBA* (a, reprinted with permission from ref. 138, Copyright © 2009 Elsevier B.V); dark-field STEM image of a PEP-*b*-PEO-*b*-PHMA aluminosilicate hybrid material (b, reprinted with permission from ref. 140, Copyright © 2008 American Chemical Society); representation of hybrid micelles of PEO-*b*-PS-*b*-P4VP and stabilized Au nanoparticles (c, reprinted with permission from ref. 144, Copyright © 2008 American Chemical Society); TEM micrograph of hollow CaCO<sub>3</sub> nanospheres (d, reprinted with permission from ref. 151, Copyright © 2010 American Chemical Society). New scale bars have been added to the figures.

## Acknowledgements

The work of M. J. B. forms part of the research programme of the Dutch Polymer Institute (DPI), project #690. F. H. S. is grateful for a fellowship from the Fonds der Chemischen Industrie (FCI). Furthermore, the authors want to acknowledge the Thuringian Ministry for Education, Science and Culture (TMBWK; #B515-10065, ChaPoNano; #B514-09051, NanoConSens).

## References

- 1 A. Blanz, S. P. Armes and A. J. Ryan, *Macromol. Rapid Commun.*, 2009, **30**, 267–277.
- 2 S. B. Darling, *Prog. Polym. Sci.*, 2007, **32**, 1152–1204.
- 3 F. H. Schacher, P. A. Rugar and I. Manners, *Angew. Chem., Int. Ed.*, 2012, **51**, 7898–7921.
- 4 Y. Y. Mai and A. Eisenberg, *Chem. Soc. Rev.*, 2012, **41**, 5969–5985.
- 5 C. T. Black, R. Ruiz, G. Breyta, J. Y. Cheng, M. E. Colburn, K. W. Guarini, H. C. Kim and Y. Zhang, *IBM J. Res. Dev.*, 2007, **51**, 605–633.
- 6 K. Knoll and N. Niessner, *Macromol. Symp.*, 1998, **132**, 231–243.
- 7 D. H. Richards and M. Szwarc, *Trans. Faraday Soc.*, 1959, **55**, 1644–1650.
- 8 T. Sakai and P. Alexandridis, *Langmuir*, 2004, **20**, 8426–8430.
- 9 K. Knop, R. Hoogenboom, D. Fischer and U. S. Schubert, *Angew. Chem., Int. Ed.*, 2010, **49**, 6288–6308.
- 10 C. Monfardini and F. M. Veronese, *Bioconjugate Chem.*, 1998, **9**, 418–450.
- 11 M. Hruby, C. Konak and K. Ulbrich, *J. Appl. Polym. Sci.*, 2005, **95**, 201–211.
- 12 P. Dimitrov, S. Rangelov, A. Dworak, N. Haraguchi, A. Hirao and C. B. Tsvetanov, *Macromol. Symp.*, 2004, **215**, 127–139.
- 13 M. J. Barthel, T. Rudolph, S. Crotty, F. H. Schacher and U. S. Schubert, *J. Polym. Sci., Part A: Polym. Chem.*, 2012, **50**, 4958–4965.
- 14 B. Obermeier, F. Wurm, C. Mangold and H. Frey, *Angew. Chem., Int. Ed.*, 2011, **50**, 7988–7997.
- 15 V. Abetz and P. F. W. Simon, *Adv. Polym. Sci.*, 2005, **189**, 125–212.
- 16 D. Leckband, S. Sheth and A. Halperin, *J. Biomater. Sci., Polym. Ed.*, 1999, **10**, 1125–1147.
- 17 C. Allen, D. Maysinger and A. Eisenberg, *Colloids Surf., B*, 1999, **16**, 3–27.
- 18 M. Hruby, C. Konak and K. Ulbrich, *J. Controlled Release*, 2005, **103**, 137–148.
- 19 C. Price, T. P. Lally and R. Stubbers, *Polymer*, 1974, **15**, 541–543.
- 20 K. Arai, T. Kotaka, Y. Kitano and K. Yoshimura, *Macromolecules*, 1980, **13**, 455–457.
- 21 Y. Mogi, H. Kotsuji, Y. Kaneko, K. Mori, Y. Matsushita and I. Noda, *Macromolecules*, 1992, **25**, 5408–5411.
- 22 C. Auschra and R. Stadler, *Macromolecules*, 1993, **26**, 2171–2174.
- 23 J. Beckmann, C. Auschra and R. Stadler, *Macromol. Rapid Commun.*, 1994, **15**, 67–72.
- 24 Y. Mogi, M. Nomura, H. Kotsuji, K. Ohnishi, Y. Matsushita and I. Noda, *Macromolecules*, 1994, **27**, 6755–6760.
- 25 J. L. Huang, X. Y. Huang, W. B. Hu and W. K. Lou, *Sci. China, Ser. B: Chem.*, 1997, **40**, 663–669.
- 26 X. Y. Huang, S. Chen and J. L. Huang, *J. Polym. Sci., Part A: Polym. Chem.*, 1999, **37**, 825–833.
- 27 N. Hadjichristidis, H. Iatrou, M. Pitsikalis, S. Pispas and A. Avgeropoulos, *Prog. Polym. Sci.*, 2005, **30**, 725–782.
- 28 O. Altintas and U. Tunca, *Chem. – Asian J.*, 2011, **6**, 2584–2591.
- 29 M. J. Barthel, K. Babiuch, T. Rudolph, J. Vitz, S. Hoepfener, M. Gottschaldt, M. D. Hager, F. H. Schacher and U. S. Schubert, *J. Polym. Sci., Part A: Polym. Chem.*, 2012, **50**, 2914–2923.
- 30 M. J. Barthel, U. Mansfeld, S. Hoepfener, J. A. Czaplewska, F. H. Schacher and U. S. Schubert, *Soft Matter*, 2013, **9**, 3509–3520.
- 31 M. Gervais, A. L. Brocas, G. Cendejas, A. Deffieux and S. Carloti, *Macromolecules*, 2010, **43**, 1778–1784.
- 32 M. L. Arnal, V. Balsamo, F. Lopez-Carrasquero, J. Contreras, M. Carrillo, H. Schmalz, V. Abetz, E. Laredo and A. J. Müller, *Macromolecules*, 2001, **34**, 7973–7982.
- 33 C. Deng, G. Z. Rong, H. Y. Tian, Z. H. Tang, X. S. Chen and X. B. Jing, *Polymer*, 2005, **46**, 653–659.
- 34 X. H. He, L. Y. Liang, M. R. Xie, Y. Q. Zhang, S. L. Lin and D. Y. Yan, *Macromol. Chem. Phys.*, 2007, **208**, 1797–1802.
- 35 J. Jin, M. M. Zhang, Q. Q. Xiong, P. C. Sun and H. Y. Zhao, *Soft Matter*, 2012, **8**, 11809–11816.
- 36 R. K. Jing, G. W. Wang, Y. N. Zhang and J. L. Huang, *Macromolecules*, 2011, **44**, 805–810.
- 37 R. K. Jing, W. C. Lin, G. W. Wang and J. L. Huang, *J. Polym. Sci., Part A: Polym. Chem.*, 2011, **49**, 2594–2600.
- 38 H. Durmaz, A. Dag, O. Altintas, T. Erdogan, G. Hizal and U. Tunca, *Macromolecules*, 2007, **40**, 191–198.
- 39 M. Glassner, K. K. Oehlenschlaeger, T. Gruending and C. Barner-Kowollik, *Macromolecules*, 2011, **44**, 4681–4689.
- 40 C. Ott, R. Hoogenboom, S. Hoepfener, D. Wouters, J. F. Gohy and U. S. Schubert, *Soft Matter*, 2009, **5**, 84–91.
- 41 T. S. Bailey, C. M. Hardy, T. H. Epps and F. S. Bates, *Macromolecules*, 2002, **35**, 7007–7017.
- 42 T. H. Epps, T. S. Bailey, R. Waletzko and F. S. Bates, *Macromolecules*, 2003, **36**, 2873–2881.
- 43 A. J. Meuler, C. J. Ellison, J. Qin, C. M. Evans, M. A. Hillmyer and F. S. Bates, *J. Chem. Phys.*, 2009, **130**.
- 44 H. Schmalz, A. Knoll, A. J. Müller and V. Abetz, *Macromolecules*, 2002, **35**, 10004–10013.
- 45 H. Schmalz, A. J. Müller and V. Abetz, *Macromol. Chem. Phys.*, 2003, **204**, 111–124.
- 46 A. Boschetti-De-Fierro, L. Spindler, G. Reiter, D. Olmos, S. Magonov and V. Abetz, *Macromolecules*, 2007, **40**, 5487–5496.
- 47 A. Boschetti-De-Fierro, A. J. Müller and V. Abetz, *Macromolecules*, 2007, **40**, 1290–1298.
- 48 M. Vivas, J. Contreras, F. Lopez-Carrasquero, A. T. Lorenzo, M. L. Arnal, V. Balsamo, A. J. Müller, E. Laredo, H. Schmalz and V. Abetz, *Macromol. Symp.*, 2006, **239**, 58–67.

- 49 H. M. Xiong, C. K. Chen, K. Lee, R. M. Van Horn, Z. Liu, B. Ren, R. P. Quirk, E. L. Thomas, B. Lotz, R. M. Ho, W. B. Zhang and S. Z. D. Cheng, *Macromolecules*, 2011, **44**, 7758–7766.
- 50 J. G. Li, R. B. Lin and S. W. Kuo, *Macromol. Rapid Commun.*, 2012, **33**, 678–682.
- 51 R. T. Yu and S. X. Zheng, *Macromolecules*, 2011, **44**, 8546–8557.
- 52 J. Bang, S. H. Kim, E. Drockenmuller, M. J. Misner, T. P. Russell and C. J. Hawker, *J. Am. Chem. Soc.*, 2006, **128**, 7622–7629.
- 53 J. Bang, B. J. Kim, G. E. Stein, T. P. Russell, X. Li, J. Wang, E. J. Kramer and C. J. Hawker, *Macromolecules*, 2007, **40**, 7019–7025.
- 54 C. B. Tang, J. Bang, G. E. Stein, G. H. Fredrickson, C. J. Hawker, E. J. Kramer, M. Sprung and J. Wang, *Macromolecules*, 2008, **41**, 4328–4339.
- 55 J. Y. Zhang, Y. H. Deng, J. Wei, Z. K. Sun, D. Gu, H. Bongard, C. Liu, H. H. Wu, B. Tu, F. Schuth and D. Y. Zhao, *Chem. Mater.*, 2009, **21**, 3996–4005.
- 56 Y. A. Meng, X. H. Zhang, B. Y. Du, B. X. Zhou, X. Zhou and G. R. Qi, *Polymer*, 2011, **52**, 391–399.
- 57 M. Aizawa and J. M. Buriak, *J. Am. Chem. Soc.*, 2006, **128**, 5877–5886.
- 58 W. H. Huang, C. X. Luo, J. L. Zhang and Y. C. Han, *J. Chem. Phys.*, 2007, 126.
- 59 W. H. Huang, C. X. Luo, J. L. Zhang, K. Yu and Y. C. Han, *Macromolecules*, 2007, **40**, 8022–8030.
- 60 J. F. Gohy, N. Lefevre, C. D'Haese, S. Hoepfener, U. S. Schubert, G. Kostov and B. Ameduri, *Polym. Chem.*, 2011, **2**, 328–332.
- 61 X. L. Mao, H. Peng, J. Q. Ling, T. Friis, A. K. Whittaker, R. Crawford and Y. Xiao, *Biomaterials*, 2009, **30**, 6903–6911.
- 62 M. D. Dimitriou, Z. L. Zhou, H. S. Yoo, K. L. Killops, J. A. Finlay, G. Cone, H. S. Sundaram, N. A. Lynd, K. P. Barteau, L. M. Campos, D. A. Fischer, M. E. Callow, J. A. Callow, C. K. Ober, C. J. Hawker and E. J. Kramer, *Langmuir*, 2011, **27**, 13762–13772.
- 63 T. X. Viegas, M. D. Bentley, J. M. Harris, Z. F. Fang, K. Yoon, B. Dizman, R. Weimer, A. Mero, G. Pasut and F. M. Veronese, *Bioconjugate Chem.*, 2011, **22**, 976–986.
- 64 G. Y. Li, L. Guo, S. M. Ma and J. S. Liu, *J. Polym. Sci., Part A: Polym. Chem.*, 2009, **47**, 1804–1810.
- 65 I. W. Wyman and G. J. Liu, *Polymer*, 2013, **54**, 1950–1978.
- 66 S. L. Lin, W. J. Zhu, X. H. He, Y. H. Xing, L. Y. Liang, T. Chen and J. P. Lin, *J. Phys. Chem. B*, 2013, **117**, 2586–2593.
- 67 Y. Zhang, W. C. Lin, R. K. Jing and J. L. Huang, *J. Phys. Chem. B*, 2008, **112**, 16455–16460.
- 68 A. Walther, P. E. Millard, A. S. Goldmann, T. M. Lovestead, F. Schacher, C. Barner-Kowollik and A. H. E. Müller, *Macromolecules*, 2008, **41**, 8608–8619.
- 69 R. C. Hayward and D. J. Pochan, *Macromolecules*, 2010, **43**, 3577–3584.
- 70 A. Khanal, Y. Li, N. Takisawa, N. Kawasaki, Y. Oishi and K. Nakashima, *Langmuir*, 2004, **20**, 4809–4812.
- 71 A. Khanal, S. Yusa and K. Nakashima, *Langmuir*, 2007, **23**, 10511–10517.
- 72 J. F. Gohy, B. G. G. Lohmeijer, S. K. Varshney, B. Decamps, E. Leroy, S. Boileau and U. S. Schubert, *Macromolecules*, 2002, **35**, 9748–9755.
- 73 A. O. Moughton and R. K. O'Reilly, *Macromol. Rapid Commun.*, 2010, **31**, 37–52.
- 74 E. S. Read and S. P. Armes, *Chem. Commun.*, 2007, 3021–3035.
- 75 X. W. Xu, A. E. Smith, S. E. Kirkland and C. L. McCormick, *Macromolecules*, 2008, **41**, 8429–8435.
- 76 Y. T. Li, B. S. Lokitz and C. L. McCormick, *Macromolecules*, 2006, **39**, 81–89.
- 77 G. Jiang, *J. Appl. Polym. Sci.*, 2009, **114**, 3472–3478.
- 78 S. Chavda, S. Yusa, M. Inoue, L. Abezgauz, E. Kesselman, D. Danino and P. Bahadur, *Eur. Polym. J.*, 2013, **49**, 209–216.
- 79 Y. L. Cai and S. P. Armes, *Macromolecules*, 2004, **37**, 7116–7122.
- 80 S. Y. Yu, T. Azzam, I. Rouiller and A. Eisenberg, *J. Am. Chem. Soc.*, 2009, **131**, 10557–10566.
- 81 S. Y. Liu, J. V. M. Weaver, M. Save and S. P. Armes, *Langmuir*, 2002, **18**, 8350–8357.
- 82 S. Y. Liu, J. V. M. Weaver, Y. Q. Tang, N. C. Billingham, S. P. Armes and K. Tribe, *Macromolecules*, 2002, **35**, 6121–6131.
- 83 V. Schmidt, R. Borsali and C. Giacomelli, *Langmuir*, 2009, **25**, 13361–13367.
- 84 G. Koutalas, S. Pispas and N. Hadjichristidis, *Eur. Phys. J. E*, 2004, **15**, 457–464.
- 85 J. Sun, C. Deng, X. S. Chen, H. J. Yu, H. Y. Tian, J. R. Sun and X. B. Jing, *Biomacromolecules*, 2007, **8**, 1013–1017.
- 86 G. R. Sun, H. G. Cui, L. Y. Lin, N. S. Lee, C. Yang, W. L. Neumann, J. N. Freskos, J. J. Shieh, R. B. Dorshow and K. L. Wooley, *J. Am. Chem. Soc.*, 2011, **133**, 8534–8543.
- 87 C. Zhou, M. A. Hillmyer and T. P. Lodge, *Macromolecules*, 2011, **44**, 1635–1641.
- 88 Y. C. Zheng, L. Wang, R. T. Yu and S. X. Zheng, *Macromol. Chem. Phys.*, 2012, **213**, 458–469.
- 89 W. Q. Zhang, X. W. Jiang, Z. P. He, D. Xiong, P. W. Zheng, Y. L. An and L. Q. Shi, *Polymer*, 2006, **47**, 8203–8209.
- 90 A. Walther, C. Barner-Kowollik and A. H. E. Müller, *Langmuir*, 2010, **26**, 12237–12246.
- 91 S. L. Lin, Y. Y. Wang, C. H. Cai, Y. H. Xing, J. P. Lin, T. Chen and X. H. He, *Nanotechnology*, 2013, 24.
- 92 M. Rabnawaz and G. J. Liu, *Macromolecules*, 2012, **45**, 5586–5595.
- 93 S. Menon and S. Das, *J. Polym. Sci., Part A: Polym. Chem.*, 2011, **49**, 4448–4457.
- 94 X. Z. Jiang, S. Z. Luo, S. P. Armes, W. F. Shi and S. Y. Liu, *Macromolecules*, 2006, **39**, 5987–5994.
- 95 J. S. Kim, H. J. Jeon, J. J. Park, M. S. Park and J. H. Youk, *J. Polym. Sci., Part A: Polym. Chem.*, 2009, **47**, 4963–4970.
- 96 S. Reinicke and H. Schmalz, *Colloid Polym. Sci.*, 2011, **289**, 497–512.
- 97 C. H. Luo, Y. Liu and Z. B. Li, *Soft Matter*, 2012, **8**, 2618–2626.
- 98 I. Koonar, C. Zhou, M. A. Hillmyer, T. P. Lodge and R. A. Siegel, *Langmuir*, 2012, **28**, 17785–17794.



- 99 R. R. Taribagil, M. A. Hillmyer and T. P. Lodge, *Macromolecules*, 2010, **43**, 5396–5404.
- 100 S. Reinicke, J. Schmelz, A. Lapp, M. Karg, T. Hellweg and H. Schmalz, *Soft Matter*, 2009, **5**, 2648–2657.
- 101 S. Reinicke, M. Karg, A. Lapp, L. Heymann, T. Hellweg and H. Schmalz, *Macromolecules*, 2010, **43**, 10045–10054.
- 102 S. Reinicke, S. Döhler, S. Tea, M. Krekhova, R. Messing, A. M. Schmidt and H. Schmalz, *Soft Matter*, 2010, **6**, 2760–2773.
- 103 M. L. Adams, A. Lavasanifar and G. S. Kwon, *J. Pharm. Sci.*, 2003, **92**, 1343–1355.
- 104 T. Yamaoka, Y. Tabata and Y. Ikada, *J. Pharm. Sci.*, 1994, **83**, 601–606.
- 105 L. Sun, L. J. Shen, M. Q. Zhu, C. M. Dong and Y. Wei, *J. Polym. Sci., Part A: Polym. Chem.*, 2010, **48**, 4583–4593.
- 106 X. B. Zhu, M. Fryd, B. D. Tran, M. A. Ilies and B. B. Wayland, *Macromolecules*, 2012, **45**, 660–665.
- 107 L. Yuan, W. L. Chen, J. Li, J. H. Hu, J. J. Yan and D. Yang, *J. Polym. Sci., Part A: Polym. Chem.*, 2012, **50**, 4579–4588.
- 108 M. Q. Zhu, L. Xiang, K. Yang, L. J. Shen, F. Long, J. B. Fan, H. Q. Yi, J. Xiang and M. P. Aldred, *J. Polym. Res.*, 2012, **19**.
- 109 Z. L. Tyrrell, Y. G. Shen and M. Radosz, *Macromolecules*, 2012, **45**, 4809–4817.
- 110 L. F. Xu, Z. Q. Zhang, F. Wang, D. D. Xie, S. Yang, T. Wang, L. J. Feng and C. C. Chu, *J. Colloid Interface Sci.*, 2013, **393**, 174–181.
- 111 G. J. Liu, S. B. Ma, S. K. Li, R. Cheng, F. H. Meng, H. Y. Liu and Z. Y. Zhong, *Biomaterials*, 2010, **31**, 7575–7585.
- 112 M. Gadzinowski and S. Sosnowski, *J. Polym. Sci., Part A: Polym. Chem.*, 2003, **41**, 3750–3760.
- 113 R. Wang, X. L. Hu, J. Yue, W. J. Zhang, L. Y. Cai, Z. G. Xie, Y. B. Huang and X. B. Jing, *J. Mater. Chem. B*, 2013, **1**, 293–301.
- 114 T. Endres, M. Y. Zheng, M. Beck-Broichsitter and T. Kissel, *Int. J. Pharm.*, 2012, **428**, 121–124.
- 115 T. K. Endres, M. Beck-Broichsitter, O. Samsonova, T. Renette and T. H. Kissel, *Biomaterials*, 2011, **32**, 7721–7731.
- 116 L. Zhou, Z. F. Chen, F. F. Wang, X. Q. Yang and B. L. Zhang, *Acta Biomater.*, 2013, **9**, 6019–6031.
- 117 Z. F. Yuan, F. Li, M. Ma, S. X. Cheng and R. X. Zhuo, *J. Appl. Polym. Sci.*, 2011, **121**, 666–674.
- 118 M. Ma, F. Li, X. H. Liu, Z. F. Yuan, F. J. Chen and R. X. Zhuo, *J. Mater. Sci.: Mater. Med.*, 2010, **21**, 2817–2825.
- 119 D. J. Gary, H. Lee, R. Sharma, J. S. Lee, Y. Kim, Z. Y. Cui, D. Jia, V. D. Bowman, P. R. Chipman, L. Wan, Y. Zou, G. Z. Mao, K. Park, B. S. Herbert, S. F. Konieczny and Y. Y. Won, *ACS Nano*, 2011, **5**, 3493–3505.
- 120 W. Zhu, Y. L. Li, L. X. Liu, W. L. Zhang, Y. M. Chen and F. Xi, *J. Biomed. Mater. Res., Part A*, 2011, **96A**, 330–340.
- 121 J. S. Kim and J. H. Youk, *Macromol. Res.*, 2009, **17**, 926–930.
- 122 J. S. Kim, H. J. Jeon, M. S. Park, Y. C. You and J. H. Youk, *Eur. Polym. J.*, 2009, **45**, 1918–1923.
- 123 K. Wang, Y. Liu, W. J. Yi, C. Li, Y. Y. Li, R. X. Zhuo and X. Z. Zhang, *Soft Matter*, 2013, **9**, 692–699.
- 124 Y. F. Du, W. Chen, M. Zheng, F. H. Meng and Z. Y. Zhong, *Biomaterials*, 2012, **33**, 7291–7299.
- 125 K. Van Butsele, S. Cajot, S. Van Vlierberghe, P. Dubruel, C. Passirani, J. P. Benoit, R. Jerome and C. Jerome, *Adv. Funct. Mater.*, 2009, **19**, 1416–1425.
- 126 K. Van Butsele, M. Morille, C. Passirani, P. Legras, J. P. Benoit, S. K. Varshney, R. Jerome and C. Jerome, *Acta Biomater.*, 2011, **7**, 3700–3707.
- 127 R. Liu, D. Li, B. He, X. H. Xu, M. M. Sheng, Y. S. Lai, G. Wang and Z. W. Gu, *J. Controlled Release*, 2011, **152**, 49–56.
- 128 J. Yao, Y. L. Ruan, T. Zhai, J. Guan, G. P. Tang, H. R. Li and S. Dai, *Polymer*, 2011, **52**, 3396–3404.
- 129 S. J. Lee, K. H. Min, H. J. Lee, A. N. Koo, H. P. Rim, B. J. Jeon, S. Y. Jeong, J. S. Heo and S. C. Lee, *Biomacromolecules*, 2011, **12**, 1224–1233.
- 130 T. Thambi, V. G. Deepagan, H. Ko, D. S. Lee and J. H. Park, *J. Mater. Chem.*, 2012, **22**, 22028–22036.
- 131 P. J. Sun, Y. Zhang, L. Q. Shi and Z. H. Gan, *Macromol. Biosci.*, 2010, **10**, 621–631.
- 132 Y. Zhang, P. J. Sun and Z. H. Gan, *Sci. China: Chem.*, 2010, **53**, 519–527.
- 133 H. F. Xu, F. H. Meng and Z. Y. Zhong, *J. Mater. Chem.*, 2009, **19**, 4183–4190.
- 134 R. Cheng, F. H. Meng, S. B. Ma, H. F. Xu, H. Y. Liu, X. B. Jing and Z. Y. Zhong, *J. Mater. Chem.*, 2011, **21**, 19013–19020.
- 135 C. Cheng, H. Wei, J. L. Zhu, C. Chang, H. Cheng, C. Li, S. X. Cheng, X. Z. Zhang and R. X. Zhuo, *Bioconjugate Chem.*, 2008, **19**, 1194–1201.
- 136 C. Kang, E. Kim, H. Baek, K. Hwang, D. Kwak, Y. Kang and E. L. Thomas, *J. Am. Chem. Soc.*, 2009, **131**, 7538–7539.
- 137 Y. L. Su, H. R. Yang, W. X. Shi, H. X. Guo, Y. Zhao and D. J. Wang, *Colloids Surf., A*, 2010, **355**, 158–162.
- 138 Y. L. Su, D. X. Wang, H. R. Yang and D. J. Wang, *Colloids Surf., A*, 2009, **342**, 122–126.
- 139 J. Song, J. W. Choi, E. Lee, J. K. Lee, W. C. Zin and B. K. Cho, *Polymer*, 2010, **51**, 4419–4423.
- 140 G. E. S. Toombes, S. Mahajan, M. Thomas, P. Du, M. W. Tate, S. M. Gruner and U. Wiesner, *Chem. Mater.*, 2008, **20**, 3278–3287.
- 141 G. E. S. Toombes, S. Mahajan, M. Weyland, A. Jain, P. Du, M. Kamperman, S. M. Gruner, D. A. Müller and U. Wiesner, *Macromolecules*, 2008, **41**, 852–859.
- 142 H. J. Niu, L. W. Zhang, M. Y. Gao and Y. M. Chen, *Langmuir*, 2005, **21**, 4205–4210.
- 143 N. Duxin, F. T. Liu, H. Vali and A. Eisenberg, *J. Am. Chem. Soc.*, 2005, **127**, 10063–10069.
- 144 T. Azzam, L. Bronstein and A. Eisenberg, *Langmuir*, 2008, **24**, 6521–6529.
- 145 A. Khanal, K. Nakashima, N. Kawasaki, Y. Oishi, M. Uehara, H. Nakamura and Y. Tajima, *Colloid Polym. Sci.*, 2005, **283**, 1226–1232.
- 146 J. M. Hu, T. Wu, G. Y. Zhang and S. Y. Liu, *J. Am. Chem. Soc.*, 2012, **134**, 7624–7627.
- 147 D. A. Liu, M. Sasidharan and K. Nakashima, *J. Colloid Interface Sci.*, 2011, **358**, 354–359.
- 148 M. Sasidharan, D. Liu, N. Gunawardhana, M. Yoshio and K. Nakashima, *J. Mater. Chem.*, 2011, **21**, 13881–13888.

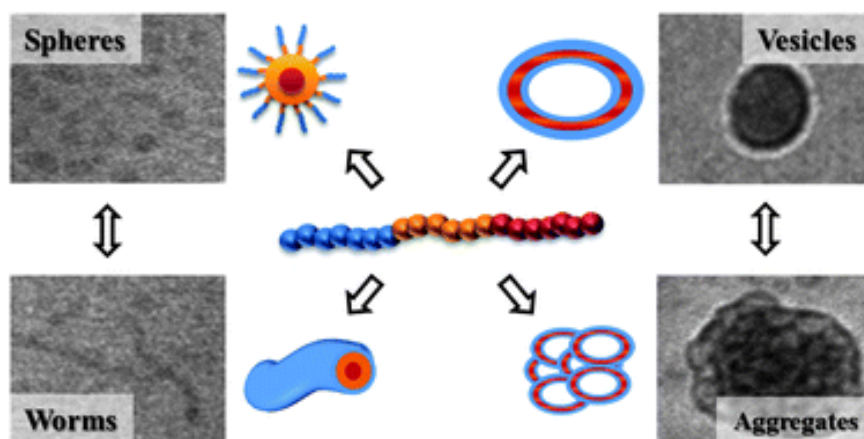
- 149 M. Sasidharan, N. Gunawardhana, H. N. Luitel, T. Yokoi, M. Inoue, S. Yusa, T. Watari, M. Yoshio, T. Tatsumi and K. Nakashima, *J. Colloid Interface Sci.*, 2012, **370**, 51–57.
- 150 B. P. Bastakoti, S. Guragain, Y. Yokoyama, S. Yusa and K. Nakashima, *New J. Chem.*, 2012, **36**, 125–129.
- 151 B. P. Bastakoti, S. Guragain, Y. Yokoyama, S. Yusa and K. Nakashima, *Langmuir*, 2011, **27**, 379–384.
- 152 J. Yao, H. A. Wu, Y. L. Ruan, J. Guan, A. N. Wang and H. R. Li, *Polymer*, 2011, **52**, 793–803.
- 153 J. Xiao, W. Q. Chen, F. Y. K. Wang and J. Z. Du, *Macromolecules*, 2013, **46**, 375–383.



## Publication P2

### Understanding and tuning the self-assembly of polyether-based triblock terpolymers in aqueous Solution

Markus J. Barthel, Ulrich Mansfeld, Stephanie Hoepfner, Justyna A. Czaplewska,  
Felix H. Schacher, Ulrich S. Schubert  
*Soft Matter* **2013**, *9*, 3509-3520.



## Understanding and tuning the self-assembly of polyether-based triblock terpolymers in aqueous solution†

Cite this: *Soft Matter*, 2013, **9**, 3509

Markus J. Barthel,<sup>abc</sup> Ulrich Mansfeld,<sup>abc</sup> Stephanie Hoepfner,<sup>abc</sup>  
Justyna A. Czaplewska,<sup>ab</sup> Felix H. Schacher<sup>\*ab</sup> and Ulrich S. Schubert<sup>\*abc</sup>

The synthesis and self-assembly of well-defined poly(ethylene oxide)-*block*-poly(allyl glycidyl ether)-*block*-poly(*tert*-butyl glycidyl ether) (PEO-*b*-PAGE-*b*-PtBGE) triblock terpolymers with varying block lengths of PAGE and PtBGE are reported. The materials were synthesized using sequential living anionic ring-opening polymerization (AROP). The middle block, PAGE, was further modified by post-polymerization addition of 2,3,4,6-tetra-*O*-acetyl-1-thio- $\beta$ -D-galactopyranose *via* thiol-ene chemistry, resulting in PEO-*b*-PAGE<sub>Gal</sub>-*b*-PtBGE. Self-assembly of the terpolymers in aqueous media resulted in the predominant formation of core-shell-corona architectures and the aggregates featured a PtBGE core, a PAGE shell, and a PEO corona. The structures were investigated using dynamic light scattering (DLS) and cryogenic transmission electron microscopy (cryo-TEM) measurements. In addition, the presence of a PEO corona rendered the formed micellar structures thermo-responsive, as demonstrated using turbidimetry. Depending on the ratio of hydrophilic to hydrophobic segments and on the thermal history of the samples, several micellar morphologies could be identified, including spheres of different size, worm-like structures, and vesicles. More important, both reversible and irreversible structural rearrangements could be identified during the heating-cooling cycles.

Received 5th November 2012  
Accepted 28th January 2013

DOI: 10.1039/c3sm00151b

[www.rsc.org/softmatter](http://www.rsc.org/softmatter)

### Introduction

Nanostructures generated *via* bottom-up self-assembly processes of well-defined macromolecules are of great interest in the fields of polymer science, nanotechnology, and also biomedicine.<sup>1-3</sup> In particular in the latter case, but also in biochemistry or medicine, soft and solution-borne structures, *i.e.* micelles, vesicles, or multicompartiment polymer particles, are discussed regarding potential applications as sensors or delivery vehicles.<sup>4-6</sup> Among many materials investigated, linear ABC triblock terpolymers hold great potential for the controlled formation of core-shell-corona or compartmentalized structures, where either the core or the shell is further subdivided.<sup>2,7,8</sup> Besides typically observed nanostructures from diblock copolymers, which have been investigated in detail, these materials offer a greater diversity of accessible morphologies and the presence of a third segment allows the introduction of

additional functionalities or responsive properties.<sup>9</sup> Concerning their synthesis, controlled/living polymerization techniques are crucial to achieve well-defined triblock terpolymers with respect to molar masses, block structure, block length ratio, and/or the controlled introduction of functional groups at either end of the polymer backbone or within the side chains. One powerful method is living anionic polymerization, enabling the facile synthesis of materials with predictable molar masses, quantitative crossover between individual segments, and highly defined architectures.<sup>10</sup> Regarding possible applications of these polymers in, *e.g.*, biological systems, the materials should be water soluble, non-toxic and chemically inert. All these requirements are fulfilled by poly(ethylene oxide) (PEO) and, partially, by poly(glycidyl ethers) containing additional functionalities in the side chain, for instance, double bonds, hydroxyl groups or furan moieties.<sup>11</sup> For several monomers such as allyl glycidyl ether, 1-ethoxy ethyl glycidyl ether, *N,N'*-dibenzyl amino glycidol, or furfuryl glycidyl ether and combinations thereof, the preparation of well-defined side-chain functionalized polyether materials has already been achieved.<sup>12-16</sup>

One further possibility to tune the solution properties of block copolymers and related materials (or nanostructures) is post-polymerization functionalization, *e.g.*, by thiol-ene reactions involving the pendant double bonds of allyl glycidyl ether segments or Diels-Alder modifications employing the furan groups in the case of furfuryl glycidyl ether.<sup>17-23</sup> These processes

<sup>a</sup>Laboratory of Organic and Macromolecular Chemistry (IOMC), Friedrich-Schiller-University Jena, Humboldtstr. 10, 07743 Jena, Germany. E-mail: [ulrich.schubert@uni-jena.de](mailto:ulrich.schubert@uni-jena.de); [felix.schacher@uni-jena.de](mailto:felix.schacher@uni-jena.de)

<sup>b</sup>Jena Center for Soft Matter (JCSM), Friedrich-Schiller-University Jena, Philosophenweg 7, 07743 Jena, Germany

<sup>c</sup>Dutch Polymer Institute (DPI), John F. Kennedylaan 2, 5612 AB Eindhoven, The Netherlands

† Electronic supplementary information (ESI) available. See DOI: 10.1039/c3sm00151b

enable the incorporation of additional functionality or the block-specific attachment of markers, such as fluorescent dyes. Nevertheless, controlled structure formation or, more precisely, the successful prediction of solution structures generated *via* the self-assembly of triblock terpolymers still remains challenging. Whereas in most studies the volume fractions of the individual segments, the overall block sequence, or the polarity of one or more compartments are varied, recent approaches focus on the influence of the assembly pathway or the kinetic control.<sup>24–26</sup> In particular in the latter case, systematic access to non-equilibrium morphologies with a wide size distribution can be achieved.

This work focuses on the synthesis of a library of ABC triblock terpolymers, poly(ethylene oxide)-*block*-poly(allyl glycidyl ether)-*block*-poly(*tert*-butyl glycidyl ether) (PEO-*b*-PAGE-*b*-PtBGE), *via* sequential living anionic ring-opening polymerization. The materials exhibit a constant length of the first block, PEO (42 repeating units), whereas the lengths of the middle block, PAGE (2 to 17 repeating units), and the last segment, PtBGE (9 to 15 repeating units), were varied. In this way, six different terpolymer compositions were prepared and their behavior in aqueous solution was investigated. In addition, the PAGE segment was further modified using thiol-ene chemistry by the attachment of acetylated thiogalactose. The length of the PAGE block drastically influences the hydrophilic-to-hydrophobic balance of the materials and, hence, the micellar morphology in aqueous media. Among the observed morphologies were spherical, cylindrical, and vesicular aggregates of different size and stability. The terpolymers were analyzed using size exclusion chromatography (SEC), <sup>1</sup>H NMR spectroscopy, turbidimetry, dynamic light scattering (DLS), and cryogenic transmission electron microscopy (cryo-TEM).

## 1 Experimental section

### 1.1 Materials

Monomethoxy poly(ethylene glycol) (PEO-OH) ( $M_n = 2000 \text{ g mol}^{-1}$ ), allyl glycidyl ether, *tert*-butyl glycidyl ether, sodium hydride, 2,2-dimethoxy-2-phenylacetophenone (DMPA), *n*-hexane, *N,N*-dimethylformamide (DMF), toluene, tetrahydrofuran (THF) and ethanol were purchased from Aldrich. 2,3,4,6-Tetra-*O*-acetyl-1-thio- $\beta$ -D-galactopyranose was synthesized as reported previously.<sup>27,28</sup> PEO was dried *via* azeotropic distillation under vacuum from dry toluene. THF and toluene were first dried using a solvent purification system (PureSolv, Innovative Technology) and afterwards freshly distilled from sodium/benzophenone. Allyl glycidyl ether and *t*-butyl glycidyl ether were purified by stirring over calcium hydride for 24 h, followed by distillation under reduced pressure into Schlenk flasks, stored at  $-18 \text{ }^\circ\text{C}$  under an argon atmosphere and were used within three days. Sodium hydride was purified by removing the mineral oil with purified *n*-hexane.

### 1.2 Methods

After the thiol-ene reaction with acetylated thiogalactose, all triblock terpolymers were purified by preparative size exclusion chromatography using Bio-Beads® S-8 (Bio-Rad) in THF.

<sup>1</sup>H NMR spectra were recorded on a Bruker AC 300 MHz using the residual solvent resonance as the internal standard. Size exclusion chromatography was performed on a Shimadzu SCL-10A system (a controller with a LC-10AD pump, a RID-10A refractive index detector and a PL gel 5  $\mu\text{m}$  mixed-D column at  $50 \text{ }^\circ\text{C}$ ). The eluent was a mixture of chloroform : triethylamine : iso-propanol (94 : 4 : 2) with a flow rate of  $1 \text{ mL min}^{-1}$ . The system was calibrated with PEO standards from PSS ( $1470 \text{ g mol}^{-1}$  to  $42\,000 \text{ g mol}^{-1}$ ). Cryo-TEM measurements were carried out on a Philips-CM 120 equipped with a  $1\text{k} \times 1\text{k}$  CCD camera. Sample preparation was performed on Quantifoil grids (R2/2) after plasma cleaning. Vittrification of the samples was carried out in a homebuilt system with a temperature control unit. A drop of the polymer solution ( $5 \mu\text{L}$ ) was placed on a perforated carbon grid (Quantifoil® R2/2) and was blotted as well as subsequently plunged into a cryogen reservoir containing liquid ethane. The samples were afterwards stored in liquid nitrogen and were transferred to the TEM by a Gatan cryo transfer system keeping the temperature below  $-176 \text{ }^\circ\text{C}$  to avoid the formation of crystalline ice layers. Cloud points were determined using a Crystal 16 from Avantium Technologies connected to a chiller (Julabo FP 40) at a wavelength of  $500 \text{ nm}$ . Therefore, polymer solutions with a concentration of  $5 \text{ g L}^{-1}$  were prepared by direct dissolution in water or in THF, followed by addition of a selective solvent (water). DLS was performed at a scattering angle of  $90^\circ$  on an ALV CGS-3 instrument and a He-Ne laser operating at a wavelength of  $\lambda = 633 \text{ nm}$  at  $25 \text{ }^\circ\text{C}$ . The CONTIN algorithm was applied to analyze the obtained correlation functions. Apparent hydrodynamic radii were calculated according to the Stokes-Einstein equation. All CONTIN plots are number-weighted. Samples were prepared as described for the turbidimetry measurements.

### 1.3 Synthesis of PEO-*b*-PAGE-*b*-PtBGE

The following procedure with the respective stoichiometry was used for the synthesis of all triblock terpolymers reported here.

The reaction was performed in a Schlenk flask with argon/vacuum connection.  $3.00 \text{ g}$  ( $1.5 \text{ mmol}$ ) PEO-OH were added to the flask and heated to  $60 \text{ }^\circ\text{C}$ . The melt was evacuated for  $15 \text{ min}$  to remove any traces of water and solvent. Afterwards,  $45 \text{ mg}$  ( $1.88 \text{ mmol}$ ) of sodium hydride (slight excess) were added and the melt was stirred for  $1.5 \text{ h}$  at  $110 \text{ }^\circ\text{C}$ . Then,  $0.36 \text{ mL}$  AGE ( $3.0 \text{ mmol}$ ) were added and the mixture was stirred for  $21 \text{ h}$ . Afterwards,  $3.2 \text{ mL}$  tBGE ( $22.5 \text{ mmol}$ ) were added and the mixture was stirred for  $24 \text{ h}$ . The reaction was terminated by the addition of  $0.2 \text{ mL}$  of a degassed methanol-acetic acid mixture. Eventually remaining monomer was removed under high vacuum and the product (here PEO<sub>42</sub>-*b*-PAGE<sub>2</sub>-*b*-PtBGE<sub>9</sub>) was dried.

Yield:  $6.2 \text{ g}$  ( $98.7\%$ ), <sup>1</sup>H NMR ( $300 \text{ MHz}$ , CDCl<sub>3</sub>,  $\delta$ , ppm):  $1.16$  (s, 9H),  $4.05$ – $3.21$  (m, PEO backbone),  $5.20$  (dd, <sup>3</sup>J<sub>trans</sub> =  $17 \text{ Hz}$ , <sup>3</sup>J =  $11 \text{ Hz}$ , 2H),  $5.87$  (m, 1H). SEC:  $M_n = 2800 \text{ g mol}^{-1}$ ,  $M_w = 2900 \text{ g mol}^{-1}$ , PDI =  $1.04$ .

### 1.4 Thiol-ene modification of PEO-*b*-PAGE-*b*-PtBGE triblock terpolymers

The following procedure with the respective stoichiometry was used for the functionalization of all triblock terpolymers.

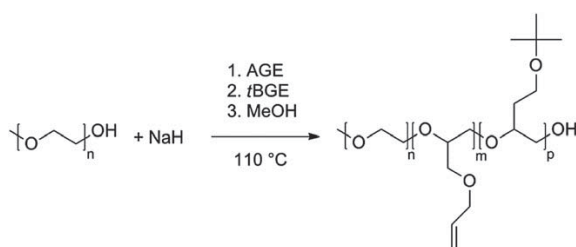
A mixture of 150 mg (corresponding to 0.44 mmol of PAGE) of the triblock terpolymer (PEO<sub>42</sub>-*b*-PAGE<sub>15</sub>-*b*-PtBGE<sub>12</sub>), 22.7 mg (0.088 mmol) of 2,2-dimethoxy-2-phenylacetophenone (DMPA), and 321 mg (0.88 mmol) of 2,3,4,6-tetra-*O*-acetyl-1-thio-β-*D*-galactopyranose was dissolved in 1.5 mL of a DMF : EtOH (3 : 1) mixture. The reaction mixture was degassed and stirred under UV irradiation (366 nm, 6 W) overnight. The increase of the molar mass (*M*<sub>n</sub>) and the decrease of the signal intensity of the peaks of the double bond were monitored by SEC and <sup>1</sup>H NMR, respectively. After 24 h no further conversion of the double bond could be detected, the reaction was stopped, and the reaction mixture was purified by size exclusion chromatography (Biobeads SX-1). The purified product was dried under vacuum.

<sup>1</sup>H NMR (300 MHz, CDCl<sub>3</sub>, δ, ppm): 1.34–1.06 (s, 9H), 1.91–1.65 (m, 2H and H<sub>2</sub>O), 2.21–1.91 (m, 12H), 2.82–2.62 (m, 2H), 3.76–3.24 (m, PEO backbone), 4.18–3.80 (m, 3H, Gal), 4.54–4.43 (m, 1H, Gal), 5.7–4.9 (m, 3H, Gal). SEC: *M*<sub>n</sub> = 3100 g mol<sup>-1</sup>, PDI = 1.03.

## 2 Results and discussion

The synthesis of the triblock terpolymers was carried out using sequential living anionic ring-opening polymerization (AROP) as described previously (Scheme 1).<sup>23</sup>

Briefly, a commercial hydroxyl-terminated PEO-OH (*M*<sub>n</sub> = 2000 g mol<sup>-1</sup>) macroinitiator was activated using sodium hydride and the sequential addition of allyl glycidyl ether (AGE) and *tert*-butyl glycidyl ether (*t*BGE) resulted in the formation of



**Scheme 1** Schematic representation of the synthesis of PEO-*b*-PAGE-*b*-PtBGE triblock terpolymers using sequential living anionic ring-opening polymerization (AROP).

PEO-*b*-PAGE-*b*-PtBGE triblock terpolymers. The materials were characterized by size exclusion chromatography (SEC) and <sup>1</sup>H NMR spectroscopy. We have recently shown that such materials featuring a hydrophilic PEO and two hydrophobic PAGE and PtBGE segments self-assemble in aqueous solution into spherical core-shell-corona micelles (at a certain composition). As the micellar morphology depends crucially on the volume fractions of the constituting segments, our aim here was to study the self-assembly behavior of a triblock terpolymer library with varying compositions. We therefore kept the length of the first block, PEO, constant and added a PAGE segment of 2 to 17 repeating units. For the third block, PtBGE, lengths of 9 and 15 repeating units were chosen, resulting in two triblock terpolymer series, PEO<sub>42</sub>-*b*-PAGE<sub>2/9/17</sub>-*b*-PtBGE<sub>9</sub> and PEO<sub>42</sub>-*b*-PAGE<sub>2/7/15</sub>-*b*-PtBGE<sub>15/14/12</sub>. The subscripts denote the degree of polymerization of the corresponding segments. Exemplarily, the SEC traces for the polymers PEO<sub>42</sub>-*b*-PAGE<sub>2/7/15</sub>-*b*-PtBGE<sub>15/14/12</sub> series are shown in Fig. 1. The SEC traces for PEO<sub>42</sub>-*b*-PAGE<sub>2/9/17</sub>-*b*-PtBGE<sub>9</sub> can be found in Fig. S1.†

In all cases (except for PEO<sub>42</sub>-*b*-PAGE<sub>2</sub>, where only a slight shift could be seen), a significant shift in the SEC elution traces could be observed for the PEO-*b*-PAGE diblock copolymers, as well as for the final triblock terpolymers. Furthermore, all samples exhibit narrow and monomodal distributions (PDI < 1.07). The detailed characterization is also listed in Table 1.

The final compositions were determined using <sup>1</sup>H NMR (Table 1 and Fig. S2†). For samples with a shorter PAGE segment (DP = 2), the obtained block length ratios were in good agreement with the theoretical values, whereas in the case of longer blocks (DP = 20) the conversion of AGE did not reach 100%. We attribute this to a rather slow polymerization rate in the case of AGE, as already observed during earlier studies and in the literature.<sup>23,29</sup> Nevertheless, full crossover to *t*BGE could be achieved, indicating a controlled reaction. Another indication for the successful block formation is that the ratio of PEO:PAGE signals in <sup>1</sup>H NMR is constant if PEO-*b*-PAGE and PEO-*b*-PAGE-*b*-PtBGE materials from the same reaction are compared.

The attachment of side chains *via* post-polymerization modification represents one straightforward possibility to influence the solution behavior of such macromolecules. In our case, this can be easily achieved by thiol-ene chemistry. We therefore attached acetylated galactose to the PAGE

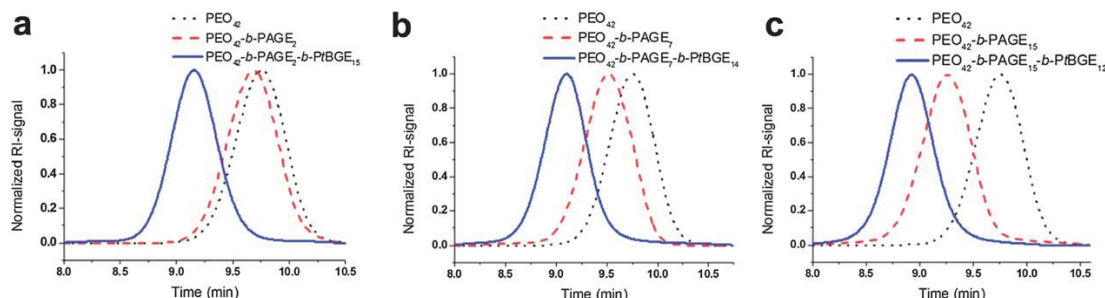
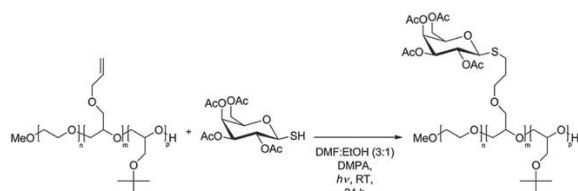


**Fig. 1** SEC traces for PEO<sub>42</sub>-*b*-PAGE<sub>2</sub>-*b*-PtBGE<sub>15</sub> (a), PEO<sub>42</sub>-*b*-PAGE<sub>7</sub>-*b*-PtBGE<sub>14</sub> (b) and PEO<sub>42</sub>-*b*-PAGE<sub>15</sub>-*b*-PtBGE<sub>12</sub> (c) obtained *via* living AROP; PEO macroinitiator (pointed black lines), PEO-*b*-PAGE diblock copolymer (dashed red lines), and PEO-*b*-PAGE-*b*-PtBGE triblock terpolymers (solid blue lines).

**Table 1** Molecular characteristics of the synthesized triblock terpolymers

Sample	$M_{\text{theo}}$ [g mol <sup>-1</sup> ]	$M_n^a$ [g mol <sup>-1</sup> ]	$M_w^a$ [g mol <sup>-1</sup> ]	PDI <sup>a</sup>	Ratio <sub>theo</sub> n/m/p	Ratio <sup>b</sup> n/m/p
PEO <sub>42</sub> - <i>b</i> -PAGE <sub>2</sub> - <i>b</i> -PtBGE <sub>15</sub>	4000	2800	2900	1.04	42/2/15	42/2/15
PEO <sub>42</sub> - <i>b</i> -PAGE <sub>7</sub> - <i>b</i> -PtBGE <sub>14</sub>	4950	2900	3100	1.05	42/10/15	42/7/14
PEO <sub>42</sub> - <i>b</i> -PAGE <sub>15</sub> - <i>b</i> -PtBGE <sub>12</sub>	6100	3400	3500	1.06	42/20/15	42/15/12
PEO <sub>42</sub> - <i>b</i> -PAGE <sub>2</sub> - <i>b</i> -PtBGE <sub>9</sub>	3250	2350	2450	1.05	42/2/9	42/2/9
PEO <sub>42</sub> - <i>b</i> -PAGE <sub>9</sub> - <i>b</i> -PtBGE <sub>9</sub>	4150	2400	2600	1.07	42/10/9	42/9/9
PEO <sub>42</sub> - <i>b</i> -PAGE <sub>17</sub> - <i>b</i> -PtBGE <sub>9</sub>	5300	2950	3150	1.07	42/20/9	42/17/9

<sup>a</sup> Obtained by SEC (CHCl<sub>3</sub> : *i*-Prop. : TEA 94 : 4 : 2, using PEO standards). <sup>b</sup> Determined by <sup>1</sup>H NMR spectroscopy.



**Scheme 2** Schematic representation of the post-polymerization functionalization of PEO-*b*-PAGE-*b*-PtBGE triblock terpolymers by the attachment of acetylated galactose *via* thiol-ene chemistry.

compartment of the as-synthesized triblock terpolymers (Scheme 2). This increases the volume fraction of the hydrophobic middle block, PAGE, but also enables subsequent deprotection of the galactose moieties towards double hydrophilic sugar-modified terpolymers.<sup>30</sup>

The modification reaction was monitored using SEC (Fig. 2) and <sup>1</sup>H NMR (Fig. S3<sup>†</sup>) spectroscopy.

As shown for the triblock terpolymer series with the longer PtBGE block (DP = 15), a significant shift of the SEC traces can be observed for PAGE segments with 7 and 15 repeating units. The increase in molar mass for the short PAGE segments in PEO<sub>42</sub>-PAGE<sub>2</sub>-*b*-PtBGE<sub>15</sub> might be too low to be directly observed in SEC, but the successful modification can nevertheless be confirmed in <sup>1</sup>H NMR spectroscopy. The final degree of functionalization (*f*) was calculated according to the decrease of the double bond signal and the appearance of the sugar signals in the <sup>1</sup>H NMR spectra. The detailed characterization of the obtained triblock terpolymers is shown in Table 2.

It has to be noted that only for the triblock terpolymers containing the PAGE block with the highest DP nearly full conversion could be observed. Even when using a rather long reaction time (3 days) only a degree of functionalization of 40 to 85% could be achieved for the materials with shorter PAGE segments. Our tentative explanation is that different lengths of the PAGE block lead to different solubility of the materials in the solvent mixture used for the thiol-ene reaction. This might cause aggregation, leading to less accessible PAGE domains. Nevertheless, also incomplete degrees of thiol-ene modification influence the solution properties of the materials in aqueous media (selective for the PEO block). Table 3 lists the volume fractions of the as-synthesized and functionalized triblock terpolymers, as determined according to the degrees of polymerization by <sup>1</sup>H NMR.

The attachment of protected thiogalactose to the PAGE segments leads to a significant change of the hydrophilic (PEO)/hydrophobic (PAGE + PtBGE) ratio of the terpolymers. For example, in the case of PEO<sub>42</sub>-*b*-PAGE<sub>15</sub>-*b*-PtBGE<sub>12</sub> the hydrophilic weight fraction decreases from 36% to 17%. As shown earlier, this directly influences the solution properties in aqueous media, *i.e.* the micellar morphology and the temperature-dependent stability of the structures. This can be accessed *via* turbidimetry, thereby probing the lower critical solution temperature (LCST) of the PEO corona chains under these conditions (comparable to spherical brushes).<sup>23</sup> To elucidate this, solutions with a concentration of 5 mg mL<sup>-1</sup> in water were prepared for each sample. As samples containing lower weight fractions of PEO (*e.g.*, PEO<sub>42</sub>-*b*-PAGE<sub>15</sub>-*b*-PtBGE<sub>12</sub> or PEO<sub>42</sub>-*b*-PAGE<sub>17</sub>-*b*-PtBGE<sub>9</sub>) could not be directly dissolved in water, the

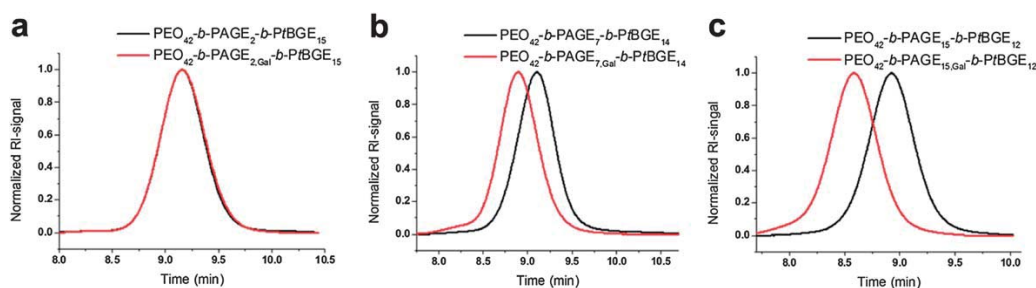


**Fig. 2** SEC traces for the thiol-ene click reaction of acetylated thiogalactose onto the PAGE segment of PEO<sub>42</sub>-*b*-PAGE<sub>2</sub>-*b*-PtBGE<sub>15</sub> (a), PEO<sub>42</sub>-*b*-PAGE<sub>7</sub>-*b*-PtBGE<sub>14</sub> (b) and PEO<sub>42</sub>-*b*-PAGE<sub>15</sub>-*b*-PtBGE<sub>12</sub> (c) triblock copolymers; the elution traces correspond to the starting materials (solid black lines) and the respective modified triblock terpolymers afterwards (solid red lines).



**Table 2** Molecular characteristics of the functionalized triblock terpolymers

Sample	$M_{\text{theo}}$ [g mol <sup>-1</sup> ]	$M_n^a$ [g mol <sup>-1</sup> ]	$M_w^a$ [g mol <sup>-1</sup> ]	PDI <sup>a</sup>	$f^b$ [%]
PEO <sub>42</sub> - <i>b</i> -PAGE <sub>2,Gal</sub> - <i>b</i> -PtBGE <sub>15</sub>	4800	2850	2950	1.03	65
PEO <sub>42</sub> - <i>b</i> -PAGE <sub>7,Gal</sub> - <i>b</i> -PtBGE <sub>14</sub>	7000	3500	3650	1.05	50
PEO <sub>42</sub> - <i>b</i> -PAGE <sub>15,Gal</sub> - <i>b</i> -PtBGE <sub>12</sub>	10 600	4600	4800	1.05	100
PEO <sub>42</sub> - <i>b</i> -PAGE <sub>2,Gal</sub> - <i>b</i> -PtBGE <sub>9</sub>	4000	2400	2500	1.03	85
PEO <sub>42</sub> - <i>b</i> -PAGE <sub>9,Gal</sub> - <i>b</i> -PtBGE <sub>9</sub>	7300	3025	3150	1.04	40
PEO <sub>42</sub> - <i>b</i> -PAGE <sub>17,Gal</sub> - <i>b</i> -PtBGE <sub>9</sub>	11 100	4150	4450	1.08	95

<sup>a</sup> Obtained by SEC (CHCl<sub>3</sub>; *i*-Prop.: TEA 94 : 4 : 2, using PEO standards). <sup>b</sup> Determined by <sup>1</sup>H NMR spectroscopy.

**Table 3** Block ratios before and after post-polymerization functionalization of the polymers

Sample	Volume fraction [%]	Volume fraction after functionalization [%]
PEO <sub>42</sub> - <i>b</i> -PAGE <sub>2</sub> - <i>b</i> -PtBGE <sub>15</sub>	46/6/48	41/16/43
PEO <sub>42</sub> - <i>b</i> -PAGE <sub>7</sub> - <i>b</i> -PtBGE <sub>14</sub>	41/18/41	32/36/32
PEO <sub>42</sub> - <i>b</i> -PAGE <sub>15</sub> - <i>b</i> -PtBGE <sub>12</sub>	36/33/31	17/68/15
PEO <sub>42</sub> - <i>b</i> -PAGE <sub>2</sub> - <i>b</i> -PtBGE <sub>9</sub>	57/7/36	48/22/30
PEO <sub>42</sub> - <i>b</i> -PAGE <sub>9</sub> - <i>b</i> -PtBGE <sub>9</sub>	46/25/29	28/55/17
PEO <sub>42</sub> - <i>b</i> -PAGE <sub>17</sub> - <i>b</i> -PtBGE <sub>9</sub>	37/39/24	17/72/11

materials were first dissolved in a minimum amount of THF (~15 g L<sup>-1</sup>). Afterwards, water was added dropwise until a slightly turbid solution was obtained (approx. 0.5 mL), followed by stirring for further 30 min. Finally, 2.5 mL water was added and the remaining THF was allowed to evaporate.

The temperature-dependent turbidity of the as-prepared samples was measured afterwards within a heating-cooling cycle (heating-cooling rate: 1 K min<sup>-1</sup>). For this purpose, 1 mL of the solution was transferred into a glass vial and heated to 100 °C under vigorous stirring, kept at this temperature for 5 minutes and was afterwards cooled down to 25 °C. This temperature cycle was repeated three times to also study the reversibility of any changes observed (Fig. 3).

As depicted in Fig. 3a and c, the PEO-*b*-PAGE-*b*-PtBGE triblock terpolymers exhibit LCST behavior at elevated temperatures (between 84 and 97 °C). As linear PEO typically shows LCST behavior at temperatures above 100 °C under such conditions, the decrease of the cloud point temperature can be attributed to the presence of the hydrophobic PAGE and PtBGE segments.<sup>31</sup> This is in accordance with our earlier studies.<sup>23</sup> Therefore, longer hydrophobic segments are expected to decrease the cloud point temperature. As depicted in Table 4,

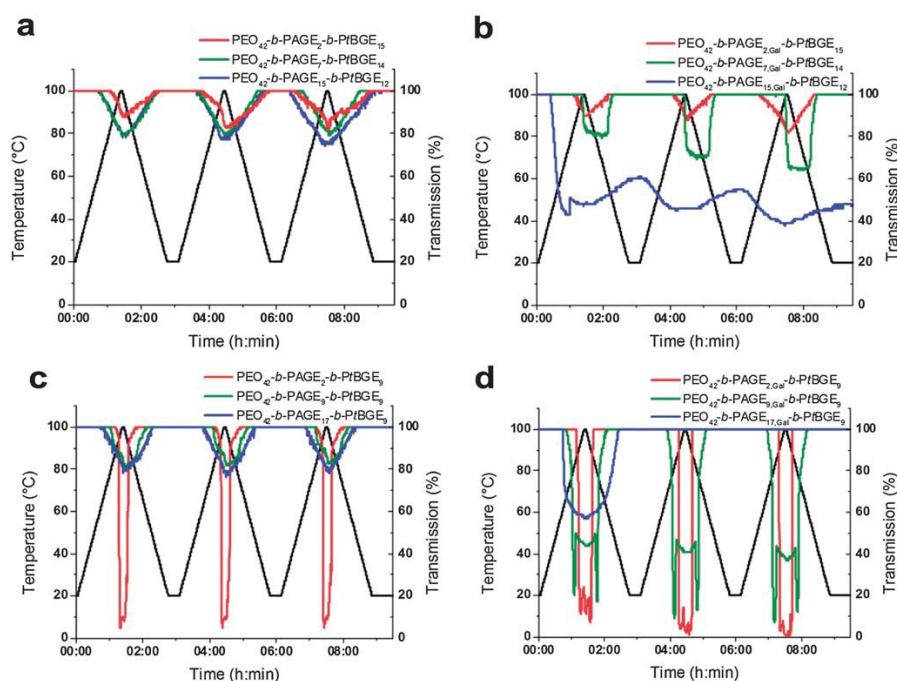


**Fig. 3** Turbidimetry measurements of the as-synthesized (a and c) and galactose-functionalized triblock terpolymers (b and d) at a concentration of 5 mg mL<sup>-1</sup>; in each case three consecutive heating-cooling cycles have been performed.

**Table 4** Cloud point temperatures of the micellar structures before and after post-polymerization functionalization of the triblock terpolymers

Sample	Cloud point	Cloud point after functionalization
PEO <sub>42</sub> - <i>b</i> -PAGE <sub>2</sub> - <i>b</i> -PtBGE <sub>15</sub>	97 °C	98 °C
PEO <sub>42</sub> - <i>b</i> -PAGE <sub>7</sub> - <i>b</i> -PtBGE <sub>14</sub>	85 °C	99 °C
PEO <sub>42</sub> - <i>b</i> -PAGE <sub>15</sub> - <i>b</i> -PtBGE <sub>12</sub>	84 °C	51 °C
PEO <sub>42</sub> - <i>b</i> -PAGE <sub>2</sub> - <i>b</i> -PtBGE <sub>9</sub>	96 °C	91 °C
PEO <sub>42</sub> - <i>b</i> -PAGE <sub>9</sub> - <i>b</i> -PtBGE <sub>9</sub>	88 °C	82 °C
PEO <sub>42</sub> - <i>b</i> -PAGE <sub>17</sub> - <i>b</i> -PtBGE <sub>9</sub>	83 °C	63 °C

the influence of an increasing block length of the hydrophobic PAGE-*b*-PtBGE segment could be observed for both series of the as-synthesized triblock terpolymers. For PEO<sub>42</sub>-*b*-PAGE<sub>2</sub>-*b*-PtBGE<sub>9</sub>, PEO<sub>42</sub>-*b*-PAGE<sub>9</sub>-*b*-PtBGE<sub>9</sub> and PEO<sub>42</sub>-*b*-PAGE<sub>17</sub>-*b*-PtBGE<sub>9</sub>, a decrease of the cloud point temperature from 96 °C to 88 °C to 83 °C could be observed, whereas for PEO<sub>42</sub>-*b*-PAGE<sub>2</sub>-*b*-PtBGE<sub>15</sub>, PEO<sub>42</sub>-*b*-PAGE<sub>7</sub>-*b*-PtBGE<sub>14</sub> and PEO<sub>42</sub>-*b*-PAGE<sub>12</sub>-*b*-PtBGE<sub>15</sub> the values decreased from 97 °C to 85 °C to 84 °C, thereby confirming the assumptions.

A further increase of the hydrophobic weight fractions of the triblock terpolymers *via* attachment of acetylated thiogalactose should result in a decrease of the cloud point temperature in aqueous media. The obtained values are displayed in Table 4 for all investigated materials. In the case of PEO<sub>42</sub>-*b*-PAGE<sub>2,Gal</sub>-*b*-PtBGE<sub>15</sub>, no significant change ( $T_{cl} = 97$  °C and  $T_{cl}' = 98$  °C) could be observed (Fig. 3b, red line). This can be attributed to the rather low length of the PAGE segment and the small fraction of sugar units. A moderate effect was observed for the cloud point temperature of PEO<sub>42</sub>-*b*-PAGE<sub>2,Gal</sub>-*b*-PtBGE<sub>9</sub>, which decreased from 96 °C to 91 °C after functionalization (Fig. 3d, red line). As in this particular case the PtBGE segment is short, the attachment of even small amounts of sugar units has more influence. This effect was even more pronounced for the terpolymers with higher PAGE contents: for PEO<sub>42</sub>-*b*-PAGE<sub>9,Gal</sub>-*b*-PtBGE<sub>9</sub>, a decrease from  $T_{cl} = 88$  °C to  $T_{cl}' = 82$  °C was observed (Fig. 3d, green line), whereas the strongest changes were detected for PEO<sub>42</sub>-*b*-PAGE<sub>17,Gal</sub>-*b*-PtBGE<sub>9</sub> (83 to 63 °C) (Fig. 3d, blue line) and PEO<sub>42</sub>-*b*-PAGE<sub>15,Gal</sub>-*b*-PtBGE<sub>12</sub> (84 to 51 °C) (Fig. 3b, blue line). Slightly different behavior has been observed for PEO<sub>42</sub>-*b*-PAGE<sub>17,Gal</sub>-*b*-PtBGE<sub>9</sub> (Fig. 3d, blue line); a cloud point temperature of 63 °C was observed during the first heating-cooling cycle and the transmission remained at 100% during runs #2 and #3. We tentatively ascribe this to a decreasing turbidity of the sample after being cooled back to room temperature, whereas the initial turbidity of the aqueous solution is used as a reference by the machine.

As can be seen in Fig. 3b, for PEO<sub>42</sub>-*b*-PAGE<sub>15,Gal</sub>-*b*-PtBGE<sub>12</sub> (blue line), the triblock terpolymers with the highest weight fraction of hydrophobic segments, the LCST behavior seems not to be reversible. This may hint at the formation of a different type of micellar morphology or even superstructures during the first heating-cooling cycle. This will be further discussed using DLS and cryo-TEM experiments at the corresponding section of this manuscript. Another exception was observed for PEO<sub>42</sub>-*b*-PAGE<sub>7,Gal</sub>-*b*-PtBGE<sub>14</sub>, where an unusual shift of the cloud point

temperature from 84.5 to 99.7 °C after thiol-ene functionalization could be observed. While the  $T_{cl}$  during the heating is shifted to higher temperatures, the temperature at which re-dissolution occurs during cooling is lowered (Fig. 3b, green curve). We again propose non-reversible aggregation processes to be responsible for this phenomenon, like already considered in the case of (PEO<sub>42</sub>-*b*-PAGE<sub>15,Gal</sub>-*b*-PtBGE<sub>12</sub>). This will be further discussed later using cryo-TEM experiments.

In summary, a decrease of the cloud point temperature with increasing hydrophobicity of the materials can be observed. For the as-synthesized triblock terpolymers a decrease from 96 °C to 83 °C and from 97 °C to 84 °C, respectively, could be measured. The functionalization of the PAGE middle block with thiogalactose has a great impact on the cloud point temperature. Here changes from 84 to 51 °C and from 83 to 63 °C could be observed for the polymers with the highest PAGE content and, hence, the largest hydrophobic weight fraction (PEO<sub>42</sub>-*b*-PAGE<sub>15,Gal</sub>-*b*-PtBGE<sub>12</sub> and PEO<sub>42</sub>-*b*-PAGE<sub>17,Gal</sub>-*b*-PtBGE<sub>9</sub>).

One straightforward method to assess the size of micellar aggregates in solution is dynamic light scattering (DLS). Concerning the materials investigated here, we expect the formation of core-shell-corona architectures. The hydrophobic PtBGE segment is supposed to form the core, covered by a shell of the middle block, PAGE. The hydrophilic corona is formed by the PEO segment, like already observed in earlier studies.<sup>23</sup> We therefore studied aqueous solutions of both triblock terpolymer series (PEO<sub>42</sub>-*b*-PAGE<sub>2-17</sub>-*b*-PtBGE<sub>9-15</sub> before functionalization by thiol-ene chemistry) at concentrations of 5 g L<sup>-1</sup> by DLS (Fig. 4). As the collapse of the PEO segments during the heating-cooling cycles might lead to structural rearrangements and changes in the micellar morphology, each sample has been investigated prior to (solid black lines) and after turbidity measurements (solid red lines).

The hydrodynamic radii for these samples are also listed in Table 5. All triblock terpolymers initially form micelles with hydrodynamic radii in the range of 5 to 10 nm (number-weighted) in aqueous solution at a concentration of 5 g L<sup>-1</sup>.

First, the terpolymer series with the longer core-forming PtBGE block will be discussed. For PEO<sub>42</sub>-*b*-PAGE<sub>2</sub>-*b*-PtBGE<sub>15</sub>, particles with  $\langle R_h \rangle_{n,app} = 6$  nm (Fig. 4a) can be detected initially. This increases to  $\langle R_h \rangle_{n,app} = 9$  nm after three heating-cooling cycles, and a minor fraction of  $\langle R_h \rangle_{n,app} = 18$  nm was found as well (not shown here). We attribute this to the occurrence of an aggregation process and the formation of micellar clusters. Similar results were observed for PEO<sub>42</sub>-*b*-PAGE<sub>7</sub>-*b*-PtBGE<sub>14</sub>. Here, structures with  $\langle R_h \rangle_{n,app} = 5$  nm (Fig. 4b) before, and a bimodal distribution with  $\langle R_h \rangle_{n,app} = 7$  nm and 21 nm can be found after heating. The situation is slightly different for the triblock terpolymer with the highest content of hydrophobic segments, PEO<sub>42</sub>-*b*-PAGE<sub>15</sub>-*b*-PtBGE<sub>12</sub>: in this case a rather distinct increase of the particle size from 7 to 21 nm occurred, and a unimodal distribution is observed. We assume that this corresponds to fusion processes of the initially formed micelles into larger aggregates during the heating process.

The initial micellar size is slightly larger for the terpolymer series with the shorter PtBGE segment ( $\langle R_h \rangle_{n,app} = 7$  to 9 nm, Fig. 4d-f). After three consecutive heating-cooling cycles, no

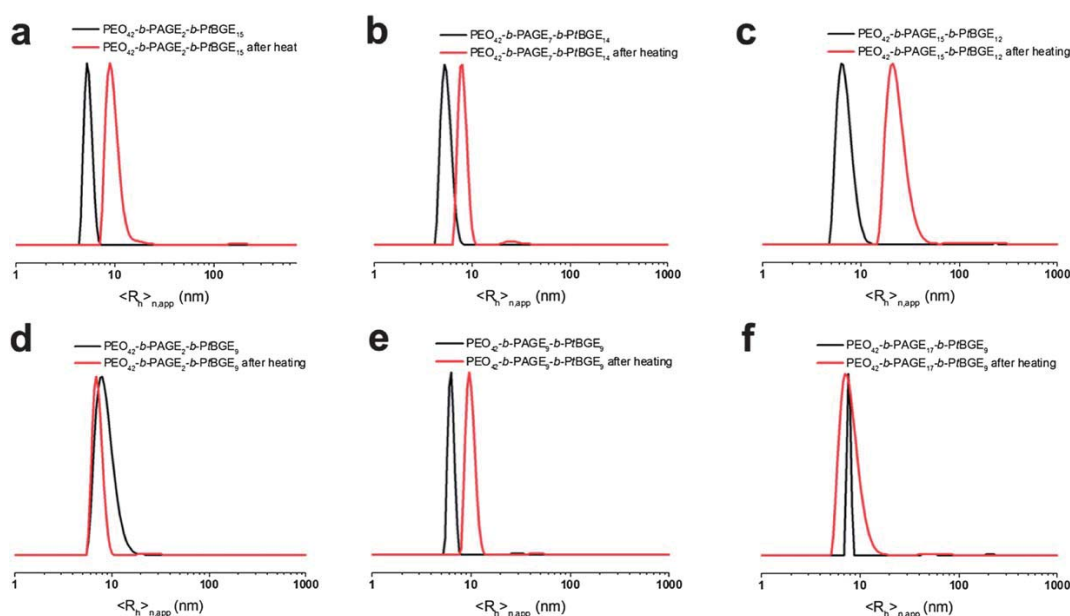


**Fig. 4** DLS CONTIN plots for PEO<sub>42</sub>-b-PAGE<sub>2</sub>-b-PtBGE<sub>15</sub> before (solid black line,  $\langle R_h \rangle_{n,app} = 6$  nm) and after three consecutive heating-cooling cycles (solid red line,  $\langle R_h \rangle_{n,app} = 9$  nm, (a)); PEO<sub>42</sub>-b-PAGE<sub>7</sub>-b-PtBGE<sub>14</sub> before (solid black line,  $\langle R_h \rangle_{n,app} = 5$  nm) and after heating (solid red line,  $\langle R_h \rangle_{n,app} = 7$  nm, (b)); PEO<sub>42</sub>-b-PAGE<sub>15</sub>-b-PtBGE<sub>12</sub> before (solid black line,  $\langle R_h \rangle_{n,app} = 7$  nm) and after heating (solid red line,  $\langle R_h \rangle_{n,app} = 21$  nm, (c)); PEO<sub>42</sub>-b-PAGE<sub>2</sub>-b-PtBGE<sub>9</sub> before (solid black line,  $\langle R_h \rangle_{n,app} = 7$  nm) and after heating (solid red line,  $\langle R_h \rangle_{n,app} = 7$  nm, (d)); PEO<sub>42</sub>-b-PAGE<sub>9</sub>-b-PtBGE<sub>9</sub> before (solid black line,  $\langle R_h \rangle_{n,app} = 7$  nm) and after heating (solid red line,  $\langle R_h \rangle_{n,app} = 10$  nm, (e)); PEO<sub>42</sub>-b-PAGE<sub>17</sub>-b-PtBGE<sub>9</sub> before (solid black line,  $\langle R_h \rangle_{n,app} = 8$  nm) and after heating (solid red line,  $\langle R_h \rangle_{n,app} = 8$  nm, (f)).

significant changes were observed for PEO<sub>42</sub>-b-PAGE<sub>2</sub>-b-PtBGE<sub>9</sub> ( $\langle R_h \rangle_{n,app} = 9$  nm before and 7 nm afterwards, with a second distribution with  $\langle R_h \rangle_{n,app} = 24$  nm). In some cases, while maintaining the radius a broadening or narrowing of the distribution can be observed. For PEO<sub>42</sub>-b-PAGE<sub>9</sub>-b-PtBGE<sub>9</sub> a slight shift from  $\langle R_h \rangle_{n,app} = 7$  nm to  $\langle R_h \rangle_{n,app} = 10$  nm was observed, and a monomodal distribution could be seen (Fig. 4e). This was different for PEO<sub>42</sub>-b-PAGE<sub>17</sub>-b-PtBGE<sub>9</sub>: initially, a bimodal distribution with  $\langle R_h \rangle_{n,app} = 8$  and 50 nm was found (Fig. 4f), whereas after heating a monomodal distribution with  $\langle R_h \rangle_{n,app} = 8$  nm prevailed. This might indicate the formation of non-equilibrium structures in the beginning.

To study if the sample preparation procedure has an influence on the particle size, the triblock terpolymers were directly dissolved in water under stirring for up to 3 days (except for PEO<sub>42</sub>-b-PAGE<sub>15</sub>-b-PtBGE<sub>12</sub> and PEO<sub>42</sub>-b-PAGE<sub>17</sub>-b-PtBGE<sub>9</sub>, where this was not possible). As shown in Table 5, the observed hydrodynamic radii were slightly higher for PEO<sub>42</sub>-b-PAGE<sub>2</sub>-b-PtBGE<sub>15</sub> and PEO<sub>42</sub>-b-PAGE<sub>7</sub>-b-PtBGE<sub>14</sub> and constant in the case of PEO<sub>42</sub>-b-PAGE<sub>2</sub>-b-PtBGE<sub>9</sub> and PEO<sub>42</sub>-b-PAGE<sub>9</sub>-b-PtBGE<sub>9</sub>.

Comparable studies were performed for the materials after the attachment of acetylated thioalactose *via* thiol-ene chemistry (Fig. 5). Again, the terpolymer series comprising the longer PtBGE segment will be discussed first: after preparation of micellar solutions from PEO<sub>42</sub>-b-PAGE<sub>2,Gal</sub>-b-PtBGE<sub>15</sub>, particles with  $\langle R_h \rangle_{n,app} = 8$  nm can be observed, and no significant changes occur during the heating-cooling cycles

**Table 5** DLS data for the as-synthesized triblock terpolymers before and after three consecutive heating-cooling cycles

Sample	Prepared in THF		
	Before heat-treatment $R_h$ [nm]	After heat-treatment $R_h$ [nm]	After direct dissolution in water $R_h$ [nm]
PEO <sub>42</sub> -b-PAGE <sub>2</sub> -b-PtBGE <sub>15</sub>	6	9	8
PEO <sub>42</sub> -b-PAGE <sub>7</sub> -b-PtBGE <sub>14</sub>	5	7	8
PEO <sub>42</sub> -b-PAGE <sub>15</sub> -b-PtBGE <sub>12</sub>	7	21	—
PEO <sub>42</sub> -b-PAGE <sub>2</sub> -b-PtBGE <sub>9</sub>	9	7	8
PEO <sub>42</sub> -b-PAGE <sub>9</sub> -b-PtBGE <sub>9</sub>	7	10	8
PEO <sub>42</sub> -b-PAGE <sub>17</sub> -b-PtBGE <sub>9</sub>	8	8	—

( $\langle R_h \rangle_{n,app} = 9$  nm, Fig. 5a). Also in the case of PEO<sub>42</sub>-b-PAGE<sub>7,Gal</sub>-b-PtBGE<sub>14</sub>, the initially formed particles with  $\langle R_h \rangle_{n,app} = 7$  nm can also be found after the heating treatment, as well as a small fraction of larger aggregates, presumably micellar clusters ( $\langle R_h \rangle_{n,app} = 7$  and 25 nm, Fig. 5b). The situation is different for the triblock terpolymer with the highest weight fraction of hydrophobic segments (PEO<sub>42</sub>-b-PAGE<sub>15,Gal</sub>-b-PtBGE<sub>12</sub>), where significant changes can be observed: at first, micelles with  $\langle R_h \rangle_{n,app} = 8$  nm are formed, which transform into larger aggregates after the heat treatment (Fig. 5c). More precisely, a bimodal distribution with  $\langle R_h \rangle_{n,app} = 30$  and 145 nm is found afterwards. This can be attributed to irreversible aggregation processes, leading to changes in micellar size and, potentially,



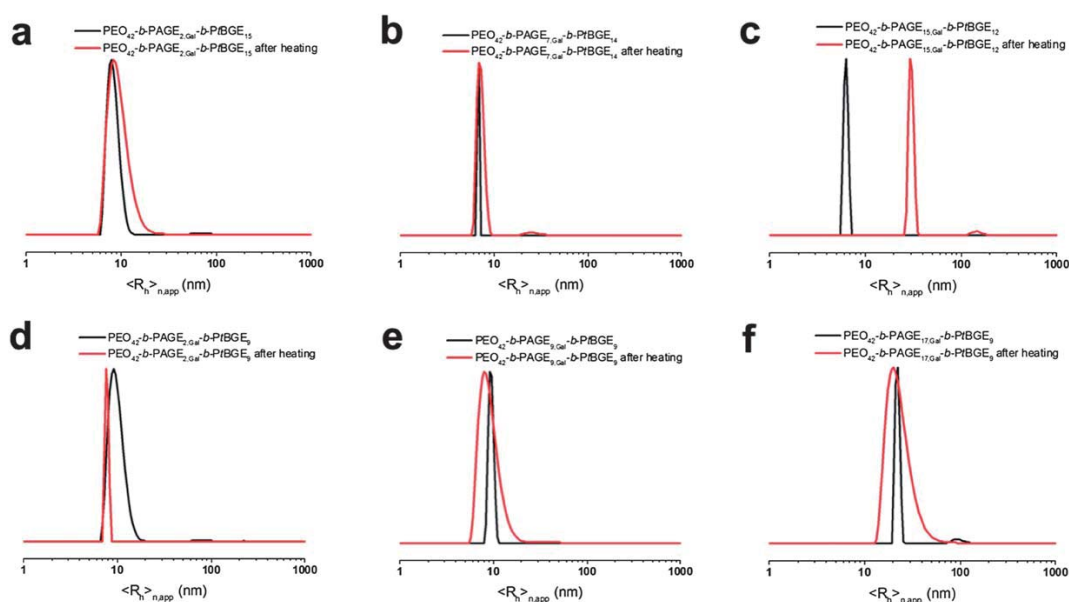


**Fig. 5** Number-weighted DLS CONTIN plots for PEO<sub>42</sub>-b-PAGE<sub>2,Gal</sub>-b-PtBGE<sub>15</sub> before (solid black line,  $\langle R_h \rangle_{n,app} = 8$  nm) and after three consecutive heating-cooling cycles (solid red line,  $\langle R_h \rangle_{n,app} = 9$  nm, (a)); PEO<sub>42</sub>-b-PAGE<sub>7,Gal</sub>-b-PtBGE<sub>14</sub> before (solid black line,  $\langle R_h \rangle_{n,app} = 7$  nm) and after heating (solid red line,  $\langle R_h \rangle_{n,app} = 7$  nm, (b)); PEO<sub>42</sub>-b-PAGE<sub>15,Gal</sub>-b-PtBGE<sub>12</sub> before (solid black line,  $\langle R_h \rangle_{n,app} = 8$  nm) and after heating (solid red line,  $\langle R_h \rangle_{n,app} = 30$  nm, (c)); PEO<sub>42</sub>-b-PAGE<sub>2,Gal</sub>-b-PtBGE<sub>9</sub> before (solid black line,  $\langle R_h \rangle_{n,app} = 10$  nm) and after heating (solid red line,  $\langle R_h \rangle_{n,app} = 8$  nm, (d)); PEO<sub>42</sub>-b-PAGE<sub>9,Gal</sub>-b-PtBGE<sub>9</sub> before (solid black line,  $\langle R_h \rangle_{n,app} = 9$  nm) and after heating (solid red line,  $\langle R_h \rangle_{n,app} = 9$  nm, (e)); and PEO<sub>42</sub>-b-PAGE<sub>17,Gal</sub>-b-PtBGE<sub>9</sub> before (solid black line,  $\langle R_h \rangle_{n,app} = 21$  nm) and after heating (solid red line,  $\langle R_h \rangle_{n,app} = 24$  nm, (f)).

morphology. This observation corresponds to the data obtained in turbidimetry measurements (see also Fig. 3).

For the terpolymer series with the shorter PtBGE core-forming block the same behavior was observed. In the case of PEO<sub>42</sub>-b-PAGE<sub>2,Gal</sub>-b-PtBGE<sub>9</sub>, a slight decrease of the particle size was found, from  $\langle R_h \rangle_{n,app} = 10$  to 8 nm (Fig. 5d). No significant changes were observed for PEO<sub>42</sub>-b-PAGE<sub>9,Gal</sub>-b-PtBGE<sub>9</sub>, as both before and after the heating-cooling cycles aggregates with  $\langle R_h \rangle_{n,app} = 9$  nm were present (Fig. 5e). Again, the situation was different for the sample with the highest weight fraction of hydrophobic blocks (of this series): PEO<sub>42</sub>-b-PAGE<sub>17,Gal</sub>-b-PtBGE<sub>9</sub> already forms larger particles with a bimodal distribution ( $\langle R_h \rangle_{n,app} = 21$  and 92 nm) at RT (Fig. 5f). During heating, an equilibration process seems to take place, as afterwards a unimodal distribution with  $\langle R_h \rangle_{n,app} = 24$  nm was detected. This is in accordance with the results obtained for the as-synthesized sample, PEO<sub>42</sub>-b-PAGE<sub>17</sub>-b-PtBGE<sub>9</sub> (Table 6).

While DLS measurements are a powerful tool to assess the average size and dynamics of micellar aggregates in solution, a detailed assignment of the involved morphologies requires further information. A straightforward and elegant tool to achieve this is cryo-TEM. Thereby, the self-assembled structures of individual macromolecules can be (ideally) visualized without drying artifacts in, typically, aqueous media.<sup>32–34</sup> Due to a rather time consuming sample preparation we focused only on the triblock terpolymer series with the longer core-forming PtBGE segment for cryo-TEM investigations.

First, the samples before modification by thiol-ene chemistry were investigated (Fig. 6). It can be clearly seen that all

**Table 6** DLS data for the triblock terpolymers after modification via thiol-ene chemistry before and after heat treatment

Sample	Before heat-treatment N [nm]	After heat-treatment N [nm]
PEO <sub>42</sub> -b-PAGE <sub>2,Gal</sub> -b-PtBGE <sub>15</sub>	8	9
PEO <sub>42</sub> -b-PAGE <sub>7,Gal</sub> -b-PtBGE <sub>14</sub>	7	7
PEO <sub>42</sub> -b-PAGE <sub>15,Gal</sub> -b-PtBGE <sub>12</sub>	8	30
PEO <sub>42</sub> -b-PAGE <sub>2,Gal</sub> -b-PtBGE <sub>9</sub>	10	8
PEO <sub>42</sub> -b-PAGE <sub>9,Gal</sub> -b-PtBGE <sub>9</sub>	9	9
PEO <sub>42</sub> -b-PAGE <sub>17,Gal</sub> -b-PtBGE <sub>9</sub>	21	24

materials of this series, PEO<sub>42</sub>-b-PAGE<sub>2</sub>-b-PtBGE<sub>15</sub> (Fig. 6a), PEO<sub>42</sub>-b-PAGE<sub>7</sub>-b-PtBGE<sub>14</sub> (Fig. 6b), and PEO<sub>42</sub>-b-PAGE<sub>15</sub>-b-PtBGE<sub>12</sub> (Fig. 6c), form small spherical micelles of 10 to 20 nm diameter, confirming the results obtained by DLS. For all three cases, the initially proposed micellar morphology, *i.e.* a PtBGE core, a PAGE shell, and a PEO corona, can be assumed. This is also depicted in the upper part of Fig. 8.

After the heating-cooling cycles, no changes in size or morphology could be seen according to cryo-TEM for PEO<sub>42</sub>-b-PAGE<sub>2</sub>-b-PtBGE<sub>15</sub> (Fig. 6d). For PEO<sub>42</sub>-b-PAGE<sub>7</sub>-b-PtBGE<sub>14</sub>, a bimodal distribution has been indicated by DLS measurements. In the cryo-TEM image (Fig. 6e), mainly spherical micelles of approximately 10 nm diameter could be detected, but also a few larger aggregates are present with sizes of 20 to 30 nm. Presumably, the heating of the solution above the cloud point

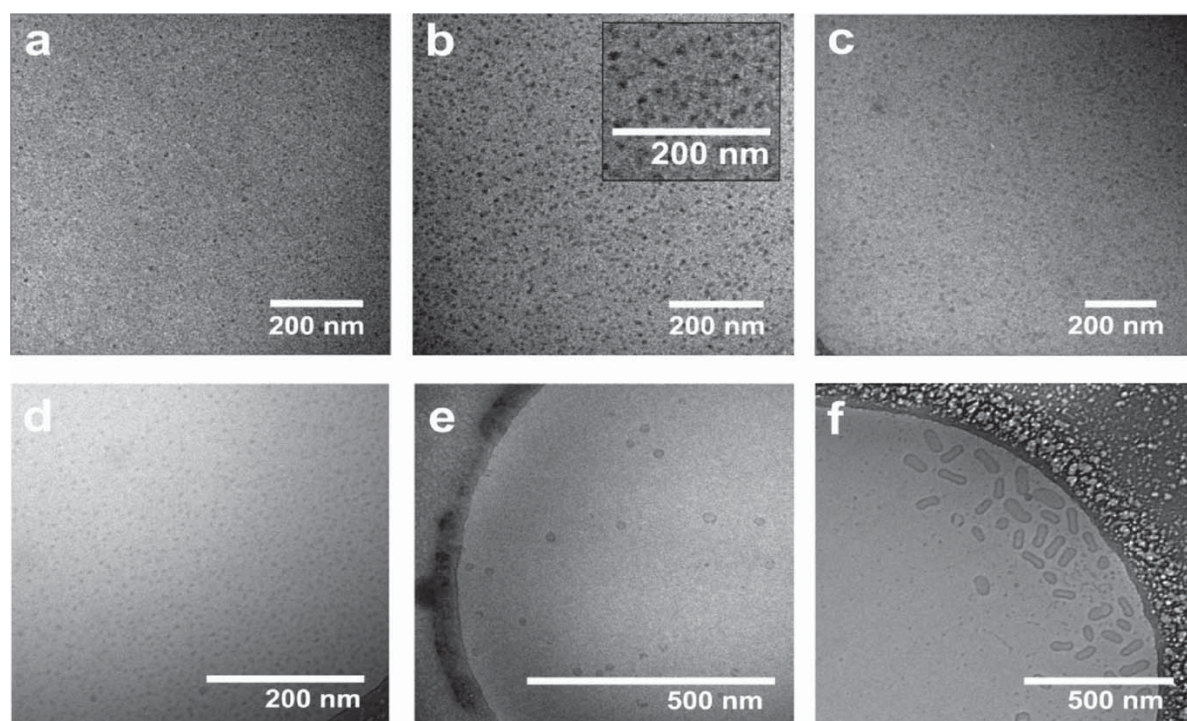


**Fig. 6** Cryo-TEM measurements of the as-synthesized triblock terpolymers before (a; PEO<sub>42</sub>-*b*-PAGE<sub>2</sub>-*b*-PtBGE<sub>15</sub>; b; PEO<sub>42</sub>-*b*-PAGE<sub>7</sub>-*b*-PtBGE<sub>14</sub>; and c; PEO<sub>42</sub>-*b*-PAGE<sub>15</sub>-*b*-PtBGE<sub>12</sub>) and after heating (d; PEO<sub>42</sub>-*b*-PAGE<sub>2</sub>-*b*-PtBGE<sub>15</sub>; e; PEO<sub>42</sub>-*b*-PAGE<sub>7</sub>-*b*-PtBGE<sub>14</sub>; and f; PEO<sub>42</sub>-*b*-PAGE<sub>15</sub>-*b*-PtBGE<sub>12</sub>) at a concentration of 5 mg mL<sup>-1</sup>.

temperature of PEO leads to the formation of a small fraction of vesicles. This is even more pronounced for PEO<sub>42</sub>-*b*-PAGE<sub>15</sub>-*b*-PtBGE<sub>12</sub> (Fig. 6f). DLS already demonstrated a threefold increase of the hydrodynamic radius after heating and this can be clearly seen in the cryo-TEM micrographs. A mixture of spherical micelles (*ca.* 10 to 15 nm diameter), worm-like micelles (thickness of *ca.* 10 to 15 nm), cylindrical vesicular structures (width 30 to 40 nm, lengths up to 100 nm), and vesicular aggregates with a diameter of 40 to 50 nm can be seen. Also worm-like structures (lengths up to 100 nm) derived from

the degradation of the vesicles can be found. Fig. 7 presents a higher magnification of the respective sample area, including spherical micelles, cylindrical structures, and two examples where the formation of vesicles from cylindrical intermediates can be observed. These findings are in good agreement with the results obtained by DLS.

Mainly, the as-synthesized PEO-*b*-PAGE-*b*-PtBGE triblock terpolymers with a long PtBGE segment form spherical core-shell-corona micelles in aqueous media. Heating above the cloud point temperature induces small changes for PEO<sub>42</sub>-*b*-PAGE<sub>2</sub>-*b*-PtBGE<sub>15</sub> (cluster formation), rearrangements into a

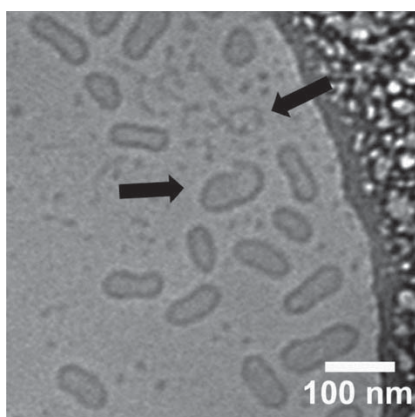


**Fig. 7** Higher magnification of a cryo-TEM micrograph for PEO<sub>42</sub>-*b*-PAGE<sub>15</sub>-*b*-PtBGE<sub>12</sub> after heating at a concentration of 5 mg mL<sup>-1</sup>.

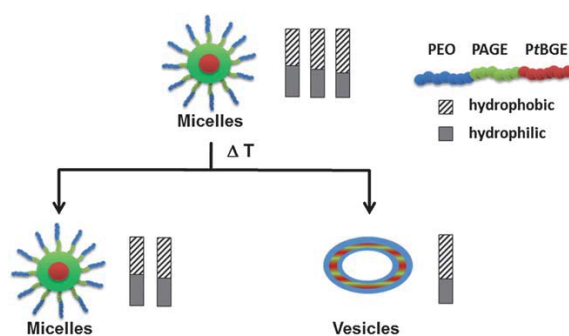


**Fig. 8** Schematic representation of the self-assembly behavior of the as-synthesized triblock terpolymers; color code: PEO (blue), PAGE (green), and PtBGE (red); the ratio of hydrophilic/hydrophobic blocks is schematically shown by the corresponding bars (grey = hydrophilic, black/white stripes = hydrophobic).



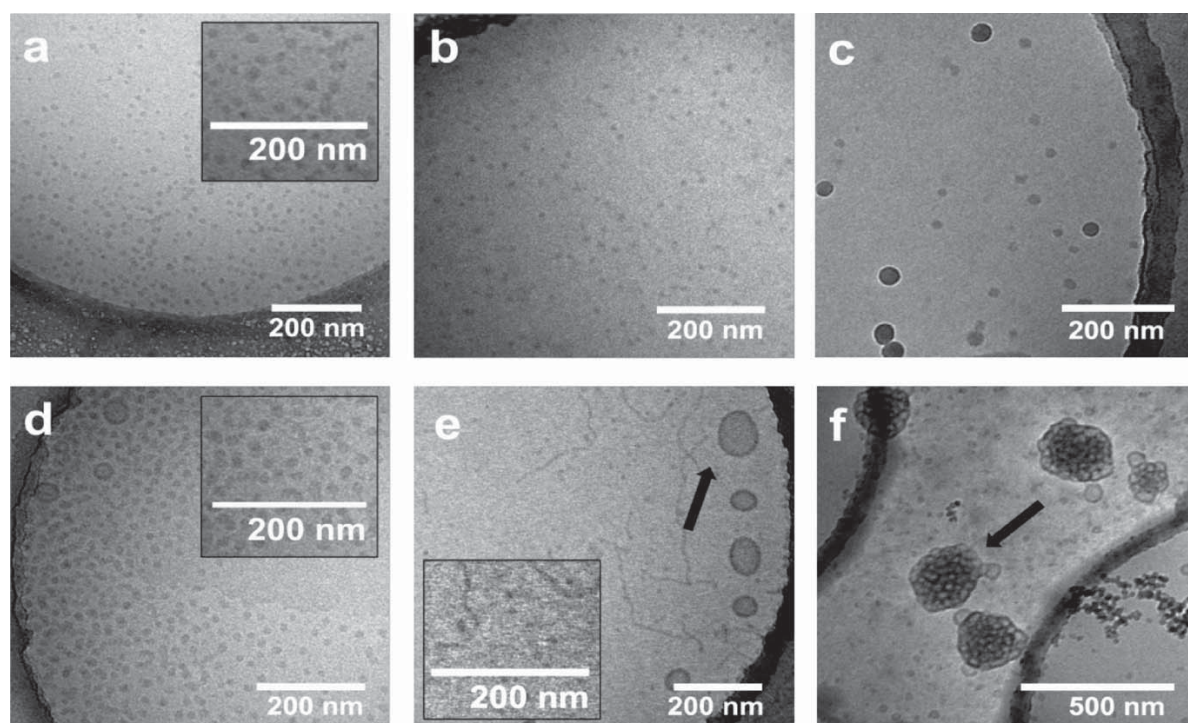


**Fig. 9** Cryo-TEM measurements of the triblock terpolymers after the attachment of thiogalactose before (a; PEO<sub>42</sub>-*b*-PAGE<sub>2,Gal</sub>-*b*-PtBGE<sub>15</sub>; b; PEO<sub>42</sub>-*b*-PAGE<sub>7,Gal</sub>-*b*-PtBGE<sub>14</sub>; and c; PEO<sub>42</sub>-*b*-PAGE<sub>15,Gal</sub>-*b*-PtBGE<sub>12</sub>) and after heating (d; PEO<sub>42</sub>-*b*-PAGE<sub>2,Gal</sub>-*b*-PtBGE<sub>15</sub>; e; PEO<sub>42</sub>-*b*-PAGE<sub>7,Gal</sub>-*b*-PtBGE<sub>14</sub>; and f; PEO<sub>42</sub>-*b*-PAGE<sub>15,Gal</sub>-*b*-PtBGE<sub>12</sub>) at a concentration of 5 mg mL<sup>-1</sup>.

small fraction of vesicles for PEO<sub>42</sub>-*b*-PAGE<sub>7</sub>-*b*-PtBGE<sub>14</sub>, and, most significant, the formation of worms and vesicles for PEO<sub>42</sub>-*b*-PAGE<sub>15</sub>-*b*-PtBGE<sub>12</sub>. This is also depicted in Fig. 8, the bars next to the different micellar morphologies represent the hydrophilic/hydrophobic ratio (block volume fractions) of the respective triblock terpolymer sample (same accounts for Fig. 10).

As already indicated by DLS measurements, the modification of the PAGE segment by the attachment of thiogalactose directly influences the solution behavior of the triblock terpolymers. To compare the morphologies obtained for the terpolymer series with the longer PtBGE segment before and after thiol-ene modification, the respective samples (PEO<sub>42</sub>-*b*-PAGE<sub>2,Gal</sub>-*b*-PtBGE<sub>15</sub>, PEO<sub>42</sub>-*b*-PAGE<sub>7,Gal</sub>-*b*-PtBGE<sub>14</sub>, and PEO<sub>42</sub>-*b*-PAGE<sub>15,Gal</sub>-*b*-PtBGE<sub>12</sub>) were also investigated using cryo-TEM measurements before and after heating-cooling cycles (Fig. 9).

Micellar solutions from PEO<sub>42</sub>-*b*-PAGE<sub>2,Gal</sub>-*b*-PtBGE<sub>15</sub> did not show significant changes in the particle size, as shown *via* DLS measurements (Fig. 5a). This can also be confirmed by the cryo-TEM images (Fig. 9a and d) before and after heating. Furthermore, a small fraction of vesicular structures was obtained afterwards. The behavior was different in the case of PEO<sub>42</sub>-*b*-PAGE<sub>7,Gal</sub>-*b*-PtBGE<sub>14</sub>, where a homogeneous distribution of spherical micelles can be observed initially, but worm-like structures and vesicles are predominant afterwards. We ascribe this to the increase of the hydrophobic weight fractions from 59 to 68% *via* thiol-ene chemistry, presumably crossing the transition point from spherical micelles to larger structures. For the sample with the highest content of PAGE (PEO<sub>42</sub>-*b*-PAGE<sub>15,Gal</sub>-*b*-PtBGE<sub>12</sub>), light scattering pointed towards larger structures (30 nm) being formed after heating. As shown *via* cryo-TEM (Fig. 9c and f), vesicles of a rather broad size distribution are formed initially, which agglomerate to larger clusters while heating. Further, this process seems to be irreversible, taking

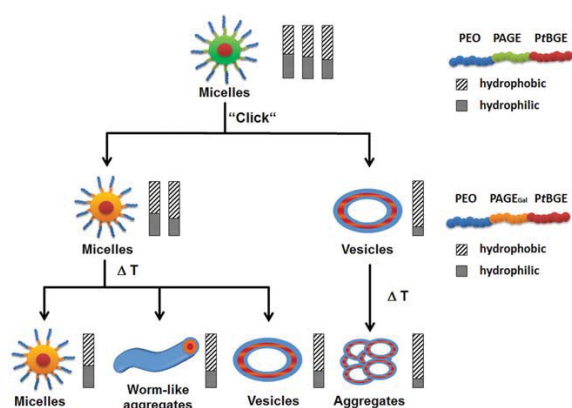


**Fig. 10** Schematic representation of the self-assembly behavior of the galactose-functionalized triblock terpolymers; color code: PEO (blue), PAGE<sub>Gal</sub> (orange), and PtBGE (red); the ratio of hydrophilic/hydrophobic blocks is schematically shown by the corresponding bars (grey = hydrophilic, black/white stripes = hydrophobic).

into account that the solution remained highly turbid during the turbidimetry measurements. The self-assembly behavior of the three described PEO-*b*-PAGE<sub>Gal</sub>-*b*-PtBGE triblock terpolymers before and after heat-treatment is also depicted in Fig. 10. Initially, spherical micelles are formed in all cases. After modification *via* thiol-ene chemistry, PEO<sub>42</sub>-*b*-PAGE<sub>2,Gal</sub>-*b*-PtBGE<sub>15</sub> and PEO<sub>42</sub>-*b*-PAGE<sub>7,Gal</sub>-*b*-PtBGE<sub>14</sub> still form spherical micelles, whereas vesicular structures are found for PEO<sub>42</sub>-*b*-PAGE<sub>15,Gal</sub>-*b*-PtBGE<sub>12</sub>. Heating above the cloud point does not change the morphology for PEO<sub>42</sub>-*b*-PAGE<sub>2,Gal</sub>-*b*-PtBGE<sub>15</sub>, whereas cylindrical micelles and vesicles are formed in the case of PEO<sub>42</sub>-*b*-PAGE<sub>7,Gal</sub>-*b*-PtBGE<sub>14</sub>. The vesicles found for PEO<sub>42</sub>-*b*-PAGE<sub>15,Gal</sub>-*b*-PtBGE<sub>12</sub>, on the other hand, aggregate and form clusters of multiple individual particles.

### 3 Conclusion

The precise prediction of micellar morphologies from amphiphilic triblock terpolymers in aqueous solution remains challenging due to a high number of influential parameters. Our aim was to use a small library of six samples of PEO-*b*-PAGE-*b*-PtBGE triblock terpolymers with varying degrees of polymerization for the hydrophobic segments (PAGE, PtBGE) to screen the formation of different morphologies. In addition, the successful attachment of acetylated thiogalactose by thiol-ene chemistry to the PAGE domains further increased the weight fraction of the hydrophobic parts, resulting in materials with 12 different compositions.

Clearly, the mere weight fraction of hydrophobic segments has a strong influence, as the terpolymers with only 17 wt% PEO could not be directly dissolved in water. To analyze the structure, temperature-dependent solubility, and potential dynamics, a combination of turbidimetry, DLS and cryo-TEM measurements was employed. As expected, the increase of the hydrophobic fractions was accompanied by decreasing cloud points. Furthermore, heat-induced transformations from spherical micelles to worm-like and vesicular structures (PEO<sub>42</sub>-*b*-PAGE<sub>15</sub>-*b*-PtBGE<sub>12</sub>, PEO<sub>42</sub>-*b*-PAGE<sub>7,Gal</sub>-*b*-PtBGE<sub>14</sub>, and in parts PEO<sub>42</sub>-*b*-PAGE<sub>2,Gal</sub>-*b*-PtBGE<sub>15</sub>) were found. In one particular case, the direct formation of vesicular aggregates (PEO<sub>42</sub>-*b*-PAGE<sub>15,Gal</sub>-*b*-PtBGE<sub>12</sub>) has been observed.

We believe that our results contribute to a comprehensive understanding of the solution self-assembly of amphiphilic triblock terpolymers, at least concerning polyether-based materials of rather low molar mass – if compared to most ternary systems made by anionic polymerization. This enables the formation of well-defined and functionalized micellar structures of rather small size with diameters from 10 to 30 nm. Such particles (as well as vesicles) are of particular interest for biomedical applications, where combinations of a hydrophobic core, a biocompatible corona, and a shell, which can be potentially functionalized, are targeted. In the future, the influence of the deprotection of the acetylated thiogalactose on the solution properties of the terpolymers will be investigated. With regard to a possible biomedical application as, *e.g.*, drug carriers, bio tests of the terpolymer series will also be performed.

### Acknowledgements

The authors thank S. Crotty for MALDI-TOF MS measurements and K. Babiuch for support during the thiol-ene click reactions. Furthermore the authors wish to acknowledge the Dutch Polymer Institute (DPI, technology area HTE, project #690) and the Thuringian Ministry for Education, Science and Culture (TMBWK, grant #B514-09051, NanoConSens) for financial support of this study. F. H. S. is grateful to the Thuringian Ministry for Education, Science, and Culture (TMBWK, grant #B515-10065, ChaPoNano) and the “Fonds der chemischen Industrie” (FCI) for financial support.

### References

- 1 S. Grund, M. Bauer and D. Fischer, *Adv. Eng. Mater.*, 2011, **13**, B61–B87.
- 2 F. H. Schacher, P. A. Rupa and I. Manners, *Angew. Chem., Int. Ed.*, 2012, **51**, 7898–7921.
- 3 G. Riess, *Prog. Polym. Sci.*, 2003, **28**, 1107–1170.
- 4 G. S. Kwon and K. Kataoka, *Adv. Drug Delivery Rev.*, 1995, **16**, 295–309.
- 5 D. E. Discher and A. Eisenberg, *Science*, 2002, **297**, 967–973.
- 6 G. Gaucher, M. H. Dufresne, V. P. Sant, N. Kang, D. Maysinger and J. C. Leroux, *J. Controlled Release*, 2005, **109**, 169–188.
- 7 A. O. Moughton, M. A. Hillmyer and T. P. Lodge, *Macromolecules*, 2012, **45**, 2–19.
- 8 F. Schacher, A. Walther, M. Ruppel, M. Drechsler and A. H. E. Müller, *Macromolecules*, 2009, **42**, 3540–3548.
- 9 E. Betthausen, M. Drechsler, M. Förtsch, F. H. Schacher and A. H. E. Müller, *Soft Matter*, 2011, **7**, 8880–8891.
- 10 D. Baskaran and A. H. E. Müller, *Prog. Polym. Sci.*, 2007, **32**, 173–219.
- 11 C. Mangold, F. Wurm and H. Frey, *Polym. Chem.*, 2012, **3**, 1714–1721.
- 12 B. Obermeier, F. Wurm, C. Mangold and H. Frey, *Angew. Chem., Int. Ed.*, 2011, **50**, 7988–7997.
- 13 P. Dimitrov, S. Rangelov, A. Dworak and C. B. Tsvetanov, *Macromolecules*, 2004, **37**, 1000–1008.
- 14 M. Backes, L. Messenger, A. Mourran, H. Keul and M. Möller, *Macromolecules*, 2010, **43**, 3238–3248.
- 15 B. F. Lee, M. J. Kade, J. A. Chute, N. Gupta, L. M. Campos, G. H. Fredrickson, E. J. Kramer, N. A. Lynd and C. J. Hawker, *J. Polym. Sci., Part A: Polym. Chem.*, 2011, **49**, 4498–4504.
- 16 A. A. Toy, S. Reinicke, A. H. E. Müller and H. Schmalz, *Macromolecules*, 2007, **40**, 5241–5244.
- 17 J. C. Persson and P. Jannasch, *Chem. Mater.*, 2006, **18**, 3096–3102.
- 18 J. N. Hunt, K. E. Feldman, N. A. Lynd, J. Deek, L. M. Campos, J. M. Spruell, B. M. Hernandez, E. J. Kramer and C. J. Hawker, *Adv. Mater.*, 2011, **23**, 2327–2331.
- 19 F. Özdemir, H. Keul, A. Mourran and M. Möller, *Macromol. Rapid Commun.*, 2011, **32**, 1007–1013.

- 20 Y. Koyama, M. Umehara, A. Mizuno, M. Itaba, T. Yasukouchi, K. Natsume, A. Suginaka and K. Watanabe, *Bioconjugate Chem.*, 1996, **7**, 298–301.
- 21 M. J. Barthel, T. Rudolph, S. Crotty, F. H. Schacher and U. S. Schubert, *J. Polym. Sci., Part A: Polym. Chem.*, 2012, **50**, 4958–4965.
- 22 B. Obermeier and H. Frey, *Bioconjugate Chem.*, 2011, **22**, 436–444.
- 23 M. J. Barthel, K. Babiuch, T. Rudolph, J. Vitz, S. Hoepfner, M. Gottschaldt, M. D. Hager, F. H. Schacher and U. S. Schubert, *J. Polym. Sci., Part A: Polym. Chem.*, 2012, **50**, 2914–2923.
- 24 H. G. Cui, Z. Y. Chen, S. Zhong, K. L. Wooley and D. J. Pochan, *Science*, 2007, **317**, 647–650.
- 25 R. C. Hayward and D. J. Pochan, *Macromolecules*, 2010, **43**, 3577–3584.
- 26 A. H. Gröschel, F. H. Schacher, H. Schmalz, O. V. Borisov, E. B. Zhulina, A. Walther and A. H. E. Müller, *Nat. Commun.*, 2012, **3**, 710.
- 27 M. Gottschaldt, D. Koth, D. Mueller, I. Klette, S. Rau, H. Goerls, B. Schafer, R. P. Baum and S. Yano, *Chem.–Eur. J.*, 2007, **13**, 10273–10280.
- 28 F. M. Ibatullin, K. A. Shabalin, J. V. Janis and A. G. Shavva, *Tetrahedron Lett.*, 2003, **44**, 7961–7964.
- 29 M. Hruby, C. Konak and K. Ulbrich, *J. Appl. Polym. Sci.*, 2005, **95**, 201–211.
- 30 K. Kempe, C. Weber, K. Babiuch, M. Gottschaldt, R. Hoogenboom and U. S. Schubert, *Biomacromolecules*, 2011, **12**, 2591–2600.
- 31 S. Saeki, N. Kuwahara, M. Nakata and M. Kaneko, *Polymer*, 1976, **17**, 685–689.
- 32 H. Cui, T. K. Hodgdon, E. W. Kaler, L. Abezgauz, D. Danino, M. Lubovsky, Y. Talmon and D. J. Pochan, *Soft Matter*, 2007, **3**, 945–955.
- 33 S. J. Holder and N. A. J. M. Sommerdijk, *Polym. Chem.*, 2011, **2**, 1018–1028.
- 34 S. Zhong and D. J. Pochan, *Polym. Rev.*, 2010, **50**, 287–320.

# Supporting information for

## “Understanding and Tuning the Self-Assembly of Polyether-based Triblock Terpolymers in Aqueous Solution”

Markus J. Barthel,<sup>1,2,3</sup> Ulrich Mansfeld,<sup>1,2,3</sup> Stephanie Hoepfener,<sup>1,2,3</sup> Justyna Czaplewska,<sup>1,2</sup> Felix H. Schacher,<sup>1,2\*</sup> and Ulrich S. Schubert<sup>1,2,3\*</sup>

<sup>1</sup> Laboratory of Organic and Macromolecular Chemistry (IOMC), Friedrich-Schiller-University Jena, Humboldtstr. 10, 07743 Jena, Germany.

<sup>2</sup> Jena Center for Soft Matter (JCSM), Friedrich-Schiller-University Jena, Philosophenweg 7, 07743 Jena, Germany.

<sup>3</sup> Dutch Polymer Institute (DPI), John F. Kennedylaan 2, 5612 AB Eindhoven, The Netherlands.

Email: [ulrich.schubert@uni-jena.de](mailto:ulrich.schubert@uni-jena.de); [felix.schacher@uni-jena.de](mailto:felix.schacher@uni-jena.de);

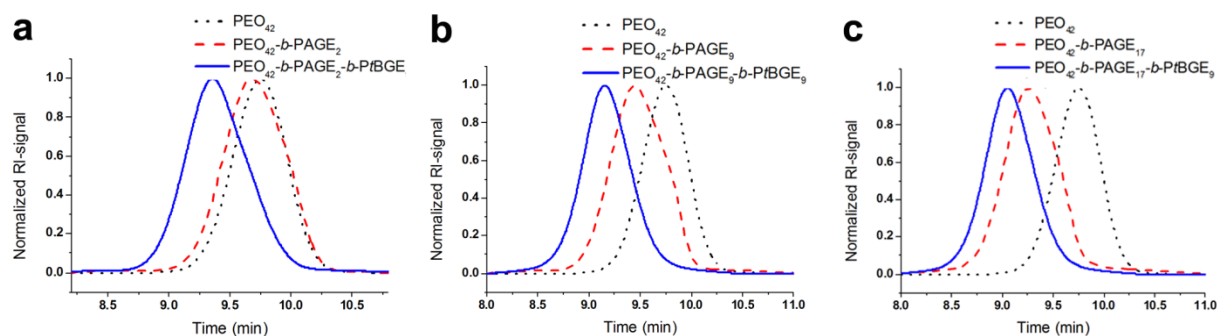


**Fig. S1:** SEC traces for PEO<sub>42</sub>-b-PAGE<sub>2</sub>-b-PtBGE<sub>9</sub> (a), PEO<sub>42</sub>-b-PAGE<sub>9</sub>-b-PtBGE<sub>9</sub> (b) and PEO<sub>42</sub>-b-PAGE<sub>17</sub>-b-PtBGE<sub>9</sub> (c) obtained via living AROP; PEO macroinitiator (solid black lines), PEO-b-PAGE diblock copolymer (solid red lines), and PEO-b-PAGE-b-PtBGE triblock terpolymers (solid blue lines).

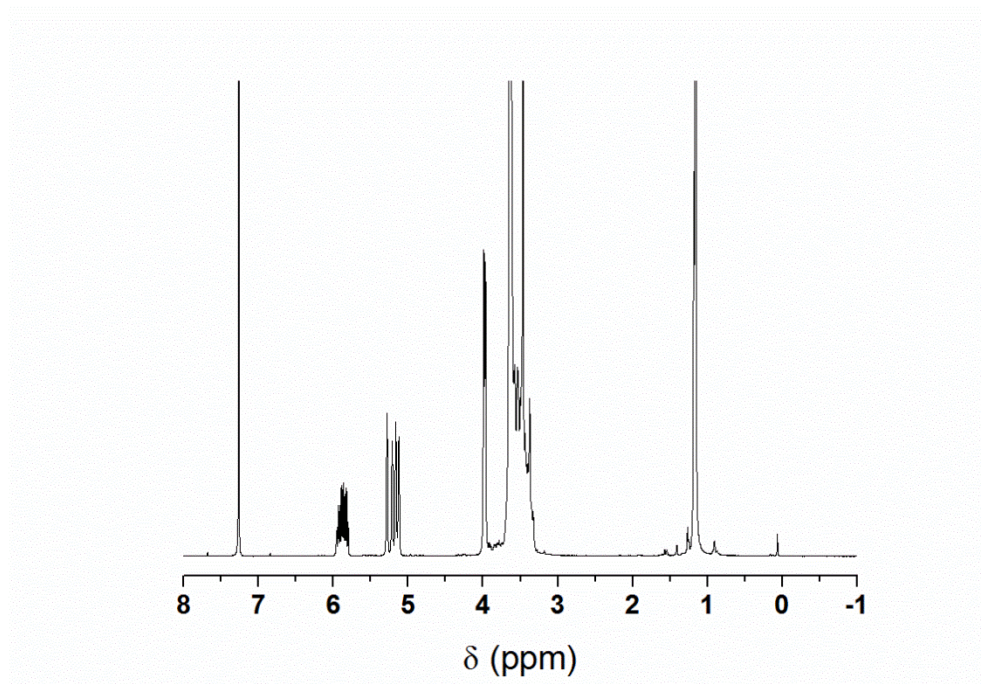


Fig. S2: <sup>1</sup>H NMR spectrum of PEO<sub>42</sub>-*b*-PAGE<sub>17</sub>-*b*-PtBGE<sub>9</sub> in CDCl<sub>3</sub>.

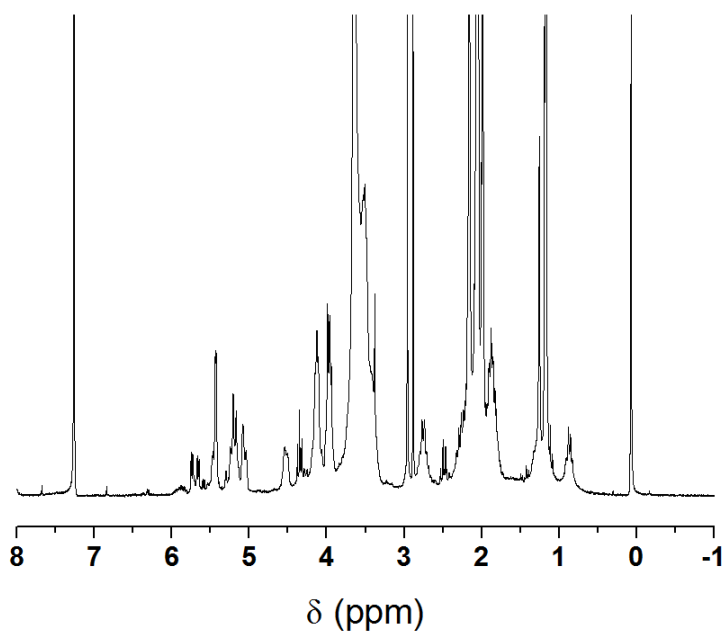


Fig. S3: <sup>1</sup>H NMR spectrum of PEO<sub>42</sub>-*b*-PAGE<sub>17,Gal</sub>-*b*-PtBGE<sub>9</sub> in CDCl<sub>3</sub>.



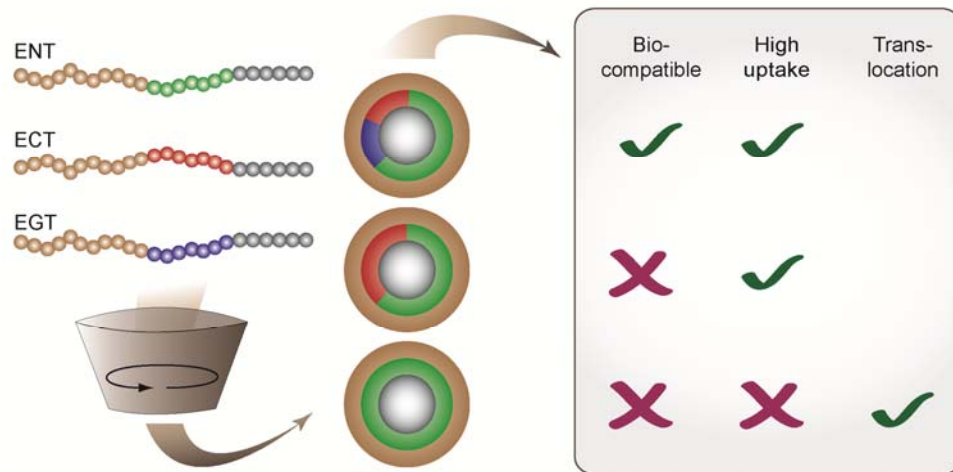
## Publication P3

“Small but powerful: Co-assembly of polyether-based triblock terpolymers into sub-30nm micelles and synergistic effects on cellular interactions”

Markus J. Barthel<sup>#</sup>, Alexandra Rinkenauer<sup>#</sup>, Michael Wagner, Ulrich Mansfeld, Stephanie Hoepfener, Justyna A. Czaplewska, Michael Gottschaldt, Anja Schallon, Felix H. Schacher, Ulrich S. Schubert

<sup>#</sup>Both authors contributed equally to this work.

*Manuscript submitted to Adv. Funct. Mater.*





# “Small but powerful: Co-assembly of polyether-based triblock terpolymers into sub-30 nm micelles and synergistic effects on cellular interactions”

Markus J. Barthel<sup>#, 1,2,3</sup> Alexandra C. Rinkenauer<sup>#, 1,2</sup> Michael Wagner,<sup>1,2</sup> Ulrich Mansfeld,<sup>1,2</sup> Stephanie Hoepfener,<sup>1,2</sup> Justyna A. Czaplewska,<sup>1,2</sup> Michael Gottschaldt,<sup>1,2</sup> Anja Schallon,<sup>1,2</sup> Felix H. Schacher,<sup>\*1,2</sup> Ulrich S. Schubert<sup>\*1,2,3</sup>

<sup>#</sup>Both authors contributed equally to this work.

<sup>1</sup> Laboratory of Organic and Macromolecular Chemistry (IOMC), Friedrich Schiller University Jena, Humboldtstrasse 10, 07743 Jena, Germany.

<sup>2</sup> Jena Center for Soft Matter (JCSM), Friedrich Schiller University Jena, Philosophenweg 7, 07743 Jena, Germany.

<sup>3</sup> Dutch Polymer Institute (DPI), P.O. Box 902, 5600 AX Eindhoven, the Netherlands.

Email: [ulrich.schubert@uni-jena.de](mailto:ulrich.schubert@uni-jena.de); [felix.schacher@uni-jena.de](mailto:felix.schacher@uni-jena.de)

## Abstract

We introduce a versatile ABC triblock terpolymer platform based on poly(ethylene oxide)-*block*-poly(allyl glycidyl ether)-*block*-poly(*tert*-butyl glycidyl ether) (PEO-*b*-PAGE-*b*-PtBGE) and subsequent functionalization of the PAGE segment with thiogalactose (hydroxyl), cysteamine (amino) and 2-mercaptopropionic acid (carboxy) by thiol-ene chemistry. These materials are used to prepare core-shell-corona micelles with a PtBGE core, a PAGE shell, and a PEO corona and sizes below 30 nm in aqueous media. We investigate the influence of different functional groups on micelle formation and cellular uptake. Moreover, co-assembly of differently functionalized materials allows to create micelles with a mixed shell and adjustable charge and, in that way, important characteristics such as cell uptake or cytotoxicity can be controlled. Furthermore, we demonstrate that even the uptake mechanism depends on the substitution pattern of the underlying triblock terpolymer.

## Keywords

Anionic ring-opening polymerization, triblock terpolymers, co-assembly, thiol-ene chemistry, cellular uptake, poly(ethylene oxide)

## Introduction

The synthesis and self-assembly of amphiphilic block copolymers into micellar structures of defined size, shape, and composition represents a very active field of research and such nanostructures show high potential for their use in potential biomedical and pharmaceutical applications.<sup>1,2</sup> The introduction of further functionalities or stimuli-responsive segments as well as the morphological variety being accessible benefit from the introduction of a third segment (C) resulting in ABC triblock terpolymers.<sup>3</sup> Since first attempts in the 1980s and the pioneering work of Stadler and coworkers later in the 1990s, increasing research efforts have been devoted to the preparation and application of such materials.<sup>4-7</sup> One intriguing aspect of ternary materials is that multicompartment micelles can be realized, structures which are further subdivided in core, shell, or corona. In consequence of their architecture, multicompartment micelles can be used to simultaneously store two different payloads within one micellar core or to implement several responsive segments.<sup>8-11</sup> In this context, we recently reported that multicompartment micelles with pH-dependent charge and morphology bear enormous potential as non-viral gene transfection agents, enabling high delivery efficiency in combination with low cytotoxicities.<sup>12,13</sup> Typically, each segment of ABC triblock terpolymers is attributed a specific “task” in solution: One block (*e.g.* A) ensures solubility in the desired environment. In water, often poly(ethylene oxide) (PEO) is used as this material is water-soluble, non-toxic, and prevents unspecific protein interactions (“stealth”-effect).<sup>14-17</sup> Another segment (B) can be used to introduce functional groups or the possibility to carry out post-polymerization functionalization reactions (*e.g.* allyl glycidyl ether) to further fine-tune the material properties or to attach targeting moieties.<sup>18-21</sup> The third block (C) often is utilized as solvophobic block, resulting in amphiphilic triblock terpolymers in case of hydrophobic segments. Related to this, we recently reported that hydrophobic glycidyl ethers *e.g.*, *tert*-butyl glycidyl ether or furfuryl glycidyl ether can be used as

core forming segments in micellar aggregates.<sup>18, 19, 22, 23</sup> These micellar cores can be applied, for example, to encapsulate hydrophobic guest compounds such as drugs or dyes.<sup>24</sup> If suitable building blocks are realized, the response of block copolymer nanostructures towards changes in temperature or pH value can be easily realized.<sup>25, 26</sup> This often induces quite drastic changes of the material properties and can be used to trigger the controlled release of encapsulated cargo or to enable endosomal release after cell internalization.<sup>12, 27, 28</sup> Nevertheless, to date the number of solution applications involving ABC triblock terpolymers are rather low, probably due to high synthetic efforts which often involve the combination of different polymerization techniques, modification sequences, or step-wise assembly procedures.

An alternative approach for the design of complex block copolymer micelles is the simple mixing of block copolymers. For instance, AB and AC diblock copolymers – where A represents identical hydrophobic blocks – are mixed in non-selective solvents and then transferred to a solvent or solvent mixture selective for B and C. It is generally believed that comparable degrees of polymerization (DP) for block A are beneficial. This could be shown, *e.g.*, for PEO-*b*-PLA and PNIPAM-*b*-PLA diblock copolymers. Co-assembly in aqueous solution leads to the formation of micelles with a PLA core and a mixed PEO/PNIPAM shell. These materials showed potential as smart carriers in drug delivery processes.<sup>29-32</sup> In this context, Kabanov and coworkers have demonstrated that co-micelles prepared from mixtures of amphiphilic and cationic copolymers based on Pluronics® can be applied for an efficient delivery of oligonucleotide sequences.<sup>33</sup> Such concepts have also been employed for the preparation of multicompartiment micelles.<sup>34, 35</sup>

Besides efforts to design structures of increased complexity for drug delivery applications, Kataoka *et al.* demonstrated that size does indeed matter and showed that micelles with diameters below 100 nm are highly interesting candidates in such approaches.<sup>36</sup> Commonly, nanostructures with diameters between 50 to 200 nm are used because endocytosis as predominant

internalization process can be assumed, the interaction with the immune system is reduced, and renal clearance can be avoided.<sup>37, 38</sup> In contrast, polymeric micelles with sizes far below 100 nm are scarce in literature and, up to now, rarely studied with regard to interactions with biological matter.<sup>37</sup> In this context, spherical core-shell micellar structures of approximately 30 nm were found to effectively penetrate poorly permeable tumor membranes.<sup>36</sup> Besides size, also charge significantly influences cell interactions of polymeric micelles, as well as their cytotoxicity and hemocompatibility. In general, the presence of cationic charges leads to increased interactions with the negatively charged cell membrane. Although this is advantageous for uptake, it also favors membrane destabilization and increases cytotoxicity. These side effects can be circumvented by using PEO as corona, but often at the cost of decreased cell interaction.<sup>39, 40</sup> As an alternative, the presence of negatively charged segments allows to decrease both the cytotoxicity and non-specific interactions with serum proteins.<sup>41</sup> Hence, direct control over the charge balance in (block co-) polymer nanostructures seems to be a promising strategy to balance cellular interactions, efficient uptake, and simultaneously suppress non-specific interactions and lower cytotoxicity. This can be achieved, *e.g.*, *via* the combination of positively and negatively charged blocks in block copolymers and has been recently demonstrated for multicompartment micelles from polybutadiene-*block*-poly(methacrylic acid)-*block*-poly(2-dimethylaminoethyl methacrylate) (BMAAD) triblock terpolymers. These structures comprise a polybutadiene core, a patchy shell consisting of *intra*-micellar interpolyelectrolyte complexes (*im*-IPEC) between PMAA and PDMAEMA, and a cationic corona of excess PDMAEMA.<sup>12</sup> We could demonstrate that the presence of the *im*-IPECs and the inherent pH-dependent dynamics of the system favor cellular uptake, whilst the PMAA middle segment acts as competing polyelectrolyte during delivery of pDNA and, at the same time, reduces cytotoxicity and facilitates release of the genetic material. Nevertheless, this approach suffers from a severe drawback: Preparation conditions,

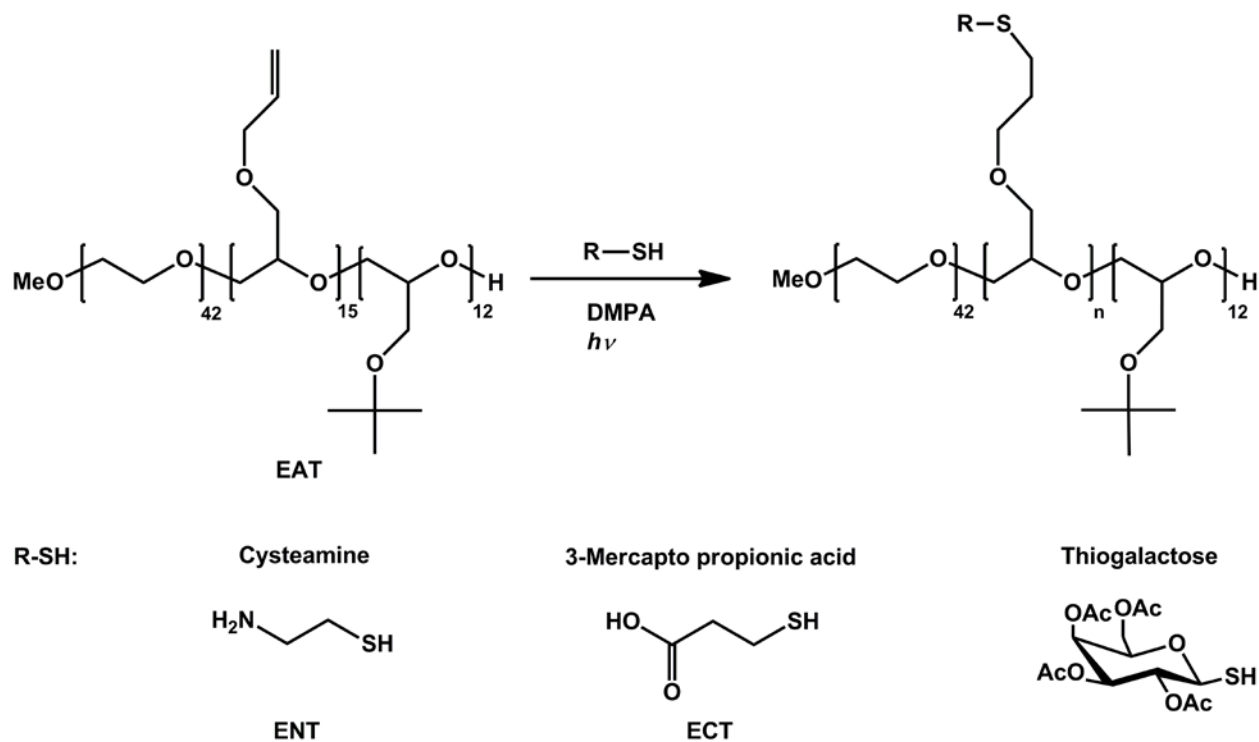
micellar size, and pH-dependent characteristics depend strongly on the terpolymer composition and, thus, have to be investigated and optimized for each new material being synthesized. This motivated us to probe a different, more versatile and general approach: Co-assembly of a small library of structurally similar ABC triblock terpolymers with different functional groups being present within the segment B.

We therefore introduce a triblock terpolymer platform based on poly(ethylene oxide)-*block*-poly(allyl glycidyl ether)-*block*-poly(*tert*-butyl glycidyl ether) (PEO-*b*-PAGE-*b*-PtBGE), synthesized by sequential living anionic ring-opening polymerization (AROP), as versatile carriers for hydrophobic compounds. The pendant double bonds of the PAGE block were functionalized by thiol-ene chemistry to introduce model ligands (thiogalactose), amine groups to provide positive charges (cysteamine), as well as carboxylic groups to generate negative charges (3-mercapto propionic acid). The obtained triblock terpolymers are subsequently used for the co-assembly into well-defined spherical core-shell-corona micelles with diameters below 30 nm and precisely adjustable charge and composition. Depending on the latter, we found synergistic effects regarding cellular uptake and cytotoxicity. In addition, the internalization efficiency (and pathway) was analyzed under serum reduced and serum containing conditions, showing an effective shielding by the PEO corona and providing first insights into the underlying uptake mechanism.

## Results and Discussion

### Synthesis and post-polymerization functionalization of PEO<sub>42</sub>-*b*-PAGE<sub>15</sub>-*b*-PtBGE<sub>12</sub>:

Based on earlier studies regarding the synthesis and functionalization, we used polyether-based triblock terpolymers, poly(ethylene oxide)-*block*-poly(allyl glycidyl ether)-*block*-poly(*tert*-butyl glycidyl ether) (PEO-*b*-PAGE-*b*-PtBGE), as starting material for the synthesis of triblock terpolymers with identical A and C segments but different functionalities present in the B block.<sup>18, 19</sup> The synthesis of PEO<sub>42</sub>-*b*-PAGE<sub>15</sub>-*b*-PtBGE<sub>12</sub> by AROP has been described previously (the subscripts denote the degrees of polymerization of the respective segment).<sup>19</sup> To generate differently functionalized examples for co-assembly, PEO<sub>42</sub>-*b*-PAGE<sub>15</sub>-*b*-PtBGE<sub>12</sub> was modified by thiol-ene chemistry: Cysteamine (2-aminoethanethiol) was used to introduce NH<sub>2</sub>-groups and the possibility to form cationic charges in aqueous media, 3-mercapto propionic acid enables to introduce carboxylic acid moieties and, hence, negative charges, and thiogalactose represents a model targeting moiety to ensure selective cellular uptake in hepatocytes.<sup>42, 43</sup> In the latter case, acetyl protected thiogalactose was used initially (**Scheme 1**).



**Scheme 1:** Schematic representation of the thiol-ene modification of PEO<sub>42</sub>-*b*-PAGE<sub>15</sub>-*b*-PtBGE<sub>12</sub> using cysteamine (N), 3-mercapto propionic acid (C) and acetylated thiogalactose. The abbreviations (EAT, ENT, ECT) will be used later on for the nomenclature of the micelles generated *via* self-assembly of the modified triblock terpolymers.

The reactions were performed in mixtures of DMF/EtOH for tetraacetyl thiogalactose and 3-mercapto propionic acid, whereas a mixture of DMF/EtOH/MeOH was used for cysteamine due to the rather low solubility of this compound. The reaction progress was monitored by size exclusion chromatography (SEC, shift to lower elution volumes in all cases) and <sup>1</sup>H NMR spectroscopy (**Figures S1 to S3**). The degree of functionalization was determined by <sup>1</sup>H NMR spectroscopy through the decrease in intensity of the characteristic signals for the pendant double bonds of PAGE at 5.85 and 5.20 ppm compared to the *t*-butyl group of the PtBGE block at 1.15 ppm (**Table 1**). For the functionalization with 3-mercapto propionic acid, full conversion could be reached after 24 h of irradiation. In contrast, only 50% functionalization could be obtained for cysteamine despite probing longer reaction times, higher irradiation intensity, or different triblock terpolymer/thiol ratios. We attribute this to the lower solubility observed for cysteamine.

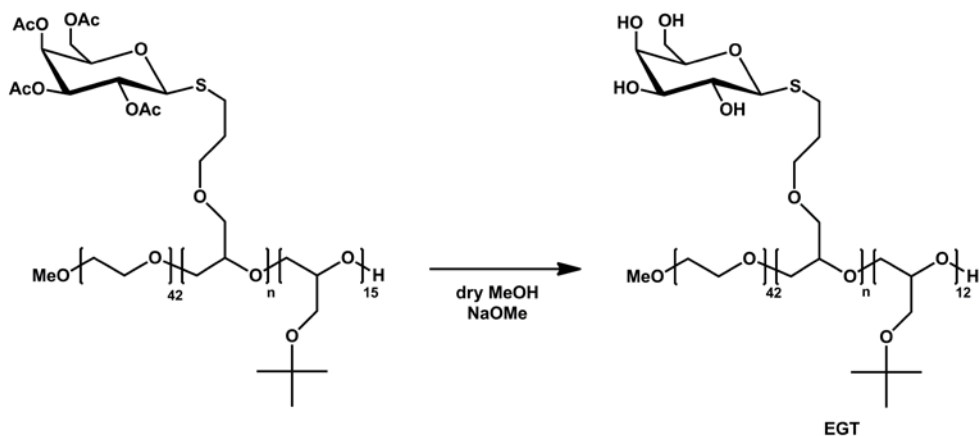
Similarly, in case of the acetylated thiogalactose only 70% functionalization could be reached, presumably also due to solubility issues of either the starting material or the triblock terpolymer after modification. Therefore, PEO<sub>42</sub>-*b*-(PAGE<sub>8,NH<sub>2</sub></sub>-*co*-PAGE<sub>7</sub>)-*b*-PtBGE<sub>12</sub> (ENT), PEO<sub>42</sub>-*b*-PAGE<sub>15,COOH</sub>-*b*-PtBGE<sub>12</sub> (ECT), and PEO<sub>42</sub>-*b*-(PAGE<sub>10,AcGal</sub>-*co*-PAGE<sub>5</sub>)-*b*-PtBGE<sub>12</sub> (EGT after deprotection) could be successfully prepared using thiol-ene chemistry.

**Table 1:** Characterization data of the synthesized triblock terpolymers. The subscripts represent the degree of polymerization. The shown abbreviations are used later on when describing self-assembled structures of the materials.

Sample	Abbreviation	SEC			<sup>1</sup> H NMR	
		M <sub>n</sub> (g/mol)	M <sub>w</sub> (g/mol)	PDI	M <sub>n</sub> (g/mol)	f (%)
PEO <sub>42</sub> - <i>b</i> -PAGE <sub>15</sub> - <i>b</i> -PtBGE <sub>12</sub>	EAT	3,350	3,500	1.05	5,100	---
PEO <sub>42</sub> - <i>b</i> -(PAGE <sub>8,NH<sub>2</sub></sub> - <i>co</i> -PAGE <sub>7</sub> )- <i>b</i> -PtBGE <sub>12</sub>	ENT	3,500	3,600	1.06	5,750	53
PEO <sub>42</sub> - <i>b</i> -PAGE <sub>15,COOH</sub> - <i>b</i> -PtBGE <sub>12</sub>	ECT	3,550	3,700	1.05	6,700	100
PEO <sub>42</sub> - <i>b</i> -(PAGE <sub>10,AcGal</sub> - <i>co</i> -PAGE <sub>5</sub> )- <i>b</i> -PtBGE <sub>12</sub>	---	4,200	4,350	1.04	8,800	70
PEO <sub>42</sub> - <i>b</i> -(PAGE <sub>10,Gal</sub> - <i>co</i> -PAGE <sub>5</sub> )- <i>b</i> -PtBGE <sub>12</sub>	EGT	10,400	11,500	1.10	7,100	70

In a second step the acetylated galactose was deprotected by treatment with sodium methanolate (**Scheme 2**). For this purpose, the polymer was dissolved in dry methanol, an excess of sodium methanolate was added and the solution was stirred for 1 h. The crude product was purified by dialysis and the complete deprotection was confirmed by <sup>1</sup>H NMR measurements (**Figure S3**, **Table 1**). For simplicity, the nomenclature ENT, ECT, and EGT will be used for micellar structures generated by self-assembly or co-assembly of these compounds.





**Scheme 2:** Schematic representation of the deprotection of acetylated thiogalactose (G) attached to a PEO-*b*-PAGE-*b*-PtBGE triblock terpolymer. The abbreviation EGT will be used later on for the nomenclature of micelles generated *via* self-assembly of the modified triblock terpolymer.

### Micelle formation in aqueous media

We have shown earlier that PEO-*b*-PAGE-*b*-PtBGE triblock terpolymers as well as their thiogalactose-functionalized counterparts undergo self-assembly in aqueous media into micelles with a PtBGE core, a PAGE shell, and a PEO corona (**Figure 1**).<sup>19</sup> Prior to co-assembly studies, micelles separately formed by EAT (before thiol-ene modification), ENT, ECT, and EGT in aqueous solution were investigated.

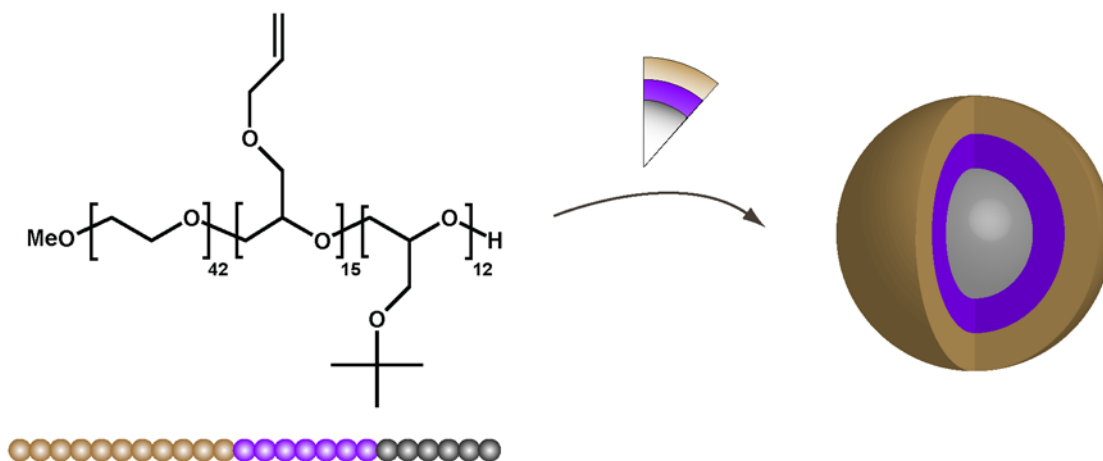


**Figure 1:** Schematic representation of a core-shell-corona micelle formed by PEO<sub>42</sub>-*b*-PAGE<sub>15</sub>-*b*-PtBGE<sub>12</sub> in aqueous media with a PtBGE core (gray), a PAGE shell (purple), and a PEO corona (brown).

Micellar solutions with a concentration of 10 g/L were prepared by the addition of THF solutions of the respective triblock terpolymer to water, followed by evaporation of the organic solvent. Subsequently, the solutions were analyzed by dynamic light scattering (DLS) and cryogenic transmission electron microscopy (cryo-TEM). In **Figure 2** the number weighted hydrodynamic radii from DLS are depicted. For all samples, radii ( $R_h$ ) in the range of 4 to 7 nm were detected in MilliQ water (pH = 7) and the results are summarized in **Table 2**.

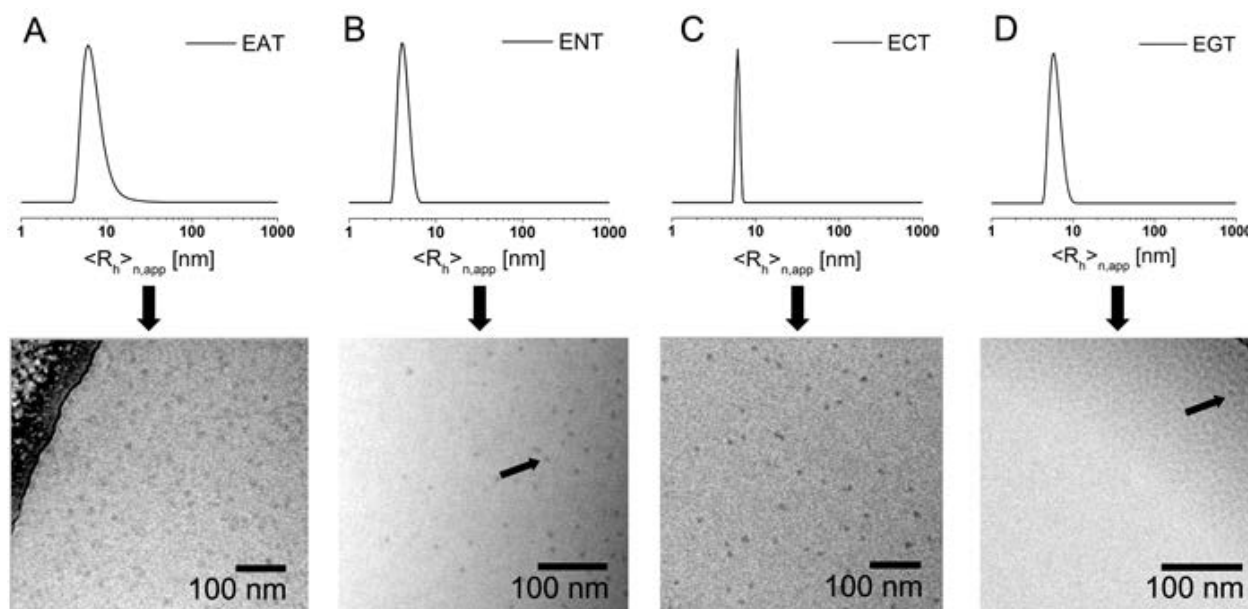


**Figure 2:** Number-weighted DLS CONTIN plots (upper section) for EAT (A,  $\langle R_h \rangle_{n,app} = 7$  nm), ENT (B,  $\langle R_h \rangle_{n,app} = 4$  nm), ECT (C,  $\langle R_h \rangle_{n,app} = 6$  nm) and EGT (D,  $\langle R_h \rangle_{n,app} = 6$  nm), as well as the corresponding cryo-TEM images (lower section) of the prepared self-assembled micelles. Due to the rather low contrast an arrow highlights representative ENT (B) and EGT (D) micellar cores. All cryo-TEM images are displayed as recorded.

In addition to DLS experiments, also cryo-TEM measurements were performed. In that way, block copolymer nanostructures in aqueous solution can be visualized without drying artifacts.<sup>44-</sup>

<sup>46</sup> As shown in **Figure 2**, spherical micelles were found for all samples discussed here. For micelles formed by ENT (**Figure 1B**) and EGT (**Figure 1D**) black arrows were added to highlight a representative micellar core. In some cases, a small distribution of worm-like

structures was also found in cryo-TEM, presumably due to aggregation of spherical micelles (**Figure S4**). This phenomenon was also observed in our previous studies.<sup>18, 19</sup> In general, for all samples micelles with a particle diameter ranging from 10 to 15 nm could be detected confirming the results from DLS studies.

### **Mixed micelles formed *via* co-assembly of triblock terpolymers**

We have recently shown that a combination of positively and negatively charged segments within triblock terpolymers (*i.e.* ampholytic materials) and the resulting multicompartment micelles in aqueous media led to pH-dependent interaction with cells, enhanced cellular uptake, and superior transfection efficiencies for pDNA.<sup>12, 28</sup> However, in this particular case one single material has been used and it can be anticipated that the charge ratio (cationic/anionic) plays an important role. We were, therefore, interested in the co-assembly of different triblock terpolymers as an alternative strategy to control charge and functionality within such micelles.<sup>29, 30</sup> In this context, the above described triblock terpolymers (ENT, ECT, EGT) represent a versatile and highly flexible tool-box. Co-assembly should again lead to the formation of core-shell-corona micelles, featuring a PEO corona and a hydrophobic P $\beta$ BGE core formed by identical segments A and C. The shell (B segment), however, should now be composed of different functional groups, depending on which material combinations are used. As a first example, micelles with different charge ratios (NH<sub>2</sub>/COOH) were prepared by co-assembly of ENT and ECT. For this purpose, mixtures of both triblock terpolymers were dissolved in THF and slowly added into water. Binary co-micelles with an excess of positive charges (ENT/ECT)<sup>3.5:1</sup>, a slight excess of positive charges (ENT/ECT)<sup>1.2:1</sup>, and an excess of negative charges (ENT/ECT)<sup>1:2.6</sup> were assembled using this pathway. In all cases, the superscripts represent the mixing ratio regarding the functional groups of the involved triblock terpolymers. The micellar solutions were afterwards analyzed by DLS

and cryo-TEM (**Figure 4**, the DLS CONTIN plots for (ENT/ECT)<sup>1:2:1</sup> and (ENT/ECT)<sup>1:2:6</sup> can be found in **Figure S5**). A schematic representation of the co-assembly and the formation of co-micelles is presented in **Figure 5**.

Again, spherical micelles with hydrodynamic radii of 4 to 6 nm were obtained by DLS and this results were confirmed by cryo-TEM measurements (diameters of 12 to 14 nm were observed). As both middle blocks of ENT (NH<sub>2</sub>) and ECT (COOH) are weak polyelectrolytes, we anticipated that the pH value might have an influence during the assembly process. Therefore, the co-assembly was carried out under acidic (pH ~ 4) as well as basic conditions (pH ~ 12) and the results were compared to the data obtained under neutral conditions (pH ~ 7). Additionally, also the preparation pathway was changed, *i.e.*, addition of water to THF solutions instead of *vice versa*. In all cases, no significant influence on the micellar size and the dispersity was observed (**Table S1**) and, therefore, all subsequent co-assembly procedures were carried out at pH 7 and *via* the addition of the THF solution containing the triblock terpolymers into water.

Subsequently, a detailed characterization of the micelles and co-micelles regarding charge was carried out using zeta-potential measurements. As structures of rather small size were obtained, it is at the same time highly demanding and crucial to investigate if, *e.g.*, co-micelles of ENT and ECT or if two separate populations are formed. This is difficult to estimate using only DLS and cryo-TEM. For the zeta-potential measurements and, also later for AF4 measurements, gel electrophoresis, and cell uptake studies Nile red, a hydrophobic red fluorescent dye, was encapsulated into the hydrophobic PtBGE core. Nile red is poorly soluble in water and exhibits a strong fluorescence in hydrophobic environment.<sup>47</sup> Therefore, the respective triblock terpolymer (or mixtures) and a small amount of the dye were dissolved in THF and slowly added into a defined amount of water (identical preparation pathway as has been described earlier).

Afterwards, the organic solvent was evaporated and the excess of non-encapsulated dye was filtered off.

In a first approach, the zeta potential of different micellar populations at a pH value of 7 was analyzed and the results are depicted in **Figure 6A**. As expected, a negative value is found for ECT (−36 mV) whereas the zeta potential for ENT is positive (47.5 mV). Both EAT and EGT revealed negative values (−39.5 mV and −27 mV), which can be attributed to the complexation of ions within the PEO corona or charge-dipole and dipole-dipole interactions, which are both known to influence the zeta potential.<sup>48</sup>

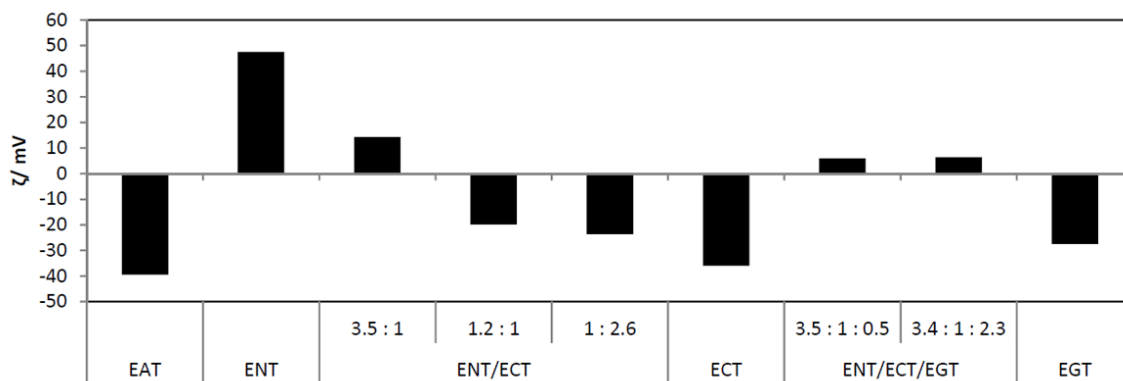


**Figure 3:** Zeta-potential measurements of different triblock terpolymer micelles and co-micelles in water.

For binary co-micelles (ENT/ECT), a clear dependence of the zeta potential on the mixing ratio can be observed, as with increasing amount of ENT the zeta potential increases (from −23.6 mV for (ENT/ECT)<sup>1:2.6</sup> to 14.2 mV for (ENT/ECT)<sup>3.5:1</sup>). Thus, zeta potential measurements indicate that co-micelles are formed. If the co-assembly in case of, *e.g.*, (ENT/ECT)<sup>3.5:1</sup> would lead to two separate populations of ENT and ECT, aggregation of oppositely charged micelles due to electrostatic interactions might be expected. In this case, an increase of the aggregates size and, presumably, precipitation might occur. As an attempt to clarify this, mixtures of ENT and ECT micelles after self-assembly *via* the above described protocol were prepared at comparable charge

ratios and were investigated using time-dependent DLS measurements (**Figure S8**), revealing an increase of the  $R_h$  from 4 to 10 nm within 2 h and partial precipitation of the material after 12 h (**Figure S8**). As the co-micelles proved to be stable over several weeks as confirmed by zeta-potential measurements and the presence of a monomodal size distribution (DLS), an efficient preparation of co-micelles by our protocol can be assumed.

Beside charge control in binary systems, also ternary systems were targeted where  $\text{NH}_2$ -groups (ENT), COOH moieties (ECT), and galactose as model targeting ligand (EGT) are combined. Galactose was chosen to enable selective cellular uptake into hepatocytes which has been already demonstrated.<sup>42, 43</sup> For the ternary systems, two ratios were prepared *via* co-assembly: (ENT/ECT/EGT)<sup>3.5:1:0.5</sup> and (ENT/ECT/EGT)<sup>3.4:1:2.3</sup>, featuring almost identical charge ratios and mainly differing in the amount of incorporated galactose. The as-prepared micellar solutions were characterized by DLS and cryo-TEM and the results are depicted in **Figure 4B** and **C** and **Table 2**. In both cases, spherical micelles with  $R_h = 7$  nm for (ENT/ECT/EGT)<sup>3.5:1:0.5</sup> and 8 nm in case of (ENT/ECT/EGT)<sup>3.4:1:2.6</sup> were found in DLS experiments. In cryo-TEM, again spherical micelles with diameters of 10 to 16 nm could be detected. A decreased contrast was observed for higher amounts of incorporated sugar moieties.

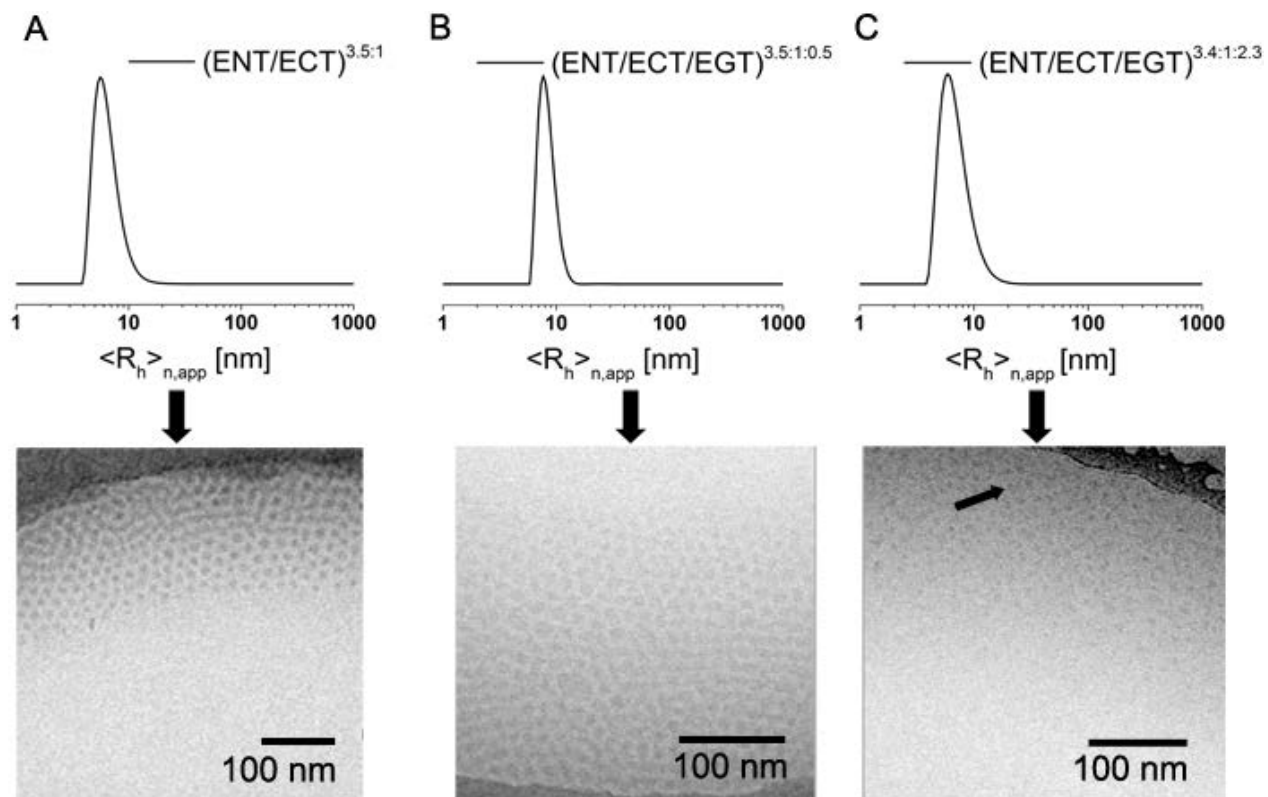


**Figure 4:** Number-weighted DLS CONTIN plots (upper row), for  $(ENT/ECT)^{3.5:1}$  (A,  $\langle R_h \rangle_{n,app} = 6$  nm),  $(ENT/ECT/EGT)^{3.5:1:0.5}$  (B,  $\langle R_h \rangle_{n,app} = 8$  nm) and  $(ENT/ECT/EGT)^{3.4:1:2.3}$  (C,  $\langle R_h \rangle_{n,app} = 7$  nm), as well as the corresponding cryo-TEM images (lower row) of the prepared co-micelles. Due to the low contrast one micellar core is highlighted with an arrow for  $(ENT/ECT/EGT)^{3.4:1:2.3}$  (C). All cryo-TEM images are displayed as recorded.

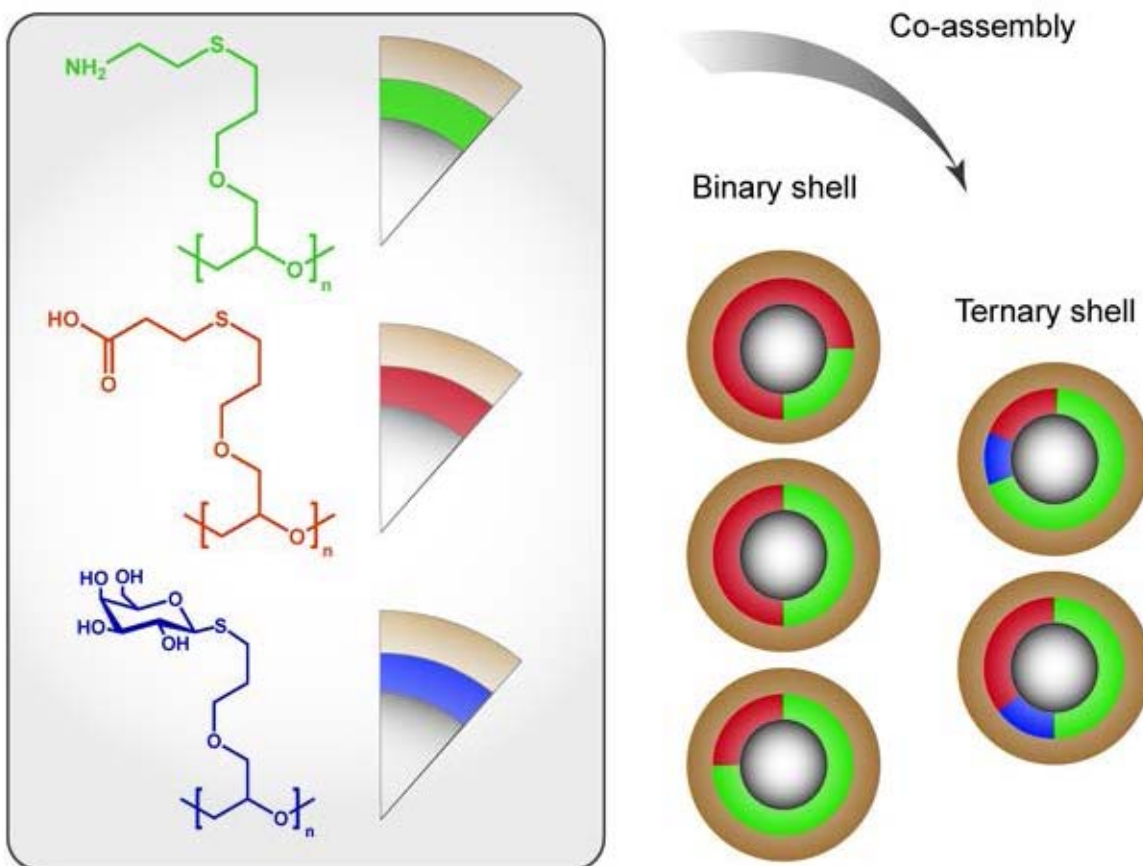


**Figure 5:** Schematic representation of the co-assembly of functionalized triblock terpolymers into binary and ternary core-shell-corona micelles with a mixed shell. The fractions of the modified PAGE shell (color code: green = cysteamine functionalized, red = 3-mercaptopropionic acid functionalized, blue = thiogalactose functionalized) represent the mixing ratio during co-assembly.

In all cases, evaluation by DLS and cryo-TEM led to comparable results regarding size and shape of both binary and ternary co-micelles. Moreover, the ternary co-micelles exhibit a decreased zeta potential if compared to the binary (ENT/ECT)<sup>3.5:1</sup> structures with 6 mV for (ENT/ECT/EGT)<sup>3.5:1:0.5</sup> and 6.5 mV for (ENT/ECT/EGT)<sup>3.4:1:2.3</sup>, thus indicating the presence of EGT within the structures (**Figure 3**). Also in this case the zeta potential measurements indicate that co-micelles are formed.



### Asymmetric flow field-flow fractionation of triblock terpolymer micelles

To obtain further insights into size, shape, and aggregation number of micelles formed by different triblock terpolymers (and combinations), asymmetric flow field-flow fractionation (AF4) coupled online to multi-angle light scattering (MALS) and DLS was applied. Here, a 10,000 g/mol membrane of regenerated cellulose and an aqueous eluent containing 20 mM NaCl was used for all systems investigated. Fractograms are shown in **Figure 6** and **Figure S6**. For all samples, the main peak represents spherical micelles and, in addition, a small second aggregate population could be detected after the cross-flow reaches zero (labeled “aggregates” in **Figure 6**). We attribute this to the presence of a small fraction of worm-like structures in accordance with earlier observations and the cryo-TEM experiments.<sup>18</sup> In case of EGT and (ENT/ECT/EGT)<sup>3.4:1:2.3</sup>, also a small fraction of triblock terpolymer unimers could be identified. Number weighted molar masses  $M_n$  of the aggregates, aggregation numbers  $N_{agg}$ , as well as the different radii ( $R_g$ ,  $R_h$ ) and the shape ratio ( $R_g/R_h$ ) derived from AF4 measurements are listed in **Table 2**. Thereby, the ratio  $R_g/R_h$  provides information about the shape of a macromolecule or colloid. Typical values are 0.778 for a hard sphere, 1.0 for a soft sphere, or 1.78 for a monodisperse linear polymer chain in a good solvent.<sup>49</sup> Additional characteristics ( $dn/dc$  values,  $M_w$ ,  $M_z$  and PDI) can be found in **Table S2**. Aggregation numbers  $N_{agg}$  were calculated by dividing the molar mass ( $M_n$ ) of the micelles by the molar mass ( $M_n$ , <sup>1</sup>H NMR) of the single triblock terpolymer chain. The hydrodynamic radii measured by AF4-MALS-DLS were significantly higher (around 10 to 15 nm) in contrast to batch DLS experiments for all samples. We attribute this to the different medium (20 mM NaCl) and, indeed, DLS measurements under these conditions could confirm the results from AF4. The increase in size in the presence of salt might originate from the complexation of sodium ions by the PEO corona or, in case of micelles prepared *via* co-assembly of ENT and ECT, an increase in ionic strength and the screening of

attractive electrostatic forces between differently charged side chains ( $\text{COO}^-$  for ECT;  $\text{NH}_3^+$  for ENT) within the shell.<sup>50</sup> Nevertheless, in all cases the ratio  $R_g/R_h$  scales between 0.775 (hard sphere) and 1.0 (soft sphere), indicating a spherical shape.<sup>49, 51</sup>

By AF4 experiments, also the absolute molar mass of the micelles could be detected: Comparable values ( $M_n$ ) of 1,000 to 2,000 kg/mol were obtained for EAT, ENT and ECT micelles, whereas only 220 kg/mol were found in case of EGT. This corresponds to  $N_{\text{agg}} = 30$  (EGT) and 225 (EAT), 323 (ENT), and 156 (ECT), respectively. At this point, we attribute the lower values observed for EGT to the steric demand of the thiogalactose side chains within the PAGE shell, preventing a more compact assembly. This is also in good accordance with the observation of a small fraction of triblock terpolymer unimers in the AF4 fractograms (**Figure S5B**). The aggregation numbers  $N_{\text{agg}}$  of binary and ternary co-micelles were calculated by consideration of the different molar masses of the terpolymers and under the assumption that the ratios of polymer chains in the micelles are the same as the mixing ratios of the triblock terpolymers.

Molar masses of binary and ternary co-micelles are in between 620 kg/mol [(ENT/ECT)<sup>1:2.6</sup>,  $N_{\text{agg}} = 99$ ] and 1,200 kg/mol [(ENT/ECT)<sup>3.5:1</sup>,  $N_{\text{agg}} = 204$ ]. This indicates the formation of more compact structures with increasing amounts of ENT for the investigated range of charge ratios.

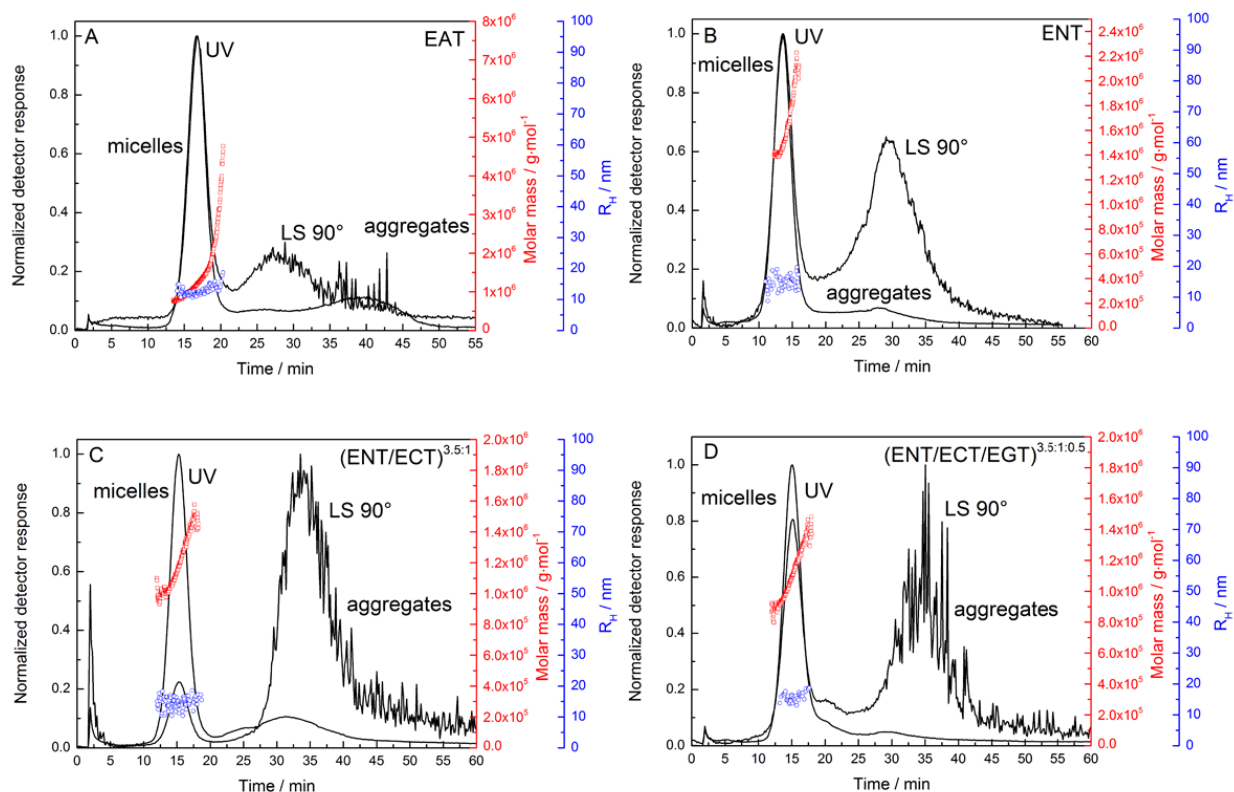


**Figure 6:** AF4 fractograms of triblock terpolymer micelles from EAT (A), ENT (B),  $(\text{ENT}/\text{ECT})^{3.5:1}$  (C), and  $(\text{ENT}/\text{ECT}/\text{EGT})^{3.5:1:0.5}$  (D) in 20 mM NaCl solution.

**Table 2:** DLS and AF4 data for the investigated triblock terpolymer micelles and co-micelles. AF4 was performed using aqueous 20 mM NaCl solution.

Sample	$M_n \cdot 10^{-5}$ (g/mol)	$\langle R_h \rangle_{n,app}$ (nm) <sup>a</sup>	$N_{agg}$	$\langle R_g \rangle$ (nm)	$\langle R_h \rangle$ (nm) <sup>b</sup>	$\langle R_g/R_h \rangle^c$	$\langle R_h \rangle$ (nm) <sup>d</sup>
EAT	11.48±0.078	7.0	225±2	10.1±0.6	13.0±0.4	0.777±0.021	11.8±0.1
ENT	18.58±0.314	4.2	323±56	15.8±1.1	17.4±1.8	0.916±0.148	9.5±0.3
ECT	10.45±0.007	6.1	156±1	12.2±0.8	14.4±0.1	0.844±0.054	13.5±0.3
EGT	2.224±0.070	6.0	31±1	5.4±0.6	5.3±0.3	1.018±0.136	7.1±0.3
$(\text{ENT}/\text{ECT})^{3.5:1}$	11.97±0.366	6.3	204±6	12.3±0.4	15.2±0.5	0.810±0.042	-
$(\text{ENT}/\text{ECT})^{1.2:1}$	7.323±0.127	4.3	121±2	8.9±0.8	10.6±1.5	0.844±0.051	10.5±0.2
$(\text{ENT}/\text{ECT})^{1:2.6}$	6.192±0.039	4.9	99±1	9.0±1.6	10.4±0.5	0.875±0.196	10.5±0.1
$(\text{ENT}/\text{ECT}/\text{EGT})^{3.5:1:0.5}$	11.34±0.714	8.2	190±12	13.6±1.2	15.9±0.1	0.856±0.084	12.3±0.5
$(\text{ENT}/\text{ECT}/\text{EGT})^{3.4:1:2.3}$	9.654±0.482	6.7	155±8	13.5±1.2	15.1±0.1	0.899±0.076	11.5±0.5

<sup>a</sup> batch DLS in pure water

<sup>b</sup> online DLS (AF4-DLS) in 20 mM NaCl

<sup>c</sup>  $R_h$  from AF4-DLS

<sup>d</sup> batch DLS in 20 mM NaCl

## Gel-electrophoresis

In addition to zeta potential measurements, another powerful method for the separation of charged macromolecules (e.g., DNA) is gel-electrophoresis. Here, the samples are placed in an agarose gel and an electrical field is applied. The electrical field induces movement within the gel towards the positive or negative pole, depending on the charge of the sample investigated.

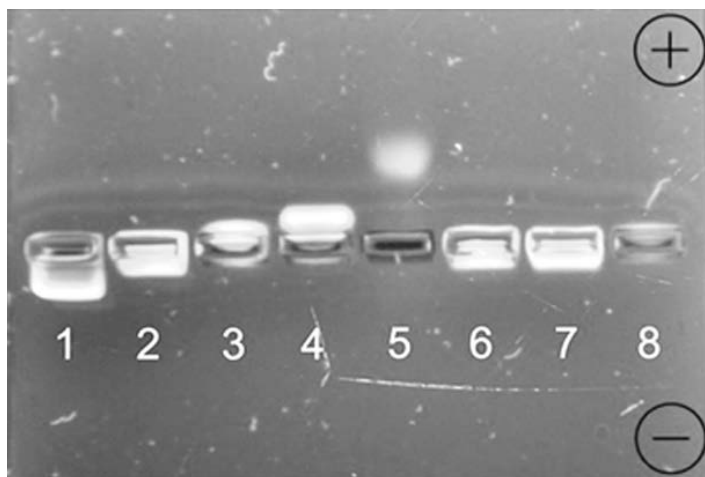


**Figure 7:** Gel-electrophoresis using 1% agarose gel and TBE buffer (1 = ENT, 2 = (ENT/ECT)<sup>3.5:1</sup>, 3 = (ENT/ECT)<sup>1.2:1</sup>, 4 = (ENT/ECT)<sup>1:2.6</sup>, 5 = ECT, 6 = (ENT/ECT/EGT)<sup>3.5:1:0.5</sup>, 7 = (ENT/ECT/EGT)<sup>3.4:1:2.3</sup>, 8 = EGT).

A small amount of labeled micelles and co-micelles was placed in an agarose gel and an electric field was applied. We anticipated that co-micelles should feature only one band, as additional confirmation of the zeta-potential measurements. As shown in **Figure 7**, micelles formed by ENT reveal the highest shift to the negative pole, whereas ECT moved towards the positive pole. The bands observed for ENT/ECT co-micelles of different mixing ratios are, in accordance with their zeta-potential, in between. If two separate populations of ENT and ECT would be formed, two separate bands in gel electrophoresis towards opposite poles might be expected. As only one band is visible for all samples, we regard this as another indication for an efficient co-assembly. In addition, ternary ENT/ECT/EGT exhibited movement towards the negative pole, again confirming the results from zeta-potential measurements. EGT did not show any movement in gel electrophoresis. Contrary to the negative zeta potential of  $-39.5$  mV, EAT micelles exhibited a

clear shift to the negative pole (**Figure S7**). Up to now, we have no conclusive explanation for this behavior as also zeta potential measurements in comparable buffer solutions (the exact composition is given in the experimental part) yielded negative values.

## **Cellular interactions**

### **Cytotoxicity and hemolysis of triblock terpolymer micelles**

Aiming for a later use of such triblock terpolymer micelles in targeting and/or delivery applications, their cytotoxicity was investigated using an Alamar blue assay. At first, triblock terpolymer micelles formed *via* the self-assembly of one single material were investigated. Micelles formed of EAT, ECT, or EGT did not show any cytotoxic effects for concentrations up to 0.5 mg/mL (cell viability was above 70%), only in case of ENT the situation was different (**Figure 8A**). Regarding EAT, ECT, and EGT these results are in accordance with literature as all structures exhibited negative zeta potentials.<sup>39, 52</sup> For micelles based on ENT, the IC<sub>50</sub> of 300 µg/mL can be explained by the presence of cationic charges within the shell (zeta potential of +47.5 mV), which could lead to stronger interactions with or even disruption of the cell membrane. These results can be taken as further proof that the functionalization of the middle block (PAGE) significantly influences interactions of such micelles with biological matter, even though all structures feature a rather long PEO corona (compared to the degrees of polymerization for PAGE and P $\tau$ BGE).<sup>53</sup>

A hemolysis assay was performed to gain deeper insight into the interaction of EAT, ENT, ECT, and EGT micelles with negatively charged cell membranes: Here, ENT exhibited slight hemolytic activity at concentrations of 50 µg/mL ( $3.8 \pm 0.6\%$  hemolysis, **Figure 8B**). No hemolytic activity was found for both EAT and ECT. In contrast,  $2.9 \pm 0.6\%$  hemolysis was

observed for EGT micelles. We attribute this to hydrophobic interactions with the cell membrane, possibly even incorporation of EGT into the latter.

### **Internalization of triblock terpolymer micelles**

Furthermore, the internalization efficiency of micelles from EAT, ENT, ECT, and EGT into human embryonic kidney (HEK) cells, a model cell line for unspecific uptake studies, was analyzed under serum reduced and serum containing conditions. Under serum reduced conditions the critical concentration, *i.e.*, the concentration where EAT shows nearly no uptake ( $1 \pm 1.1\%$ ), was determined to be  $10 \mu\text{g/mL}$  (**Figure 8**). From this data set, it becomes obvious that ENT revealed the best uptake into  $79.7 \pm 4.5\%$  (at  $10 \mu\text{g/mL}$ ) of the cells. This can be attributed to the presence of positive charges in the shell and an increased interaction with the cell membrane, also confirmed by the earlier discussed hemolysis assay. Higher concentrations of  $50 \mu\text{g/mL}$  could not be analyzed as the cell viability was too low under serum reduced condition. Compared to ENT, the decreased uptake of ECT and EGT at a concentration of  $10 \mu\text{g/mL}$  with  $26.8 \pm 6.3\%$  and  $15.3 \pm 21.7\%$ , respectively, can be explained by the negative zeta potential of these particles, resulting in decreased interactions with cells. Nevertheless, even ECT and EGT show significantly increased cellular uptake induced either by the introduction of charges (COOH) or targeting units (thiogalactose) if compared to EAT at  $10 \mu\text{g/mL}$  ( $1 \pm 1.11\%$ ). As the presence of a PEO corona has been shown in many examples to prevent unspecific protein adsorption (“stealth effect”),<sup>17</sup> the uptake was also analyzed in the presence of serum (**Figure 8D**). Here, only the uptake of ENT decreased significantly from  $86 \pm 11\%$  to  $13 \pm 0.6\%$  at  $10 \mu\text{g/mL}$  ( $p < 0.005$ ), presumably due to stronger interactions with negatively charged serum proteins.<sup>54, 55</sup> Nevertheless, the uptake of both, ENT and ECT, is significantly higher compared to EAT with  $2\% \pm 0.5$  ( $p < 0.05$ ). The internalization of EGT is similar to EAT at  $10 \mu\text{g/mL}$  thus also reduced from 15 to 2.9% in the

presence of serum proteins. As the functionalization with thiogalactose is supposed to result in specific uptake into liver cells, we also incubated the EGT micelles with HepG2 cells.<sup>42</sup> Unfortunately, no increased uptake at low concentrations ( $3.9\% \pm 5$  at  $10 \mu\text{g/mL}$ ) could be detected, which would hint towards a targeted internalization process (**Figure S9**). One explanation might be that the galactose side chains are not sufficiently exposed at the surface and, thus, the interaction with the asialoglycoprotein receptor, specific for galactose in HepG2 cells, is hampered. Further, the PEO corona might form hydrogen bonds with the galactose residues,<sup>56</sup> additionally reducing their accessibility.

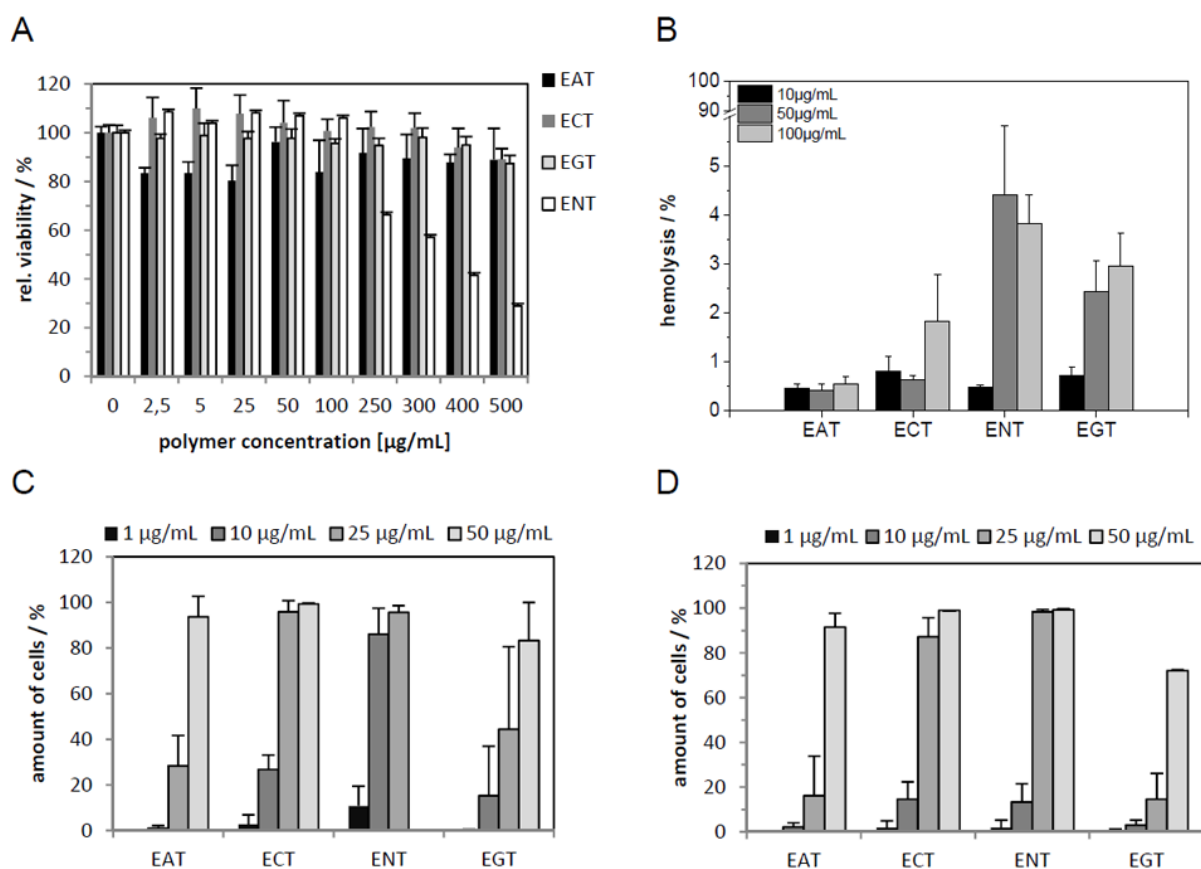


**Figure 8:** Cytotoxicity test of triblock terpolymer micelles using L929 cells (A) and hemolysis assay using three different donors (B). Cellular uptake under serum reduced (C) and serum containing conditions (D) in HEK cells. Values represent the mean  $\pm$  S.D.

## Cytotoxicity and internalization of co-micelles

As the up to now used triblock terpolymer micelles (EAT, ENT, ECT, and EGT) already showed significant differences regarding cellular uptake and cytotoxicity, the influence of the composition in binary and ternary co-micelles on the cytotoxicity was studied. (ENT/ECT)<sup>3.5:1</sup> exhibited a positive zeta potential and a similar cytotoxicity (IC<sub>50</sub> of 350 µg/mL), if compared to ENT (**Figure 8A**). In case of (ENT/ECT)<sup>1.2:1</sup> and (ENT/ECT)<sup>1:2.6</sup>, no cytotoxicity was observed, in accordance with the negative zeta potential.

Interestingly, both the ternary co-micelles, (ENT/ECT/EGT)<sup>3.5:1:0.5</sup> and (ENT/ECT/EGT)<sup>3.4:1:2.3</sup>, which feature the same charge ratio as (ENT/ECT)<sup>3.5:1</sup> and exhibited positive zeta potentials, did not show any cytotoxicity at all tested concentrations. This is indeed remarkable, and we propose that this originates from the presence of EGT terpolymer chains in these structures. All prepared co-micelles were further investigated regarding their internalization behavior. In this case, (ENT/ECT)<sup>3.5:1</sup> demonstrated outstanding uptake compared to all other samples as already at 10 µg/mL under serum containing conditions 75% ± 11.5 of the cells showed internalization (**Figure 9B**). These results are comparable to ENT micelles under serum reduced conditions, thus indicating decreased non-specific interactions of (ENT/ECT)<sup>3.5:1</sup> with serum proteins. For both (ENT/ECT)<sup>1.2:1</sup> and (ENT/ECT)<sup>1:2.6</sup>, reduced uptake with 8.9 ± 11% and 6.7 ± 5.5% (compared to (ENT/ECT)<sup>3.5:1</sup>) was found. In case of ternary co-micelles, (ENT/ECT/EGT)<sup>3.5:1:0.5</sup> exhibited decreased uptake compared to (ENT/ECT)<sup>3.5:1</sup>, presumably due to the presence of EGT (**Figure 9B**). Further increase of the galactose content leads to even lower values, which is in accordance with lower uptake of EGT compared to ECT and ENT. Nevertheless, it should be noted that, in contrast to (ENT/ECT)<sup>3.5:1</sup>, both (ENT/ECT/EGT)<sup>3.5:1:0.5</sup> and (ENT/ECT/EGT)<sup>3.4:1:2.3</sup> did not show any cytotoxicity. In summary, by adjusting the micellar composition *via* co-assembly of



ENT, ECT, and EGT both cellular uptake and cytotoxicity can be controlled and optimized (according to our results).

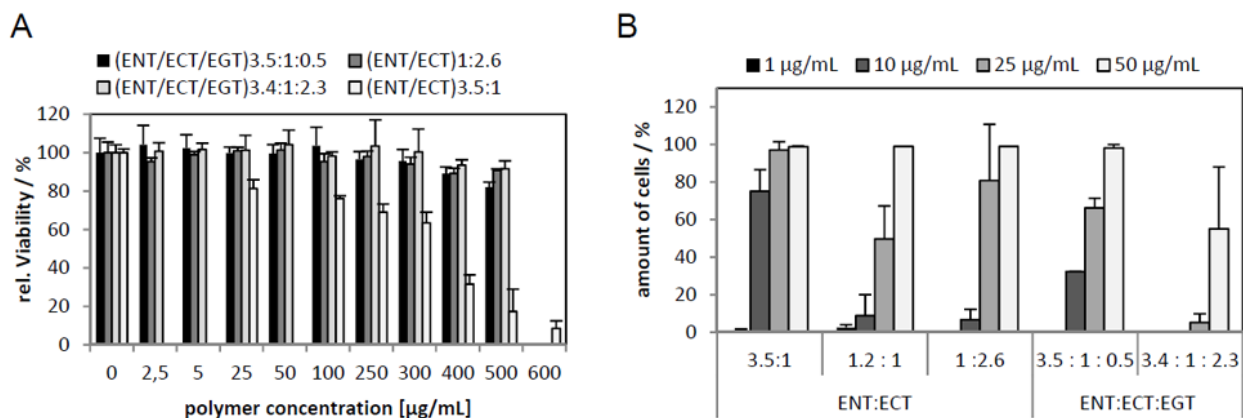


**Figure 9:** Cytotoxicity test of binary and ternary co-micelles using L929 cells (A) and cellular uptake in HEK cells (B). Values represent the mean  $\pm$  S.D. n = 3.

### Further investigations regarding the pathway for cellular uptake

We were also interested in a more detailed analysis of the internalization process. The size of the core-shell-corona micelles used in the present study is below 30 nm in diameter, a size where studies on the internalization process are rarely found, as normally nanostructures between 50 to 200 nm are used in drug delivery applications. Here, internalization *via* endocytosis is under debate, as this process is usually observed for structures with sizes between 50 to 500 nm.<sup>57, 58</sup> As endocytosis is energy dependent, the uptake efficiencies were investigated at 4 °C, conditions which are known to inhibit energy dependent mechanisms (**Figure 10A**).<sup>59</sup> Interestingly, no significant changes under these conditions were found for EAT, ECT and ENT if compared to 37 °C. In contrast, the internalization efficiency for EGT decreased significantly to 15%  $\pm$  7.8 (at 50 µg/mL), indicating an energy dependent mechanism.

Besides, ENT micelles are already cytotoxic at a concentration of 50 µg/mL at 4 °C, in contrast to 37 °C. The increased cytotoxicity at 4 °C might originate from the reduced fluidity of the cell membrane at low temperatures. Therefore, it might occur that cationically charged micelles lead

to destabilization and local disruption of the membrane.<sup>60</sup> As the size of the micelles is rather small, these perforations can be easily closed at 37 °C at normal membrane fluidity. At 4 °C, however, this process is significantly slowed down, leading to cell leakage. It has been described in the literature that structures of a few nanometers in size can lead to pore formation and translocation through the cell membrane.<sup>61, 62</sup> To evaluate if cell leakage is caused in our case, a lactate dehydrogenase (LDH) assay was performed,<sup>63</sup> which was used to detect the release of cytosolic LDH into the surrounding media through membrane perforations. For ECT and EAT micelles, no significant LDH release could be observed in contrast to ENT (**Figure 10B**). This provides a first hint and supports our assumption that EAT and ECT micelles cross the cellular membrane by the formation of reversible membrane pores or penetrate the cell membrane *via* diffusion. ENT seems to cause larger pores, resulting in LDH release. These first investigations of the internalization process demonstrate that differences in shell composition and functionality of triblock terpolymer micelles influence not only cytotoxicity and uptake efficiency, but also alter the overall internalization process. In that respect, the herein presented toolbox of triblock terpolymers represents an ideal starting point for the purposeful variation of micellar composition and charge and more detailed investigations of the uptake mechanism will follow.

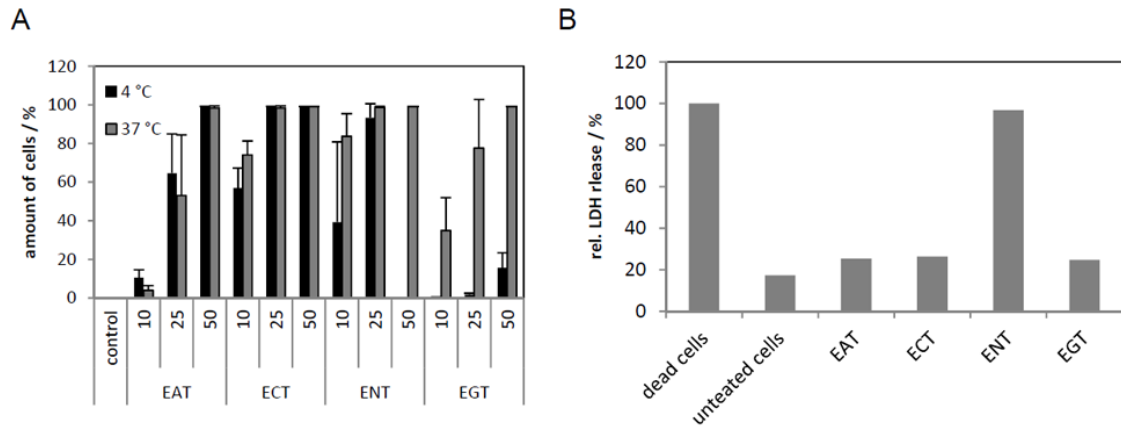


**Figure 10:** Cellular uptake of triblock terpolymer micelles at 4 °C and 37 °C in HEK cells after 4 h (A) and lactate dehydrogenase assay with HEK cells and 25 µg/mL of the micelles (B). Values represent the mean ± S.D, n = 3.

## Conclusion

Multifunctional and well-defined triblock terpolymers represent very promising materials for the preparation of efficient drug delivery vehicles. Here, we introduce a concept for the co-assembly of ABC triblock terpolymers with identical A and C segments but different functionalities in the middle block (B) into core-shell-corona micelles with a mixed shell. In that way, sub-30 nm particles with superior control over charge and the location of targeting ligands with the micellar shell were formed. The materials employed are poly(ethylene oxide)-*block*-poly(allyl glycidyl ether)-*block*-poly(*tert*-butyl glycidyl ether) (PEO-*b*-PAGE-*b*-PtBGE) triblock terpolymers where the PAGE segments has been subsequently modified using thiol-ene chemistry to introduce -NH<sub>2</sub> (cysteamine, ENT), -COOH (3-mercaptopropionic acid, ECT), and thiolgalactose residues (EGT). Depending on whether binary (ENT/ECT) or ternary co-micelles (ENT/ECT/EGT) were prepared, charge and, directly linked to that, cytotoxicity of the resulting nanoparticle could be adjusted. In case of ENT/ECT/EGT co-micelles, efficient cellular uptake (even in the presence of serum proteins) could be combined with low cytotoxicity. Different characterization methods, including dynamic light scattering (DLS), asymmetric flow field-flow fractionation (AF4), zeta potential measurements, and cryo-TEM indicate that indeed co-micellization occurs. Moreover, first insights into the internalization process of these sub-30 nm micelles could be provided and our results hint towards uptake *via* direct penetration through the cell membrane and not *via* endocytosis, offering interesting possibilities for further detailed studies.

## Experimental part

### Instruments

$^1\text{H NMR}$  spectra were recorded on a Bruker AC 300 MHz spectrometer in chloroform. **Size exclusion chromatography (SEC)** was performed on a Shimadzu SCL-10A system (with a LC-10AD pump, a RID-10A refractive index detector, and a PL gel 5  $\mu\text{m}$  mixed-D column at RT), the eluent was a mixture of chloroform:triethylamine:*iso*-propanol (94:4:2) with a flow rate of 1 mL/min. The system was calibrated with poly(ethylene glycol) standards from PSS ( $M_n = 1,470$  g/mol to 42,000 g/mol). **MALDI-ToF** mass spectra were obtained using an Ultraflex III ToF/ToF mass spectrometer (Bruker Daltonics) with *trans*-2-[3-(4-*tert*-butylphenyl)-2-methyl-2-propenylidene] malononitrile (DCTB) or 2,5-dihydroxybenzoic acid (DHB) as matrix in reflector as well as in linear mode. The instrument was calibrated prior to each measurement with an external PMMA standard from PSS Polymer Standards Services GmbH. **Dynamic light scattering (DLS)** was performed at a scattering angle of  $90^\circ$  on an ALV CGS-3 instrument and a He-Ne laser operating at a wavelength of  $\lambda = 633$  nm at  $25^\circ\text{C}$ . The CONTIN algorithm was applied to analyze the obtained correlation functions. Apparent hydrodynamic radii were calculated according to the Stokes-Einstein equation. All CONTIN plots are number-weighted. **Cryo-TEM measurements** were carried out at 120 kV using a Philips-CM 120 equipped with a  $1\text{k} \times 1\text{k}$  CCD camera. Sample preparation was performed on Quantifoil® grids (holey carbon R2/2) after plasma cleaning. Vitrification of the samples was carried out in a home-built system with a temperature control unit. A drop of the polymer solution (5  $\mu\text{L}$ ) was placed on the grid, which was blotted and subsequently plunged into a cryogen reservoir containing liquid ethane. The samples were afterwards stored in liquid nitrogen and were transferred to the TEM keeping the temperature below  $-176^\circ\text{C}$  to avoid the formation of crystalline ice layers.

### ***Asymmetric flow field-flow fractionation (AF4)***

Asymmetric flow field-flow fractionation (AF4) was performed on a n AF2000 MT System (Postnova Analytics, Landsberg, Germany) coupled to an UV (PN3211, 260 nm), RI (PN3150), MALLS (PN3070, 633 nm) and DLS (ZetaSizer Nano ZS) detector. The eluent is delivered by three different pumps (tip, focus, cross-flow) and the sample is injected by an autosampler (PN5300) into the channel. The channel has a trapezoidal geometry and an overall area of 31.6 cm<sup>2</sup>. The nominal height of the spacer was 500 μm and a regenerated cellulose membrane with a molar mass cut-off of 10 kDa was used as accumulation wall. All experiments were carried out at 25 °C and the eluent was degassed water containing 20 mM NaCl. The detector flow rate was set to 0.5 mL/min for all samples and 20 μL (5 mg/mL) were injected with an injection flow rate of 0.2 mL/min for 7 min. For EAT the cross-flow was set to 2 mg/mL and decreased under an exponential gradient (0.5) to 0 within 20 min. For EGT the cross-flow was set to 2 mg/mL and decreased under a linear gradient to 0 within 20 min. For ECT the cross-flow was set to 2 mg/mL and decreased under an exponential gradient (0.5) to 0 within 25 min. For ENT the cross-flow was set to 1.3 mg/mL and decreased under an exponential gradient (0.7) to 0 within 25 min. For (ENT/ECT)<sup>1:2:6</sup> the cross-flow was set to 2 mg/mL and decreased under a linear gradient to 0 within 35 min. For (ENT/ECT)<sup>1:2:1</sup> the cross-flow was set to 2 mg/mL and decreased under a linear gradient to 0 within 30 min. For (ENT/ECT)<sup>3:5:1</sup>, (ENT/ECT/EGT)<sup>3:5:1:0.5</sup> and (ENT/ECT/EGT)<sup>3:4:1:2:3</sup> the cross-flow was set to 1.3 mg/mL and decreased under an exponential gradient (0.7) to 0 within 25 min. After the cross-flow reaches zero, for all samples, the cross-flow was kept constant at zero for at least 30 min to ensure complete elution. For calculation of the molar mass and the radius of gyration a Berry plot was used.<sup>64</sup> All measurements were repeated three times. The refractive index increment (dn/dc) of all samples was measured by manual injection of a known concentration directly into the channel without

any focusing or cross-flow. The  $dn/dc$  was calculated as the average of at least three injections from the area under the RI curve ( $AUC_{RI}$ ).

### ***Electrophoretic light scattering (ELS)***

Electrophoretic light scattering was used to measure the electrokinetic potential, also known as zeta potential. The measurements were performed on a Zetasizer Nano ZS (Malvern Instruments, Herrenberg, Germany) by applying laser Doppler velocimetry.<sup>65</sup> For each measurement, 20 runs were carried out using the slow-field reversal and fast-field reversal mode at 150 V. Each experiment was performed in triplicate at 25 °C. The zeta potential ( $\zeta$ ) was calculated from the electrophoretic mobility ( $\mu$ ) according to the Henry Equation. Henry coefficient  $f(ka)$  was calculated according to Oshima.<sup>66</sup>

### **Materials**

The triblock terpolymer precursor PEO<sub>42</sub>-*b*-PAGE<sub>15</sub>-*b*-PtBGE<sub>12</sub> (SEC:  $M_n = 3,400$  g/mol;  $M_w = 3,500$  g/mol; PDI = 1.06; obtained with PEO calibration; NMR:  $M_n = 5122$  g/mol) as well as 2,3,4,6-tetra-*O*-acetyl-1-thio- $\beta$ -D-galactopyranose (acetylated thiogalactose) were synthesized as reported previously.<sup>19, 67, 68</sup> 2,2-Dimethoxy-2-phenylacetophenone (DMPA), cysteamine, 3-mercaptopropionic acid, sodium methanolate (0.5 M in methanol), Nile Red, DOWEX 50WX8-200, methanol, *N,N*-dimethylformamide (DMF), tetrahydrofuran (THF) and ethanol were purchased from Aldrich and used as received. AlamarBlue, was obtained from Life Technologies (Darmstadt, Germany). If not stated otherwise, cell culture materials, cell culture media, and solutions were obtained from PAA (Pasching, Austria). All other chemicals were purchased from Sigma Aldrich (Steinhausen, Germany) and are of analytical grade or better and were used without further purification.

### **Cysteamine functionalization of PEO<sub>42</sub>-*b*-PAGE<sub>15</sub>-*b*-PtBGE<sub>12</sub>:**

300 mg (0.059 mmol, corresponding to 0.88 mmol of PAGE) of the triblock terpolymer were dissolved in 5 mL of a mixture of DMF, EtOH and MeOH (ratio 1:0.3:1). 45 mg (0.18 mmol, 0.2 eq.) DMPA and 339 mg cysteamine (4.39 mmol, 5 eq.) were added to the mixture. The reaction mixture was degassed and stirred under UV irradiation (366 nm, 6 W) for 24 h. The increase of the molar mass ( $M_n$ ) and the decrease of the signal intensity of the peaks of the double bond were monitored by SEC and <sup>1</sup>H NMR, respectively. The reaction mixture was purified by dialysis against water, a THF/water mixture (1:1) and pure THF. The solvent was removed by distillation under reduced pressure and the product dried under vacuum.

Yield: 250 mg

<sup>1</sup>H NMR (300 MHz, CDCl<sub>3</sub>-*d*<sub>6</sub>,  $\delta$  in ppm): 6.00–5.75 (m, 1H), 5.34–5.07 (m, 2H), 4.04–3.9 (m, 2H), 3.9–3.2 (m, PEO backbone), 2.74–1.94 (br, 4H, CH<sub>2</sub>-CH<sub>2</sub>-S), 2.74–1.93 (br, 2H, S-CH<sub>2</sub>), 1.3–0.97 (s, 9H).  $f = 50\%$ .

SEC:  $M_n = 3,500$  g/mol,  $M_w = 3,600$  g/mol, PDI = 1.06

### **3-Mercapto propionic acid functionalization of PEO<sub>42</sub>-*b*-PAGE<sub>15</sub>-*b*-PtBGE<sub>12</sub>:**

450 mg (0.088 mmol, corresponding to 1.32 mmol of PAGE) of the triblock terpolymer were dissolved in 5 mL of a mixture of DMF/EtOH (ratio 3:1). Subsequently, 68 mg (0.27 mmol, 0.2 eq.) DMPA and 0.23 mL 3-mercapto propionic acid (2.64 mmol, 2 eq.) were added. The reaction mixture was degassed and stirred under UV irradiation (366 nm, 6 W) for 24 h. The increase of the molar mass ( $M_n$ ) and the decrease of the signal intensity of the peaks of the double bond were monitored by SEC and <sup>1</sup>H NMR, respectively. The reaction mixture was purified by dialysis against a THF/water mixture (5:1) and pure THF. The solvent was removed by distillation under reduced pressure and the product dried under vacuum.

Yield: 600 mg



$^1\text{H}$  NMR (300 MHz,  $\text{CDCl}_3-d_6$ ,  $\delta$  in ppm): 3.94–3.24 (m, PEO backbone), 2.87–2.72 (m, 4H,  $\text{CH}_2$  linker), 1.92–1.76 (m, 2H), 1.24–1.09 (s, 9H). Degree of functionalization  $f = 50\%$ .

SEC:  $M_n = 3,550$  g/mol,  $M_w = 3,700$  g/mol, PDI = 1.05

#### **Thiogalactose functionalization of $\text{PEO}_{42}$ -*b*- $\text{PAGE}_{15}$ -*b*- $\text{PtBGE}_{12}$ :**

450 mg (0.088 mmol, corresponding to 1.32 mmol of PAGE) of the triblock terpolymer were dissolved in 5 mL of a mixture of DMF/EtOH (ratio 3:1). To the mixture 68 mg (0.27 mmol, 0.2 eq.) DMPA and 963 mg acetylated thiogalactose (2.64 mmol, 2 eq.) were added. The reaction mixture was degassed and stirred under UV irradiation (366 nm, 6 W) for 72 h. The increase of the molar mass ( $M_n$ ) and the decrease of the signal intensity of the peaks of the double bond were monitored by SEC and  $^1\text{H}$  NMR, respectively. The reaction mixture was purified by size exclusion chromatography (Biobeads SX-1) and the product was dried under vacuum.

Yield: 600 mg

$^1\text{H}$  NMR (300 MHz,  $\text{CDCl}_3-d_6$ ,  $\delta$  in ppm): 6.00–5.76 (m, 1H), 5.7–4.9 (m, 3H, Gal), 4.56–4.43 (m, 1H, Gal), 4.40–4.21 (m, 3H, Gal), 4.20–3.03 (m, PEO backbone), 2.86–2.62 (m, 2H), 2.57–1.47 (m, 12H-Ac), 1.28–1.04 (s, 9H). Degree of functionalization  $f = 70\%$ .

SEC:  $M_n = 4,200$  g/mol,  $M_w = 4,350$  g/mol, PDI = 1.04

#### **Deprotection of $\text{PEO}_{42}$ -*b*-( $\text{PAGE}_5$ -*co*- $\text{PAGE}_{10,\text{Gal}}$ )-*b*- $\text{PtBGE}_{12}$ :**

600 mg (0.066 mmol, corresponding to 2.64 mmol of acetyl groups) of the triblock terpolymer were dissolved in 15 mL of dry methanol. To the mixture 7 mL (3.5 mmol, 1.3 eq.) of a 0.5 M sodium methanolate solution were added and the mixture was allowed to stir for 1 h. Afterwards a DOWEX 50WX8-200 ion exchange resin was added and stirred for 15 min to neutralize the reaction mixture. The resin was filtered off and the crude product was dialyzed against a water/THF mixture (5:1), pure water and pure THF. The solvent was removed by distillation under reduced pressure and product was dried under vacuum.

Yield: 250 mg

$^1\text{H}$  NMR (300 MHz,  $\text{CDCl}_3-d_6$ ,  $\delta$  in ppm): 6.0–5.76 (m, 1H), 5.5–4.84 (m, 3H-Gal), 4.10–2.80 (m, PEO backbone), 1.26–1.01 (s, 9H).

SEC:  $M_n = 10,400$  g/mol,  $M_w = 11,500$  g/mol, PDI = 1.10

#### **Preparation of triblock terpolymer micelles:**

The following procedures with the respective stoichiometry were used for the preparation of all micellar nanostructures with a concentration of 10 g/L in aqueous solution.

100 mg of the corresponding triblock terpolymer were dissolved in 5 mL THF and 4 mg of Nile Red was added to the solution. To the mixture was then added slowly 10 mL of MilliQ water *via* a syringe and the THF was allowed to evaporate by stirring overnight. Non-encapsulated dye was filtered off by a 0.45  $\mu\text{m}$  nylon syringe filter. In case of evaporation of water the solution was filled up again to a volume of 10 mL. After filtration a clear pink solution could be obtained.

#### **Binary co-micelles:**

Here, the preparation of a 1.2/1 mixture of  $\text{PEO}_{42}\text{-}b\text{-(PAGE}_{8,\text{NH}_2}\text{-}co\text{-PAGE}_7)\text{-}b\text{-PtBGE}_{12}$  and  $\text{PEO}_{42}\text{-}b\text{-PAGE}_{15,\text{COOH}}\text{-}b\text{-PtBGE}_{12}$  is reported. Due to the different degrees of functionalization a 2/1 ratio regarding the masses was used.

6.6 mg of  $\text{PEO}_{42}\text{-}b\text{-(PAGE}_{8,\text{NH}_2}\text{-}co\text{-PAGE}_7)\text{-}b\text{-PtBGE}_{12}$  and 3.3 mg of  $\text{PEO}_{42}\text{-}b\text{-PAGE}_{15,\text{COOH}}\text{-}b\text{-PtBGE}_{12}$  were dissolved in 0.3 mL of THF and approx. 2 mg of Nile Red were added to the solution. The solution was then slowly added to 1 mL of MilliQ water and the THF was allowed to evaporate by stirring overnight. Non-encapsulated dye remained as precipitate in the solution and was filtered by 0.45  $\mu\text{m}$  nylon syringe filter. In case of evaporation of water the solution was filled up again to a volume of 1 mL. After filtration a clear pink solution could be obtained.

### **Ternary co-micelles:**

Here, the preparation of a 3.4/1/2.3 mixture of PEO<sub>42</sub>-*b*-(PAGE<sub>8,NH2</sub>-*co*-PAGE<sub>7</sub>)-*b*-PtBGE<sub>12</sub>, PEO<sub>42</sub>-*b*-PAGE<sub>15,COOH</sub>-*b*-PtBGE<sub>12</sub> and PEO<sub>42</sub>-*b*-(PAGE<sub>10,AcGal</sub>-*co*-PAGE<sub>5</sub>)-*b*-PtBGE<sub>12</sub> is reported. Due to the different degrees of functionalization a 6/1/3.5 ratio regarding the stoichiometry of the amino and carboxy functionalized triblock terpolymers was used.

12 mg of PEO<sub>42</sub>-*b*-(PAGE<sub>8,NH2</sub>-*co*-PAGE<sub>7</sub>)-*b*-PtBGE<sub>12</sub>, 2 mg of PEO<sub>42</sub>-*b*-PAGE<sub>15,COOH</sub>-*b*-PtBGE<sub>12</sub> and 7 mg PEO<sub>42</sub>-*b*-(PAGE<sub>10,AcGal</sub>-*co*-PAGE<sub>5</sub>)-*b*-PtBGE<sub>12</sub> were dissolved in 0.4 mL of THF and approx. 3 mg of Nile Red were added to the solution. The solution was then slowly added to 2.1 mL of MilliQ water and the THF was allowed to evaporate by stirring overnight. Non-encapsulated dye remained as precipitate in the solution and was filtered by 0.45 μm nylon syringe filter. In case of evaporation of water the solution was filled up again to a volume of 2.1 mL. After filtration a clear pink solution could be obtained.

### **Gel migration assay**

The micelles (40 μg) were incubated with 5 μL loading buffer (0.25% bromophenolblue, 40% saccharose). Afterwards the solutions were loaded to an 1% agarose gel, electrophoresis (Bio-Rad, Munich, Germany, Mini-Sub Cell GT System) was carried out with a current of 80 V (PowerPac<sup>TM</sup> Basic as power supply) for 30 min in TBE running buffer solution (107.8 g/L Tris-base, 7.4 g/L EDTA, 55 g/L borate). Subsequently, the agarose gel was irradiated with an UV-lamp to induce fluorescence of the bands.

HEK-293 cells (CRL-1573, ATCC) were maintained in RPMI 1640 culture medium, L929 cells (CCL-1, ATCC) in DMEM culture medium and HepG2 (HB-8065, ATCC) in DMEM-F12 culture medium. Both media were supplemented with 10% fetal calf serum (FCS), 100 μg/mL streptomycin, 100 IU/mL penicillin, and 2 mM L-glutamine. Cells were cultivated at 37 °C in a humidified 5% CO<sub>2</sub> atmosphere.

### ***Cytotoxicity***

For L929 cells, the cytotoxicity assay was performed as described by ISO10993-5. In detail, cells were seeded at  $1 \times 10^4$  cells per well in a 96-well plate and incubated for 24 h. No cells were seeded in the outer wells. Afterwards, polymers at the indicated concentrations were added, and the cells were incubated at 37 °C for further 24 h. Subsequently, the medium was replaced by D-PBS and AlamarBlue as recommended by the supplier. After incubation for 4 h, the fluorescence was measured at Ex 570/Em 610 nm, with untreated cells on the same well plate serving as controls.

### ***Hemolysis Assay***

The membrane damaging properties of the polymers were quantified by analyzing the release of hemoglobin from human erythrocytes. The erythrocytes-containing blood was centrifuged at 700 g for 10 min. The obtained pellet was washed three times with D-PBS pH 7.4 by centrifugation at 700 g for 10 min and resuspended in HBG buffer of pH 4 to 8. Polymer solutions were added to the erythrocytes (100  $\mu$ L) and incubated for 60 min under constant shaking at 37 °C. After centrifugation (700 g, 10 min), the supernatant was analyzed for released hemoglobin at 580 nm. The absorbance was measured using a plate reader (Genios Pro, Tecan, Germany). For comparison, collected erythrocytes were washed with DPBS and either lysed with 0.2% Triton X-100 yielding the 100% lysis control value ( $A_{100}$ ) or resuspended in DPBS as reference ( $A_0$ ). The analysis was repeated with blood from at least six independent donors. The hemolytic activity of the polycations was calculated as follow:

$$\% \text{ hemolysis} = 100 * (A_{\text{sample}} - A_0) / (A_{100} - A_0) \quad (1)$$

Here,  $A_{\text{sample}}$ ,  $A_0$ , and  $A_{100}$  are the absorbance intensities of a given sample, erythrocytes incubated with D-PBS, and erythrocytes lysed with Titon X-100.

### ***Uptake studies***

For uptake of the adherent cell lines, cells were seeded at a density of  $10^5$  cells per well in 12-well plates one day before transfection. One hour prior to addition of micelles, cells were rinsed with PBS and supplemented with 1 mL OptiMEM (Life Technologies) or fresh serum containing growth media. Micelles were added at indicated end concentration to the cells and the plates were incubated for 24 h in the incubator. For analysis, the cells were harvested by trypsinization and 10% trypan blue was added. Subsequently the cells were analysed *via* flow cytometry using a Cytomics FC 500 (Beckman Coulter). For determination of the viability during flow cytometry, dead cells were identified in the SSC/FSC dot plot. The relative uptake of encapsulated nil red fluorescence of  $10^4$  cells was quantified. For determination of the uptake efficiency viable cells containing nil red were gated. The experiments were performed at least independently three times.

### **Acknowledgements**

The work of M. J. B. forms part of the research programme of the Dutch Polymer Institute (DPI), project #690. A. C. R, A. S. and M. W. thanks the Carl Zeiss Foundation for financial support and C. Fritzsche for hemolysis studies and Alamar Blue assay. F. H. S. is grateful for a fellowship from the Fonds der Chemischen Industrie (FCI). Furthermore, the authors want to acknowledge the Thuringian Ministry for Education, Science and Culture (TMBWK; #B515-10065, ChaPoNano; #B514-09051, NanoConSens).

## References

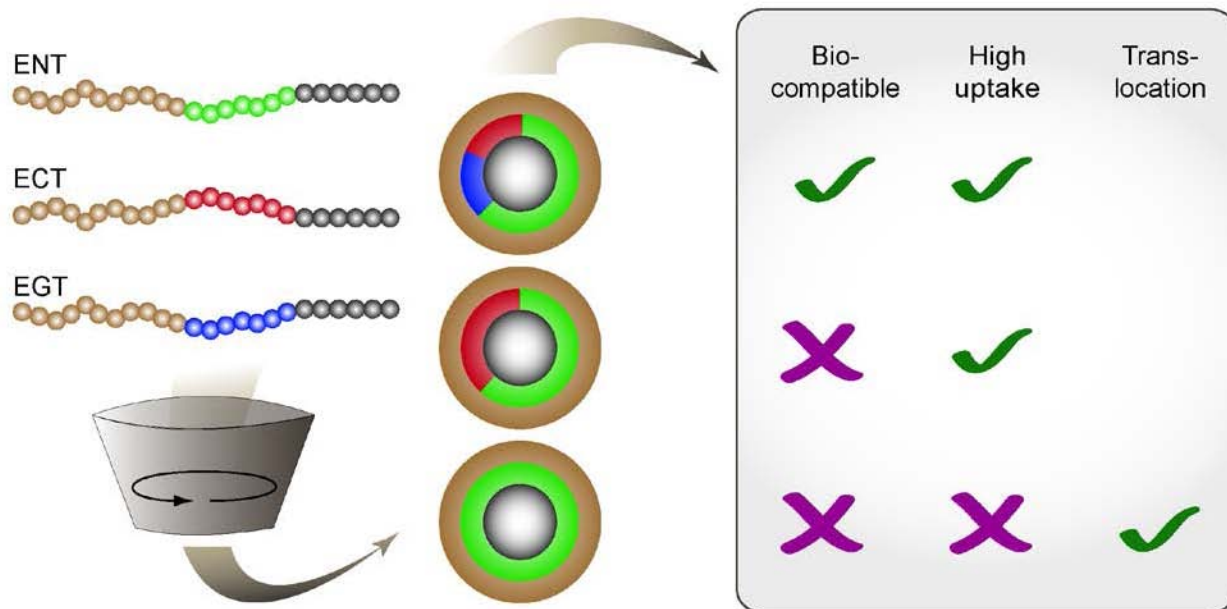
1. Y. Y. Mai, A. Eisenberg, *Chem. Soc. Rev.* **2012**, *41*, 5969-5985.
2. F. H. Schacher, P. A. Rupar, I. Manners, *Angew. Chem. Int. Ed.* **2012**, *51*, 7898-7921.
3. M. J. Barthel, F. H. Schacher, U. S. Schubert, *Polym. Chem.* **2014**, DOI: 10.1039/C1033PY01666H.
4. C. Price, T. P. Lally, R. Stubbers, *Polymer* **1974**, *15*, 541-543.
5. K. Arai, T. Kotaka, Y. Kitano, K. Yoshimura, *Macromolecules* **1980**, *13*, 455-457.
6. Y. Mogi, H. Kotsuji, Y. Kaneko, K. Mori, Y. Matsushita, I. Noda, *Macromolecules* **1992**, *25*, 5408-5411.
7. C. Auschra, R. Stadler, *Macromolecules* **1993**, *26*, 2171-2174.
8. T. P. Lodge, A. Rasdal, Z. B. Li, M. A. Hillmyer, *J. Am. Chem. Soc.* **2005**, *127*, 17608-17609.
9. E. Betthausen, M. Drechsler, M. Fortsch, F. H. Schacher, A. H. E. Müller, *Soft Matter* **2011**, *7*, 8880-8891.
10. A. H. Gröschel, F. H. Schacher, H. Schmalz, O. V. Borisov, E. B. Zhulina, A. Walther, A. H. E. Müller, *Nat. Commun.* **2012**, *3*, 710.
11. A. H. Gröschel, A. Walther, T. I. Löbling, F. H. Schacher, H. Schmalz, A. H. E. Müller, *Nature* **2013**, *503*, 247-251.
12. A. C. Rinkenauer, A. Schallon, U. Günther, M. Wagner, E. Betthausen, U. S. Schubert, F. H. Schacher, *ACS Nano* **2013**, *7*, 9621-9631.
13. A. Schallon, C. V. Synatschke, V. Jerome, A. H. E. Müller, R. Freitag, *Biomacromolecules* **2012**, *13*, 3463-3474.
14. X. Y. Huang, S. Chen, J. L. Huang, *J. Polym. Sci., Part A: Polym. Chem.* **1999**, *37*, 825-833.
15. M. L. Arnal, V. Balsamo, F. Lopez-Carrasquero, J. Contreras, M. Carrillo, H. Schmalz, V. Abetz, E. Laredo, A. J. Müller, *Macromolecules* **2001**, *34*, 7973-7982.
16. R. K. Jing, G. W. Wang, Y. N. Zhang, J. L. Huang, *Macromolecules* **2011**, *44*, 805-810.
17. K. Knop, R. Hoogenboom, D. Fischer, U. S. Schubert, *Angew. Chem. Int. Ed.* **2010**, *49*, 6288-6308.
18. M. J. Barthel, K. Babiuch, T. Rudolph, J. Vitz, S. Hoepfener, M. Gottschaldt, M. D. Hager, F. H. Schacher, U. S. Schubert, *J. Polym. Sci., Part A: Polym. Chem.* **2012**, *50*, 2914-2923.
19. M. J. Barthel, U. Mansfeld, S. Hoepfener, J. A. Czaplewska, F. H. Schacher, U. S. Schubert, *Soft Matter* **2013**, *9*, 3509-3520.
20. B. Obermeier, H. Frey, *Bioconjugate Chem.* **2011**, *22*, 436-444.
21. M. Hruby, C. Konak, K. Ulbrich, *J. Control. Release* **2005**, *103*, 137-148.
22. S. L. Lin, W. J. Zhu, X. H. He, Y. H. Xing, L. Y. Liang, T. Chen, J. P. Lin, *J. Phys. Chem. B* **2013**, *117*, 2586-2593.
23. M. Libera, B. Trzebicka, A. Kowalczyk, W. Walach, A. Dworak, *Polymer* **2011**, *52*, 250-257.
24. K. Kataoka, A. Harada, Y. Nagasaki, *Adv. Drug. Deliv. Rev.* **2001**, *47*, 113-131.
25. P. J. Sun, Y. Zhang, L. Q. Shi, Z. H. Gan, *Macromol. Biosci.* **2010**, *10*, 621-631.
26. K. Van Butsele, S. Cajot, S. Van Vlierberghe, P. Dubruel, C. Passirani, J. P. Benoit, R. Jerome, C. Jerome, *Adv. Funct. Mater.* **2009**, *19*, 1416-1425.
27. S. Fukushima, K. Miyata, N. Nishiyama, N. Kanayama, Y. Yamasaki, K. Kataoka, *J. Am. Chem. Soc.* **2005**, *127*, 2810-2811.

28. Y. Lee, K. Miyata, M. Oba, T. Ishii, S. Fukushima, M. Han, H. Koyama, N. Nishiyama, K. Kataoka, *Angew. Chem. Int. Ed.* **2008**, *47*, 5163-5166.
29. C. L. Wu, R. J. Ma, H. He, L. Z. Zhao, H. J. Gao, Y. L. An, L. Q. Shi, *Macromol. Biosci.* **2009**, *9*, 1185-1193.
30. A. B. E. Attia, Z. Y. Ong, J. L. Hedrick, P. P. Lee, P. L. R. Ee, P. T. Hammond, Y. Y. Yang, *Curr. Opin. Colloid Interface Sci.* **2011**, *16*, 182-194.
31. X. Liu, Y. Liu, Z. K. Zhang, F. Huang, Q. Tao, R. J. Ma, Y. L. An, L. Q. Shi, *Chem. Eur. J.* **2013**, *19*, 7437-7442.
32. J. P. Lin, J. Q. Zhu, T. Chen, S. L. Lin, C. H. Cai, L. S. Zhang, Y. Zhuang, X. S. Wang, *Biomaterials* **2009**, *30*, 108-117.
33. S. V. Vinogradov, E. V. Batrakova, S. Li, A. V. Kabanov, *J. Drug Targeting* **2004**, *12*, 517-526.
34. R. Zheng, G. Liu, X. Yan, *J. Am. Chem. Soc.* **2005**, *127*, 15358-15359.
35. Z. Li, M. A. Hillmyer, T. P. Lodge, *Macromolecules* **2006**, *39*, 765-771.
36. H. Cabral, Y. Matsumoto, K. Mizuno, Q. Chen, M. Murakami, M. Kimura, Y. Terada, M. R. Kano, K. Miyazono, M. Uesaka, N. Nishiyama, K. Kataoka, *Nat. Nanotechnol.* **2011**, *6*, 815-823.
37. H. Dong, N. Dube, J. Y. Shu, J. W. Seo, L. M. Mahakian, K. W. Ferrara, T. Xu, *ACS Nano* **2012**, *6*, 5320-5329.
38. F. Alexis, E. Pridgen, L. K. Molnar, O. C. Farokhzad, *Mol. Pharm.* **2008**, *5*, 505-515.
39. J. Nguyen, X. Xie, M. Neu, R. Dumitrascu, R. Reul, J. Sitterberg, U. Bakowsky, R. Schermuly, L. Fink, T. Schmehl, T. Gessler, W. Seeger, T. Kissel, *J. Gene. Med.* **2008**, *10*, 1236-1246.
40. S. Mishra, P. Webster, M. E. Davis, *Eur. J. Cell. Biol.* **2004**, *83*, 97-111.
41. J. Sun, F. Zeng, H. Jian, S. Wu, *Biomacromolecules* **2013**, *14*, 728-736.
42. K. Babiuch, D. Pretzel, T. Tolstik, A. Vollrath, S. Stanca, F. Foertsch, C. R. Becer, M. Gottschaldt, C. Biskup, U. S. Schubert, *Macromol. Biosci.* **2012**, *12*, 1190-1199.
43. R. Yang, F. H. Meng, S. B. Ma, F. S. Huang, H. Y. Liu, Z. Y. Zhong, *Biomacromolecules* **2011**, *12*, 3047-3055.
44. H. Cui, T. K. Hodgdon, E. W. Kaler, L. Abezgauz, D. Danino, M. Lubovsky, Y. Talmon, D. J. Pochan, *Soft Matter* **2007**, *3*, 945-955.
45. S. J. Holder, N. A. J. M. Sommerdijk, *Polym. Chem.* **2011**, *2*, 1018-1028.
46. S. Zhong, D. J. Pochan, *Polym. Rev.* **2010**, *50*, 287-320.
47. P. Greenspan, E. P. Mayer, S. D. Fowler, *J. Cell. Biol.* **1985**, *100*, 965-973.
48. M. Wagner, K. Reiche, A. Blume, P. Garidel, *Colloids Surf., A.* **2012**, *415*, 421-430.
49. W. Burchard, *Adv. Polym. Sci.* **1999**, *143*, 113-194.
50. M. A. Benincasa, K. D. Caldwell, *J. Chromatogr., A* **2001**, *925*, 159-169.
51. M. Glantz, A. Hakansson, H. L. Mansson, M. Paulsson, L. Nilsson, *Langmuir* **2010**, *26*, 12585-12591.
52. A. Vollrath, D. Pretzel, C. Pietsch, I. Perevyazko, S. Schubert, G. M. Pavlov, U. S. Schubert, *Macromol. Rapid Commun.* **2012**, *33*, 1791-1797.
53. F. J. Verbaan, C. Oussoren, C. J. Snel, D. J. A. Crommelin, W. E. Hennink, G. Storm, *J. Gene Med.* **2004**, *6*, 64-75.
54. M. Ogris, S. Brunner, S. Schuller, R. Kircheis, E. Wagner, *Gene Ther.* **1999**, *6*, 595-605.
55. J. Y. Cherng, P. vandeWetering, H. Talsma, D. J. A. Crommelin, W. E. Hennink, *Pharmaceut. Res.* **1996**, *13*, 1038-1042.
56. S. Belbekhouche, V. Dulong, L. Picton, D. Le Cerf, *Colloid Surf., A* **2013**, *428*, 25-31.

57. A. Albanese, P. S. Tang, W. C. Chan, *Annu. Rev. Biomed. Eng.* **2012**, *14*, 1-16.
58. J. Rejman, V. Oberle, I. S. Zuhorn, D. Hoekstra, *Biochem. J.* **2004**, *377*, 159-169.
59. R. M. Steinman, I. S. Mellman, W. A. Muller, Z. A. Cohn, *J. Cell Biol.* **1983**, *96*, 1-27.
60. P. R. Leroueil, S. Y. Hong, A. Mecke, J. R. Baker, B. G. Orr, M. M. B. Holl, *Accounts Chem. Res.* **2007**, *40*, 335-342.
61. C. L. Ting, Z. G. Wang, *Soft Matter* **2012**, *8*, 12066-12071.
62. H. M. Ding, W. D. Tian, Y. Q. Ma, *ACS Nano* **2012**, *6*, 1230-1238.
63. S. Choksakulnimitr, S. Masuda, H. Tokuda, Y. Takakura, M. Hashida, *J. Controlled Release* **1995**, *34*, 233-241.
64. M. Andersson, B. Wittgren, K. G. Wahlund, *Anal. Chem.* **2003**, *75*, 4279-4291.
65. A. V. Delgado, F. Gonzalez-Caballero, R. J. Hunter, L. K. Koopal, J. Lyklema, *J. Colloid Interf. Sci.* **2007**, *309*, 194-224.
66. H. Ohshima, *J. Colloid Interf. Sci.* **1994**, *168*, 269-271.
67. M. Gottschaldt, D. Koth, D. Müller, I. Klette, S. Rau, H. Görls, B. Schafer, R. P. Baum, S. Yano, *Chem. Eur. J.* **2007**, *13*, 10273-10280.
68. F. M. Ibatullin, K. A. Shabalin, J. V. Janis, A. G. Shavva, *Tetrahedron Lett.* **2003**, *44*, 7961-7964.



## Table of Content



We present the influence of the functionalization of a triblock terpolymer poly(ethylene oxide)-*block*-poly(allyl glycidyl ether)-*block*-poly(*tert*-butyl glycidyl ether) (PEO-*b*-PAGE-*b*-PtBGE) with thiogalactose (sugar), cysteamine (amino) and 2-mercaptopropionic acid (carboxy) groups on micelle formation and cellular uptake.

## Supporting information for

### “Small but powerful: Co-assembly of polyether-based triblock terpolymers into sub-30nm micelles and synergistic effects on cellular interactions”

Markus J. Barthel<sup>#, 1,2,3</sup> Alexandra C. Rinkenauer<sup>#, 1,2</sup> Michael Wagner,<sup>1,2</sup> Ulrich Mansfeld,<sup>1,2</sup> Stephanie Hoepfener,<sup>1,2</sup> Justyna A. Czaplewska,<sup>1,2</sup> Michael Gottschald,<sup>1,2</sup> Anja Schallon,<sup>1,2</sup> Felix H. Schacher,<sup>\*1,2</sup> Ulrich S. Schubert<sup>\*1,2,3</sup>

<sup>#</sup>Both authors contributed equally to this work.

<sup>1</sup> Laboratory of Organic and Macromolecular Chemistry (IOMC), Friedrich Schiller University Jena, Humboldtstrasse 10, 07743 Jena, Germany.

<sup>2</sup> Jena Center for Soft Matter (JCSM), Friedrich Schiller University Jena, Philosophenweg 7, 07743 Jena, Germany.

<sup>3</sup> Dutch Polymer Institute (DPI), P.O. Box 902, 5600 AX Eindhoven, the Netherlands.

Email: [ulrich.schubert@uni-jena.de](mailto:ulrich.schubert@uni-jena.de); [felix.schacher@uni-jena.de](mailto:felix.schacher@uni-jena.de)

**Table S1:** Influence of the pH value of the solution on the self-assembly process.

Sample	$\langle R_h \rangle_{n,app}$ [nm]
(ENT/ECT) <sup>3.5:1</sup> pH = 7	6
(ENT/ECT) <sup>3.5:1</sup> pH = 3	7
(ENT/ECT) <sup>3.5:1</sup> pH = 11	7

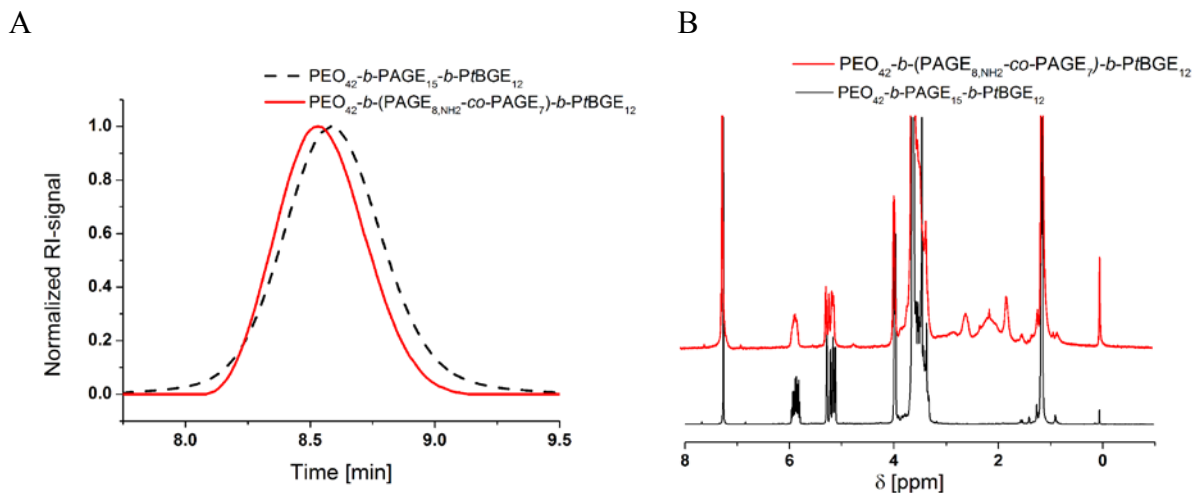


**Figure S1:** SEC traces (A) and  $^1\text{H}$  NMR spectrum (B) of the  $\text{PEO}_{42}\text{-}b\text{-PAGE}_{15}\text{-}b\text{-PtBGE}_{12}$  precursor as well as the cysteamine functionalized triblock terpolymer.

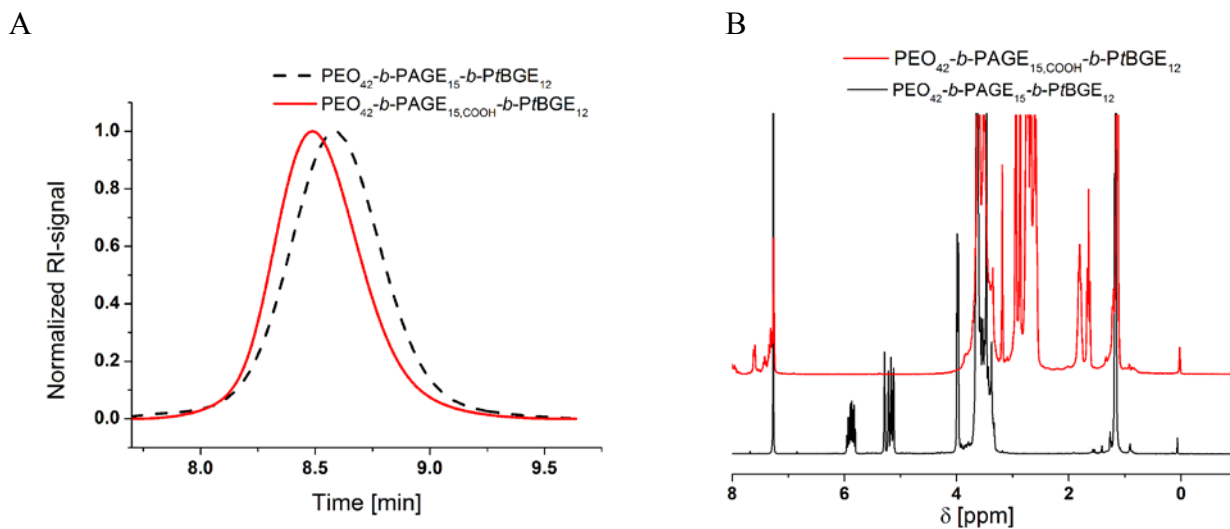


**Figure S2:** SEC traces (A) and  $^1\text{H}$  NMR spectrum (B) of the  $\text{PEO}_{42}\text{-}b\text{-PAGE}_{15}\text{-}b\text{-PtBGE}_{12}$  precursor as well as the 3-mercaptopropionic acid functionalized triblock terpolymer.

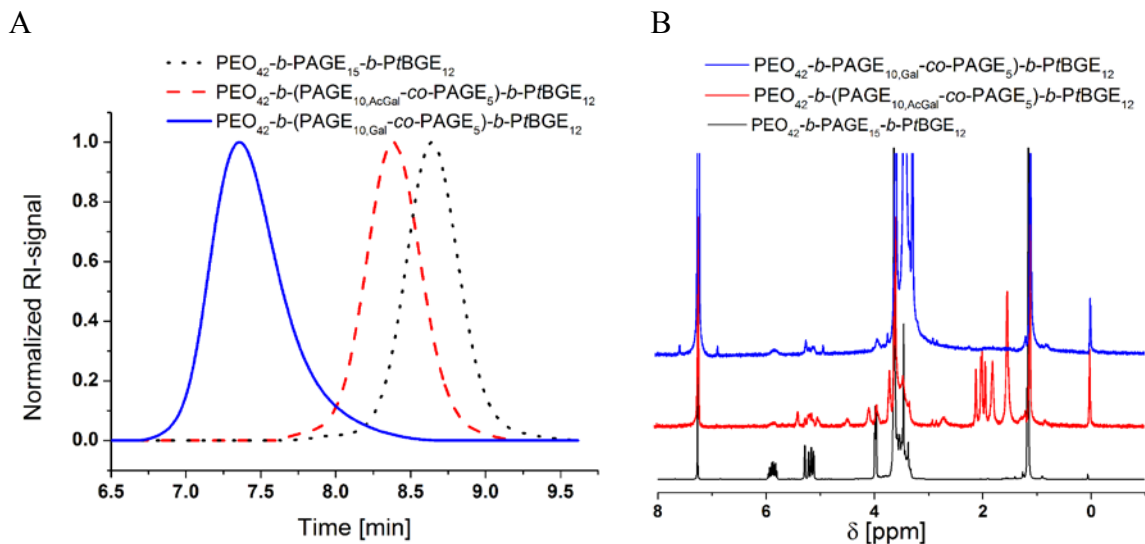


**Figure S3:** SEC traces (A) and  $^1\text{H}$  NMR spectrum (B) of the  $\text{PEO}_{42}\text{-}b\text{-PAGE}_{15}\text{-}b\text{-PtBGE}_{12}$  precursor, the acetylated thiogalactose functionalized triblock terpolymer as well as the deprotected product.

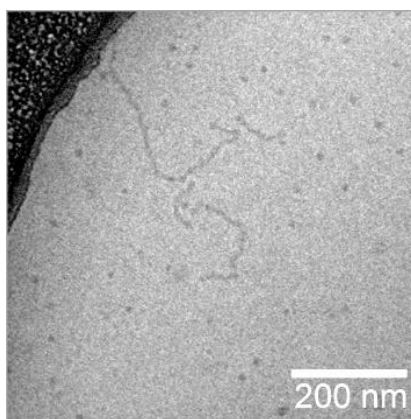


**Figure S4:** Cryo-TEM image of  $\text{PEO}_{42}\text{-}b\text{-PAGE}_{15,\text{COOH}}\text{-}b\text{-PtBGE}_{12}$  (ECT) as example displaying the minor distribution of worm-like structures.

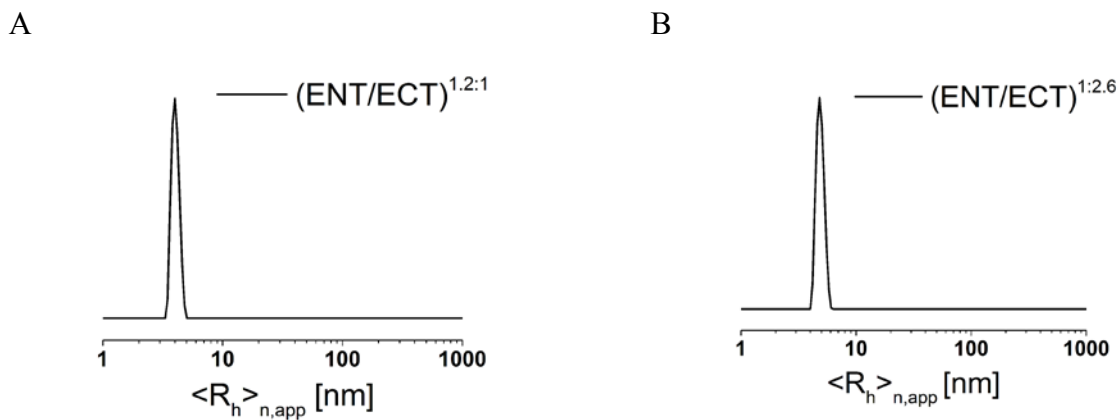


**Figure S5:** Number-weighted DLS CONTIN plots for the 1.2:1 (A) and 1:2.6 (B) mixture of  $\text{PEO}_{42}\text{-}b\text{-PAGE}_{8,\text{NH}_2}\text{-}b\text{-PtBGE}_{12}$  /  $\text{PEO}_{42}\text{-}b\text{-PAGE}_{15,\text{COOH}}\text{-}b\text{-PtBGE}_{12}$  (ENT/ECT).

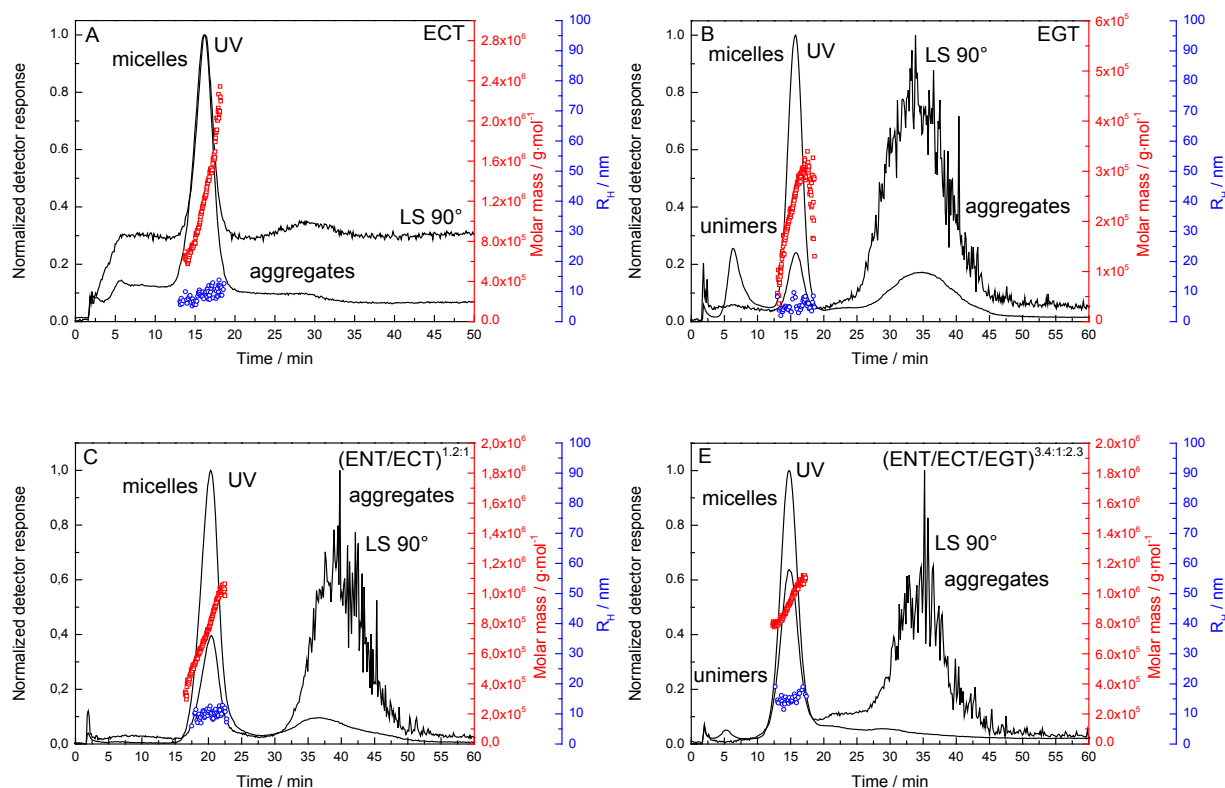


**Figure S6:** AF4 fractograms of self-assembled structures of PEO<sub>42</sub>-*b*-PAGE<sub>15,COOH</sub>-*b*-PtBGE<sub>12</sub> (ECT, A), PEO<sub>42</sub>-*b*-(PAGE<sub>10,Gal-co</sub>-PAGE<sub>5</sub>)-*b*-PtBGE<sub>12</sub> (EGT, B), PEO<sub>42</sub>-*b*-(PAGE<sub>8,NH2-co</sub>-PAGE<sub>7</sub>)-*b*-PtBGE<sub>12</sub> / PEO<sub>42</sub>-*b*-PAGE<sub>15,COOH</sub>-*b*-PtBGE<sub>12</sub> ((ENT/ECT)<sup>1.2:1</sup>, C), PEO<sub>42</sub>-*b*-(PAGE<sub>8,NH2-co</sub>-PAGE<sub>7</sub>)-*b*-PtBGE<sub>12</sub> / PEO<sub>42</sub>-*b*-PAGE<sub>15,COOH</sub>-*b*-PtBGE<sub>12</sub> ((ENT/ECT)<sup>1:2.6</sup>, D) and PEO<sub>42</sub>-*b*-(PAGE<sub>8,NH2-co</sub>-PAGE<sub>7</sub>)-*b*-PtBGE<sub>12</sub> / PEO<sub>42</sub>-*b*-PAGE<sub>15,COOH</sub>-*b*-PtBGE<sub>12</sub> / PEO<sub>42</sub>-*b*-(PAGE<sub>10,Gal-co</sub>-PAGE<sub>5</sub>)-*b*-PtBGE<sub>12</sub> ((ENT/ECT/EGT)<sup>3.4:1:2.3</sup>, E) in 20 mM NaCl.

**Table S2:** Experimental dn/dc values of the different polymer systems in 20 mM NaCl.

Sample	dn/dc (mL/g)	M <sub>w</sub> (g/mol)	M <sub>z</sub> (g/mol)	PDI
EAT	0.111±0.001	1.226E6±7,371	1.353E6±14,572	1.07±0.001
ENT	0.092±0.008	1.888E6±37,165	1.926E6±36,501	1.02±0.003
ECT	0.128±0.002	1.140E6±8,485	1.239E6±11,314	1.09±0.001
EGT	0.144±0.001	2.428E5±4,327	2.551E5±5,667	1.09±0.037
(ENT/ECT)3.5:1	0.116±0.001	1.213E6±36,638	1.230E6±36,638	1.01±0.001
(ENT/ECT)1.2:1	0.096±0.004	7.665E5±11,067	7.981E5±10,152	1.05±0.003
(ENT/ECT)1:2.6	0.114±0.001	6.386E5±2,113	6.569E5±2,223	1.03±0.004
(ENT/ECT/EGT)3.5:1:0.5	0.101±0.001	1.154E6±74,661	1.175E6±79,952	1.02±0.002
(ENT/ECT/EGT)3.4:1:2.3	0.113±0.002	9.743E5±48,431	9.820E5±46,701	1.01±0.001

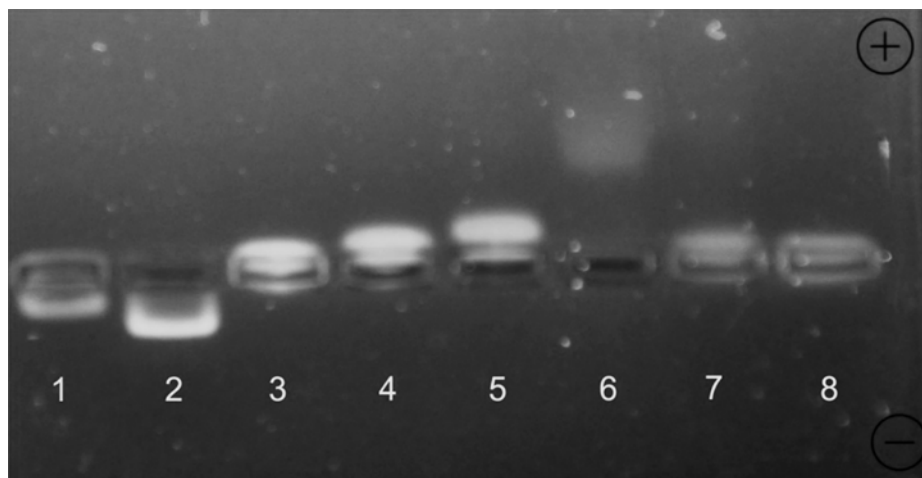


**Figure S7:** Gel-electrophoresis study of the as synthesized material EAT (1), ENT (2), mixtures of ENT and ECT in ratios of 3:1 (3), 1:1 (4), 1:3 (5), ECT (6), a mixture of ECT and EGT in a ratio of 1:1 (7) and EGT(8).

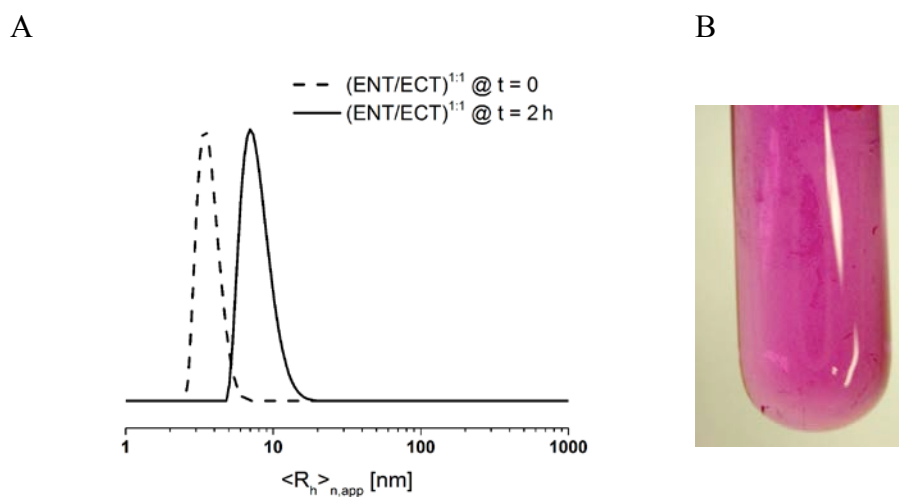


**Figure S8:** Number-weighted DLS CONTIN plots of a 1:1 mixture of  $\text{PEO}_{42}$ -*b*-( $\text{PAGE}_{8,\text{NH}_2}$ -*co*- $\text{PAGE}_7$ )-*b*- $\text{PtBGE}_{12}$  (ENT) micelles with  $\text{PEO}_{42}$ -*b*- $\text{PAGE}_{15,\text{COOH}}$ -*b*- $\text{PtBGE}_{12}$  (ENT/ECT) directly after mixing and 2 h (ENT/ECT) (A) and a photograph of the solution after 12 h showing precipitated material (B).

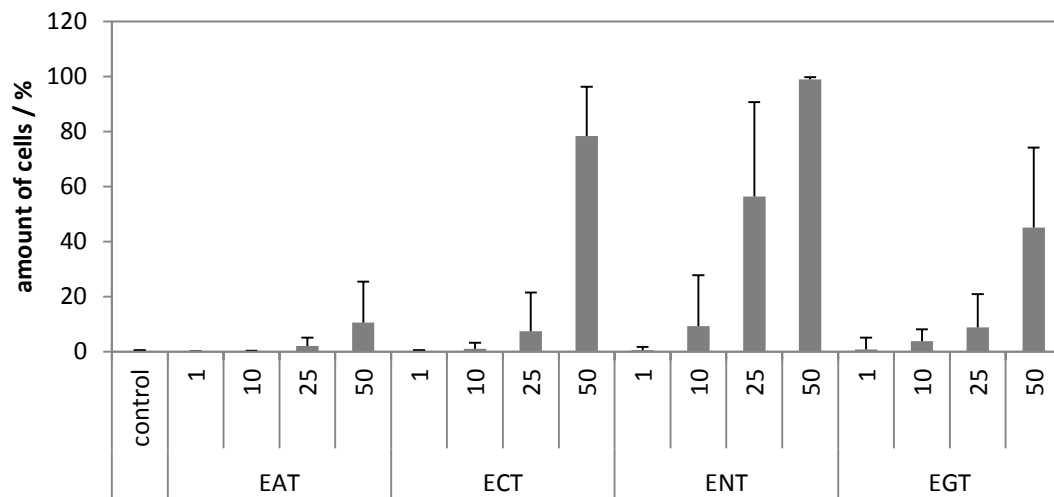


**Figure S9:** Internalization efficiency of triblock terpolymer micelles in HepG2 cells.

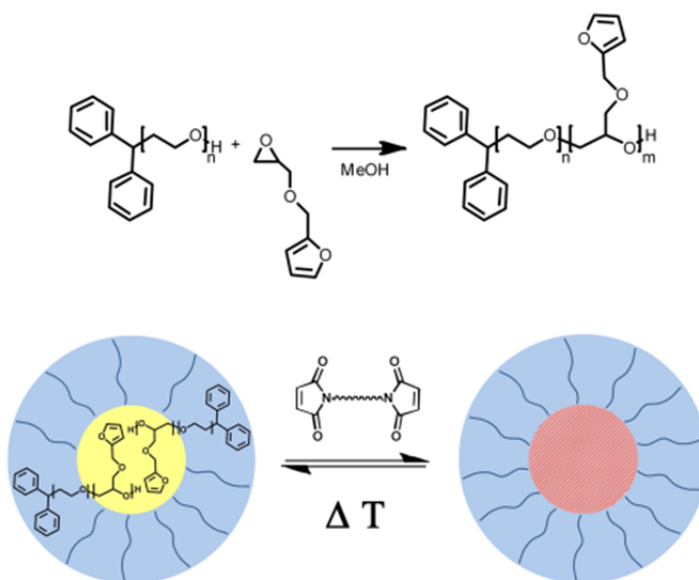
## Publication P4

Homo- and block copolymers of poly(furfuryl glycidyl ether) by living anionic polymerization: Towards reversibly core-crosslinked micelles

Markus J. Barthel<sup>#</sup>, Tobias Rudolph<sup>#</sup>, Sarah Crotty, Felix H. Schacher, Ulrich S. Schubert

<sup>#</sup> Both authors contributed equally to this work.

*J. Polym. Sci., Part A: Polym. Chem.* **2012**, *50*, 4958-4965.





# Homo- and Diblock Copolymers of Poly(furfuryl glycidyl ether) by Living Anionic Polymerization: Toward Reversibly Core-Crosslinked Micelles

Markus J. Barthel,<sup>1,2,3\*</sup> Tobias Rudolph,<sup>1,2\*</sup> Sarah Crotty,<sup>1,2,3</sup> Felix H. Schacher,<sup>1,2</sup> Ulrich S. Schubert<sup>1,2,3</sup>

<sup>1</sup>Laboratory of Organic and Macromolecular Chemistry (IOMC), Friedrich-Schiller-University Jena, Humboldtstr 10, 07743 Jena, Germany

<sup>2</sup>Jena Center for Soft Matter (JCSM), Friedrich-Schiller-University Jena, Humboldtstr. 10, 07743 Jena, Germany

<sup>3</sup>Dutch Polymer Institute (DPI), John F. Kennedylaan 2, 5612 AB Eindhoven, The Netherlands

Correspondence to: U. S. Schubert (E-mail: ulrich.schubert@uni-jena.de) or F. H. Schacher (E-mail: felix.schacher@uni-jena.de)

Received 26 July 2012; accepted 6 August 2012; published online 29 August 2012

DOI: 10.1002/pola.26327

**ABSTRACT:** We report the synthesis and characterization of well-defined homo- and diblock copolymers containing poly(furfuryl glycidyl ether) (PFGE) via living anionic ring-opening polymerization using different initiators. The obtained materials were characterized by SEC, MALDI-TOF MS, and <sup>1</sup>H NMR spectroscopy and molar masses of up to 9400 g/mol were obtained for PFGE homopolymers. If the amphiphilic diblock copolymer PEG-*block*-PFGE was dissolved in water, micelles with a PFGE core and a PEG corona were formed. Hereby, the hydrophobic PFGE core

domains were used for the incorporation of a suitable bismaleimide and heating to 60 °C induced the crosslinking of the micellar core via Diels-Alder chemistry. This process was further shown to be reversible. © 2012 Wiley Periodicals, Inc. *J Polym Sci Part A: Polym Chem* 50: 4958–4965, 2012

**KEYWORDS:** anionic polymerization; block copolymers; cross-linking; furfuryl glycidyl ether; poly(ethylene glycol); ring-opening polymerization; self-assembly; self-healing

**INTRODUCTION** The preparation of micellar structures with controlled size, solubility, and surface chemistry for example, the controlled uptake and/or delivery of guest substances in selected compartments has rapidly increased over the last years.<sup>1,2</sup> Quite often, poly(ethylene glycol) (PEG) has been employed as the hydrophilic block, as PEG is non-toxic, chemically inert and highly water-soluble.<sup>3,4</sup>

For the preparation of well-defined, functionalized PEG and related poly(glycidyl ethers) with controlled molar masses, low polydispersity indices (PDIs), and predictable architectures, living anionic ring-opening polymerization (ROP) represents a powerful tool. Poly(glycidyl ethers) offer the possibility to introduce additional side-chain functionality into polyether-based polymers and block copolymers. This has been shown for example, PEG-*block*-poly(allyl glycidyl ether) block copolymers and their self-assembly into micelles in aqueous solution.<sup>5</sup> The PAGE segment enables post-polymerization modifications using thiol-ene chemistry and, therefore, the covalent attachment of drugs or bioactive moieties.<sup>6–10</sup> In that respect, Hrubý reported the attachment of doxorubicin, a drug commonly used in cancer therapy, to the

PAGE compartment featuring a pH-sensitive linker to enable the selective cleavage of the drug at the target.<sup>11</sup> Besides PAGE, ethoxy ethyl glycidyl ether (EEGE),<sup>12,13</sup> or isopropylidene glyceryl glycidyl ether can be used for the synthesis of functional polyethers.<sup>14</sup>

An additional possibility for a (reversible) post-polymerization functionalization is the introduction of furfuryl groups. Kavita et al. used furfuryl methacrylate as a comonomer in the ATRP of methacrylates.<sup>15</sup> After polymerization, the furfuryl groups could be used in a subsequent Diels-Alder reaction for example, cross-linking and network formation.<sup>16,17</sup> Further heating above a certain temperature can be used to induce a retro-Diels-Alder reaction, resulting in a cleavage of the network junctions. Subsequent cooling restores the network and the process was shown to be fully reversible. One possible application field for these systems are self-healing materials, as recently demonstrated for PEG-based networks.<sup>18,19</sup> As an example for polyethers carrying furfuryl moieties in the side-chain, poly(furfuryl glycidyl ether) (PFGE) has been prepared using condensation reactions but with limited control over molar mass, molecular architecture, and PDI values.<sup>20</sup>

\*Author Markus J. Barthel and Author Tobias Rudolph contributed equally to this work.

Additional Supporting Information may be found in the online version of this article.

© 2012 Wiley Periodicals, Inc.

Here, we report the synthesis of well-defined PFGE homopolymers and the corresponding poly(ethylene glycol)-*block*-poly(furfuryl glycidyl ether) (PEG<sub>139</sub>-*b*-PFGE<sub>12</sub>) diblock copolymer by living anionic ROP using different initiators [Diphenylmethyl potassium DPMK, sodium hydride (NaH), cesium hydroxide monohydrate (CsOH), and potassium *t*-butanolate (*t*-BuOK)]. Due to the hydrophobic nature of the PFGE block, poly(ethylene glycol)-*block*-PFGE (PEG-*b*-PFGE) diblock copolymers undergoes self-assembly in dilute aqueous solution into micelles with a PFGE core and a PEG corona. We show that a suitable crosslinker, 1-1'-(methylenedi-4,1-phenylene)bismaleimide (BMA), can be successfully encapsulated within the PFGE core domains and used for core-crosslinking upon heating of the micellar solution to 60 °C. This could be verified by dialysis of the aggregates into non-selective solvents (THF, DMF) where the micellar structure could be retained. We further demonstrate that the crosslinking process is reversible to a certain extent.

## EXPERIMENTAL

### Instruments

<sup>1</sup>H NMR spectra were recorded on a Bruker AC 300 MHz. Size exclusion chromatography was performed on either a Shimadzu SCL-10 A system (with a LC-10AD pump, a RID-10 A refractive index detector, and a PL gel 5 μm mixed-D column at 25 °C) where the eluent was a mixture of chloroform:triethylamine:isopropanol (94:4:2) with a flow rate of 1 mL/min or on an Agilent Technologies 1200 Series SEC system equipped with a G131A isocratic pump, a G1329A autosampler, a G1362A refractive index detector, and both a PSS Gram 30 and a PSS Gram 1000 columns in series. 2.1% LiCl solution in DMA was used as eluent at 1 mL/min flow rate at a column oven temperature of 40 °C. Both systems were calibrated with PEG standards from PSS ( $M_n = 1470\text{--}42000$  g/mol).

MALDI-TOF mass spectra were obtained using an Ultraflex III TOF/TOF mass spectrometer (Bruker Daltonics) with *trans*-2-[3-(4-*tert*-butylphenyl)-2-methyl-2-propenylidene] malononitrile or 2,5-dihydroxybenzoic acid as matrix in reflector as well as in linear mode. The instrument was calibrated prior to each measurement with an external PMMA standard from PSS Polymer Standards Services GmbH.

DLS was performed at a scattering angle of 90° on an ALV GGS-3 instrument and a He-Ne laser operating at a wavelength of  $\lambda = 633$  nm at 25 °C. The CONTIN algorithm was applied to analyze the correlation functions obtained. Apparent hydrodynamic radii were calculated according to the Stokes-Einstein equation. All CONTIN plots are number-weighted.

Transmission electron microscopy (TEM) was performed on a Zeiss-CEM 902A, Oberkochen, Germany operating at 80 kV. Images were recorded using a 1k TVIPS FastScan CCD camera. No staining of the samples was necessary. For sample preparation, a drop of the micellar solution was cast onto carbon-coated TEM grids, the solvent was blotted away using filter paper, and the structures were imaged after drying.

### Materials

Ethylene oxide (EO), furfuryl glycidyl ether (FGE), sodium hydride in mineral oil, potassium *t*-butanolate, cesium hydroxide monohydrate, *N,N*-dimethylformamide (DMF), tetrahydrofuran (THF), and toluene were purchased from Aldrich. Toluene was used directly from a solvent purification system (PureSolv, Innovative Technology). THF was distilled from sodium/benzophenone. EO was distilled from sodium. FGE was purified by column chromatography (eluent: ethylacetate/*n*-hexane 5/1) and vacuum drying before usage. Diphenylmethyl potassium (DPMK) was synthesized as reported previously.<sup>1</sup> Sodium hydride was washed with dry cyclohexane to remove the mineral oil and stored under argon. Cesium hydroxide was suspended in dry toluene and the solvent was removed under vacuum at 90 °C to dry the cesium hydroxide. The PEG precursor was synthesized via living anionic ROP of EO with DPMK in THF in a BüchiGlasUster Pico-Clave and dried via azeotropic distillation under vacuum from dry toluene. *t*-BuOK was used as received.

### Polymerization of FGE in the Bulk

*t*-BuOK (5.6 mg, 0.05 mmol) were transferred into a Schlenk flask under inert conditions and 0.45 mL FGE (3.24 mmol, the ratio M:I was 65:1,  $M_{n,theo} = 10,000$  g/mol) were added. The mixture was kept for 24 h at 45 °C under vigorous stirring. The reaction was terminated by the addition of 0.1 mL methanol and the product was dried under vacuum. SEC:  $M_n = 5500$  g/mol, PDI = 1.18. The synthesis of PFGE using NaH, CsOH, and DPMK as initiators was carried out using the same procedure.

### Polymerization of FGE in Solution

Four milliliter of freshly prepared THF were transferred into a Schlenk flask and 0.071 mL DPMK (0.05 mmol) were added. Afterwards, 0.45 mL (FGE, 3.24 mmol, ratio of M:I was 65:1, and  $M_{n,theo} = 10,000$  g/mol) were introduced and the reaction was allowed to stir for 24 h at 45 °C. The reaction was terminated by the addition of 0.5 mL methanol and the product was dried under vacuum.

<sup>1</sup>H NMR (300 MHz, DMSO-*d*<sub>6</sub>,  $\delta$ , ppm): 3.6–3.2 (br, 5H), 3.9 (t, 1H), 4.42 (s, 2H), 6.28 (m, 2H), 7.26–7.1 (m, 10H), and 7.36 (s, 1H). SEC:  $M_n = 2900$  g/mol, PDI = 1.09; MALDI-TOF MS:  $M_p = 8200$  g/mol.

The synthesis of PFGE using NaH, CsOH, and DPMK as initiators was carried out using the same procedure.

### Synthesis of PEG-*b*-PFGE

One gram monohydroxy-functionalized PEG ( $M_{p,MALDI} = 6100$  g/mol, 0.16 mmol) was dried under vacuum at 75 °C for 2 h and dissolved in 10 mL freshly prepared THF. To activate the hydroxyl group, a stoichiometric amount of DPMK was added until the solution remained slightly red. FGE (0.73 mL, 5.3 mmol) were added and the reaction mixture was stirred for 24 h at 45 °C. The reaction was terminated by the addition of 0.5 mL methanol and the crude polymer was purified by precipitation in cold diethyl ether and dried under vacuum.

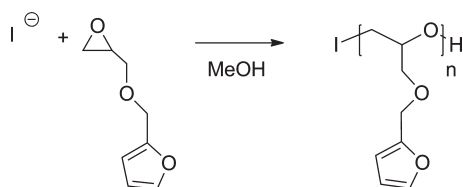


**FIGURE 1** Schematic representation of the homopolymerization of FGE.

$^1\text{H}$  NMR (300 MHz,  $\text{DMSO-}d_6$ ,  $\delta$ , ppm): 3.65–3.15 (br, PEG-backbone), 3.95 (t, 1H), 4.3 (s, 2H), 6.3 (m, 2H), 7.2–7.05 (m, 10H), 7.5 (s, 1H). SEC:  $M_n = 6000$  g/mol, PDI = 1.06; MALDI-TOF MS:  $M_p = 8050$  g/mol

## RESULTS AND DISCUSSION

### Synthesis of PFGE

The living anionic ring-opening polymerization (AROP) of allyl glycidyl ether (AGE) or EEGE represents a facile strategy for the introduction of functional groups into polyether-based materials, thus enabling post-polymerization functionalizations.<sup>14</sup> In most cases, click chemistry is used to modify the polymer and to adjust its properties, either in solution or in the bulk. FGE is another promising monomer for anionic ROP and subsequent post-polymerization functionalization via the pendant furan ring by, for example, Diels-Alder reactions. However, FGE was up to now only used in condensation reactions, exhibiting limited control over molar masses or PDI values.<sup>20</sup>

FGE was purified by column chromatography, followed by vacuum drying before usage in anionic ROP reactions. The homopolymerization in THF was first studied using DPMK as initiator, synthesized according to literature procedures.<sup>21</sup> For this system lower molar masses than expected were observed, even if longer reaction times (48 h) were used. Therefore, a general study of the FGE homopolymerization was performed. Hereby, we focused on different initiators for the AROP [DPMK, sodium hydride (NaH), cesium hydroxide monohydrate (CsOH), and potassium *t*-butanolate (*t*-BuOK)] (Fig. 1).

**TABLE 1** Characterization Data for the PFGE Homopolymers Initiated Using Different Initiators in Bulk and in Solution

Initiator	In Bulk			In THF		
	$M_n^a$	$M_w^a$	PDI <sup>a</sup>	$M_n^a$	$M_w^a$	PDI <sup>a</sup>
NaH	2700	3200	1.18	–	–	–
CsOH	2800	3300	1.18	865	900	1.06
DPMK	3100	3500	1.11	2800	3150	1.09
<i>t</i> -BuOK	5500	7000	1.28	2900	3100	1.10

<sup>a</sup> Obtained by SEC ( $\text{CHCl}_3$ ; *i*-Prop.:TEA 94:4:2, using PEG standards).

In addition, to study the influence of THF as solvent, the reactions were performed in solution as well as in the bulk. It can be clearly seen from the SEC traces [Fig. 2(a); Table 1] that *t*-BuOK (solid black line,  $M_{n,\text{app}} = 5500$  g/mol) lead to (apparently) higher molar masses than DPMK (dashed black line,  $M_{n,\text{app}} = 3100$  g/mol) under bulk conditions. CsOH (dotted black line,  $M_{n,\text{app}} = 2800$  g/mol), and NaH (black line with alternating dots and dashes,  $M_{n,\text{app}} = 2700$  g/mol) lead to even lower molar masses. However, coupling products were observed in case of *t*-BuOK, DPMK, and CsOH (bimodal distributions), as well as a broadening of the molar mass distribution using NaH as initiator.

To obtain a full picture, all initiators for the anionic ROP were also tested in THF. The results are displayed in Figure 2(b) and Table 1. The best results were obtained in case of *t*-BuOK (solid black line,  $M_{n,\text{app}} = 2900$  g/mol), leading to well-defined PFGE with higher molar masses as DPMK (dotted black line,  $M_{n,\text{app}} = 2800$  g/mol). No polymer was obtained for NaH, whereas CsOH (dashed black line,  $M_{n,\text{app}} = 865$  g/mol) again yielded lower molar masses.

For a detailed characterization of the obtained homopolymers, the DPMK initiated sample was studied using MALDI-TOF MS and  $^1\text{H}$  NMR spectroscopy [Fig. 3(a,b)].

In this case, a molar mass ( $M_p$ ) of 8200 g/mol could be determined by MALDI-TOF MS. The observed isotopic pattern in MALDI-TOF MS [Fig. 3(a), inset] corresponds well to

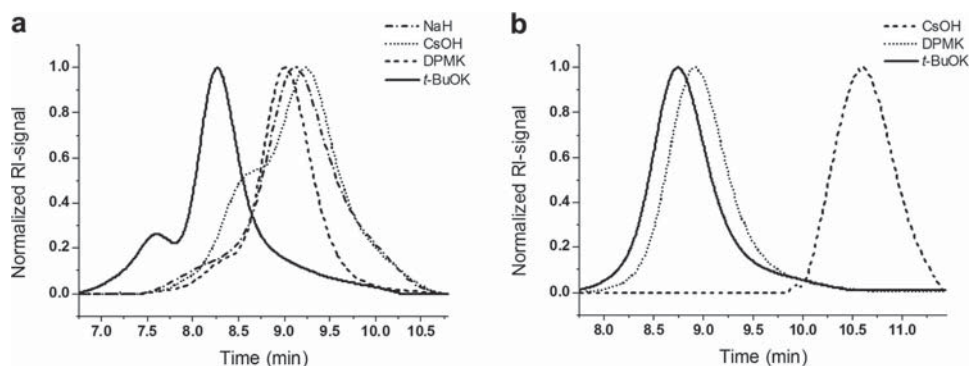


**FIGURE 2** SEC traces for PFGE obtained by homopolymerization in bulk (a) and in THF (b) using different initiators for living anionic ROP.

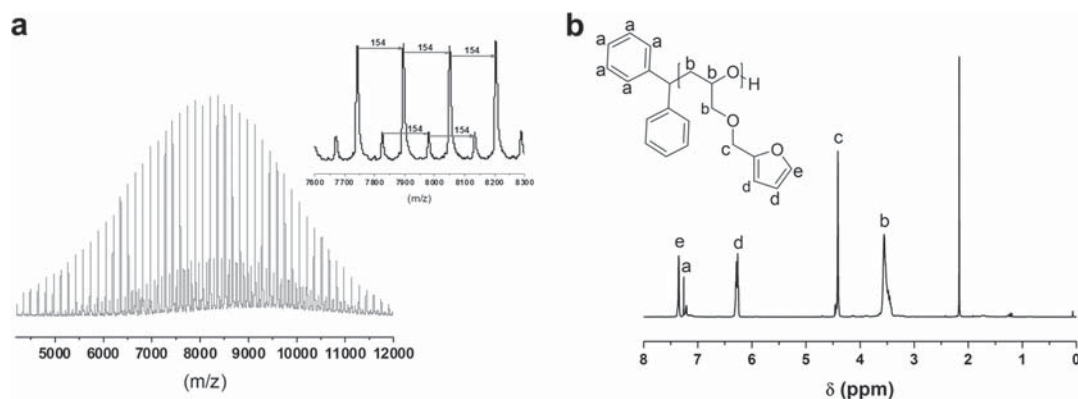


**FIGURE 3** MALDI-TOF MS spectrum (a) and  $^1\text{H}$  NMR ( $\text{DMSO}-d_6$ , 300 MHz) spectrum (b) of PFGE.

the calculated mass distribution with a repeating unit of 154 g/mol. The small second distribution can be attributed to side-reactions occurring during the measurement. In the  $^1\text{H}$  NMR spectrum [Fig. 3(b)], the characteristic peaks for the furane ring at 7.36 and 6.26 ppm (e and d), as well as the signals for the phenyl groups of the initiator at 7.26 ppm (a) could be detected. It could be observed that the polymer shows significantly lower molar masses in the SEC measurements in comparison to the values determined by NMR and MALDI-TOF MS.

To probe the reaction kinetics for FGE, a polymerization aiming at a molar mass ( $M_n$ ) of 10,000 g/mol (ratio of M:I was 65:1) using *t*-BuOK as initiator was performed in THF and monitored by a combination of SEC and  $^1\text{H}$  NMR measurements. The results are displayed in Figure 4 and Table 2.

As shown in Figure 4(a) in the SEC measurements, almost no increase in the molar mass can be seen after 12 h. The conversion of the monomer was simultaneously monitored by  $^1\text{H}$  NMR spectroscopy (Supporting Information Figure S1a) via the decrease of the characteristic signal of the

proton next to the oxirane ring at 3.05 ppm. The signal of the two protons of the furane ring [Fig. 2(d)] was used as an internal standard. For the T24 sample ( $M_{n,\text{app}} = 3450$  g/mol) a monomer conversion of  $\sim 100\%$  could be obtained, whereas T12 ( $M_{n,\text{app}} = 3450$  g/mol) yielded 90% FGE consumption. The living character of the polymerization is demonstrated by the semilogarithmic plot of the monomer concentration at  $t = 0$  ( $M_0$ ) divided by the concentration at  $t = n$  ( $M_n$ ) as displayed in Supporting Information Figure S1b. As shown in Figure 4(b), MALDI-TOF MS measurements yielded a molar mass ( $M_p$ ) of 9400 g/mol for T24, being in good agreement with the targeted value of 10,000 g/mol. The small differences can be attributed to the handling of the initiator in very small amounts (6 mg *t*-BuOK) in the glovebox.

#### Synthesis of PEG-*b*-PFGE

For the synthesis of an AB diblock copolymer, PEG-*b*-PFGE, sequential anionic ROP of EO and FGE, respectively [Fig. 5(a)] was performed. As initiator, DPMK was used due to the possibility of an exact titration of the hydroxyl groups of the PEG macroinitiator, presumably avoiding the formation of homopolymer due to an excess of initiator. The PEG

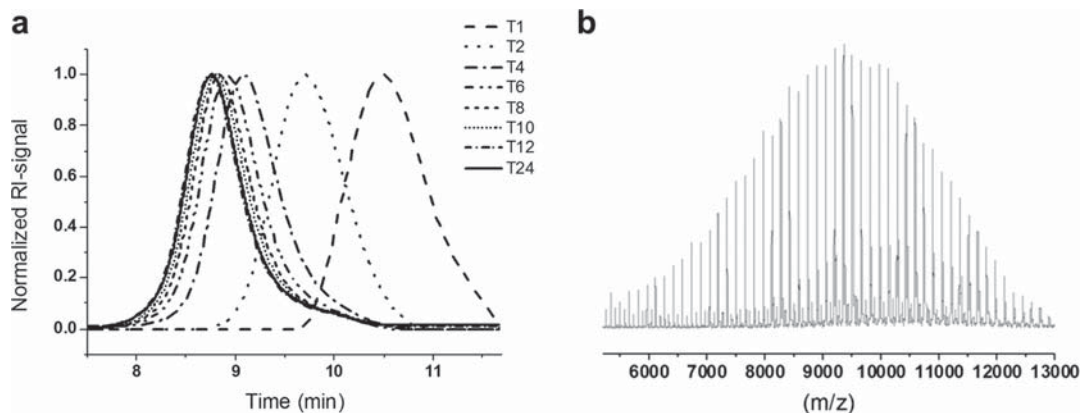


**FIGURE 4** SEC traces for a kinetic study of the PFGE homopolymerization (a) and the corresponding MALDI-TOF MS spectrum of the final product (b,  $M_p = 9400$  g/mol).

**TABLE 2** Characterization Data for the Kinetic Study of the PFGE Homopolymerization

Sample	$M_n^a$	$M_w^a$	PDI <sup>a</sup>	Conversion <sup>b</sup> (%)
PFGE T1	900	1000	1.11	11
PFGE T2	1800	1900	1.07	30
PFGE T4	2750	3050	1.11	45
PFGE T6	3150	3500	1.10	64
PFGE T8	3300	3700	1.11	77
PFGE T10	3400	3800	1.12	82
PFGE T12	3450	3850	1.12	90
PFGE T24	3450	3850	1.12	100

<sup>a</sup> Obtained by SEC (CHCl<sub>3</sub>:*i*-Prop.:TEA 94:4:2, using PEG standards).

<sup>b</sup> Determined by <sup>1</sup>H NMR.

precursor was prepared using DPMK as initiator for EO in THF.<sup>21</sup> The corresponding macroinitiator, PEG-OH with a molar mass ( $M_n$ ) of 6100 g/mol and a PDI value of 1.05, was subsequently reactivated using DPMK, followed by the addition of FGE. MALDI-TOF MS [Fig. 5(b)] revealed a molar mass ( $M_n$ ) of 8050 g/mol for the obtained PEG-*b*-PFGE diblock copolymer. Both PEG-OH and PEG-*b*-PFGE were further analyzed by SEC [Fig. 5(c)] and a shift to lower elution volume as well as a narrow PDI of 1.06 was obtained for the diblock copolymer.

The characteristic signals of the PEG backbone (3.5–3.2 ppm) and the furfuryl groups in the side-chain (7.5, 6.3, and 4.3 ppm) are also visible in the <sup>1</sup>H NMR spectrum

(Supporting Information Fig. S2), resulting in a composition of PEG<sub>139</sub>-*b*-PFGE<sub>12</sub>, where the subscripts denote the degrees of polymerization of the respective segment.

As shown in Table 3 for PEG-*b*-PFGE, the obtained molar mass ( $M_n$ ) of 8200 g/mol is significantly lower than the calculated one with 10,000 g/mol. One possible explanation for this could be the formation of aggregates during the polymerization in THF, thus limiting the molar mass. If the diblock copolymer is directly dissolved in THF, dynamic light scattering (DLS) yields mainly unimolecular polymer chains ( $R_{h,app} = 4$  nm), but also larger aggregates ( $R_{h,app} = 300$  nm) after 24 h (Supporting Information Fig. S3). This confirms the results obtained for the homopolymerization of FGE using different initiators, that is, that the ROP of FGE in THF does not reach full conversion if DPMK is used as an initiating system. Nevertheless, THF remained the solvent of choice due the even larger aggregates (~100 nm) formed immediately after dissolving PEG-*b*-PFGE in toluene and the insolubility of PEG-*b*-PFGE in cyclohexane or ethylbenzene.

### Self-Assembly of PEG-*b*-PFGE in Water

Due to its amphiphilic nature, PEG<sub>139</sub>-*b*-PFGE<sub>12</sub> forms micelles in dilute aqueous solution, as demonstrated using DLS experiments. The structures presumably consist of a hydrophobic PFGE core and a hydrophilic PEG corona [Fig. 6(a)] and we assume a spherical shape of the particles.

Directly after dissolution in water, micelles of  $R_{h,app} = 10$  nm and with a rather narrow size-distribution were obtained

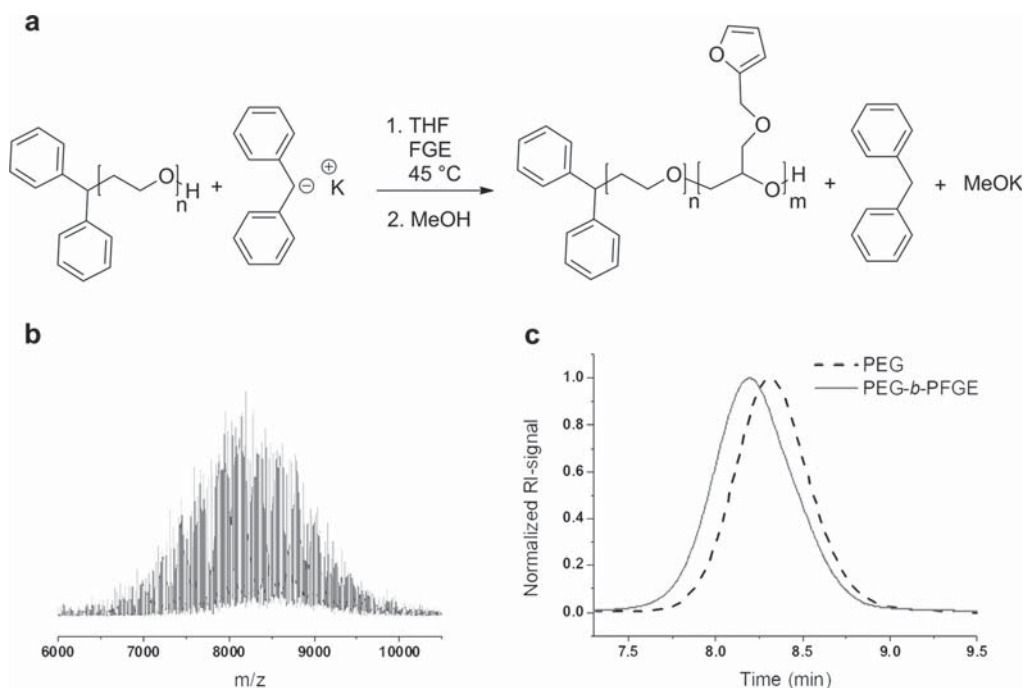


**FIGURE 5** Synthesis of PEG-*b*-PFGE using sequential living anionic ROP (a), MALDI-TOF MS spectrum (b), and SEC traces for the PEG precursor (dashed black line) and PEG-*b*-PFGE (c, solid gray line).



**TABLE 3** Characterization Data for Homopolymers and Block Copolymers

Sample	$M_{n,theo}$ (g/mol)	$M_{n,SEC}$ (g/mol)	$M_{p,MALDI}$ (g/mol)	PDI
PEG <sup>a</sup>	5000	5100 <sup>b</sup>	6100	1.05 <sup>b</sup>
PEG <sub>139</sub> - <i>b</i> -PFGE <sub>12</sub> <sup>c</sup>	10,000	6000 <sup>b</sup>	8050	1.06 <sup>b</sup>

<sup>a</sup> Precursor.

<sup>b</sup> Obtained by SEC (CHCl<sub>3</sub>:*i*-Prop.:TEA 94:4:2, using PEG standards).

<sup>c</sup> Subscripts denote the degrees of polymerization of the corresponding block determined by <sup>1</sup>H NMR spectroscopy.

(Supporting Information Fig. S3a). The core-forming block, PFGE, can now be crosslinked via a Diels-Alder reaction, using a bifunctional crosslinker, for example, a bismaleimide [Reaction scheme in Fig. 6(a)]. The controlled crosslinking of selected domains in micellar structures is desirable and can be used to enhance their resistance against degradation, limit the diffusion of guest molecules into or out of the core domains, or ensure the stability within desired environments.<sup>22–24</sup>

In our case, crosslinking of the micellar core was achieved by a [4 + 2] cycloaddition reaction [Fig. 6(a)]. For this purpose, PEG<sub>139</sub>-*b*-PFGE<sub>12</sub> and a bifunctional crosslinker, 1-1'-(methylenedi-4,1-phenylene)bismaleimide (BMA), were dissolved in DMF at a concentration of 15 g/L and a molar ratio crosslinker/PFGE of 50/1. To encapsulate the BMA linker within the hydrophobic PFGE core domains, water was slowly added until a turbid solution was obtained

(water:DMF = 2:1). The remaining DMF was then removed by dialysis against water and the resulting aqueous solution was analyzed by DLS. The exact amount of encapsulated material is difficult to estimate, as BMA is insoluble in water and partially precipitated during dialysis. For the PEG<sub>139</sub>-*b*-PFGE<sub>12</sub> micelles containing BMA in the core, a radius of  $R_{h,app} = 6$  nm was detected in water afterwards. To induce crosslinking of the core domains, the solution was subsequently heated to 60 °C for several hours. According to DLS, the micellar size did not change significantly upon the crosslinking procedure [Fig. 6(b)]. To prove the successful crosslinking of the PFGE core, the micelles were transferred to nonselective solvents for both blocks, THF and DMF. Therefore, the aqueous micellar solution was poured into an excess of, for example, THF so that the ratio was THF:H<sub>2</sub>O = 6:1 (concentration = 0.8 g/L), dialyzed against THF and again analyzed by DLS [Fig. 6(c)]. Here, micelles with a radius of  $R_{h,app} = 15$  nm could be detected. The increase in size can be explained by a certain swelling of the crosslinked PFGE core in THF as a nonselective solvent. In a next step, the solvent was removed under vacuum and DMF as an alternative nonselective solvent was added (concentration = 1.6 g/L). Again, DLS studies revealed micelles with a solvent-swollen PFGE core and a radius of  $R_{h,app} = 10$  nm even after several days [Fig. 6(d)]. These results clearly indicate a successful crosslinking of the PFGE core. The structure of the PEG-*b*-PFGE micelles was also investigated using TEM (Fig. 7). As can be seen, spherical structures with diameters of ~20 nm but also larger species, most probably due to aggregation occurring during the drying process, can be

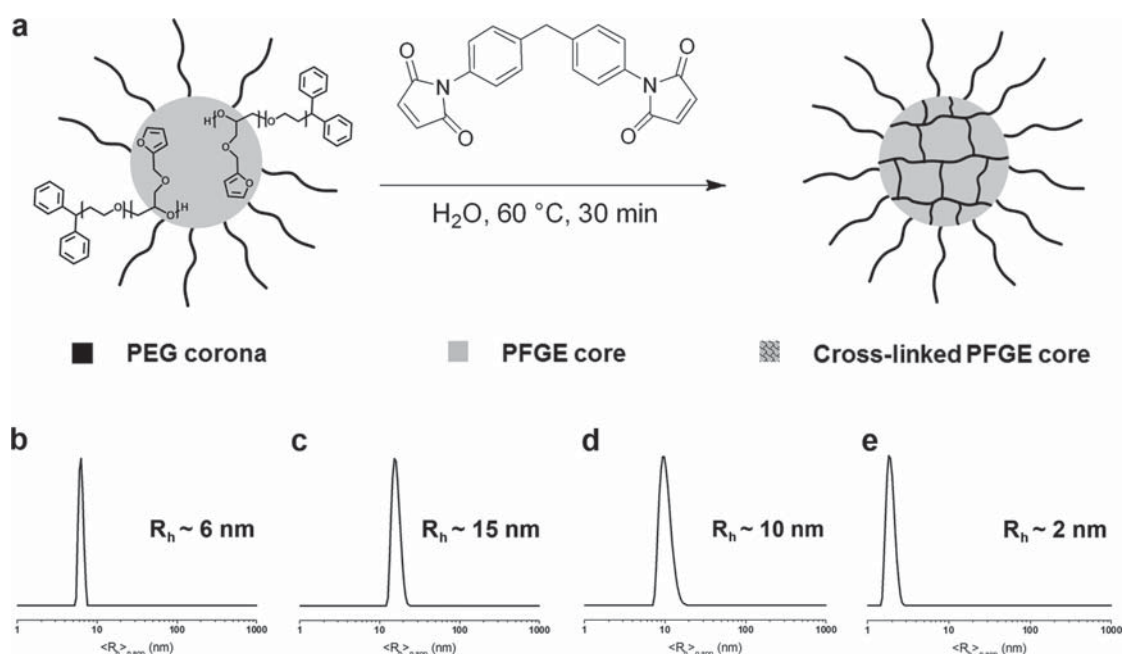


**FIGURE 6** Crosslinking of the micellar core (a), number-weighted DLS CONTIN plots for PEG-*b*-PFGE micelles in water after crosslinking (b), in THF (c), and DMF (d), and after the retro-Diels-Alder reaction in DMF (e).

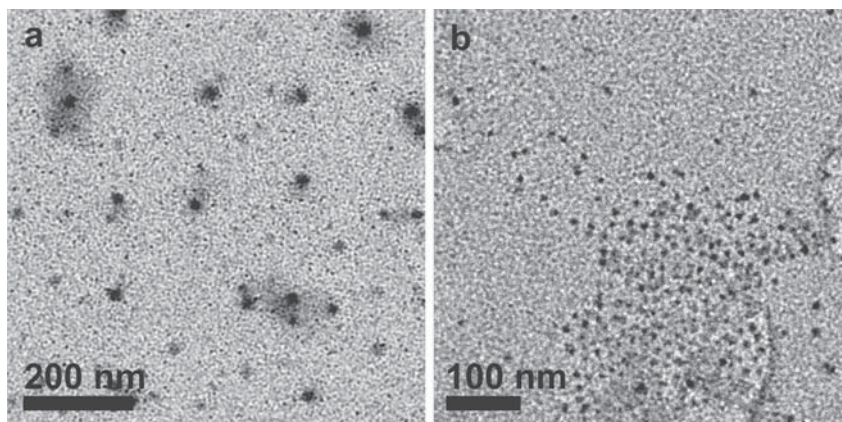


**FIGURE 7** TEM micrographs of PEG<sub>139</sub>-*b*-PFGE<sub>12</sub> micelles cast from aqueous solution (a) or after crosslinking of the PFGE core and subsequent dialysis to THF (b) onto carbon-coated TEM grids.

observed directly after dissolution of PEG<sub>139</sub>-*b*-PFGE<sub>12</sub> in water [Fig. 7(a)]. The dark spots represent the PFGE core; the PEG corona is not visible under these conditions. After crosslinking of the PFGE core and subsequent dialysis into THF, again spherical micelles can be observed [Fig. 7(b)]. Here, core sizes of 10–20 nm are observed, again proving a successful crosslinking of the PFGE core domains.

Additionally, the crosslinking could be proven by the disappearance of the furan signals (6.3 and 4.3 ppm, Fig. 8) in <sup>1</sup>H NMR after prolonged heating at 60 °C (Fig. 8). Moreover, a new signal (5.3 ppm) appears which can be assigned to the double bond formed during the DA reaction. Although this indicates complete consumption of the furan moieties, the exact amount of encapsulated BMA is unknown and the presence of unreacted PFGE cannot be excluded. As the crosslinking via Diels-Alder chemistry should be reversible, the micellar solution was further heated to higher temperatures (150 °C) for 30 min in DMSO. As shown in Figure 8, the signals for the furan ring reappear, but also the signal

for the cross-linked species is still present. Integration suggests that ~50% of the core undergo retro-DA reactions under these conditions, also for longer reaction times (6 h). Nevertheless, DLS after 2 h shows that unimolecular block copolymer chains are present [ $R_{h,app} = 2$  nm, Fig. 6(e)]. Presumably, the dissolution of the micellar core leads to increases the conformational freedom of the polymer chains and decreases the concentration of reaction sites, which might explain the incomplete retro-DA reaction.

## CONCLUSION

In summary, we synthesized well-defined homo- and diblock copolymers containing FGE with a narrow molar mass distribution (PDI < 1.1), molar masses ( $M_p$ ) of up to 9400 g/mol for PFGE, and studied the influence of different initiators and the reaction kinetics in detail. For the PEG<sub>139</sub>-*b*-PFGE<sub>12</sub> diblock copolymer, self-assembly in aqueous solution resulted in the formation of well-defined spherical micelles with a PFGE core and a PEG corona. One intriguing feature of the herein employed hydrophobic domain, PFGE, is that it can be reversibly crosslinked using Diels-Alder chemistry. The core-crosslinked micelles retain their structure in nonselective solvents like THF or DMF. For the retro-DA process, however, high temperatures are necessary and only a conversion of 50% could be observed. Nevertheless, the micellar cores were shown to disassemble into unimolecular chains. One possible improvement regarding the crosslinking process could be the use of a bismaleimide linker with a less rigid or pH-labile spacer, improving either the solubility or a triggered dissolution of the micellar cores. Although the initial results reported here describe only one single diblock copolymer (PEG<sub>139</sub>-*b*-PFGE<sub>12</sub>), the concept could be convincingly demonstrated. In the future, we will extend this to block copolymers with different weight fractions, giving access to other and also more complex morphologies in solution.<sup>25</sup> Whereas the reversible crosslinking of the core in spherical core-corona systems might be interesting for controlled release or surface patterning from non-selective solvents, such processes would be very

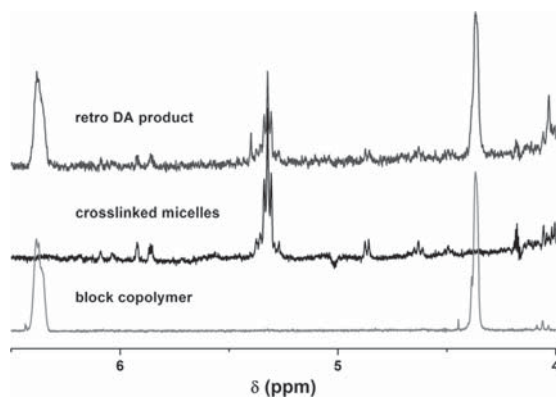


**FIGURE 8** Characteristic region of the <sup>1</sup>H NMR (DMSO, 300 MHz) spectrum of PEG-*b*-PFGE, core-crosslinked micelles, and the retro-Diels-Alder product.

appealing if applied to vesicular,<sup>26</sup> tubular, or cylindrical structures.<sup>27</sup>

#### ACKNOWLEDGMENTS

The authors wish to acknowledge the Dutch Polymer Institute (DPI, technology area high-throughput-experimentation, project #690) and the Thuringian Ministry for Education, Science and Culture (grant #B514-09051, NanoConSens) for financial support of this study. F. H. S. and T. R. are grateful to the Thuringian Ministry for Education, Science, and Culture (TMBWK; #B515-10065, ChaPoNano) for financial support.

#### REFERENCES AND NOTES

- 1 Tyrrell, Z. L.; Shen, Y. Q.; Radosz, M. *Prog. Polym. Sci.* **2010**, *35*, 1128–1143.
- 2 Schacher, F. H.; Rupar, P. A.; Manners, I. *Angew. Chem. Int. Ed.* **2012**, *51*, 7898–7921.
- 3 Harris, J. M.; Chess, R. B. *Nat. Rev. Drug. Discov.* **2003**, *2*, 214–221.
- 4 Knop, K.; Hoogenboom, R.; Fischer, D.; Schubert, U. S. *Angew. Chem. Int. Ed.* **2010**, *49*, 6288–6308.
- 5 Hruby, M.; Konak, C.; Ulbrich, K. *J. Appl. Polym. Sci.* **2005**, *95*, 201–211.
- 6 Koyama, Y.; Umehara, M.; Mizuno, A.; Itaba, M.; Yasukouchi, T.; Natsume, K.; Suginata, A.; Watanabe, K. *Bioconjugate Chem.* **1996**, *7*, 298–301.
- 7 Obermeier, B.; Frey, H. *Bioconjugate Chem.* **2011**, *22*, 436–444.
- 8 Ozdemir, F.; Keul, H.; Mourran, A.; Möller, M. *Macromol. Rapid. Commun.* **2011**, *32*, 1007–1013.
- 9 Hunt, J. N.; Feldman, K. E.; Lynd, N. A.; Deek, J.; Campos, L. M.; Spruell, J. M.; Hernandez, B. M.; Kramer, E. J.; Hawker, C. J. *Adv. Mater.* **2011**, *23*, 2327–2331.
- 10 Barthel, M. J.; Babiuch, K.; Rudolph, T.; Vitz, J.; Hoepfener, S.; Gottschaldt, M.; Hager, M. D.; Schacher, F. H.; Schubert, U. S. *J. Polym. Sci. Part A: Polym. Chem.* **2012**, *50*, 2914–2923.
- 11 Hruby, M.; Konak, C.; Ulbrich, K. *J. Controlled Release* **2005**, *103*, 137–148.
- 12 Reinicke, S.; Schmelz, J.; Lapp, A.; Karg, M.; Hellweg, T.; Schmalz, H. *Soft Matter* **2009**, *5*, 2648–2657.
- 13 Toy, A. A.; Reinicke, S.; Müller, A. H. E.; Schmalz, H. *Macromolecules* **2007**, *40*, 5241–5244.
- 14 Obermeier, B.; Wurm, F.; Mangold, C.; Frey, H. *Angew. Chem. Int. Ed.* **2011**, *50*, 7988–7997.
- 15 Kavitha, A. A.; Singha, N. K. *J. Polym. Sci. Part A: Polym. Chem.* **2007**, *45*, 4441–4449.
- 16 Kavitha, A. A.; Singha, N. K. *Macromolecules* **2010**, *43*, 3193–3205.
- 17 Bergman, S. D.; Wudl, F. *J. Mater. Chem.* **2008**, *18*, 41–62.
- 18 Imbesi, P. M.; Fidge, C.; Raymond, J. E.; Cauet, S. I.; Wooley, K. L. *ACS Macro Lett.* **2012**, *1*, 473–477.
- 19 Tian, Q. A.; Rong, M. Z.; Zhang, M. Q.; Yuan, Y. C. *Polym. Int.* **2010**, *59*, 1339–1345.
- 20 Pratama, P. A.; Peterson, A. M.; Palmese, G. R. *Macromol. Chem. Phys.* **2012**, *213*, 173–181.
- 21 Normant, H.; Angelo, B. *Bull. Soc. Chim. Fr.* **1960**, *2*, 354–359.
- 22 Kim, Y.; Pourgholami, M. H.; Morris, D. L.; Stenzel, M. H. *Biomacromolecules* **2012**, *13*, 814–825.
- 23 Schacher, F.; Walther, A.; Ruppel, M.; Drechsler, M.; Müller, A. H. E. *Macromolecules* **2009**, *42*, 3540–3548.
- 24 O'Reilly, R. K.; Hawker, C. J.; Wooley, K. L. *Chem. Soc. Rev.* **2006**, *35*, 1068–1083.
- 25 Percec, V.; Wilson, D. A.; Leowanawat, P.; Wilson, C. J.; Hughes, A. D.; Kaucher, M. S.; Hammer, D. A.; Levine, D. H.; Kim, A. J.; Bates, F. S.; Davis, K. P.; Lodge, T. P.; Klein, M. L.; DeVane, R. H.; Aqad, E.; Rosen, B. M.; Argintaru, A. O.; Sienkowska, M. J.; Rissanen, K.; Nummelin, S.; Ropponen, J. *Science* **2010**, *328*, 1009–1014.
- 26 Discher, B. M.; Won, Y.-Y.; Ege, D. S.; Lee, J. C.-M.; Bates, F. S.; Discher, D. E.; Hammer, D. A. *Science* **1999**, *284*, 1143–1146.
- 27 Zhang, X.; Tanner, P.; Graff, A.; Palivan, C. G.; Meier, W. *J. Polym. Sci. Part A: Polym. Chem.* **2012**, *50*, 2293–2318.



Supporting information for

**“Homo- and Block Copolymers of Poly (furfuryl glycidyl ether) by Living Anionic Polymerization: Towards Reversibly Core-Crosslinked Micelles”**

Markus J. Barthel,<sup>1,2,3§</sup> Tobias Rudolph,<sup>1,2§</sup> Sarah Crotty,<sup>1,2</sup> Felix H. Schacher<sup>1,2\*</sup> and Ulrich S. Schubert<sup>1,2,3\*</sup>

<sup>1</sup> Laboratory of Organic and Macromolecular Chemistry (IOMC), Friedrich-Schiller-University Jena, Humboldtstr. 10, 07743 Jena, Germany.

<sup>2</sup> Jena Center for Soft Matter (JCSM), Friedrich-Schiller-University Jena, Philosophenweg, 07743 Jena, Germany.

<sup>3</sup> Dutch Polymer Institute (DPI), John F. Kennedylaan 2, 5612 AB Eindhoven, The Netherlands.

§ These authors contributed equally to this work.

**Materials and methods:**

<sup>1</sup>H NMR spectra were recorded on a Bruker AC 300 MHz using the residual solvent signal as an internal standard.

DLS was performed at a scattering angle of 90° on an ALV CGS-3 instrument and a He–Ne laser operating at a wavelength of  $\lambda = 633$  nm at 25 °C. The CONTIN algorithm was applied to analyze the correlation functions obtained. Apparent hydrodynamic radii were calculated according to the Stokes–Einstein equation. All CONTIN plots are number-weighted.

## Kinetic study of PFGE:

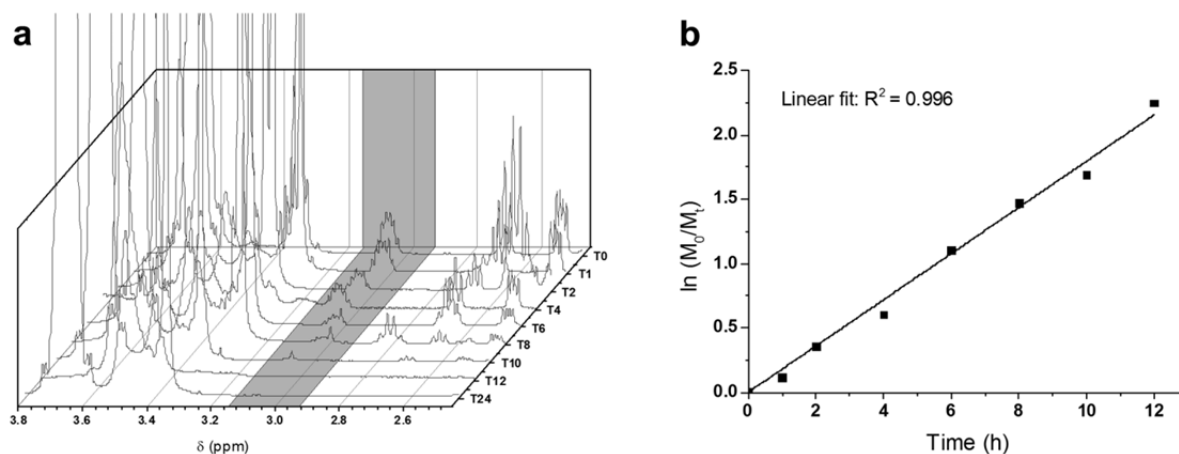


Figure S1. <sup>1</sup>H NMR traces of the kinetic study of the PFGE homopolymerization (a) and logarithmic plot of conversion against time (b).

## PEG-*b*-PFGE:

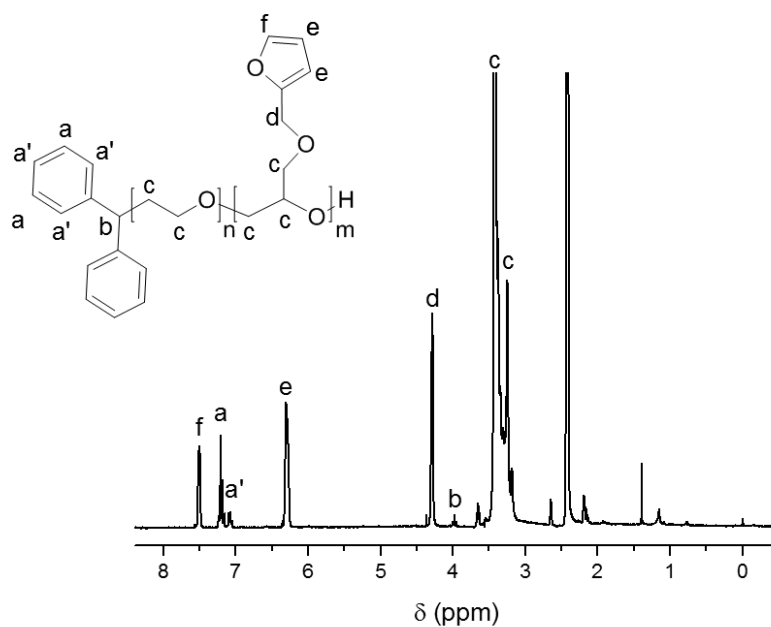
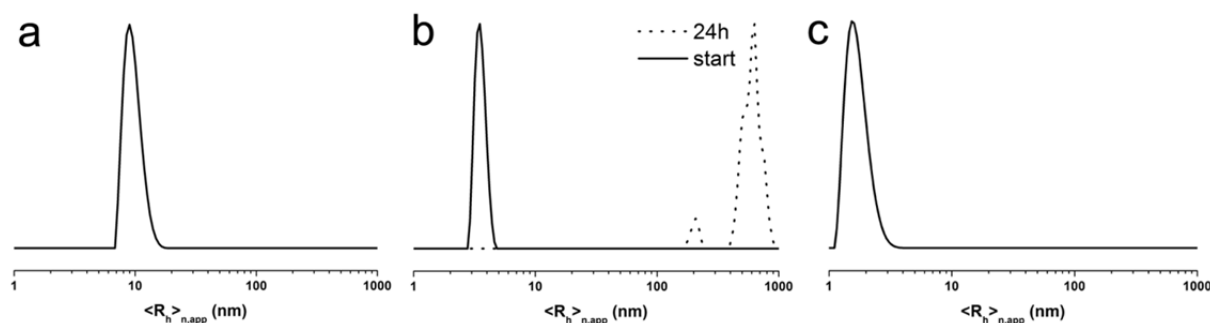


Figure S2: <sup>1</sup>H NMR (DMSO-*d*<sub>6</sub>, 300 MHz) spectrum of PEG-*b*-PFGE.

### DLS investigations of the diblock copolymer:

For DLS investigations 5 mg of the diblock copolymer PEG-*b*-PFGE were directly dissolved in 1 mL of a selective (H<sub>2</sub>O), a non-selective solvent (DMF), as well as in the reaction solvent (THF). The corresponding behavior in solution was investigated and depicted in **Figure S2**. In water the amphiphilic block copolymer forms spherical micelles with a radius of  $R_{h,app} = 10$  nm.

For the reaction solvent, THF, particles with a radius of  $R_{h,app} = 4$  nm were obtained directly after dissolution. Over 24 h, this size increased up to several hundreds of nm and the solution turned slightly turbid, which indicates the formation of large agglomerates/micelles, which might also be an explanation for the lower degree of polymerization for PFGE during the polymerization. As a non-selective solvent DMF was further used for the investigation of the diblock copolymer in solution showing a monomodal size distribution of  $R_{h,app} = 2$  nm.



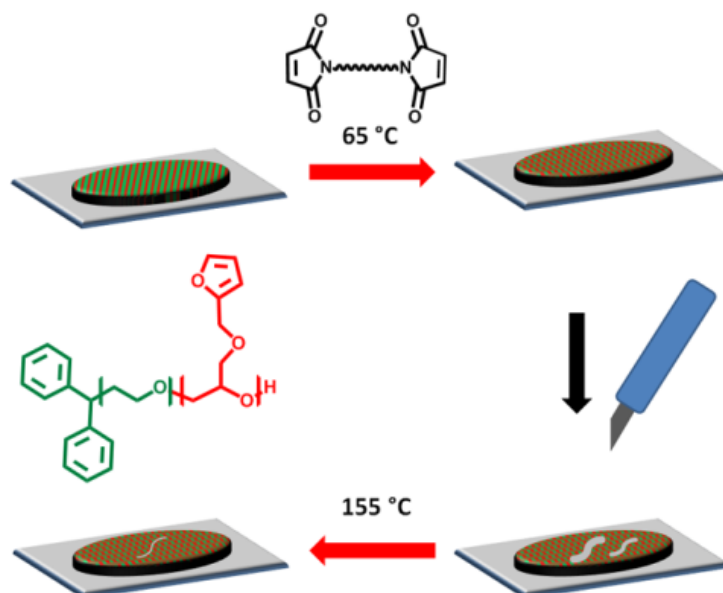
*Figure S3*: Number-weighted DLS CONTIN plots for PEG-*b*-PFGE in water (a), as well as directly after dissolving in THF and after 24 h in THF (b) or DMF (c).

1. H. Normant, B. Angelo, B. *Bull. Soc. Chim. Fr.* **1960**, 354.

## Publication P5

Self-healing materials *via* reversible crosslinking of poly(ethylene oxide)-*block*-poly(furfuryl glycidyl ether) (PEO-*b*-PFGE) block copolymer films

Markus J. Barthel, Tobias Rudolph, Anke Teichler, Renzo M. Paulus, Jürgen Vitz,  
Stephanie Hoepfener, Martin D. Hager, Felix H. Schacher, Ulrich S. Schubert  
*Adv. Funct. Mater.* **2013**, *23*, 4921-4932



# Self-Healing Materials via Reversible Crosslinking of Poly(ethylene oxide)-*Block*-Poly(furfuryl glycidyl ether) (PEO-*b*-PFGE) Block Copolymer Films

Markus J. Barthel, Tobias Rudolph, Anke Teichler, Renzo M. Paulus, Jürgen Vitz, Stephanie Hoepfener, Martin D. Hager, Felix H. Schacher\* and Ulrich S. Schubert\*

The application of well-defined poly(furfuryl glycidyl ether) (PFGE) homopolymers and poly(ethylene oxide)-*b*-poly(furfuryl glycidyl ether) (PEO-*b*-PFGE) block copolymers synthesized by living anionic polymerization as self-healing materials is demonstrated. This is achieved by thermo-reversible network formation via (retro) Diels-Alder chemistry between the furan groups in the side-chain of the PFGE segments and a bifunctional maleimide crosslinker within drop-cast polymer films. The process is studied in detail by differential scanning calorimetry (DSC), depth-sensing indentation, and profilometry. It is shown that such materials are capable of healing complex scratch patterns, also multiple times. Furthermore, microphase separation within PEO-*b*-PFGE block copolymer films is indicated by small angle X-ray scattering (lamellar morphology with a domain spacing of approximately 19 nm), differential scanning calorimetry, and contact angle measurements.

## 1. Introduction

The capability to heal inflicted damage is ubiquitous in nature as, e.g., shown via the merging of broken bones, the closure of injured blood vessels,<sup>[1–3]</sup> or the healing of byssal threads

of marine mussels.<sup>[4]</sup> The present awareness that the availability of raw materials will decrease, accompanied by increasing material and production costs, renders self-healing approaches an attractive research field in polymer chemistry and materials science. Particular interest is devoted to the facile introduction of such features into mechanically robust polymeric systems whilst maintaining synthetic feasibility and, even more important, processability of the resulting materials.

Different methods have been reported to introduce self-healing properties to a polymeric material.<sup>[5–7]</sup> One possibility is the encapsulation of reactive ingredients (a polymerizable healing agent and an initiator) within the desired material.

Scratching or crack formation leads to a release of the embedded substances (e.g., by rupture of microcapsules), followed by mixing of both ingredients and resulting in a healing process of the damaged material.<sup>[8]</sup> This approach was also extended by the introduction of vascular networks containing a healing agent, which was released upon rupture.<sup>[9]</sup> Therefore, multiple healing processes are possible. A second approach represents the use of intermolecular forces. For this purpose, reversible interactions (i.e., crosslinks) of polymer chains with, e.g., hydrogen bonds represent a widely used strategy. After being damaged, these bonds allow a healing due to the reformation of bonds without any external stimuli such as heating or irradiation being necessary. This has been achieved using highly specific donor-acceptor systems,<sup>[10–15]</sup> and could recently be also applied for “hard” epoxy networks.<sup>[16]</sup> Another example of this approach are metal-ligand interactions. Thereby, materials consisting of polymers or oligomers comprising reversible non-covalent metal-ligand interactions (e.g., 2,6-bis(1'-methylbenzimidazolyl)pyridine or terpyridine, as well as corresponding metal ions) can heal inflicted damage.<sup>[17,18]</sup> Also, this ability represents an inherent material characteristic (i.e. intrinsic self-healing materials) and does not require the encapsulation of external healing agents. Moreover, the application of  $\pi$ - $\pi$  interactions in self-healing processes has also been demonstrated for, e.g., pyrenyl units which interact with naphthalene diimide oligomers to reversibly crosslinked polymeric networks.<sup>[19,20]</sup>

M. J. Barthel, T. Rudolph, A. Teichler, R. M. Paulus,  
Dr. J. Vitz, Dr. S. Hoepfener, Dr. M. D. Hager,  
Prof. F. H. Schacher, Prof. U. S. Schubert  
Laboratory of Organic and Macromolecular  
Chemistry (IOMC)

Friedrich Schiller University Jena  
Humboldtstr. 10, 07743 Jena, Germany  
E-mail: felix.schacher@uni-jena.de;  
ulrich.schubert@uni-jena.de

M. J. Barthel, T. Rudolph, A. Teichler, R. M. Paulus, Dr. J. Vitz,  
Dr. S. Hoepfener, Dr. M. D. Hager, Prof. F. H. Schacher,  
Prof. U. S. Schubert

Jena Center for Soft Matter (JCSM)  
Friedrich-Schiller-University Jena  
Philosophenweg 7, 07743 Jena, Germany

M. J. Barthel, A. Teichler, Dr. J. Vitz, Dr. S. Hoepfener,  
Prof. U. S. Schubert

Dutch Polymer Institute (DPI)  
John F. Kennedylaan 2, 5612 AB Eindhoven, The Netherlands



DOI: 10.1002/adfm.201300469

The temperature-dependent reversible covalent crosslinking of polymers or block copolymers represents another interesting concept for the implementation of intrinsic self-healing into a material. Hereby, the Diels-Alder reaction represents a powerful tool.<sup>[21–27]</sup> One well-known example is the combination of furan and maleimide functionalities.<sup>[28–30]</sup> In this context, we have recently reported that furfuryl glycidyl ether can be used as a monomer for living anionic polymerization and the preparation of well-defined poly(ethylene oxide)-*b*-poly(furfuryl glycidyl ether) (PEO-*b*-PFGE) block copolymers comprising furan units in the side chain.<sup>[31]</sup> Subsequently, the furan units were used for the reversible core-crosslinking of the micelles formed by these block copolymers in selective solvents for the PEO segment. The application of polymer networks bearing free furan groups with a suitable linker (e.g., bismaleimides) in reversible Diels-Alder reactions represents a powerful system for potential self-healing applications.<sup>[21–24,28–30,32–34]</sup> This has been recently reported in the case of furfuryl glycidyl ether,<sup>[35,36]</sup> where the epoxy-ring was used in a condensation reaction with amino groups to create polymeric materials. These polymers can be turned into a network structure by reacting them with a bismaleimide compound.

We were now interested in exploiting the features of PEO-*b*-PFGE block copolymers for the generation of self-healing materials, in particular of nanostructured polymer films. Apart from the use of PEO-related materials in biological and medical context for PEG-ylation or drug-delivery approaches, PEO is widely used in the field of coatings. Here, antifouling properties, proliferated cell adhesion, or the coating of food supplement products have been described.<sup>[37–42]</sup> Moreover, the employment of block copolymers in self-healing applications represents an attractive approach. Such materials undergo microphase separation in bulk into a variety of well-documented morphologies.<sup>[43]</sup> In the case of AB diblock copolymers, this might be one way to solve a fundamental problem related to self-healing materials: the combination of strong reversible interactions between individual polymer chains together with dynamic properties (low glass transition temperature segments). However, such approaches have been rarely described,<sup>[44–48]</sup> as mostly statistical or random copolymers have been used for such purposes.

We herein describe the synthesis of well-defined PEO-*b*-PFGE block copolymers via living anionic ring-opening polymerization. Films of these materials were reversibly crosslinked using Diels-Alder (DA)/retro Diels-Alder (rDA) chemistry and investigated with regard to possible self-healing behavior. Multiple healing cycles as well as even complex damage patterns can be recovered, and the extent of the healing process (length, width of scratches as well as the time frame) were carefully investigated with a combination of differential scanning calorimetry (DSC), depth-sensing indentation, and profilometry studies. We further show that PEO-*b*-PFGE block copolymers undergo phase separation in the bulk, as indicated by small angle X-ray scattering, differential scanning calorimetry, and contact angle measurements.

## 2. Experimental Section

### 2.1. Instruments

<sup>1</sup>H NMR spectra were recorded on a Bruker AC 300 MHz spectrometer in chloroform. Size exclusion chromatography (SEC) was performed on a Shimadzu SCL-10A system (with a LC-10AD pump, a RID-10A refractive index detector, and a PL gel 5  $\mu$ m mixed-D column at RT), the eluent was a mixture of chloroform:triethylamine:iso-propanol (94:4:2) with a flow rate of 1 mL min<sup>-1</sup>. The system was calibrated with poly(ethylene glycol) standards from PSS ( $M_n = 1470$  g mol<sup>-1</sup> to 42 000 g mol<sup>-1</sup>). MALDI-ToF mass spectra were obtained using an Ultraflex III ToF/ToF mass spectrometer (Bruker Daltonics) with *trans*-2-[3-(4-*tert*-butylphenyl)-2-methyl-2-propenylidene] malononitrile (DCTB) or 2,5-dihydroxybenzoic acid (DHB) as matrix in reflector as well as in linear mode. The instrument was calibrated prior to each measurement with an external PMMA standard from PSS Polymer Standards Services GmbH. Surface topography as well as film thicknesses were measured using an optical interferometric profiler Wyko NT9100 (Veeco, Germany). The instrument is equipped with three objectives (2.5 $\times$ , 5 $\times$  and 20 $\times$ ), which enable effective magnifications between 1 $\times$  to 40 $\times$ . Differential scanning calorimetry (DSC) was performed on a Netzsch DSC 204 F1 equipped with a liquid nitrogen dewar. Dried samples were weighed into aluminum crucibles in amounts ranging from 5 to 20 mg, and an empty aluminum crucible was used as reference. The samples were measured with a temperature program consisting of three heating runs ranging from -150 to 150 °C with a heating rate of 20 K min<sup>-1</sup> for the first heating run and 10 K min<sup>-1</sup> for the second and third heating runs. The glass transition temperatures ( $T_g$ ) were determined from the second and third heating runs (onset value). All thermograms were exported in graphs with exo down.

**Mechanical Properties:** The elastic moduli of the materials were characterized via depth-sensing indentation (DSI) using a TriboIndenter TI 900 (Hysitron Inc., Minneapolis, MN) with a NanoDMA 06 transducer, equipped with a conospherical diamond indenter tip of  $\approx 4.7$   $\mu$ m radius. The polymer films were prepared by drop casting and dried afterwards under air. The measurements were conducted at ambient conditions, at 23  $\pm$  1 °C and 31  $\pm$  6% relative humidity (RH) for PFGE<sub>55</sub> and at 23  $\pm$  1 °C and 30.0  $\pm$  3% RH for PEO<sub>330</sub>-*b*-PFGE<sub>20</sub>, as measured with a Voltcraft DL-141TH data logger. For quasi-static testing, an open loop load function with 1 s loading, 2 s hold at maximum load, and 1 s unloading profile was applied.<sup>[49]</sup> All measurements were performed in a single automated run in less than 3 h for one sample. The reduced modulus  $E_r$  was determined from the unloading response using the analysis method proposed by Oliver and Pharr.<sup>[50]</sup> Measurements were repeated at sixteen maximum loads in a 4  $\times$  4 array, for PFGE<sub>55</sub> increasing in steps of 120  $\mu$ N from 100 to 1900  $\mu$ N or in steps of 140  $\mu$ N from 100 to 2200  $\mu$ N, respectively. PEO<sub>330</sub>-*b*-PFGE<sub>20</sub> was measured in steps of 100  $\mu$ N from 100 to 1600 for the film and in steps of 120  $\mu$ N from 100 to 1900  $\mu$ N for the crosslinked sample. Values are averaged from at least ten measurements each. From the reduced modulus  $E_r$ , the indentation modulus

$E_i$  was calculated using the elastic modulus and Poisson's ratio of the diamond indenter, 1140 GPa and 0.07, respectively, and a Poisson's ratio of 0.4 for the polymeric material, according to

$$E_{i,\text{sample}} = \frac{1 - \nu_{\text{sample}}^2}{\frac{1}{E_{r,\text{sample}}} - \frac{1 - \nu_{\text{indenter}}^2}{E_{\text{indenter}}}} \quad (1)$$

The hardness is defined as:

$$H = \frac{P_{\text{max}}}{A} \quad (2)$$

**Small and Wide Angle X-Ray Scattering:** SWAXS measurements on dried samples of PFGE<sub>55</sub> and PEO<sub>330</sub>-*b*-PFGE<sub>20</sub> were performed on a Bruker AXS Nanostar (Bruker, Karlsruhe, Germany), equipped with a microfocus X-ray source (Incoatec IuSCu E025, Incoatec, Geesthacht, Germany), operating at  $\lambda = 1.54 \text{ \AA}$ . A pinhole setup with 750  $\mu\text{m}$ , 400  $\mu\text{m}$ , and 1000  $\mu\text{m}$  (in the order from source to sample) was used and the sample-to-detector distance was 107 cm (SAXS) and 12 cm (WAXS). Samples were mounted on a metal rack and fixed using tape. The scattering patterns were corrected for the beam stop and the background (Scotch tape) prior to evaluations.

**Transmission Electron Microscopy:** performed using a TEM (Zeiss-CEM 902A, Oberkochen, Germany) operating at 80 kV. Images were recorded using a 1 k TVIPS FastScan CCD camera. The TEM samples were prepared by applying a drop of the sample solutions onto the surface of a carbon coated copper grid (Quantifoil Micro-Tools GmbH, Jena, Germany).

## 2.2. Materials

Ethylene oxide (EO) was purchased from Linde and Aldrich. Furfuryl glycidyl ether (FGE), *t*-BuOK, tetrahydrofuran (THF), *n*-hexane and toluene were purchased from Aldrich. Toluene and THF were used from a solvent purification system (PureSolv, Innovative Technology) and distilled over sodium/benzophenone. Ethylene oxide was distilled over sodium. Furfuryl glycidyl ether was purified by column chromatography (eluent: ethylacetate/*n*-hexane 5/1) and vacuum drying before usage. Diphenylmethyl potassium (DPMK) was synthesized as reported previously.<sup>[51]</sup> The PEO precursor was prepared via living anionic ring-opening polymerization of ethylene oxide with DPMK in THF in a BüchiGlasUster PicoClave and dried by azeotropic distillation under vacuum from dry toluene. *t*-BuOK was used as received.

**Polymerization of FGE:** 4 mL of freshly distilled THF were transferred into a Schlenk flask and 5.61 mg potassium *t*-butanolate (0.05 mmol) were added. Subsequently, 0.45 mL furfuryl glycidyl ether (FGE, 3.24 mmol, ratio of M:I was 65:1,  $M_{n,\text{theo}} = 10\,000 \text{ g mol}^{-1}$ ) was introduced and the reaction was allowed to stir for 24 h at 45 °C. The reaction was terminated by adding 0.5 mL methanol and the product was washed with *n*-hexane and dried under vacuum.

<sup>1</sup>H NMR (300 MHz, CDCl<sub>3</sub>-*d*<sub>6</sub>,  $\delta$ ): 7.27 (d, 1H, CH), 6.24–6.17 (m, 2H, CH), 4.35 (s, 2H, CH<sub>2</sub>), 3.55–3.29 (br, 5H, backbone), 1.18 (s, 9H, *t*-Bu CH<sub>3</sub>).

SEC:  $M_n = 2900 \text{ g mol}^{-1}$ ,  $M_w = 3100 \text{ g mol}^{-1}$ , PDI = 1.07; MALDI-ToF MS:  $M_p = 8400 \text{ g mol}^{-1}$

**Synthesis of PEO-*b*-PFGE Block Copolymers:** PEO<sub>330</sub>-*b*-PFGE<sub>10</sub>: 3.45 g monohydroxy-functionalized PEO ( $M_{n,\text{SEC}} = 14\,000 \text{ g mol}^{-1}$ , PDI = 1.05,  $M_{p,\text{MALDI}} = 14\,500 \text{ g mol}^{-1}$ , 0.24 mmol) was dried under vacuum at 75 °C for 2 h and dissolved in 30 mL freshly distilled THF. To activate the hydroxyl group, a stoichiometric amount of DPMK was added until the solution remained slightly red. 0.33 mL (2.4 mmol) FGE was added and the reaction mixture was allowed to stir for 24 h at 45 °C under inert conditions. The reaction was terminated by the addition of 0.5 mL methanol and the crude polymer was purified by precipitation in cold diethyl ether and dried under vacuum.

<sup>1</sup>H NMR (300 MHz, DMSO-*d*<sub>6</sub>,  $\delta$ ): 7.5 (s, 1H, CH), 7.2–7.05 (m, 10H, Ar H), 6.3 (m, 2H, CH), 4.3 (s, 2H, CH<sub>2</sub>), 3.95 (t, 1H, CH), 3.65–3.15 (br, PEO-backbone).

SEC:  $M_n = 15\,200 \text{ g mol}^{-1}$ ,  $M_w = 16\,100 \text{ g mol}^{-1}$ , PDI = 1.06; MALDI-ToF MS:  $M_p = 16\,000 \text{ g mol}^{-1}$

PEO<sub>330</sub>-*b*-PFGE<sub>20</sub> was synthesized according the same procedure with regard to stoichiometry.

SEC:  $M_n = 17\,600 \text{ g mol}^{-1}$ ,  $M_w = 18\,100 \text{ g mol}^{-1}$ , PDI = 1.04; MALDI-ToF MS:  $M_p = 17\,000 \text{ g mol}^{-1}$

## 3. Results and Discussion

We have recently prepared well-defined PFGE homo- and PEO-*b*-PFGE block copolymers via living anionic ring-opening polymerization (AROP).<sup>[31]</sup> Herein, PEO-*b*-PFGE materials will be used for temperature-mediated self-healing of films after the controlled application of scratches. For this purpose two PEO-*b*-PFGE block copolymers, PEO<sub>330</sub>-*b*-PFGE<sub>10</sub> and PEO<sub>330</sub>-*b*-PFGE<sub>20</sub>, were synthesized by sequential AROP and, for comparison, a PFGE<sub>55</sub> homopolymer (Figure 1 and Table 1). Both PEO-*b*-PFGE block copolymers were prepared starting from a monohydroxy-PEO precursor by activation with diphenylmethyl potassium (DPMK), followed by the addition of FGE.<sup>[31]</sup>

### 3.1. Structural and Thermal Characterization of PFGE<sub>55</sub> and PEO<sub>330</sub>-*b*-PFGE<sub>x</sub> Films

Both PFGE and PEO-*b*-PFGE block copolymers were investigated using differential scanning calorimetry (DSC, Figure 2).

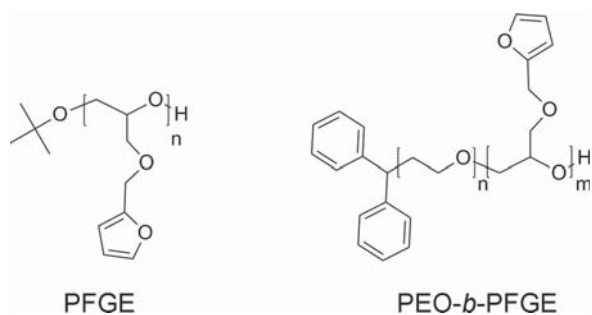


**Figure 1.** Schematic representation of the materials used in this study: PFGE and PEO-*b*-PFGE block copolymers.

**Table 1.** Characterization data of the used homo- and block copolymers.

Sample	$M_{n,theo}$ [g mol <sup>-1</sup> ]	$M_{n,SEC}$ [g mol <sup>-1</sup> ] <sup>b)</sup>	$M_{p,MALDI}$ [g mol <sup>-1</sup> ]	PDI <sup>b)</sup>
PFGE <sub>55</sub>	10 000	2900	8400	1.07
PEO <sub>330</sub> <sup>a)</sup>	14 000	14 800	14 500	1.05
PEO <sub>330</sub> - <i>b</i> -PFGE <sub>10</sub> <sup>c)</sup>	16 000	15 200	16 000	1.06
PEO <sub>330</sub> - <i>b</i> -PFGE <sub>20</sub> <sup>c)</sup>	17 600	17 400	17 000	1.04

<sup>a)</sup>Precursor; <sup>b)</sup>Obtained by SEC (CHCl<sub>3</sub>:TEA:i-Prop. 94:4:2, using PEO standards); <sup>c)</sup> Subscripts denote the degrees of polymerization of the corresponding block determined by <sup>1</sup>H NMR spectroscopy. The corresponding SEC traces, NMR spectra and MALDI-ToF MS pattern can be found in the Supporting Information, Figures S1–S3.

In addition, material degradation during the heating cycles, as well as the healing experiments discussed later, can be excluded, as thermogravimetric analysis (TGA) demonstrated thermal stability of the materials up to approximately 170 °C under air and 335 °C under nitrogen atmosphere (Supporting Information Figure S4).

As can be seen, the homopolymer PFGE<sub>55</sub> exhibits a  $T_g$  at approximately -40 °C (Figure 2a). PEO<sub>330</sub>-*b*-PFGE<sub>20</sub> shows a strong melting peak at  $T_m$  = 59 °C, which can be attributed to the PEO segments (Figure 2b). The inset in Figure 2b shows the regime below 0 °C at higher resolution and reveals two

separated glass transition temperatures at -79 and -40 °C, respectively. The first value can be assigned to PEO<sup>[52]</sup> whereas -40 °C reflects the PFGE segments. Both separate glass transition temperatures were also observed in case of PEO<sub>330</sub>-*b*-PFGE<sub>10</sub> (data not shown here). The presence of two separated  $T_g$ 's hints towards phase separation, although the overall molar mass of both PEO<sub>330</sub>-*b*-PFGE<sub>x</sub> block copolymers is rather low. To confirm this assumption, additional SAXS experiments were performed on films which were annealed at 70 °C for 30 min and afterwards cooled to room temperature (Figure 2c).

Reflections could be observed for PEO<sub>330</sub>-*b*-PFGE<sub>20</sub> at 0.46°, 0.92°, and 1.36°, corresponding to the [100]:[200]:[300] positions of a potential lamellar pattern, and the most intense [100] signal corresponds to a domain size of  $d_{lam}$  = 19 ± 2 nm. The formation of lamellae is rather surprising, as the volume fraction of PFGE in PEO<sub>330</sub>-*b*-PFGE<sub>20</sub> is of about 17.5 wt%, rather hinting towards the formation of cylindrical domains. To probe the surface properties of the investigated films, water contact angle measurements were performed on PEO<sub>330</sub>, PFGE<sub>55</sub>, and PEO<sub>330</sub>-*b*-PFGE<sub>20</sub> surfaces (Figure 2d). As expected, PEO<sub>330</sub> shows a contact angle of 34.5°, which is characteristic for a hydrophilic surface, whereas this increases to 83.6° for PFGE<sub>55</sub>. In case of PEO<sub>330</sub>-*b*-PFGE<sub>20</sub>, a value of 64.5° was obtained, showing surface characteristics in between the two corresponding homopolymers. At this point, we assume the

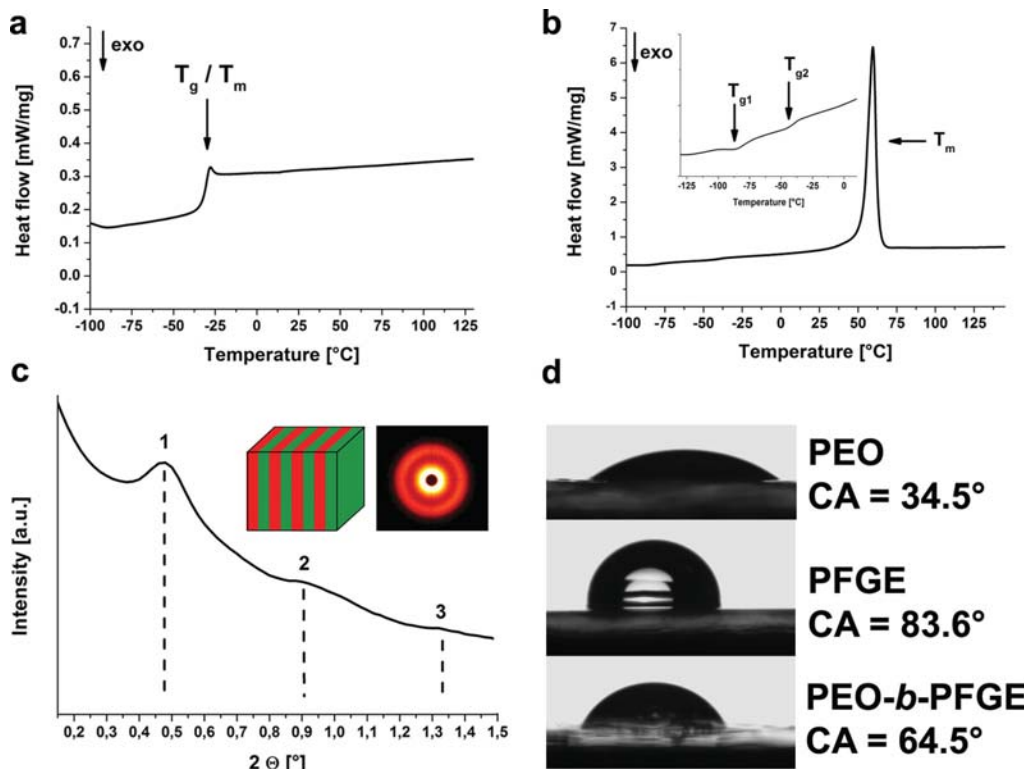


**Figure 2.** DSC thermograms of a) PFGE and b) PEO<sub>330</sub>-*b*-PFGE<sub>20</sub>. c) Zoom-in for PEO<sub>330</sub>-*b*-PFGE<sub>20</sub>. SAXS measurements of PEO<sub>330</sub>-*b*-PFGE<sub>20</sub> and schematic representation of the proposed block copolymer bulk morphology. d) Contact angle measurements for PEO<sub>330</sub>, PFGE<sub>55</sub> and PEO<sub>330</sub>-*b*-PFGE<sub>20</sub>.



formation of a lamellar bulk morphology in the case of PEO<sub>330</sub>-*b*-PFGE<sub>20</sub>. For PEO<sub>330</sub>-*b*-PFGE<sub>10</sub>, the obtained SAXS pattern (Supporting Information Figure S5a) was different, and the volume fraction of approximately 10% for PFGE hints towards the formation of PFGE spheres within a PEO matrix. This was confirmed by sonication-assisted dissolution of a crosslinked PEO<sub>330</sub>-*b*-PFGE<sub>10</sub> block copolymer film in DMF, resulting in micellar structures with a crosslinked PFGE core of about 10 nm in diameter and a PEO corona, as observed via TEM measurements (Supporting Information, Figure S5b). Unfortunately, we were not able to distinguish between both domains in case of PEO<sub>330</sub>-*b*-PFGE<sub>20</sub> block copolymers via atomic force microscopy (AFM) or TEM. In the latter case, thin samples ( $\approx 80$  nm) were prepared from a crosslinked block copolymer film using a microtome. We observed rather rapid electron beam damage and the formation of sheet-like fragments. Even staining with OsO<sub>4</sub> (addressing any remaining double bonds in the PFGE domains) did not result in an improved phase contrast. As a consequence, the assumption of lamellar structures within films from PEO<sub>330</sub>-*b*-PFGE<sub>20</sub> relies on the SAXS data, as well as contact angle measurements and the DSC results.

To exclude that the SAXS pattern in Figure 2c is merely caused by crystalline PEO domains, small (SAXS) and wide angle X-ray (WAXS) measurements at different temperatures were carried out (Figure 3). As it is clearly shown, the most intense reflection in SAXS at 0.46° is still present even above the melting point of PEO and after 16 h at 70 °C (Figure 3a). The fact that here only the [100] reflection is visible can be ascribed to shorter measurement times ( $\approx 30$  min if compared to 4 h in Figure 2c), resulting in a decreasing signal-to-noise ratio. If this is combined with WAXS measurements of the same sample under comparable conditions (Figure 3b), very intense reflections at 18.6° and 22.8° (among other less intense signals) can be assigned to semicrystalline PEO domains.<sup>[53]</sup> Upon heating, these disappear at about 64 °C (inset in Figure 3b) and a broad amorphous halo can be observed.

### 3.2. Reversible Crosslinking of PFGE-Based Materials

For self-healing studies, films were prepared from PFGE<sub>55</sub>, PEO<sub>330</sub>-*b*-PFGE<sub>10</sub> and PEO<sub>330</sub>-*b*-PFGE<sub>20</sub> via drop-casting onto polished glass slides. Typically, 20 mg of the polymer and a

stoichiometric amount of the crosslinker, 1,1-diphenylmethyl bismaleimide (BMA), were dissolved in 0.2 mL dichloromethane (DCM). The solution was applied to a glass slide using a syringe and the solvent was allowed to evaporate.

Due to the presence of BMA, slightly yellow films (depending on the amount of crosslinker) were obtained. In case of the PFGE homopolymer, the amount of BMA was reduced to 0.8 equivalents, otherwise demixing and crystallization of the crosslinker was observed. For crosslinking, the polymer films were heated to 65 °C in an oven (Figure 4a). To ensure full crosslinking, the samples were kept at this temperature for 14 h. Subsequent network formation via crosslinking of the furan groups led to a significant change in the material properties, accompanied by a color change in case of the block copolymer films from slightly yellow to red. This was not the case for films from PFGE<sub>55</sub>. We tentatively propose an aggregation of the crosslinker within the PEO domains, possibly due to the formation of  $\pi$ -complexes. This color change can also be monitored by time-dependent UV-Vis spectroscopy at 50 °C in solution (Supporting Information, Figure S6). However, the color change also depends on the temperature or the time during sample preparation. A detailed study of this phenomenon is, however, beyond the scope of this work. In all cases an increase of the film hardness was observed during crosslinking using depth sensing indentation measurements (Figure 4). We have to point out that films of PEO<sub>330</sub>-*b*-PFGE<sub>10</sub> visibly melted at 59 °C even after crosslinking. As melting of crosslinked PEO<sub>330</sub>-*b*-PFGE<sub>x</sub> films during the heating cycles would lead to film deformations, we focused on PFGE<sub>55</sub> and PEO<sub>330</sub>-*b*-PFGE<sub>20</sub> for further studies.

First, the mechanical properties of PFGE-based films prior to and after crosslinking with BMA were investigated. As pristine films from PFGE<sub>55</sub> were liquid (highly viscous) at room-temperature, no indentation measurements were possible. PEO<sub>330</sub>-*b*-PFGE<sub>20</sub> shows a hardness ( $H$ , defined as load/indentation area) of 0.038 GPa and a stiffness ( $E_i$ , Young modulus) of 0.46 GPa. All  $H$  values provided refer to a displacement of 150 nm. The  $E_i$  values represent average values of the obtained data in the linear range. After crosslinking, PFGE<sub>55</sub> shows a hardness of 0.6 GPa and a stiffness of  $E_i = 5.13$  GPa (Figure 4b,d), the values being slightly higher as reported for "hard" polymers, like poly(methyl methacrylate) (PMMA, 0.32 GPa, 4.8 GPa) as well as polystyrene (PS, 0.34 GPa,

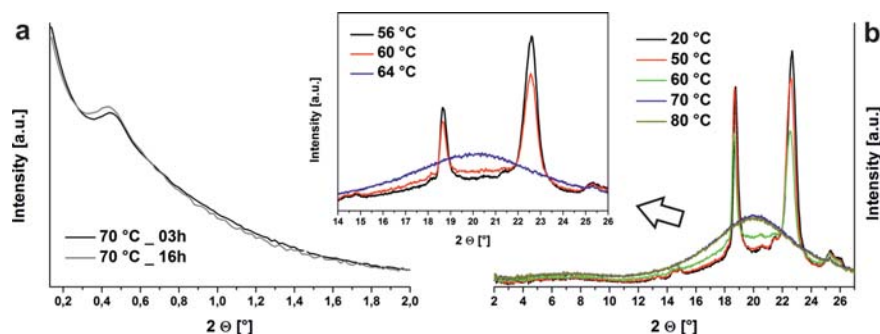


**Figure 3.** a) Small and b) wide angle X-ray patterns for PEO<sub>330</sub>-*b*-PFGE<sub>20</sub> at different temperatures; the inset in (b) shows the enlarged region containing the reflexes for semicrystalline PEO.

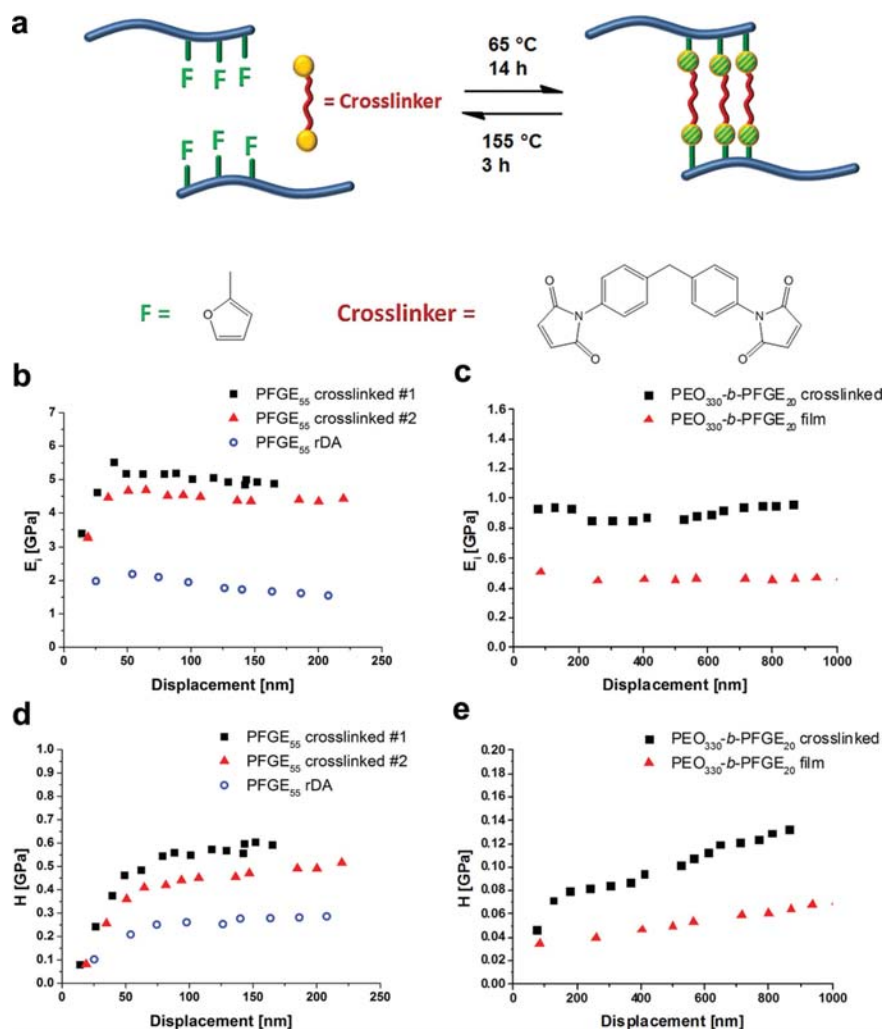


**Figure 4.** a) Schematic representation of the crosslinking of PFGE with a bifunctional maleimide BMA crosslinker. Depth-sensing indentation measurements for b,d) PFGE<sub>55</sub> and c,e) PEO<sub>330</sub>-b-PFGE<sub>20</sub> films before and after crosslinking.

4.8 GPa).<sup>[54]</sup> This can be explained by a rather high degree of crosslinking, as each monomer unit carries a furan group in the side chain. For PEO<sub>330</sub>-b-PFGE<sub>20</sub>, significantly lower values of  $H = 0.071$  GPa and  $E_i = 0.91$  GPa compared to PFGE<sub>55</sub>, but increased by a factor of two compared to the non-crosslinked state were obtained (Figure 4c,e). This can be rationalized by the presence of only 17 wt% PFGE and, hence, a lower overall degree of crosslinking.

According to the load displacement results, the block copolymer films showed visco-elastic behavior (Supporting Information, Figure S7), which is one prerequisite/driving force for a self-healing process. The PEO segments seemed to act as a softening material, whereas an increasing hardness at higher displacements was observed as well. The increase of both hardness and stiffness can be attributed to the crosslinking of PFGE<sub>55</sub> and PEO<sub>330</sub>-b-PFGE<sub>20</sub> and, therefore,

the rDA reaction is expected to invert this process. The films were therefore heated to 155 °C for 3 h and subjected to additional depth-sensing-indentation measurements at RT. At this point, a color change of the diblock copolymer film from red to brown was observed. Nevertheless, the block copolymer was shown to withstand these conditions.<sup>[31]</sup>

As expected, the  $E_i$ -modulus decreased to 1.76 GPa after the treatment at 155 °C, and the hardness was reduced to 0.26 GPa for PFGE<sub>55</sub> (Figure 4b,d). Subsequent re-crosslinking by heating to 65 °C for 14 h led to an increase to 4.51 GPa ( $E$ -modulus) and 0.45 GPa (hardness), although the values are slightly lower than after the first crosslinking procedure. We attribute this to an incomplete DA reaction. For the PEO<sub>330</sub>-b-PFGE<sub>20</sub> block copolymer film, no significant changes after the rDA reaction were observed, which can be attributed to the rather low weight fraction of the PFGE segment.

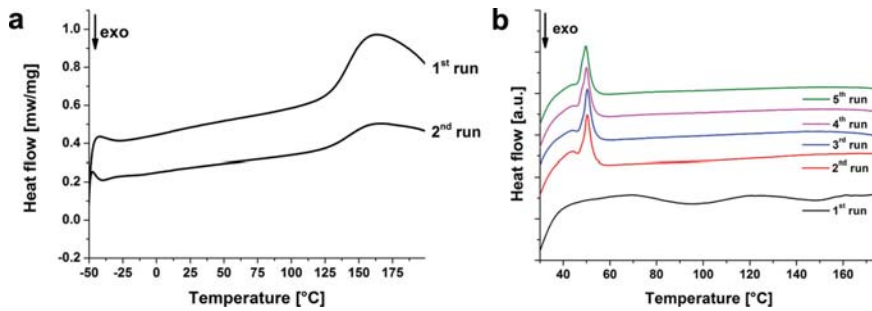


**Figure 5.** a) DSC measurements of a crosslinked PFGE<sub>55</sub> film with a heating rate of 20 K min<sup>-1</sup> for the first run and 10 K min<sup>-1</sup> for the second run. b) Multiple measurements of a crosslinked PEO<sub>330</sub>-*b*-PFGE<sub>20</sub> block copolymer film.

As the rDA is the key for a successful reversible network formation, we studied a crosslinked PFGE<sub>55</sub> film in more detail by DSC measurements (Figure 5). As shown in Figure 5a for PFGE<sub>55</sub>, the rDA reaction occurs within a temperature range of 135 to 160 °C. We attribute the fact that this is not visible for PEO<sub>330</sub>-*b*-PFGE<sub>20</sub> to the limited sensitivity of the DSC and the

low content of crosslinked furan rings. Heating of a crosslinked PEO<sub>330</sub>-*b*-PFGE<sub>20</sub> does not reveal any signal during the first heating run (Figure 5b). However, after heating above the rDA temperature, subsequent cooling, and repeated heating a slight melting peak at 50 °C can be detected, which we ascribe to partial crystallization of the PEO domains.

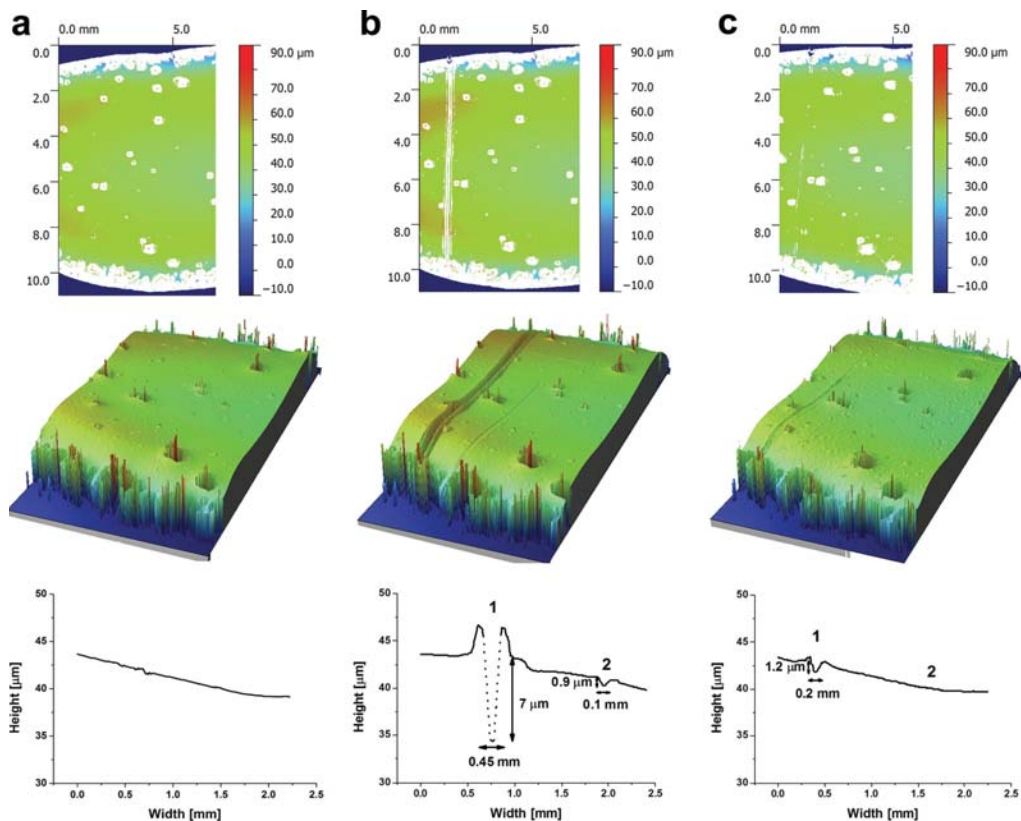


**Figure 6.** Profilometry measurements of PEO<sub>330</sub>-*b*-PFGE<sub>20</sub> block copolymer films after a) crosslinking, b) scratching with a spatula, and c) the healing process at 155 °C.

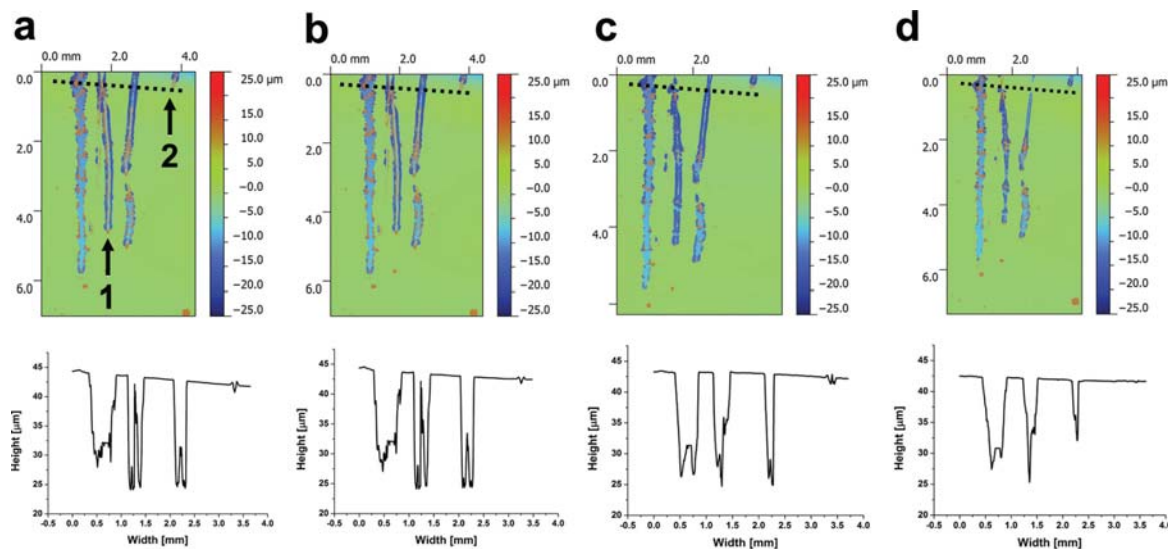


**Figure 7.** Profilometry measurements of a) a crosslinked PEO<sub>330</sub>-*b*-PFGE<sub>20</sub> film, b) after heating for 4 h at 65 °C, c) subsequent heating for 4 h at 100 °C, and d) heating for 3 h at 155 °C.

### 3.3. Self-Healing Properties of PEO<sub>330</sub>-*b*-PFGE<sub>20</sub>

In order to introduce controlled surface defects, the respective films were treated with a spatula, resulting in scratches of varying depth, length and width. At this point, it can be noticed that such films from PFGE<sub>55</sub> were very brittle and scratching led to film breakage. Therefore, it was concluded that “pure” films from PFGE<sub>55</sub> are not suitable, at least as thin films, and we focused on PEO<sub>330</sub>-*b*-PFGE<sub>20</sub> films, which were stable upon scratching.

Films containing PEO<sub>330</sub>-*b*-PFGE<sub>20</sub> and the BMA crosslinker (molar ratio was 1:1) were prepared and crosslinked at 65 °C for 14 h. In the literature, values between 50 and 70 °C were determined for this procedure by DSC.<sup>[28,29,55,56]</sup> After crosslinking, the film surface was analyzed using an optical profilometer (Figure 6) and subsequently scratched with a spatula. As it can be seen, defined scratches (Scratch 1: 7 μm depth, 0.45 mm width, length 8 mm; Scratch 2: 0.9 μm depth, 0.1 mm width, length of 3.5 mm) were created (Figure 6b, the dashed lines are a guide to the eye as the instrument is not able to resolve the steep walls of this particular scratch). Afterwards, the block copolymer film was heated for 3 h at 155 °C, allowed to cool down slowly to 65 °C, and re-crosslinked for 14 h at 65 °C.

After the rDA reaction at 155 °C and subsequent crosslinking at 65 °C, profilometry revealed that Scratch 2 disappeared completely and Scratch 1 decreased to 1.2 μm depth and 0.2 mm width. Repetition of the heating process and increasing of the heating time did not lead to a further reduction of the scratch size. During all steps of this process, the overall thickness of the PEO<sub>330</sub>-*b*-PFGE<sub>20</sub> film was monitored and shown to be constant (height ≈54 μm) (Supporting Information, Figure S8). Furthermore, defects within the block copolymer film remained unchanged, which would not be the case if the sample would undergo melting.

To ensure that the rDA reaction, followed by crosslinking at 65 °C, is responsible for the healing process, a film (Figure 7a) with defined scratches was heated for 4 h at 65 °C (over the melting temperature of the pristine block copolymer) and the surface was investigated by profilometry (Figure 7b). At this temperature, no changes were observed whereas subsequent heating to 100 °C for additional 4 h led to slight changes of the film surface (Figure 7c). In case of small scratches (max. depth 1 μm, Figure 7a,2), the depth was reduced by approximately 0.5 μm whereas deeper scratches (depth ≈6 μm or higher Figure 7a,1) remained unchanged. At this point we assume that heating to 100 °C leads to an increase of the chain mobility and possibly to the rDA reaction of small parts of the crosslinked units, which can be regarded as a kind of “pre-healing” process. Only if the film was heated to 155 °C for 3 h (Figure 7d), significant changes were observed (complete disappearance of smaller scratches as well as the decrease in length and width of larger defects). The fact that rather small gashes can already be repaired at lower temperatures has also been observed for networks from hyperbranched fluorinated polyethers created via DA chemistry.<sup>[57]</sup> Tentatively, the following mechanism is proposed to be responsible for the self-healing process: the incorporation of BMA and subsequent crosslinking leads to increasing hardness and decreasing chain mobility. At this point, the block copolymer film is damaged by mechanical force. Heating to 155 °C induces a rDA reaction and a partial decrosslinking of the network, accompanied by an increase in chain mobility leading to a kind of a reflow and, therefore, closure of the crack. The crosslinks are then partially reformed upon cooling.

We were also interested in the maximum number of possible self-healing cycles. For this purpose, a PEO<sub>330</sub>-*b*-PFGE<sub>20</sub> block copolymer film was subjected to several cycles of crosslinking-scratching-rDA-crosslinking (Figure 8).



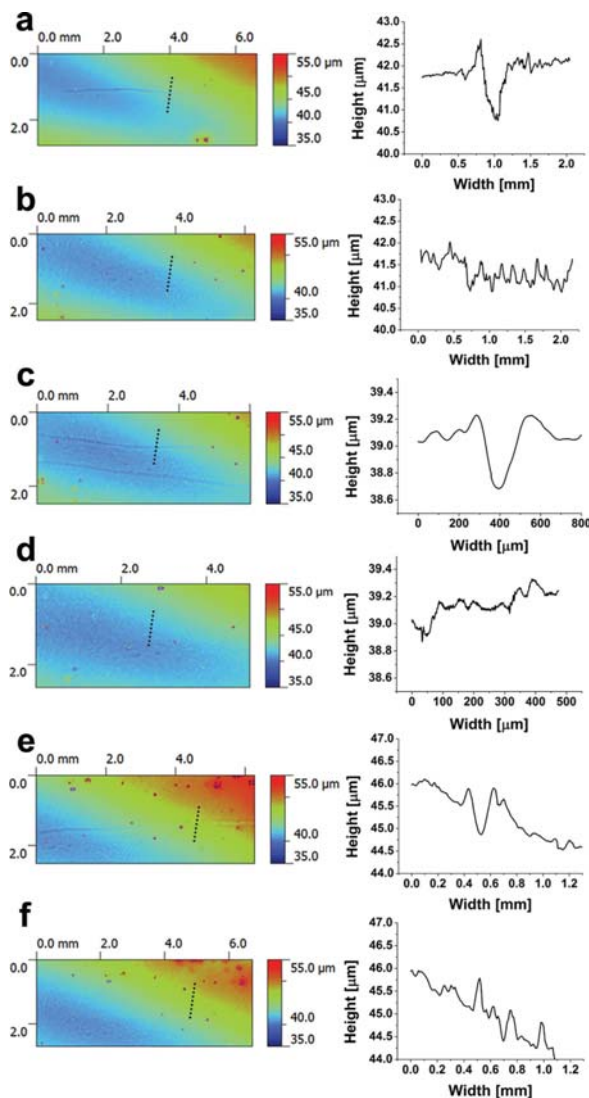


**Figure 8.** Repeated scratch healing of a  $\text{PEO}_{330}\text{-}b\text{-PFGE}_{20}$  block copolymer film: 1<sup>st</sup> cycle a) after scratching; b) after healing, c,d) 2<sup>nd</sup> cycle, and e,f) 4<sup>th</sup> cycle.

In the first cycle, a scratch of 0.13 mm width, 0.82  $\mu\text{m}$  depth and 4.4 mm length was inflicted (Figure 8a), and heating to 155  $^{\circ}\text{C}$  for 3 h, followed by subsequent crosslinking for 14 h at 65  $^{\circ}\text{C}$  lead to a disappearance of the scratch (Figure 8b). This procedure was repeated 4 times, and the 2<sup>nd</sup> healing cycle (a scratch of 0.14 mm, 0.42  $\mu\text{m}$  depth and 5.4 mm length) is shown in Figure 8c before and Figure 8d afterwards. Already here, it can be noticed that the film surface increases in roughness, particularly visible in the surface profile in Figure 8d. Nevertheless, in the fourth healing cycle, a 0.13 mm wide, 0.68  $\mu\text{m}$  deep and 5.2 mm long scratch (Figure 8e) can be still removed (Figure 8f). Whereas this can be applied to rather small scratches, the efficiency of the healing process for the

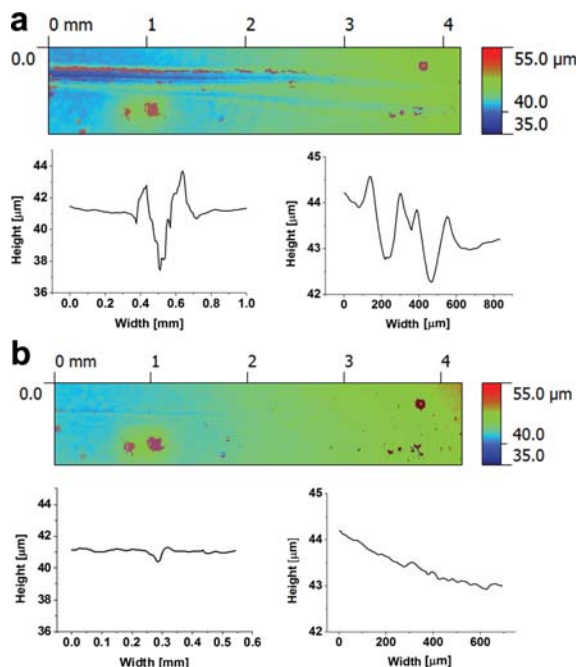


**Figure 9.** 5<sup>th</sup> scratch healing cycle of a  $\text{PEO}_{330}\text{-}b\text{-PFGE}_{20}$  block copolymer film comprising a scratch with a gradient depth and width before (a) and after self-healing (b).

block copolymer films regarding larger surface defects seems to decrease with increasing cycle number. To demonstrate this, a scratch with a depth (3.8 to 1.3  $\mu\text{m}$ ) and width (3.4 to 1.7 mm) gradient was applied to a film after 4 healing cycles (Figure 9a). After heating to 155  $^{\circ}\text{C}$  for 3 h and subsequent crosslinking, the scratch depth decreased to 0.66  $\mu\text{m}$  on the left side of the sample (Figure 9b). Also the width was reduced to 1.2 mm, whereas the thinner parts of the scratch completely disappeared. If compared to block copolymer films during the first healing cycles, where the depth of scratches could be reduced by up to 6–7  $\mu\text{m}$ , this decreased after 5 healing cycles to approx. 2 to 3  $\mu\text{m}$ .

Our explanation for this phenomenon is that with increasing number of heating cycles the amount of thermodynamically stable exo-product during the Diels-Alder reaction increases, which lead to a shift of the rDA process to higher temperatures.<sup>[58,59]</sup> As severe broadening of the signals in  $^1\text{H}$  NMR spectroscopy hints towards (at least partial) material degradation when films were heated above 170  $^{\circ}\text{C}$  in air, a complete cleavage of the DA adducts is not possible under these conditions. As this currently limits the process, the films were heated under an inert atmosphere in a glovebox as an alternative. After 30 min at temperatures of 175 to 215  $^{\circ}\text{C}$ , a color change from brownish to dark brown was visible. Nevertheless, the network structure still seemed to be intact as the  $\text{PEO}_{330}\text{-}b\text{-PFGE}_{20}$  film remained insoluble in different organic solvents (e.g., THF, DMF). To identify the origin of the color change, we heated pure  $\text{PEO}_{330}$ ,  $\text{PFGE}_{55}$  (pristine as well as crosslinked) and the BMA crosslinker was heated to 215  $^{\circ}\text{C}$ .

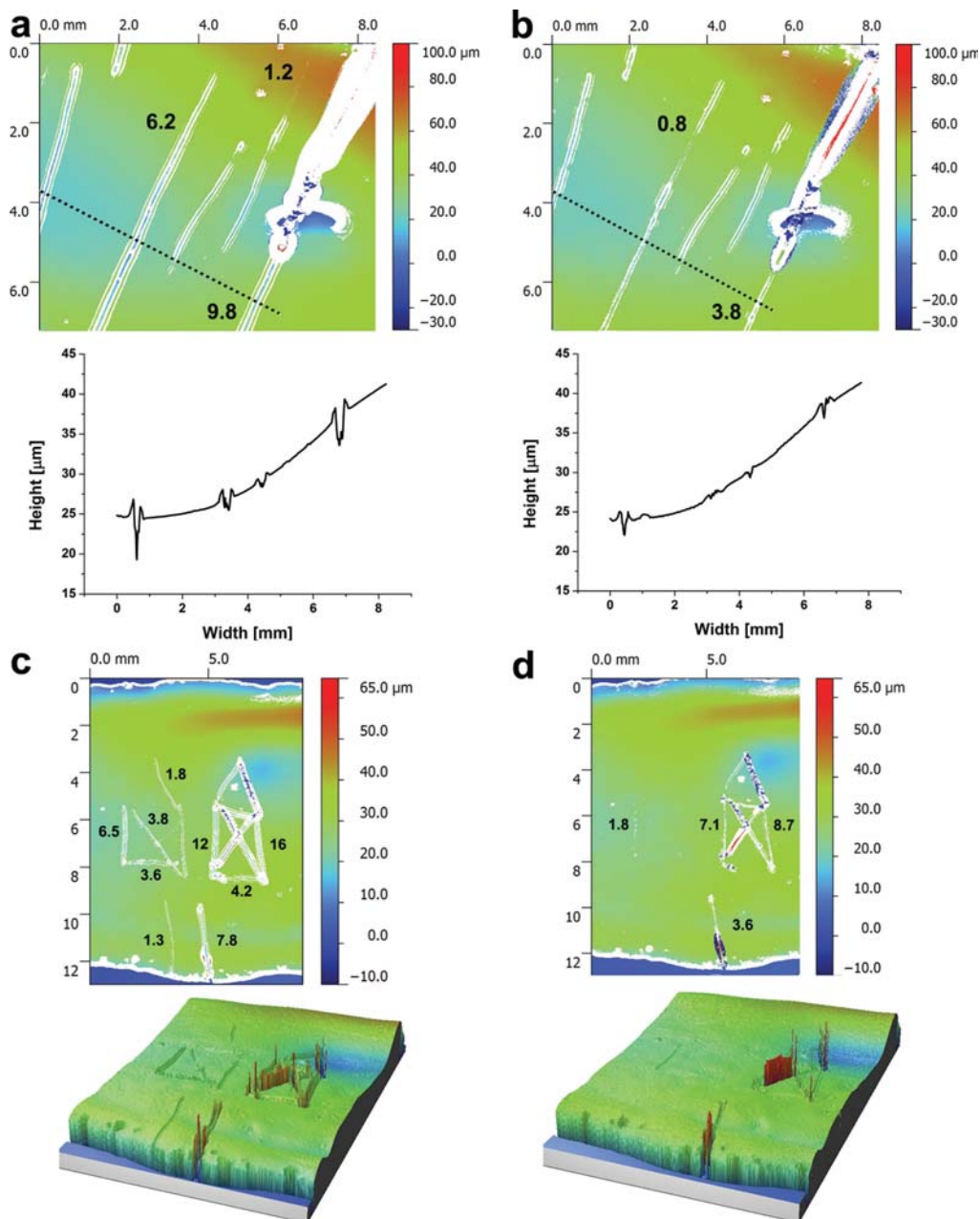


**Figure 10.** Self-healing process of a multi-scratch pattern (a) before, and b) after) as well as a complex pattern within a crosslinked PEO<sub>330</sub>-*b*-PFGE<sub>20</sub> block copolymer film (c) before, and d) after heating to 155 °C).

Both PEO<sub>330</sub> and BMA melted, whereas both PFGE samples revealed a rapid color change to dark brown, presumably due to the thermal instability of the furan moieties.<sup>[60]</sup> According to SEC measurements, no degradation occurred for PFGE<sub>55</sub> as a comparable elution trace was observed afterwards (Supporting Information, Figure S9). Nevertheless, we found that under

these rather harsh conditions the surface roughness increased rapidly. This might be explained by a fast cooling of the sample and partial breakage of the film due to mechanical stress. Even after this heat treatment, the block copolymer films exhibited self-healing abilities (a scratch of 2.9 μm depth decreased to 0.3 μm).

### 3.4. Multiple Scratches and Complex Scratch Patterns

We also applied complex scratch patterns to crosslinked PEO<sub>330</sub>-*b*-PFGE<sub>20</sub> block copolymer films (Figure 10). As shown in Figure 10b, small scratches with, e.g., a depth of 1.2 μm and a width of 0.16 mm disappeared completely, whereas deeper scratches with a depth of 6.2 or 9.8 μm and widths of 0.45 and 0.5 mm only decreased in size. The depths could be reduced to 0.8 and 3.8 μm, respectively, as well as the scratch width to 0.23 and 0.3 mm.

Figure 10c depicts a rather challenging scratch pattern, two "Santa's houses" with depths of approximately 1.8 to 6.8 μm and 4.2 to 16 μm. As shown in Figure 10d, the left (less deep) pattern vanished nearly completely. Only in case of the deeper scratch (6.5 μm), the depth was reduced to 1.8 μm, whereas the right-hand pattern comprising deeper scratches (12 to 16 μm) can still be seen afterwards (remaining scratches with 7.1 and 8.7 μm depth).

Finally, the comparison of the healing efficiency of the system presented here with literature examples was targeted. As shown before, it is possible to heal scratches of up to 6 μm depth and 1.7 mm width at elevated temperatures and on a time scale of 17 h (3 h at 155 °C and 14 h at 65 °C). One of the next targets for future studies is to reduce the required annealing times. For the initial investigation of the system the focus was placed on the complete crosslinking of the polymer films. However, self-healing approaches exploiting Diels-Alder chemistry will be necessarily limited to this temperature range in order to induce network formation or cleavage. This has also been demonstrated for comparable systems using this approach.<sup>[29,35]</sup> Self-healing processes based on  $\pi$ - $\pi$  interactions have been shown to operate at 90 °C and were able to cure scratches of up to 75 μm width within minutes.<sup>[20]</sup> In the case of systems based on hydrogen bonding it could be shown that previously cut pieces reconnect by simple surface contact at ambient temperatures, but this ability decreased the longer the pieces were kept separate (which we did not observe in the current example).<sup>[15,61]</sup> Comparable materials based on reversible metal-ligand-interactions were also healed at elevated temperatures (>100 °C) and the BMA crosslinker to 215 °C.<sup>[17,18,62]</sup>

## 4. Conclusion

We demonstrate one of the first examples for self-healing materials based on block copolymers. Films from PEO<sub>330</sub>-*b*-PFGE<sub>20</sub> diblock copolymers were shown to exhibit a smooth surface and a lamellar bulk morphology with a domain size of approximately 19 nm. The materials are capable of undergoing reversible (up to five times shown here) crosslinking/de-crosslinking and, hence, healing of inflicted damage at elevated temperatures. Comparison with PFGE<sub>55</sub> homopolymers via depth-sensing indentation revealed that this is accompanied by changes in hardness of the PFGE minority fraction. The results clearly show that PEO-*b*-PFGE block copolymers are promising candidates for self-healing surfaces (possible healing of scratches of up to 6 μm depth and 1.7 mm width), although still rather long cycles (up to 17 h) and high temperatures (155 °C) are required, and the employed BMA crosslinker

is rather toxic. In addition, the efficiency of the rDA process decreases with increasing cycle number, presumably due to the formation of the exo-product during the DA reaction. Nevertheless, our approach addresses one of the inherent problems in self-healing materials: the combination of smooth and dynamic segments with the capability of strong and reversible network formation via, here, Diels-Alder chemistry.

It will be the subject of further studies to purposefully vary the weight fraction of PFGE to access different bulk morphologies for such block copolymers as well as to identify superior crosslinking agents. Also, the use of PFGE-*b*-PEO-*b*-PFGE triblock copolymers might be advantageous.

## Supporting Information

Supporting Information is available from the Wiley Online Library or from the author.

## Acknowledgements

The authors thank Steffi Stumpf for help with AFM measurements, Sarah Crotty for MALDI-ToF-MS measurements and Ulrike Günther for help with the sample preparation for TEM measurements. We also wish to acknowledge the Dutch Polymer Institute (DPI, technology area high-throughput-experimentation, project #690) and the Thuringian Ministry for Education, Science and Culture (grants #B514-09051, NanoConSens and #B515-11028, SWAXS-JCSM) for financial support of this study. F. H. S. and T. R. are further grateful to the Thuringian Ministry for Education, Science, and Culture (TMBWK; #B515-10065, ChaPoNano). T. R. acknowledges the Carl-Zeiss foundation for a PhD-scholarship. U. S. S. and M. D. H. thank the DFG for financial support within the framework of SPP 1568.

Received: February 4, 2013

Revised: February 26, 2013

Published online: April 19, 2013

- [1] M. D. Hager, P. Greil, C. Leyens, S. van der Zwaag, U. S. Schubert, *Adv. Mater.* **2010**, *22*, 5424–5430.
- [2] R. S. Trask, H. R. Williams, I. P. Bond, *Bioinspir. Biomim.* **2007**, *2*, P1–P9.
- [3] E. W. Davie, O. D. Ratnoff, *Science* **1964**, *145*, 1310–8.
- [4] E. Vaccaro, J. H. Waite, *Biomacromolecules* **2001**, *2*, 906–911.
- [5] B. J. Blaiszik, S. L. B. Kramer, S. C. Olugebefola, J. S. Moore, N. R. Sottos, S. R. White, *Annu. Rev. Mater. Res.* **2010**, *40*, 179–211.
- [6] N. K. Guimard, K. K. Oehlenschlaeger, J. W. Zhou, S. Hilf, F. G. Schmidt, C. Barner-Kowollik, *Macromol. Chem. Phys.* **2012**, *213*, 131–143.
- [7] S. Bode, B. Sandmann, M. D. Hager, U. S. Schubert, *Metal-Complex based Self-healing Polymers in Self-Healing Polymers: From Principles to Applications* (Ed. W. Binder), Wiley-VCH, Weinheim **2013**.
- [8] S. R. White, N. R. Sottos, P. H. Geubelle, J. S. Moore, M. R. Kessler, S. R. Sriman, E. N. Brown, S. Viswanathan, *Nature* **2001**, *409*, 794–797.
- [9] H. R. Williams, R. S. Trask, P. M. Weaver, I. P. Bond, *J. R. Soc. Interface* **2008**, *5*, 55–65.
- [10] V. Berl, M. Schmutz, M. J. Krische, R. G. Khoury, J. M. Lehn, *Chem-Eur. J.* **2002**, *8*, 1227–1244.
- [11] J. L. Wietor, A. Dimopoulos, L. E. Govaert, R. A. T. M. van Benthem, G. de With, R. P. Sijbesma, *Macromolecules* **2009**, *42*, 6640–6646.

- [12] R. P. Sijbesma, F. H. Beijer, L. Brunsveld, B. J. B. Folmer, J. H. K. K. Hirsberg, R. F. M. Lange, J. K. L. Lowe, E. W. Meijer, *Science* **1997**, *278*, 1601–1604.
- [13] O. A. Scherman, G. B. W. L. Lighthart, R. P. Sijbesma, E. W. Meijer, *Angew. Chem. Int. Ed.* **2006**, *45*, 2072–2076.
- [14] H. Ohkawa, G. B. W. L. Lighthart, R. P. Sijbesma, E. W. Meijer, *Macromolecules* **2007**, *40*, 1453–1459.
- [15] P. Cordier, F. Tournilhac, C. Soulie-Ziakovic, L. Leibler, *Nature* **2008**, *451*, 977–980.
- [16] D. Montarnal, M. Capelot, F. Tournilhac, L. Leibler, *Science* **2011**, *334*, 965–968.
- [17] S. Bode, L. Zedler, F. H. Schacher, B. Dietzek, M. Schmitt, J. Popp, M. D. Hager, U. S. Schubert, *Adv. Mater.* **2013**, *25*, 1634–1638.
- [18] M. Burnworth, L. M. Tang, J. R. Kumpfer, A. J. Duncan, F. L. Beyer, G. L. Fiore, S. J. Rowan, C. Weder, *Nature* **2011**, *472*, 334–337.
- [19] S. Burattini, B. W. Greenland, W. Hayes, M. E. Mackay, S. J. Rowan, H. M. Colquhoun, *Chem. Mater.* **2011**, *23*, 6–8.
- [20] S. Burattini, H. M. Colquhoun, J. D. Fox, D. Friedmann, B. W. Greenland, P. J. F. Harris, W. Hayes, M. E. Mackay, S. J. Rowan, *Chem. Commun.* **2009**, 6717–6719.
- [21] X. X. Chen, M. A. Dam, K. Ono, A. Mal, H. B. Shen, S. R. Nutt, K. Sheran, F. Wudl, *Science* **2002**, *295*, 1698–1702.
- [22] X. X. Chen, F. Wudl, A. K. Mal, H. B. Shen, S. R. Nutt, *Macromolecules* **2003**, *36*, 1802–1807.
- [23] Y. L. Liu, C. Y. Hsieh, *J. Polym. Sci. Part A: Polym. Chem.* **2006**, *44*, 905–913.
- [24] M. Wouters, E. Craenmehr, K. Tempelaars, H. Fischer, N. Stroeks, J. van Zanten, *Prog. Org. Coat.* **2009**, *64*, 156–162.
- [25] J. Zhou, N. K. Guimard, A. J. Inglis, M. Namazian, C. Y. Lin, M. L. Coote, E. Spyrou, S. Hilf, F. G. Schmidt, C. Barner-Kowollik, *Polym. Chem.* **2012**, *3*, 628–639.
- [26] A. J. Inglis, L. Nebhani, O. Altintas, F. G. Schmidt, C. Barner-Kowollik, *Macromolecules* **2010**, *43*, 5515–5520.
- [27] J. Kötteritzsch, S. Stumpf, S. Hoepfener, J. Vitz, M. D. Hager, U. S. Schubert, *Macromol. Chem. Phys.* **2013**, DOI: 10.1002/macp.201200712.
- [28] A. Gandini, *Prog. Polym. Sci.* **2013**, *38*, 1–29.
- [29] Y. Zhang, A. A. Broekhuis, F. Picchioni, *Macromolecules* **2009**, *42*, 1906–1912.
- [30] J. A. Syrett, C. R. Becer, D. M. Haddleton, *Polym. Chem.* **2010**, *1*, 978–987.
- [31] M. J. Barthel, T. Rudolph, S. Crotty, F. H. Schacher, U. S. Schubert, *J. Polym. Sci. Part A: Polym. Chem.* **2012**, *50*, 4958–4965.
- [32] R. Gheneim, C. Perez-Berumen, A. Gandini, *Macromolecules* **2002**, *35*, 7246–7253.
- [33] Q. Tian, Y. C. Yuan, M. Z. Rong, M. Q. Zhang, *J. Mater. Chem.* **2009**, *19*, 1289–1296.
- [34] C. Gousse, A. Gandini, P. Hodge, *Macromolecules* **1998**, *31*, 314–321.
- [35] P. A. Pratama, A. M. Peterson, G. R. Palmese, *Macromol. Chem. Phys.* **2012**, *213*, 173–181.
- [36] A. M. Peterson, R. E. Jensen, G. R. Palmese, *ACS Appl. Mater. Interfaces* **2010**, *2*, 1141–1149.
- [37] T. Ekblad, G. Bergstroem, T. Ederth, S. L. Conlan, R. Mutton, A. S. Clare, S. Wang, Y. L. Liu, Q. Zhao, F. D'Souza, G. T. Donnelly, P. R. Willemsen, M. E. Pettitt, M. E. Callow, J. A. Callow, B. Liedberg, *Biomacromolecules* **2008**, *9*, 2775–2783.
- [38] H. Xu, F. Yan, E. E. Monson, R. Kopelman, *J. Biomed. Mater. Res. A* **2003**, *66A*, 870–879.
- [39] *EFSAJ.* **2006**, *4*, 414–415.
- [40] I. Banerjee, R. C. Pangule, R. S. Kane, *Adv. Mater.* **2011**, *23*, 690–718.
- [41] P. Kim, D. H. Kim, B. Kim, S. K. Choi, S. H. Lee, A. Khademhosseini, R. Langer, K. Y. Suh, *Nanotechnology* **2005**, *16*, 2420–2426.
- [42] N. A. Peppas, J. Z. Hilt, A. Khademhosseini, R. Langer, *Adv. Mater.* **2006**, *18*, 1345–1360.
- [43] F. H. Schacher, P. A. Rupar, I. Manners, *Angew. Chem. Int. Ed.* **2012**, *51*, 7898–7921.
- [44] P. Tyagi, A. Deratani, D. Bouyer, D. Cot, V. Gence, M. Barboiu, T. N. T. Phan, D. Bertin, D. Gigmès, D. Quemener, *Angew. Chem. Int. Ed.* **2012**, *51*, 7166–7170.
- [45] K. J. Henderson, T. C. Zhou, K. J. Otim, K. R. Shull, *Macromolecules* **2010**, *43*, 6193–6201.
- [46] M. D. Chipara, M. Chipara, E. Shansky, J. M. Zaleski, *Polym. Adv. Technol.* **2009**, *20*, 427–431.
- [47] J. Hentschel, A. M. Kushner, J. Ziller, Z. Guan, *Angew. Chem.* **2012**, *51*, 10561.
- [48] A. A. Kavitha, N. K. Singha, *Macromolecules* **2010**, *43*, 3193–3205.
- [49] E. F. J. Rettler, J. M. Kranenburg, H. M. L. Lambermont-Thijs, R. Hoogenboom, U. S. Schubert, *Macromol. Chem. Phys.* **2010**, *211*, 2443–2448.
- [50] W. C. Oliver, G. M. Pharr, *J. Mater. Res.* **1992**, *7*, 1564–1583.
- [51] H. Normant, B. Angelo, *B. Soc. Chim. Fr.* **1960**, 354–359.
- [52] E. Araneda, A. Leiva, L. Gargallo, N. Hadjichristidis, I. Mondragon, D. Radic, *Polym. Eng. Sci.* **2012**, *52*, 1128–1136.
- [53] F. H. Schacher, J. Elbert, S. K. Patra, S. F. M. Yusoff, M. A. Winnik, I. Manners, *Chem-Eur. J.* **2012**, *18*, 517–525.
- [54] B. J. Briscoe, L. Fiori, E. Pelillo, *J. Phys. D: Appl. Phys.* **1998**, *31*, 2395–2405.
- [55] J. A. Syrett, G. Mantovani, W. R. S. Barton, D. Price, D. M. Haddleton, *Polym. Chem.* **2010**, *1*, 102–106.
- [56] C. Toncelli, D. C. De Reus, F. Picchioni, A. A. Broekhuis, *Macromol. Chem. Phys.* **2012**, *213*, 157–165.
- [57] P. M. Imbesi, C. Fidge, J. E. Raymond, S. I. Cauët, K. L. Wooley, *ACS Macro Lett.* **2012**, *1*, 473–477.
- [58] J. Canadell, H. Fischer, G. De With, R. A. T. M. Van Benthem, *J. Polym. Sci. Part A: Polym. Chem.* **2010**, *48*, 3456–3467.
- [59] L. Rulisek, P. Sebek, Z. Havlas, R. Hrabal, P. Capek, A. Svatos, *J. Org. Chem.* **2005**, *70*, 6295–6302.
- [60] S. D. Bergman, F. Wudl, *J. Mater. Chem.* **2008**, *18*, 41–62.
- [61] G. M. L. van Gemert, J. W. Peeters, S. H. M. Sontjens, H. M. Janssen, A. W. Bosman, *Macromol. Chem. Phys.* **2012**, *213*, 234–242.
- [62] J. Yuan, X. Fang, L. Zhang, G. Hong, Y. Lin, Q. Zheng, Y. Xu, Y. Ruan, W. Weng, H. Xia, G. Chen, *J. Mater. Chem.* **2012**, *22*, 11515–11522.



# ADVANCED FUNCTIONAL MATERIALS

## Supporting Information

for *Adv. Funct. Mater.*, DOI: 10.1002/adfm.201300469

Self-Healing Materials via Reversible Crosslinking of  
Poly(ethylene oxide)- Block -Poly(furfuryl glycidyl ether)  
(PEO- b -PFGE) Block Copolymer Films

*Markus J. Barthel, Tobias Rudolph, Anke Teichler, Renzo M.  
Paulus, Jürgen Vitz, Stephanie Hoepfener, Martin D. Hager,  
Felix H. Schacher \* and Ulrich S. Schubert\**

Supporting information for

Self-Healing Materials via Reversible Crosslinking of

Poly(ethylene oxide)-*block*-poly(furfuryl glycidyl ether) (PEO-  
*b*-PFGE) Block Copolymer Films

Markus J. Barthe<sup>1,2,3</sup> Tobias Rudolph,<sup>1,2</sup> Anke Teichler,<sup>1,2,3</sup> Renzo M. Paulus,<sup>1,2</sup> Jürgen Vitz,<sup>1,2,3</sup>  
Stephanie Hoepfener,<sup>1,2,3</sup> Martin D. Hager,<sup>1,2</sup> Felix H. Schacher,<sup>1,2\*</sup> and Ulrich S. Schubert<sup>1,2,3\*</sup>

<sup>1</sup> Laboratory of Organic and Macromolecular Chemistry (IOMC), Friedrich-Schiller-University Jena, Humboldtstr. 10, 07743 Jena, Germany.

<sup>2</sup> Jena Center for Soft Matter (JCSM), Friedrich-Schiller-University Jena, Philosophenweg 7, 07743 Jena, Germany.

<sup>3</sup> Dutch Polymer Institute (DPI), John F. Kennedylaan 2, 5612 AB Eindhoven, The Netherlands.

Email: [ulrich.schubert@uni-jena.de](mailto:ulrich.schubert@uni-jena.de); [felix.schacher@uni-jena.de](mailto:felix.schacher@uni-jena.de);

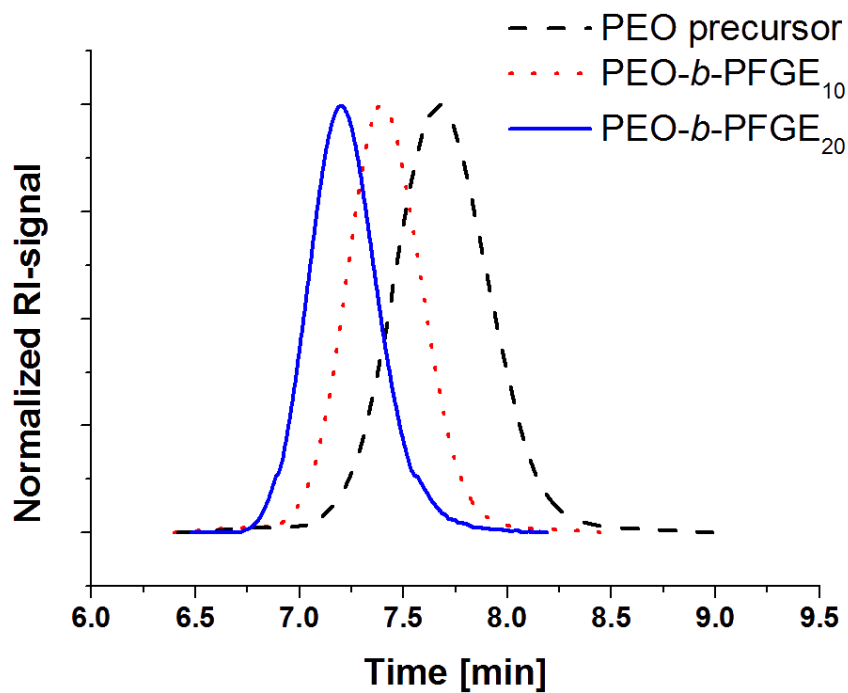


**Figure S1.** SEC traces for the PEO<sub>330</sub> precursor (dashed black line), PEO<sub>330</sub>-*b*-PFGE<sub>10</sub> (dotted red line), and PEO<sub>330</sub>-*b*-PFGE<sub>20</sub> (solid blue line) block copolymers (eluent: CHCl<sub>3</sub> / *i*-propanol / triethylamine).

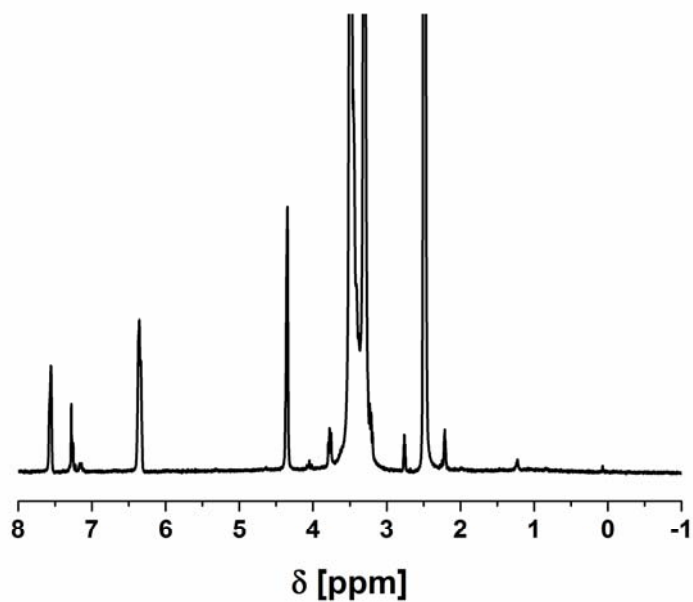


**Figure S2.** <sup>1</sup>H NMR spectrum (300 MHz) of PEO<sub>330</sub>-*b*-PFGE<sub>20</sub> in DMSO-*d*<sub>6</sub>.

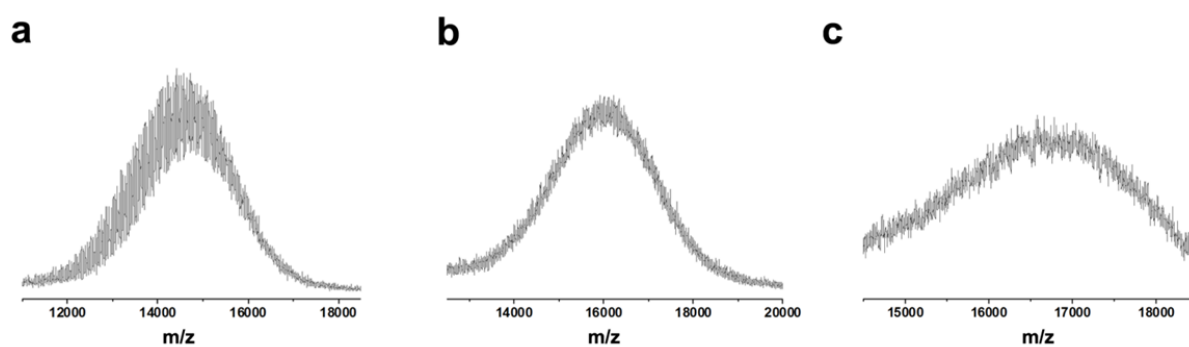


**Figure S3.** MALDI-ToF MS measurements of the PEO<sub>330</sub> precursor (a), and of PEO<sub>330</sub>-*b*-PFGE<sub>10</sub> (b) and PEO<sub>330</sub>-*b*-PFGE<sub>20</sub> (c) block copolymers.

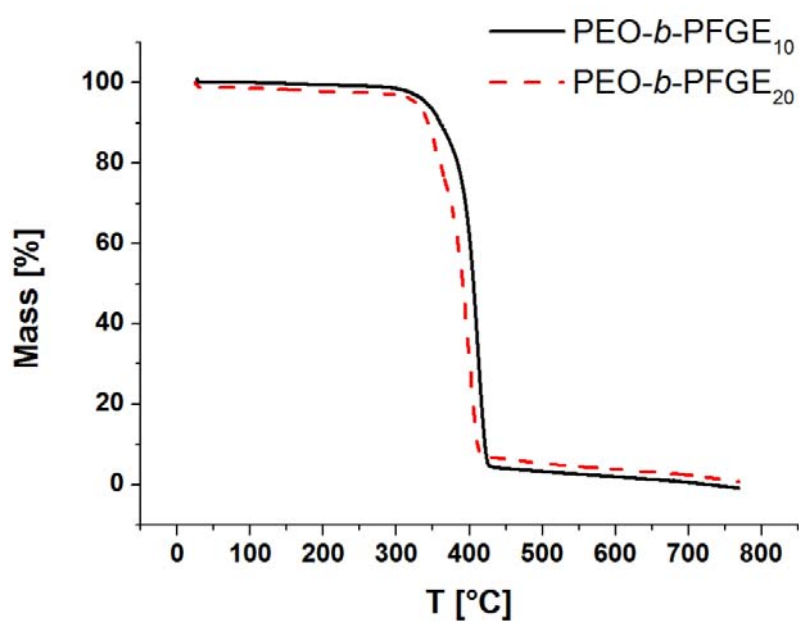


**Figure S4.** TGA measurements for PEO<sub>330</sub>-*b*-PFGE<sub>10</sub> and PEO<sub>330</sub>-*b*-PFGE<sub>20</sub> block copolymers under nitrogen atmosphere.

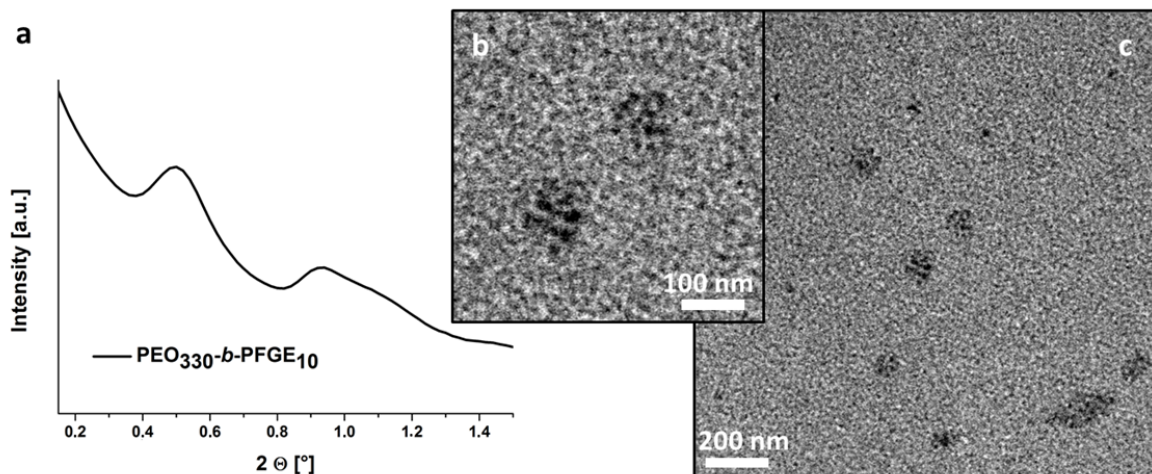


**Figure S5.** SAXS measurement for a crosslinked  $\text{PEO}_{330}\text{-}b\text{-PFGE}_{10}$  film (a) and TEM micrograph for core-crosslinked  $\text{PEO}_{330}\text{-}b\text{-PFGE}_{10}$  micelles after bulk crosslinking and sonication-assisted dissolution (b, higher magnification and c presents an overview).

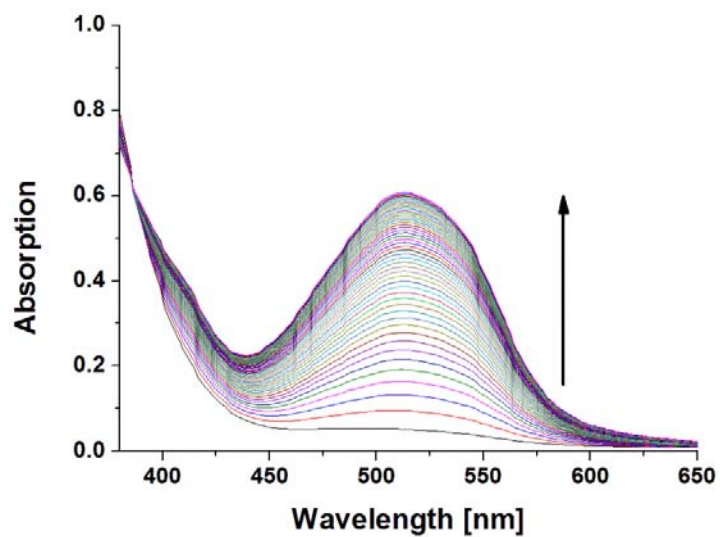


**Figure S6.** Time depending UV/Vis measurements of a  $\text{PEO}_{330}\text{-}b\text{-PFGE}_{20}$  / BMA linker mixture in DMF.

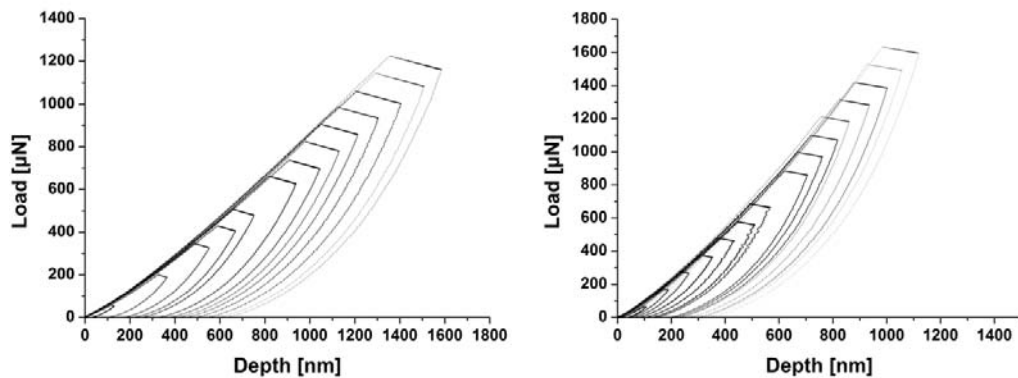


**Figure S7.** Load-depth curves of a pristine (left) and crosslinked (right)  $\text{PEO}_{330}\text{-}b\text{-PFGE}_{20}$  sample at different loadings.

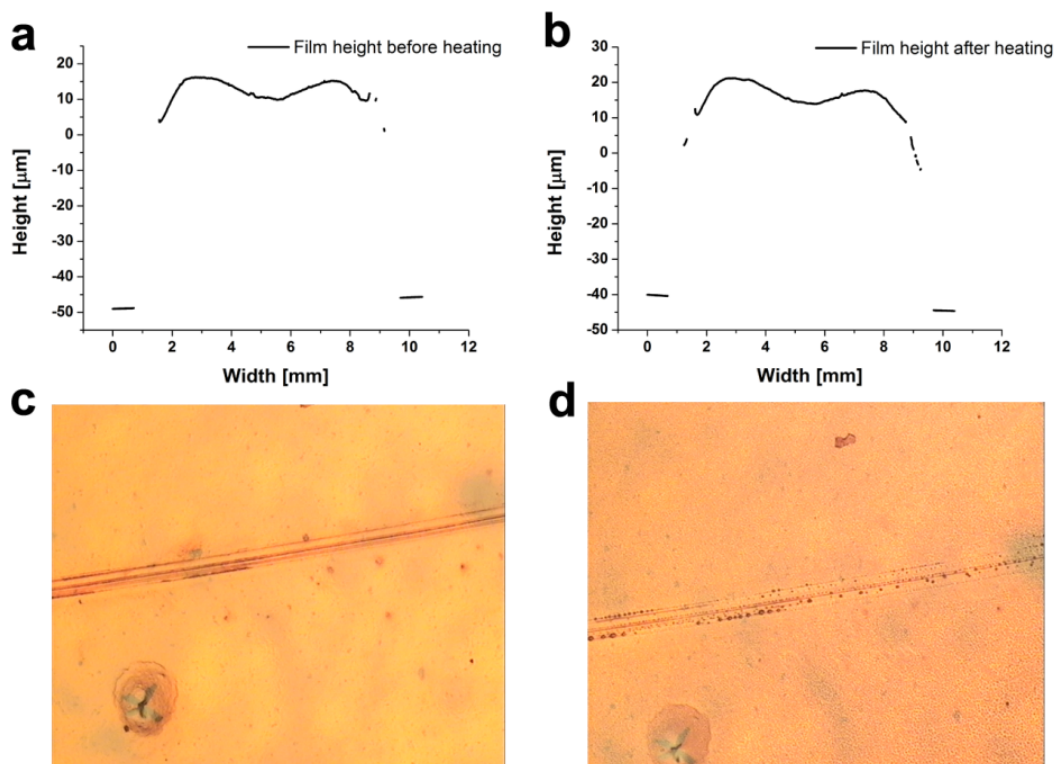


**Figure S8.** Height profiles of a  $\text{PEO}_{330}\text{-}b\text{-PFGE}_{20}$  block copolymer film before (a) and after heating (b) as well as optical microscopy images of the polymer film at room-temperature (c) and at  $155\text{ }^{\circ}\text{C}$  (d). The slight variation of the axis values in Figure 8a and b originate from a tilt of the sample during the measurement process.

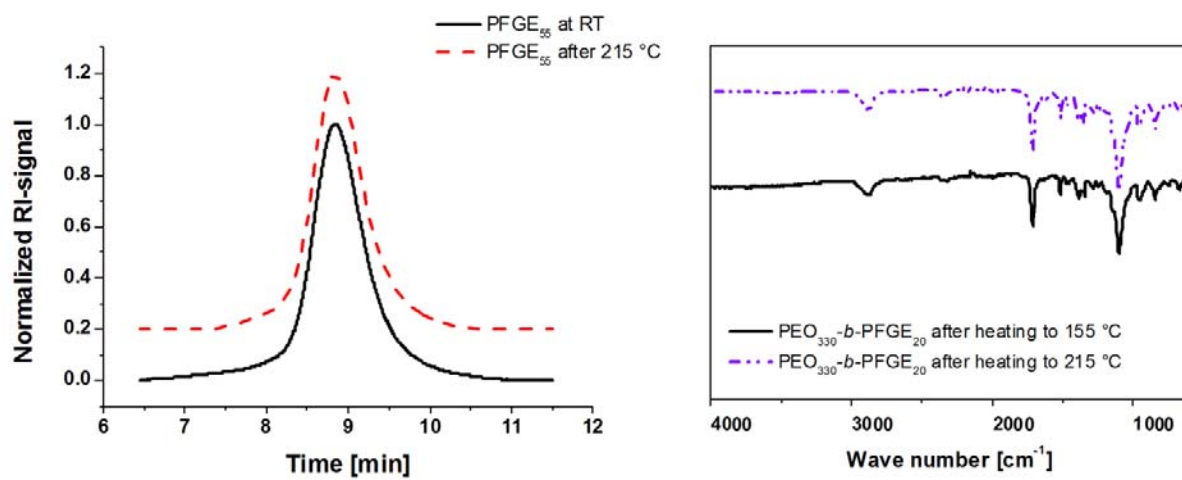


**Figure S9.** SEC traces of PFGE<sub>55</sub> before (solid black line) and after heating to 215 °C (dashed red line) (left) as well as IR spectroscopy measurements of a PEO<sub>330</sub>-b-PFGE<sub>20</sub> sample heated to 155 °C (solid line) and 215 °C (dashed line) (right).

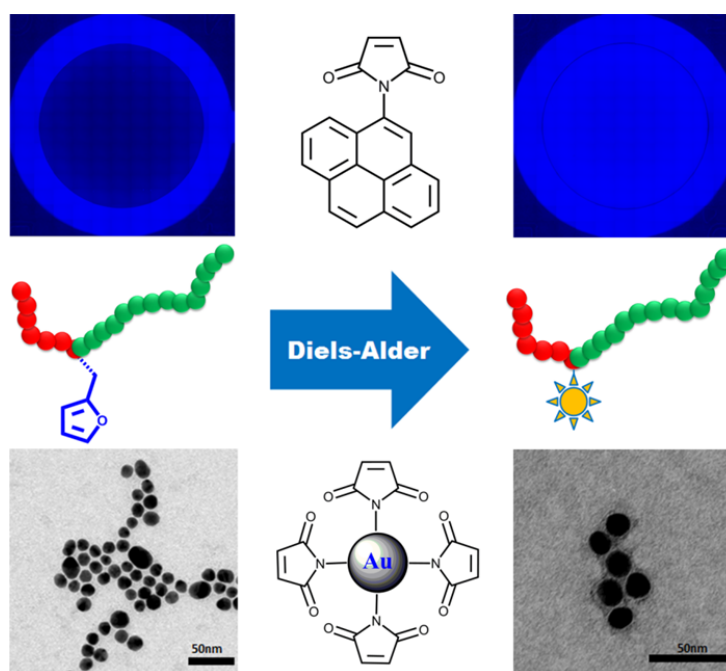
## Publication P6

### Poly(2-vinyl pyridine)-*block*-poly(ethylene oxide) featuring a furan group at the block junction – Synthesis and functionalization

Tobias Rudolph<sup>#</sup>, Markus J. Barthel<sup>#</sup>, Florian Kretschmer, Ulrich Mansfeld, Stephanie Hoepfener, Martin D. Hager, Ulrich S. Schubert, Felix H. Schacher

<sup>#</sup> Both authors contributed equally to this work.

*Macromol. Rapid Commun.* **2014**, DOI: 10.1002/marc201300875.





# **Poly(2-vinyl pyridine)-*block*-Poly(ethylene oxide) featuring a Furan Group at the Block Junction – Synthesis and Functionalization**

Tobias Rudolph,<sup>1,2,#</sup> Markus J. Barthel,<sup>1,2,3,#</sup> Florian Kretschmer,<sup>1,2</sup> Ulrich Mansfeld,<sup>1,2</sup>  
Stephanie Hoepfener,<sup>1,2</sup> Martin D. Hager,<sup>1,2</sup> Ulrich S. Schubert,<sup>1,2,3</sup> and Felix H. Schacher<sup>1,2,\*</sup>

[1] Laboratory of Organic and Macromolecular Chemistry, Friedrich Schiller University Jena, Humboldtstr. 10,  
07743 Jena, Germany

E-mail: [felix.schacher@uni-jena.de](mailto:felix.schacher@uni-jena.de)

[2] Jena Center for Soft Matter (JCSM), Friedrich Schiller University Jena, Philosophenweg 7, 07743 Jena,  
Germany

[3] Dutch Polymer Institute, P.O. Box 902, Eindhoven 5600 AX, The Netherlands

# These authors contributed equally to this work.

Keywords: anionic polymerization, furfuryl glycidyl ether, mid-chain junction, poly(ethylene oxide), Diels-Alder reaction, block copolymer

## **Abstract**

Furfuryl glycidyl ether (FGE) represents a highly versatile monomer for the preparation of reversibly crosslinkable nanostructured materials *via* Diels-Alder reactions. Here, we report the use of FGE for the mid-chain functionalization of a P2VP-*b*-PEO diblock copolymer. The material features one furan moiety at the block junction, P2VP<sub>68</sub>-FGE-*b*-PEO<sub>390</sub>, which can be subsequently addressed in Diels-Alder reactions using maleimide functionalized counterparts. The presence of the FGE moiety enables the introduction of dyes as model labels or the formation of hetero-grafted brushes as shell on hybrid Au@Polymer nanoparticles. This renders P2VP<sub>68</sub>-FGE-*b*-PEO<sub>390</sub> a powerful tool for selective functionalization reactions, including the modification of surfaces.

## **Introduction**

During the last decades well-defined block copolymers revealed high potential for a broad range of applications, mainly driven by the possibility to combine different properties within one single material and to introduce the ability to undergo self-assembly into nanostructured materials in various environments.<sup>1-5</sup> The preparation of block copolymers is usually achieved by sequential polymerization of different monomers or *via* post-polymerization modification using suitable macromolecular conjugation reactions (*e.g.*, 1,3-dipolar cycloadditions, (Hetero) Diels-Alder (DA) reactions).<sup>6-9</sup> Thereby, the precise positioning of functional groups within polymer chains is crucial for the synthesis of linear block copolymers or materials of different architectures, *e.g.*, star-shaped molecular structures.<sup>10-12</sup> Although more and more examples are found where polymeric building blocks are functionalized at one or both chain ends, examples for addressing the mid-chain junction point, *i.e.* the covalent linkage of block A and B of diblock copolymers, are scarce.<sup>13-16</sup> Such functional mid-chain junctions can be introduced by functional initiators<sup>17, 18, 19</sup> or end-capping of an active polymer chain and the

subsequent polymerization of the second block.<sup>20, 21</sup> Current examples most commonly feature a new initiating group or a clickable moiety. In that respect, epoxides can be used as straightforward and highly efficient end-capping agents during living anionic polymerization using lithium counter ions. Here, due to the strong coordination of lithium towards the alkoxide chain end further polymerization of epoxides is prevented and the attachment of one single molecule can be realized. Potential functionalized epoxides such as allyl glycidyl ether (AGE) or ethoxy ethyl glycidyl ether (EEGE) are commercially available and transform this substance class into an interesting tool for the selective mid-chain functionalization of polymer chains.

Recently, furfuryl glycidyl ether (FGE) has been established as a versatile and functional monomer for anionic ring-opening polymerization (AROP) and the subsequent use of the furan moiety for controlled and reversible crosslinking of micellar cores or individual domains within nanostructured films *via* the Diels-Alder reaction (DA) using a bismaleimide.<sup>22, 23</sup> In the latter case, the potential application of poly(ethylene oxide)-*block*-poly(furfuryl glycidyl ether) (PEO-*b*-PFGE) diblock copolymers as self-healing coatings was proposed.

Herein, we use FGE as a functional end-capping agent for the living anionic polymerization of poly(2-vinylpyridine) (P2VP), followed by the subsequent polymerization of ethylene oxide (EO) and the formation of mid-chain functionalized P2VP-*b*-PEO. After characterization *via* size exclusion chromatography (SEC), nuclear magnetic resonance (NMR) spectroscopy and MALDI-TOF MS, the furan moiety in between the two blocks was used for selective DA-reactions with maleimide functionalized model dyes and gold nanoparticles.

## Results and discussion

Mid-chain functionalized block copolymers represent interesting materials when it comes to the modification of surfaces such as on planar substrates or on (nano)particles. The introduction of a furan group at the junction point of diblock copolymers in turn is motivated by the broad accessibility of functional groups and architectures by the DA chemistry. Therefore, the synthesis of poly(2-vinylpyridine)-*block*-poly(ethylene oxide) (P2VP-FGE-*b*-PEO), featuring a furfuryl glycidyl ether moiety in between the P2VP and the PEO segment, was carried out in two steps. First, 2-vinylpyridine was polymerized after initiation *via* *sec*-butyl lithium (*sec*-BuLi). After full conversion, 1,1-diphenylethylene was added to the reaction mixture to decrease the nucleophilicity of the active chain end,<sup>15</sup> and the living P2VP chains were end-capped with furfuryl glycidyl ether (FGE, **Figure 1A**). Afterwards, the reaction was quenched by the addition of methanol and the crude product was precipitated into cold hexane. P2VP-FGE-OH was characterized *via* SEC, <sup>1</sup>H-NMR and MALDI-TOF MS (**Figure 1**, **Table S1**, and **Figure S2**). The degree of polymerization (DP) was determined to be 68, resulting in P2VP<sub>68</sub>-FGE-OH. The endgroup fidelity was assessed *via* MALDI-TOF MS and NMR and was found to be 100% within the error of the measurement. MALDI-TOF MS also revealed the presence of the lithium counterion (**Figure S2**), which however had to be removed prior to the polymerization of ethylene oxide. For this purpose, the material was intensively washed with water and precipitated into cold hexane several times (**Figure S3**). As a second step, P2VP<sub>68</sub>-FGE-OH was dissolved in THF and the hydroxyl endgroup was activated by the addition of an excess of diphenylmethyl potassium (DPMK), until a deep red color could be observed (**Figure 1A**). Under vigorous stirring ethylene oxide was added to the functionalized reaction at -20 °C, was slowly heated to 40 °C and the polymerization was terminated *via* the addition of methanol after 24 h, followed by precipitation of the block copolymer into cold diethyl ether. The obtained material was again investigated *via* SEC, <sup>1</sup>H-

NMR and MALDI-TOF MS (**Figure S4**). The SEC trace shows a clear shift to lower elution volume in comparison to P2VP<sub>68</sub>-FGE-OH (**Figure 1B** and **Table S1**), and a new peak around 3.6 ppm for the PEO-backbone appears in the <sup>1</sup>H-NMR spectrum. The exact molar mass of the block copolymer was determined by MALDI-TOF MS, leading to 24 500 g mol<sup>-1</sup>, and a composition of P2VP<sub>68</sub>-FGE-PEO<sub>390</sub> (**Figure S4**), which was also confirmed *via* <sup>1</sup>H-NMR spectroscopy.

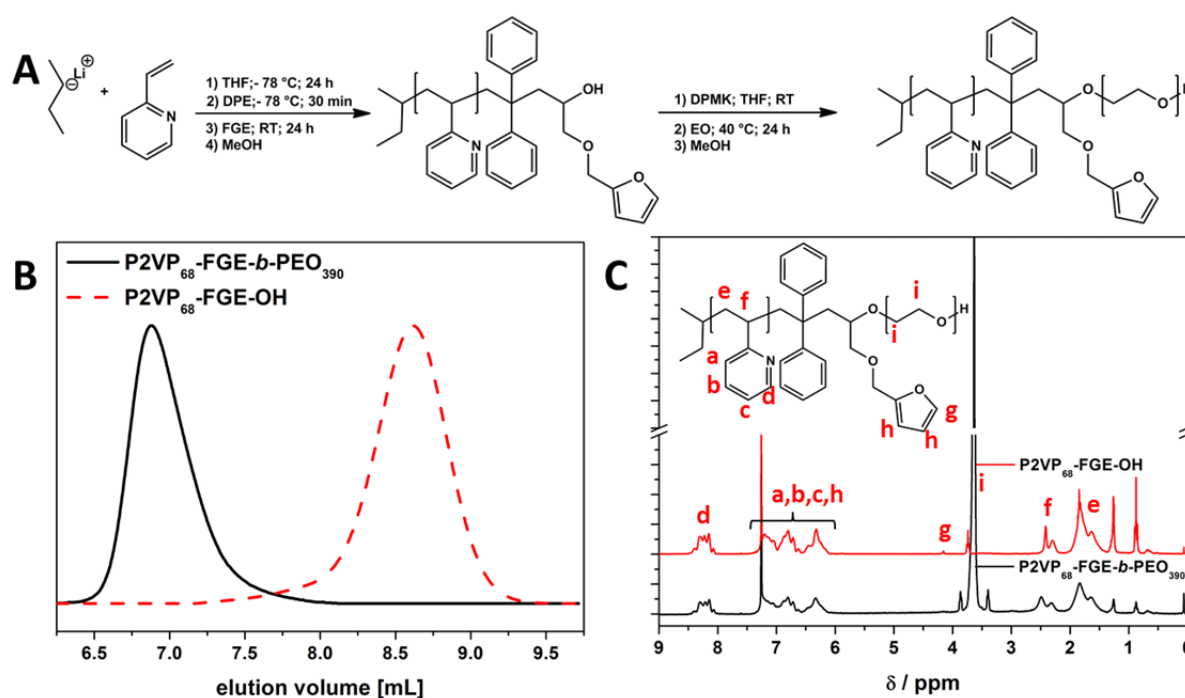


**Figure 1:** A) block copolymer synthesis *via* sequential polymerization of 2-vinylpyridine and ethylene oxide; B) comparison of SEC traces for P2VP<sub>68</sub>-FGE-OH (dashed red line) and P2VP<sub>68</sub>-FGE-*b*-PEO<sub>390</sub> (black straight line) and C) the NMR spectra for P2VP<sub>68</sub>-FGE-OH (red line) and P2VP<sub>68</sub>-FGE-*b*-PEO<sub>390</sub> (black line).

As a first proof of successful functionalization, P2VP<sub>68</sub>-FGE-*b*-PEO<sub>390</sub> was used in DA-reactions with two different maleimide-functionalized dyes (*N*-(1-pyrenyl)maleimide and 4-phenylazomaleinonil). Therefore, the block copolymer and the respective dye (20 eq.) were dissolved in 2 mL DMF separately in two vials and heated to 75 °C for 24 hours. Afterwards, the dye-functionalized materials were purified *via* size-exclusion column chromatography (BioBeads SX1) to remove any excess of the dyes. In both cases, successful functionalization with the azobenzene-, P2VP<sub>68</sub>-azo-*b*-PEO<sub>390</sub>, and the pyrene-moiety, P2VP<sub>68</sub>-pyr-*b*-PEO<sub>390</sub>, was proven by UV-Vis measurements (**Figure 2B** and **2C**). The UV-Vis spectra display that

the initial P2VP<sub>68</sub>-FGE-*b*-PEO<sub>390</sub> shows no characteristic absorption band (black line), whereas the characteristic patterns of the individual molecules (red lines, 331 nm for 4-phenylazomaleinanil and 313, 326 and 342 nm for *N*-(1-pyrenyl)maleimide) can be found for the block copolymers after successful functionalization (blue lines).

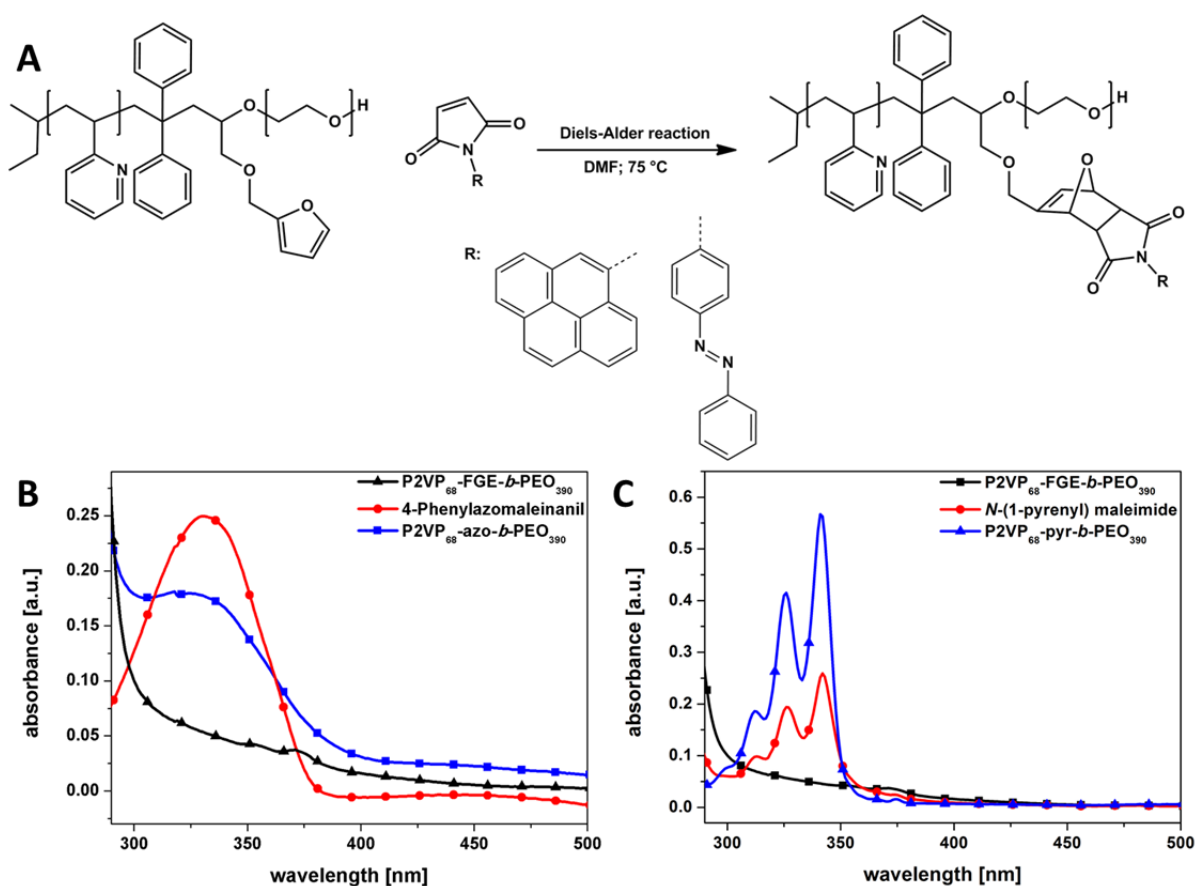


**Figure 2:** A) DA reaction between P2VP<sub>68</sub>-FGE-*b*-PEO<sub>390</sub> and maleimide functionalized dyes; comparison of UV-Vis spectra for B) P2VP<sub>68</sub>-FGE-*b*-PEO<sub>390</sub> (black curve), 4-phenylazomaleinanil (red curve), and P2VP<sub>68</sub>-azo-*b*-PEO<sub>390</sub> (blue curve); C) P2VP<sub>68</sub>-FGE-*b*-PEO<sub>390</sub> (black curve), *N*-(1-pyrenyl) maleimide (red curve), and P2VP<sub>68</sub>-pyr-*b*-PEO<sub>390</sub> (blue curve) in THF.

Pyrene is known as a hydrophobic, fluorescent dye suitable for the determination of the critical micellization concentration (cmc) of amphiphilic block copolymers.<sup>24-27</sup> In case of *N*-(1-pyrenyl)maleimide no fluorescence is described in the literature for the pristine dye in water, only after nucleophilic attack by thiols.<sup>28</sup> This can also be observed for our system after functionalization with *N*-(1-pyrenyl)maleimide and this was investigated *via* fluorescence microscopy (excitation wavelength = 357 nm; emission filter = 460 nm, **Figure 3**). Using this set-up no fluorescence could be detected for the pure dye in MilliQ water, whereas pyrene

itself showed clear fluorescence under these conditions (**Figure S6C**). Both P2VP<sub>68</sub>-pyr-*b*-PEO<sub>390</sub> and P2VP<sub>68</sub>-FGE-*b*-PEO<sub>390</sub> were transferred from THF into MilliQ water (pH7) by evaporation of the organic solvent (concentration was 5 mg mL<sup>-1</sup> in both cases). In **Figure 3** the blue circle originates from the fluorescence of the well-plate itself, while in the middle the sample solution is located. As P2VP is known to exhibit a weak autofluorescence,<sup>29</sup> some fluorescence was also observed for P2VP<sub>68</sub>-FGE-*b*-PEO<sub>390</sub>, whereas P2VP<sub>68</sub>-pyr-*b*-PEO<sub>390</sub> shows a twofold increase in fluorescence in comparison to the pristine block copolymer (**Figure 3** and **Figure S6** and **S7**). This drastic increase in fluorescence can be explained by electronic changes after the covalent attachment to the block copolymer chain by DA chemistry.

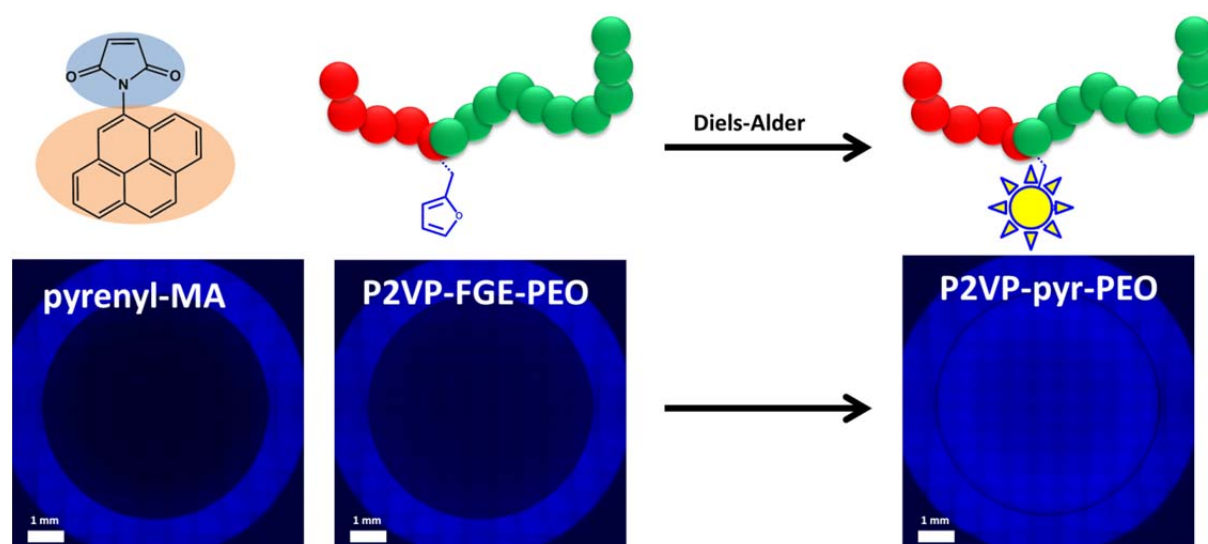


**Figure 3: Functionalization of P2VP<sub>68</sub>-FGE-*b*-PEO<sub>390</sub>; comparison of fluorescence microscope images of *N*-(1-pyrenyl)maleimide (left), P2VP<sub>68</sub>-FGE-*b*-PEO<sub>390</sub> (5 mg mL<sup>-1</sup>, middle), and P2VP<sub>68</sub>-pyr-*b*-PEO<sub>390</sub> (5 mg mL<sup>-1</sup>, right) in water.**

We were also interested in using P2VP<sub>68</sub>-FGE-*b*-PEO<sub>390</sub> for the functionalization of gold nanoparticles (Au-NP). In that way, a hetero-brush could be generated in analogy to poly(styrene)-*block*-poly(ethylene oxide) (PS-*b*-PEO) brushes on planar surfaces.<sup>21</sup> Therefore, a maleimide functionalized tri-thiol was synthesized (**Figure S1**) and used for the synthesis of maleimide-functionalized Au-NPs.<sup>30, 31</sup> Possible excess of the thiol was removed by centrifugation of the particles (60 min at 5 000 rpm), followed by re-suspension in DMF

(three cycles). The protective group was removed by heating the functionalized NP for 1 h at 140 °C. Both size and shape of the nanoparticles were confirmed *via* DLS, TEM and UV-Vis (**Figure 4**). Spherical Au-NPs with a  $\langle R_h \rangle_{z,app}$  of 8 nm were obtained according to DLS (**Figure 4D**) and TEM (**Figure 4A**). For the attachment of P2VP<sub>68</sub>-FGE-*b*-PEO<sub>390</sub> to the nanoparticle surface, Au-NP and P2VP<sub>68</sub>-FGE-*b*-PEO<sub>390</sub> were suspended together in DMF and heated for 2 days at 75 °C. After this treatment the solution was centrifuged and washed with DMF to remove any unreacted P2VP<sub>68</sub>-FGE-*b*-PEO<sub>390</sub>. After re-suspension the particles (P2VP<sub>68</sub>-DA<sub>Au</sub>-*b*-PEO<sub>390</sub>) were investigated using UV-Vis and DLS, showing a slight red-shift in the UV-Vis spectra from 527 to 538 nm (**Figure 4C**) and an increase in hydrodynamic radius ( $\langle R_h \rangle_{z,app} = 12$  nm) compared to the pristine block copolymer ( $\langle R_h \rangle_{z,app} = 4$  nm), and the maleimide-functionalized Au-NP ( $\langle R_h \rangle_{z,app} = 8$  nm, **Figure 4D**).

According to DLS, the size distribution of P2VP<sub>68</sub>-DA<sub>Au</sub>-*b*-PEO<sub>390</sub> slightly broadens, which might be due to a certain aggregation of the hybrid particles in solution. If the structures are subjected to TEM analysis, the freshly prepared Au-NPs feature sharp edges whereas this seems not to be the case after DA reaction with P2VP<sub>68</sub>-FGE-*b*-PEO<sub>390</sub>, indicating the attachment of a polymeric shell (**Figure S8**). Negative staining with uranyl acetate was applied to the NP both before and after surface modification. As expected, no changes were observed for the pristine Au-NP, except for a slight decrease of the overall contrast within the corresponding TEM micrographs due to an increase of the electron density on the whole TEM grid (**Figure S8**). For P2VP<sub>68</sub>-DA<sub>Au</sub>-*b*-PEO<sub>390</sub>, a continuous dark ring of a few nanometers thickness is observed and this further supports the assumption of the successful formation of a P2VP/PEO shell. P2VP<sub>68</sub>-DA<sub>Au</sub>-*b*-PEO<sub>390</sub> was also transferred into DMF-d<sub>7</sub> and was investigated *via* <sup>1</sup>H-NMR, but the signal intensity of the obtained spectrum was observed to be rather low (**Figure S9**). However, both the characteristic signals for P2VP and PEO could be clearly assigned.



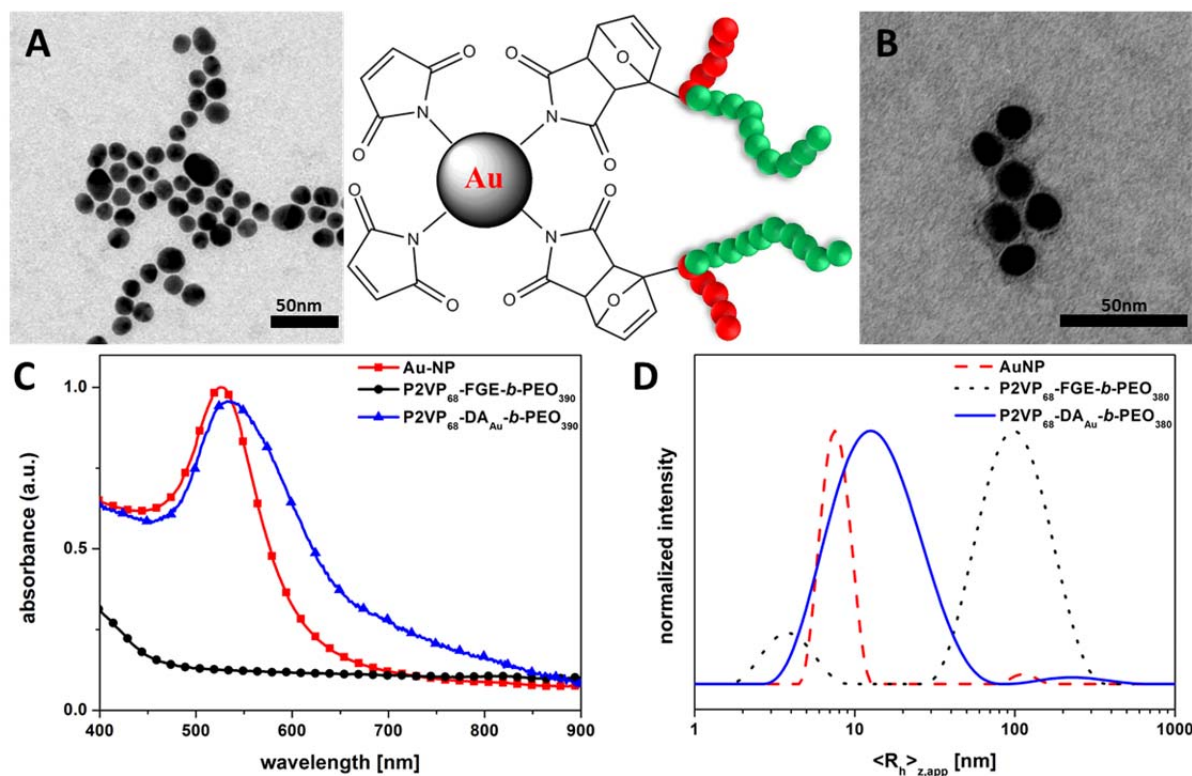


**Figure 4:** Comparison of TEM micrographs for the pristine (A, unstained) and polymer coated block copolymer AuNP (B, stained with uranyl acetate); comparison of UV-Vis spectra for P2VP<sub>68</sub>-FGE-*b*-PEO<sub>390</sub> (black curve), maleimide functionalized AuNP (red curve), and P2VP<sub>68</sub>-DA<sub>Au</sub>-*b*-PEO<sub>390</sub> (blue curve); comparison of intensity-weighted DLS CONTIN plots for P2VP<sub>68</sub>-FGE-*b*-PEO<sub>390</sub> (black dotted curve;  $\langle R_h \rangle_{z,app} = 4 \text{ nm}$  and  $100 \text{ nm}$ ;  $2 \text{ mg mL}^{-1}$ ), maleimide functionalized AuNP (red dashed curve;  $\langle R_h \rangle_{z,app} = 8 \text{ nm}$ ;  $1 \text{ mg mL}^{-1}$ ), and P2VP<sub>68</sub>-DA<sub>Au</sub>-*b*-PEO<sub>390</sub> (blue curve,  $\langle R_h \rangle_{z,app} = 12 \text{ nm}$ ;  $1 \text{ mg mL}^{-1}$ ) in DMF.

As a further proof for the successful particle coating, both P2VP<sub>68</sub>-DA<sub>Au</sub>-*b*-PEO<sub>390</sub> and the pristine AuNP were transferred from DMF into water (pH 7). While the solution containing P2VP<sub>68</sub>-DA<sub>Au</sub>-*b*-PEO<sub>390</sub> showed a red color (hinting towards well-dispersed hybrid particles), the pristine NP aggregated, indicated by a bluish color (**Figure S10A**). Under acidic conditions (pH  $\leq 4$ ), P2VP becomes protonated and positively charged. Therefore, zeta potential measurements were performed for the block copolymer and the nanoparticles, respectively (**Figure S10B**). While the pristine AuNP show a zeta potential of  $\sim -33 \text{ mV}$  at pH 7, precipitation was observed at pH 4. After coating, a zeta potential of  $-3 \text{ mV}$  at pH 7 and

+22 mV at pH 4 was found, following the trend observed for P2VP<sub>68</sub>-FGE-*b*-PEO<sub>390</sub> under this conditions (**Figure S10B**).

### *Conclusion*

We successfully synthesized a mid-chain functionalized block copolymer featuring one furan moiety, P2VP<sub>68</sub>-FGE-*b*-PEO<sub>390</sub> by sequential living anionic polymerization. The furan moiety was subsequently used in Diels-Alder reactions with maleimide functionalized counterparts to introduce dyes as model labels to the block copolymer or to create a hetero-grafted shell on Au-NP. Our results convincingly demonstrate that P2VP<sub>68</sub>-FGE-*b*-PEO<sub>390</sub> is a versatile example for (surface) functionalization and the introduction of hetero-brushes. Our results may also be used in the future for the stabilization of carbon-nanotubes (CNT) *via* P2VP<sub>68</sub>-pyr-*b*-PEO<sub>390</sub>, surface modification of nanoparticles different from Au, or the preparation of ABC miktoarm star terpolymers.

### *Acknowledgements*

The authors would like to thank Sarah Crotty for MALDI-TOF MS, Ulrike Günther for Zeta-potential measurements and David Pretzel for fluorescence microscopy measurements. F.H.S. thanks the VCI for an independent researcher fellowship, and T.R. acknowledges the Carl-Zeiss foundation for a PhD-scholarship. The work of M. J. B. forms part of the research program of the Dutch Polymer Institute (DPI), project #690. We also wish to acknowledge the Thuringian Ministry for Education, Science and Culture (grants #B514-09051, NanoConSens, #B515-10065, ChaPoNano, #B515-11028, BASIS and #B515-07008) for financial support of this study. USS, MDH and SH thank the Federal Ministry of Education and Research (Spitzencluster PHONA) for financial support.

## Table of Content

# Poly(2-vinyl pyridine)-*block*-Poly(ethylene oxide) featuring a Furan Group at the Block Junction – Synthesis and Functionalization

Tobias Rudolph,<sup>1,2,#</sup> Markus J. Barthel,<sup>1,2,3,#</sup> Florian Kretschmer,<sup>1,2</sup> Ulrich Mannsfeld,<sup>1,2</sup>  
Stephanie Hoepfener,<sup>1,2</sup> Martin D. Hager,<sup>1,2</sup> Ulrich S. Schubert,<sup>1,2,3</sup> and Felix H. Schacher<sup>1,2,\*</sup>

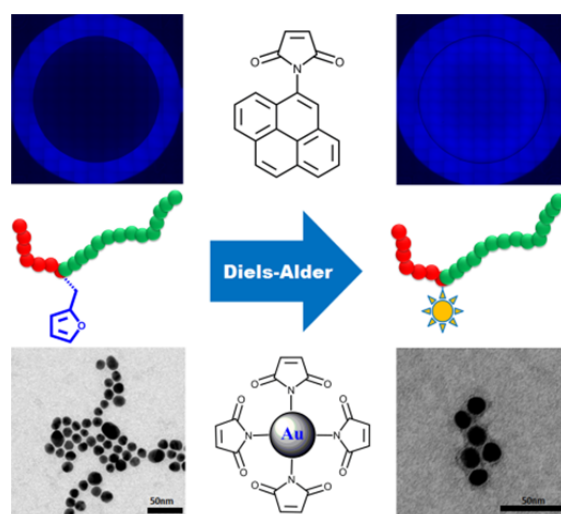
[1] Laboratory of Organic and Macromolecular Chemistry, Friedrich Schiller University Jena, Humboldtstr. 10,  
07743 Jena, Germany

E-mail: [felix.schacher@uni-jena.de](mailto:felix.schacher@uni-jena.de)

[2] Jena Center for Soft Matter (JCSM), Friedrich Schiller University Jena, Philosophenweg 7, 07743 Jena,  
Germany

[3] Dutch Polymer Institute, P.O. Box 902, Eindhoven 5600 AX, The Netherlands

# These authors contributed equally to this work.



We report the synthesis of mid-chain functionalized P2VP<sub>68</sub>-FGE-*b*-PEO<sub>390</sub> by sequential living anionic polymerization and its subsequent use for the attachment of model dyes or for the formation of a hetero-grafted shell onto Au nanoparticles by Diels-Alder reactions between the furan group and maleimides.

## References

1. F. H. Schacher, P. A. Rugar and I. Manners, *Angew. Chem. Int. Ed.*, 2012, **51**, 7898-7921.
2. A. H. Gröschel, F. H. Schacher, H. Schmalz, O. V. Borisov, E. B. Zhulina, A. Walther and A. H. E. Müller, *Nat. Commun.*, 2012, **3**, 710.
3. H.-C. Kim, S.-M. Park and W. D. Hinsberg, *Chem. Rev.*, 2009, **110**, 146-177.
4. A. Nunns, J. Gwyther and I. Manners, *Polymer*, 2013, **54**, 1269-1284.
5. S. B. Darling, *Prog. Polym. Sci.*, 2007, **32**, 1152-1204.
6. M. A. Tasdelen, M. U. Kahveci and Y. Yagci, *Prog. Polym. Sci.*, 2011, **36**, 455-567.
7. C. Barner-Kowollik, F. E. Du Prez, P. Espeel, C. J. Hawker, T. Junkers, H. Schlaad and W. Van Camp, *Angew. Chem. Int. Ed.*, 2011, **50**, 60-62.
8. K. Kempe, A. Krieg, C. R. Becer and U. S. Schubert, *Chem. Soc. Rev.*, 2012, **41**, 176-191.
9. A. S. Goldmann, M. Glassner, A. J. Inglis and C. Barner-Kowollik, *Macromol. Rapid Commun.*, 2013, **34**, 810-849.
10. T. Rudolph, S. Crotty, M. v. d. Lühe, D. Pretzel, U. S. Schubert and F. Schacher, *Polymers*, 2013, **5**, 1081-1101.
11. D. Fournier, R. Hoogenboom and U. S. Schubert, *Chem. Soc. Rev.*, 2007, **36**, 1369-1380.
12. H. Durmaz, A. Sanyal, G. Hizal and U. Tunca, *Polym. Chem.*, 2012, **3**, 825-835.
13. A. Hanisch, H. Schmalz and A. H. E. Müller, *Macromolecules*, 2012, **45**, 8300-8309.
14. C. Tonhauser and H. Frey, *Macromol. Rapid Commun.*, 2010, **31**, 1938-1947.
15. A. Natalello, C. Tonhauser, E. Berger-Nicoletti and H. Frey, *Macromolecules*, 2011, **44**, 9887-9890.
16. X.-S. Feng and C.-Y. Pan, *Macromolecules*, 2002, **35**, 4888-4893.
17. O. Altintas, U. Tunca and C. Barner-Kowollik, *Polym. Chem.*, 2011, **2**, 1146-1155.
18. O. Altintas, B. Yankul, G. Hizal and U. Tunca, *J. Polym. Sci. Part A: Polym. Chem.*, 2007, **45**, 3588-3598.
19. Z. L. Wang, J. T. Xu, B. Y. Du and Z. Q. Fan, *J. Colloid Interface Sci.*, 2011, **360**, 350-354.
20. C. Tonhauser, B. Obermeier, C. Mangold, H. Lowe and H. Frey, *Chem. Commun.*, 2011, **47**, 8964-8966.
21. C. Tonhauser, A. A. Golriz, C. Moers, R. Klein, H.-J. Butt and H. Frey, *Adv. Mater.*, 2012, **24**, 5559-5563.
22. M. J. Barthel, T. Rudolph, S. Crotty, F. H. Schacher and U. S. Schubert, *J. Polym. Sci. Part A: Polym. Chem.*, 2012, **50**, 4958-4965.
23. M. J. Barthel, T. Rudolph, A. Teichler, R. M. Paulus, J. Vitz, S. Hoepfener, M. D. Hager, F. H. Schacher and U. S. Schubert, *Adv. Funct. Mater.*, 2013, **23**, 4921-4932.
24. K. Knop, G. M. Pavlov, T. Rudolph, K. Martin, D. Pretzel, B. O. Jahn, D. H. Scharf, A. A. Brakhage, V. Makarov, U. Mollmann, F. H. Schacher and U. S. Schubert, *Soft Matter*, 2013, **9**, 715-726.
25. K. Kalyanasundaram and J. K. Thomas, *J. Am. Chem. Soc.*, 1977, **99**, 2039-2044.
26. M. Wilhelm, C. L. Zhao, Y. Wang, R. Xu, M. A. Winnik, J. L. Mura, G. Riess and M. D. Croucher, *Macromolecules*, 1991, **24**, 1033-1040.
27. G. Kwon, M. Naito, M. Yokoyama, T. Okano, Y. Sakurai and K. Kataoka, *Langmuir*, 1993, **9**, 945-949.
28. C.-W. Wu, L. R. Yarbrough and F. Y. H. Wu, *Biochemistry*, 1976, **15**, 2863-2868.
29. D. Vyprachtický, K. W. Sung and Y. Okamoto, *J. Polym. Sci. Part A: Polym. Chem.*, 1999, **37**, 1341-1345.
30. F. Kretschmer, U. Mansfeld, S. Hoepfener, M. Hager and U. S. Schubert, *Chem. Commun.*, 2013, **50**, 88-90.
31. H. Y. Song, M. H. Ngai, Z. Y. Song, P. A. MacAry, J. Hobley and M. J. Lear, *Org. Biomol. Chem.*, 2009, **7**, 3400-3406.

# Supporting Information

## **Poly(2-vinyl pyridine)-*block*-Poly(ethylene oxide) featuring a Furan Group at the Block Junction – Synthesis and Functionalization**

Tobias Rudolph,<sup>1,2,#</sup> Markus J. Barthel,<sup>1,2,3,#</sup> Florian Kretschmer,<sup>1,2</sup> Ulrich Mannsfeld,<sup>1,2</sup>  
Stephanie Hoepfener,<sup>1,2</sup> Martin D. Hager,<sup>1,2</sup> Ulrich S. Schubert,<sup>1,2,3</sup> and Felix H. Schacher<sup>1,2,\*</sup>

[1] Laboratory of Organic and Macromolecular Chemistry, Friedrich Schiller University Jena, Humboldtstr. 10,  
07743 Jena, Germany

E-mail: [felix.schacher@uni-jena.de](mailto:felix.schacher@uni-jena.de)

[2] Jena Center for Soft Matter (JCSM), Friedrich Schiller University Jena, Philosophenweg 7, 07743 Jena,  
Germany

[3] Dutch Polymer Institute, P.O. Box 902, Eindhoven 5600 AX, The Netherlands

# These authors contributed equally to this work.

## ***Instruments***

NMR: Proton nuclear magnetic resonance ( $^1\text{H-NMR}$ ) spectra were recorded in  $\text{CDCl}_3$  on a Bruker AC 300 MHz spectrometer at 298 K. Chemical shifts are given in parts per million (ppm,  $\delta$  scale) relative to the residual signal of the deuterated solvent.

SEC: Size exclusion chromatography was measured on a system equipped with a SCL-10A system controller, a LC-10AD pump and a RID-10A refractive index detector using a solvent mixture containing chloroform ( $\text{CHCl}_3$ ), triethylamine (TEA) and *iso*-propanol (*i*-PrOH) (94:4:2) at a flow rate of  $1 \text{ mL min}^{-1}$  on a PSS SDV linear M 5  $\mu\text{m}$  column. The system was calibrated using PS (100 to 100,000  $\text{g mol}^{-1}$ ) and PEO (440 to 44,700  $\text{g mol}^{-1}$ ) standards.

MALDI-ToF MS: Matrix-assisted laser desorption/ionization time of flight mass spectrometry was performed on an Ultraflex III TOF/TOF (Bruker Daltonics, Bremen, Germany), equipped with a Nd:YAG laser and with *trans*-2-[3-(4-*tert*-butylphenyl)-2-methyl-2-propenylidene] malononitrile (DCTB) as the matrix and NaCl as the doping agent in reflector and linear mode. The instrument was calibrated prior to each measurement with an external poly(methyl methacrylate) (PMMA) standard from PSS Polymer Standards Services GmbH (Mainz, Germany).

DLS: Dynamic light scattering was performed at a scattering angle of  $90^\circ$  on an ALV CGS-3 instrument equipped with a He-Ne laser operating at a wavelength of 633 nm at  $25^\circ\text{C}$ . The CONTIN algorithm was applied to analyze the obtained correlation functions. For temperature control, the DLS is equipped with a Lauda thermostat. Apparent hydrodynamic radii were calculated according to the Stokes-Einstein equation.

Transmission electron microscopy (TEM): TEM measurements were performed on a Philips CM-120. 15  $\mu\text{L}$  of the sample solution were blotted onto clean carbon coated TEM grids (Mesh 400, Quantifoil, Jena) and excess material was removed by a filter paper



(Whatman No. 1); the samples were allowed to dry prior to the transfer to the microscope. Grid cleaning was performed by UV-ozone treatment for 40 s. For staining purpose a drop of uranyl acetate ( $3 \text{ mg ml}^{-1}$ ) was applied to the grid, the supernatant solution was removed via filter paper and the sample washed with water to remove the excess of uranyl acetate.

Centrifugation was performed with a Heraeus Biofuge Primo with a fixed angle rotor in 1.5 mL Eppendorf tubes.

UV-Vis spectroscopy: UV-Vis absorption spectra were recorded with a Specord 250 spectrometer (Analytik Jena) or a Lambda 750 UV/VIS/NIR spectrometer (PerkinElmer) in Suprasil quartz glass cuvettes 104-QS (Hellma Analytics) with a thickness of 10 mm at room temperature.

Fluorescence microscope: Fluorescence images were measured on a fluorescence microscope (Cell Observer Z1, Carl Zeiss, Jena, Germany) equipped with a mercury arc UV lamp and the appropriate filter combinations for excitation and detection of emission. In this case the sample was irradiated with 357 nm and an emission filter of 460 nm. All images were measured using identical instrument settings (e.g. UV lamp power, integration time, camera gain) and spots of the well plate were addressed using an automated XY table.

Zeta Potential Measurements: The  $\zeta$ -potentials were measured on a ZetaSizer Nano ZS from Malvern *via* the M3-PALS technique with a laser beam at 633 nm. The detection angle was  $13^\circ$ . The electrophoretic mobilities ( $u$ ) were converted into  $\zeta$  –potentials *via* the Henry equation in the Smoluchowski approximation,  $z = u \eta / \epsilon_0 \epsilon$ , where  $\eta$  denotes the viscosity and  $\epsilon_0 \epsilon$  the permittivity of the solution.

## ***Experimental section***

### ***Materials***

Sec-butyl lithium, tetrahydrofuran, dimethylformamide, 2-vinyl pyridine, ethylene oxide, DPMK was synthesized as described in literature.<sup>1</sup> Furfuryl glycidyl ether was purified *via* column chromatography as described in literature.<sup>2</sup> 4-Phenylazomaleinanil and N-(1-pyrenyl)-maleimide were purchased from Sigma Aldrich and used as received. DMF (anhydrous, amine free, 99.9%) was purchased from Alfa Aesar. Dicyclohexylcarbodiimide (DCC), furane, 4-dimethylaminopyridine (DMAP) and potassium thioacetate were purchased from Sigma-Aldrich. Pentaerythritol tribromide was received from TCI Europe. Water (< 0.1 $\mu$ S/cm) was purchased from ELGA Purelab Prima. All chemicals were used as received. Compound **1**<sup>3</sup> and citrate stabilized nanoparticles<sup>4</sup> were synthesized as reported in literature.

### ***Anionic polymerization of 2-vinylpyridine and end-capping with furfuryl glycidyl ether***

In a Schlenk flask 80 mL freshly prepared THF were cooled to  $-78$  °C with an *iso*-propanol/dry ice bath and 0.71 mL (1 mmol) of *s*-BuLi was added and stirred for 10 min. Afterwards 5.1 mL (47 mmol) of freshly distilled 2-vinyl pyridine were added quickly to the reaction solution and stirred for 1 hours. Afterwards, 0.4 mL diphenylethylene (2.3 mmol) were added to the reaction mixture to decrease the nucleophilicity of the active chain end. After addition of 0.27 mL of furfuryl glycidyl ether (2.3 mmol) the solution was allowed to warm to RT and stirred overnight at 25 °C. The reaction was terminated afterwards by the addition of methanol.

The polymer was precipitated in cold hexane and the crude product was purified by dissolving in chloroform and washing with water. The solvent was removed under reduced pressure and the product was dried under vacuum.

**SEC** (CHCl<sub>3</sub>/*i*-PrOH/Et<sub>3</sub>N):  $M_n = 8\,700\text{ g mol}^{-1}$ ;  $\mathcal{D} = 1.08$  (PS-calibration); **<sup>1</sup>H NMR** (300 MHz, CDCl<sub>3</sub>,  $\delta$ ): 8.5-8.0 (br, arom. *H*), 7.4-7.1 (br, arom. *H*), 4.15 (s, CH<sub>2</sub>-furan), 3.74 (t, CH<sub>2</sub>), 2.55-2.15 (br, -CH-P2VP); **MALDI-TOF MS**:  $M_p = 7\,200\text{ g mol}^{-1}$ .

*Anionic polymerization of ethylene oxide (EO) via P2VP<sub>68</sub>-FGE-OH-macro initiator*

2.0 g of P2VP<sub>68</sub>-FGE-OH (0.28 mmol) were dissolved in 100 mL freshly distilled THF and transferred into a Büchi GlasUster PicoClave reactor. The hydroxyl-end group was activated *via* the addition of an excess of DPMK (~10 eq.) until a black color was observed. The reaction mixture was cooled to -20 °C and ethylene oxide (EO; 5.3 mL; 107 mmol) were introduced into the reaction vessel. The solution was slowly heated to 40 °C and stirred for 24 hours. The remaining pressure was released from the reactor system and the polymerization was terminated by the addition of methanol.

The desired block copolymer was obtained after precipitation into cold ether, filtering, and drying under vacuum.

**SEC** (CHCl<sub>3</sub>/*i*-PrOH/Et<sub>3</sub>N):  $M_n = 20\,000\text{ g mol}^{-1}$ ;  $\mathcal{D} = 1.11$  (-calibration); **<sup>1</sup>H NMR** (300 MHz, CDCl<sub>3</sub>,  $\delta$ ): 8.5-8.0 (br, arom. *H*), 7.4-7.1 (br, arom. *H*), 3.8-3.4 (PEO-backbone), 2.55-2.15 (br, -CH-P2VP); **MALDI-TOF MS**:  $M_p = 24\,500\text{ g mol}^{-1}$ .

### Synthesis of the thiol-linker

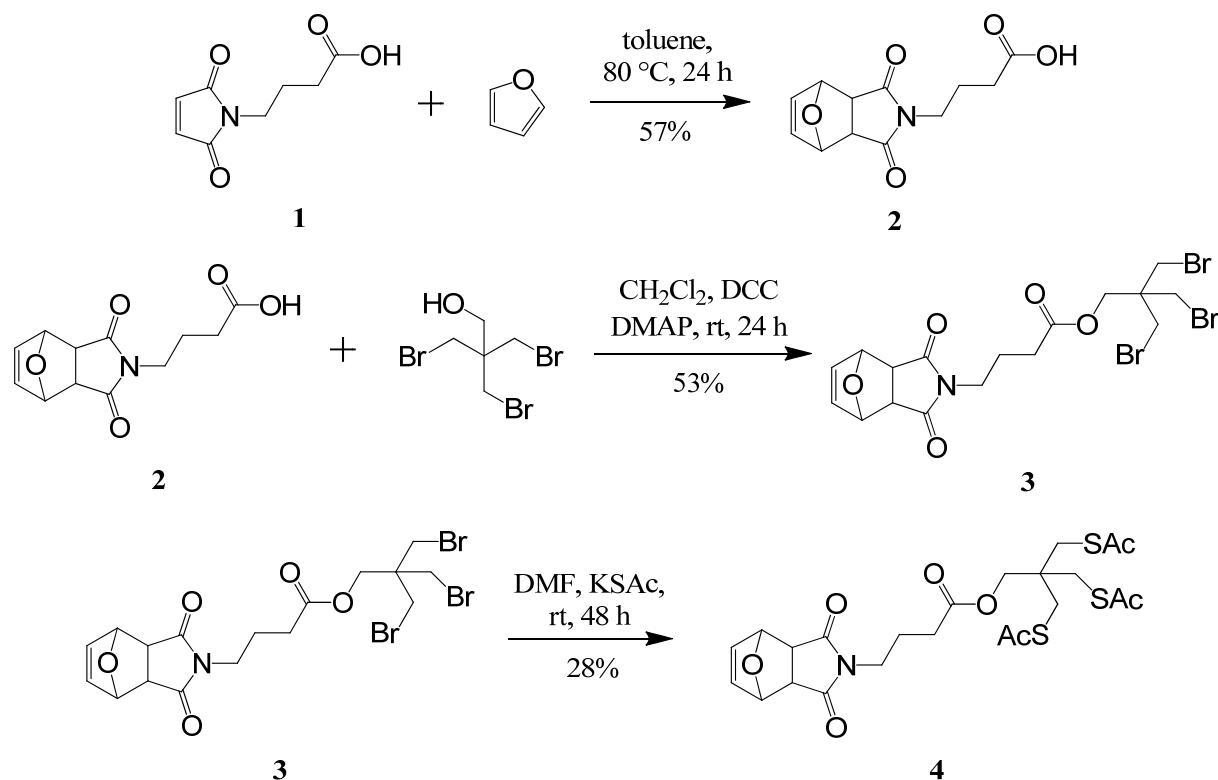


Figure S1: Synthetic strategy for the preparation of the maleimide-functionalized thiol-linker.

#### *4-(1,3-Dioxo-3a,4,7,7a-tetrahydro-1H-4,7-epoxyisoindol-2(3H)-yl)butanoic acid (2)*

**1** (1.4 g, 7.64 mmol) and furane (5.2 g, 76.40 mmol) were dissolved in 20 mL toluene and the solution was heated to 80 °C for 24 h. Subsequently, the reaction was cooled to 4 °C in the fridge. The formed precipitated was filtered off and dried to obtain **2** as white crystals. Yield 1.1 g (57% of theory).

**<sup>1</sup>H NMR** (300 MHz, CDCl<sub>3</sub>):  $\delta$  = 6.52 (s, 2 H, 2 CH), 5.28 (s, 2 H, 2 CH), 3.58 (t,  $J$  = 6.8 Hz, 2 H, CH<sub>2</sub>), 2.86 (s, 2 H, 2 CH), 2.37 (t,  $J$  = 7.42 Hz, 2 H, CH<sub>2</sub>), 1.93 (m,  $J$  = 7.22 Hz, 2 H, CH<sub>2</sub>) ppm. **<sup>13</sup>C NMR** (250 MHz, CDCl<sub>3</sub>):  $d$  = 177.31, 176.28, 136.50, 80.94, 47.40, 37.95, 30.78, 22.59 ppm.

*3-Bromo-2,2-bis(bromomethyl)propyl-4-(1,3-dioxo-3a,4,7,7a-tetrahydro-1H-4,7-epoxy-isoindol-2(3H)-yl)butanoate (3)*

**2** (1.1 g, 4.38 mmol), pentaerythritol tribromide (1.7 g, 5.23 mmol), DCC (1.36 g, 6.59 mmol) and DMAP (82 mg, 0.67 mmol) were dissolved in 50 mL methylene chloride and stirred at room temperature under nitrogen for 24 h. Afterwards the mixture was filtered and the clear solution was washed with 50 mL water. The organic phase was dried over sodium sulfate and the solvent was removed under reduced pressure. Subsequently the crude product was purified *via* column chromatography (silica gel 60, methylene chloride: ethyl acetate 95:5) and **3** was obtained as a colorless solid. Yield 1.3g (53% of theory).

**<sup>1</sup>H NMR** (300 MHz, CDCl<sub>3</sub>):  $\delta$  = 6.52 (s, 2 H, 2 CH), 5.27 (s, 2 H, 2 CH), 4.21 (s, 2 H, CH<sub>2</sub>), 3.56 (s, 6 H, 3 CH<sub>2</sub>), 3.55 (t, 2 H, CH<sub>2</sub>), 2.86 (s, 2 H, 2 CH), 2.35 (t,  $J$  = 7.31 Hz, 2 H, CH<sub>2</sub>), 1.92 (m,  $J$  = 7.08 Hz, 2 H, CH<sub>2</sub>) ppm. **<sup>13</sup>C NMR** (75 MHz, CDCl<sub>3</sub>):  $\delta$  = 176.22, 171.53, 136.49, 80.94, 63.71, 47.39, 42.73, 37.88, 34.11, 30.89, 22.71 ppm. **MS (HR-ESI)**:  $m/z$  calculated for [C<sub>17</sub>H<sub>20</sub>Br<sub>3</sub>NO<sub>5</sub>]<sup>Na+</sup>: 577.8784; found: 577.8776 [M + Na].

*3-(Acetylthio)-2,2-bis((acetylthio)methyl)propyl 4-(1,3-dioxo-3a,4,7,7a-tetrahydro-1H-4,7-epoxyisoindol-2(3H)-yl)butanoate (4)*

**3** (1 g, 1.79 mmol) and potassium thioacetate (1.22 g, 10.68 mmol) were dissolved in 10 mL DMF and stirred in a closed vial at room temperature for 48 h. Subsequently, 50 mL diethyl ether were added and the formed precipitate was filtered off. The organic solution was washed five times with 50 mL water followed by drying over sodium sulfate. Afterwards the solvent was removed under reduced pressure. The crude product was purified *via* column chromatography (silica gel 60, methylene chloride: acetonitrile 38:2) to obtain **4** as a yellow oil which solidifies upon standing. Yield 290 mg (28% of theory).

**<sup>1</sup>H NMR** (300 MHz, CDCl<sub>3</sub>): δ = 6.52 (s, 2 H, 2 CH), 5.29 (s, 2 H, 2 CH), 3.95 (s, 2 H, CH<sub>2</sub>), 3.57 (t, *J* = 6.85, 2 H, CH<sub>2</sub>), 3.07 (s, 6 H, 3 CH<sub>2</sub>), 2.86 (s, 2 H, CH<sub>2</sub>) 2.36 (s, 9 H, 3 CH<sub>3</sub>), 2.35 (t, 2 H, CH<sub>2</sub>), 1.93 (m, *J* = 7.08 Hz, 2 H, CH<sub>2</sub>) ppm. **<sup>13</sup>C NMR** (75 MHz, CDCl<sub>3</sub>): δ = 194.14, 176.20, 171.97, 136.53, 80.94, 66.09, 47.43, 42.16, 37.99, 32.94, 30.99, 30.58, 22.68 ppm. **MS (HR-ESI)**: *m/z* calculated for [C<sub>23</sub>H<sub>29</sub>NO<sub>8</sub>S<sub>3</sub>]<sup>Na+</sup>: 566.0948; found: 566.0900 [M + Na].

#### *Synthesis of maleimide stabilized gold nanoparticles (Au-NP)*

10 × 1 mL citrate stabilized gold nanoparticles were pipetted in Eppendorf tubes and centrifuged at 5000 rpm for 90 minutes. Respectively, 950 μL of the supernatant solution were taken off, subsequently, a solution of **4** (100 μL, 1 mg/mL DMF) and 850 μL DMF were added. The particles were redispersed by simple shaking. The solution was centrifuged at 5000 rpm for 90 minutes, afterwards, 900 μL of the supernatant solution were taken off and the remaining 100 μL solution of the ten tubes were combined and pipetted in a glass vial. Finally, a solution of **4** (46 μL, 1 mg/mL DMF) was added and the mixture was heated to 130 °C for 1 h in order to cleave off the furan unit.

#### *Diels-Alder reaction with maleimide-functionalized gold-nanoparticle*

P2VP<sub>68</sub>-FGE-*b*-PEO<sub>390</sub> (5 mg) and 1 mg AuNP (46 μg of **4**) were dissolved in 1.5 mL DMF and heated to 75 °C for 2 days. The excess of block copolymer was removed by centrifugation at 5000 rpm for 90 minutes. The supernatant solution was removed and the particles re-suspended in DMF.

*Diels-Alder reaction P2VP<sub>68</sub>-FGE-*b*-PEO<sub>390</sub> and N-(1-pyrenyl)maleimide*

P2VP<sub>68</sub>-FGE-*b*-PEO<sub>390</sub> (100 mg; 4 μmol) and N-(1-pyrenyl)maleimide (24 mg; 0.08 mmol) were dissolved in 2 mL DMF. The solution was heated to 75 °C overnight. The desired product was received after size exclusion column chromatography (BioBeads SX1) with THF as eluent.

SEC (CHCl<sub>3</sub>/*i*-PrOH/Et<sub>3</sub>N): M<sub>n</sub> = 17 000 g mol<sup>-1</sup>; Đ = 1.22 (PEO-calibration)

*Diels-Alder reaction P2VP<sub>68</sub>-FGE-*b*-PEO<sub>390</sub> and 4-phenylazomaleinanil*

P2VP<sub>68</sub>-FGE-*b*-PEO<sub>390</sub> (100 mg; 4 μmol) and 4-phenylazomaleinanil (24 mg; 0.08 mmol) were dissolved in 2 mL DMF. The solution was heated to 75 °C overnight. The desired product was received after size exclusion column chromatography (BioBeads SX1) with THF as eluent.

SEC (CHCl<sub>3</sub>/*i*-PrOH/Et<sub>3</sub>N): M<sub>n</sub> = 16 000 g mol<sup>-1</sup>; Đ = 1.24 (PEO-calibration)

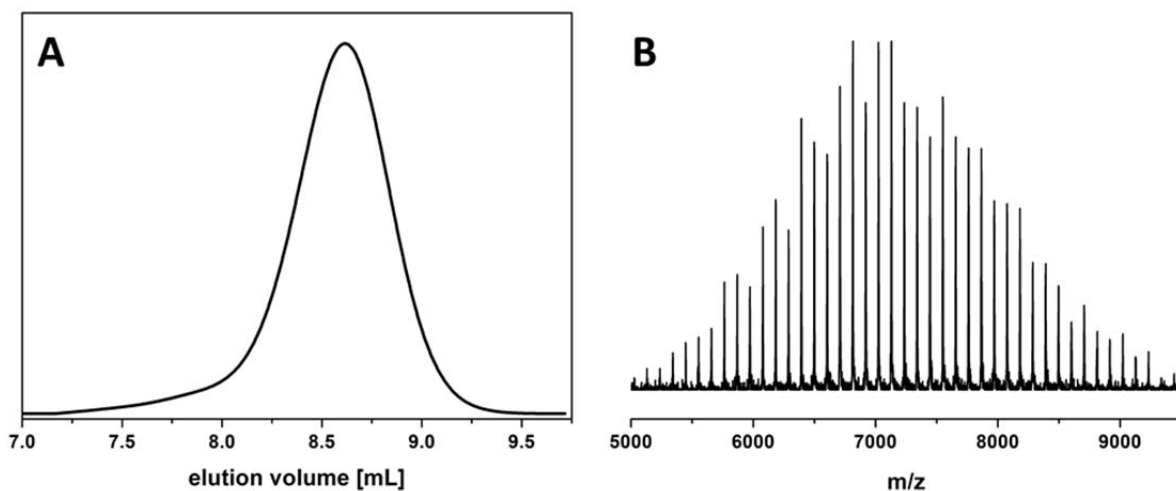


Figure S2: SEC trace (A) and MALDI-TOF MS spectra (B) for P2VP<sub>68</sub>-FGE-OH.

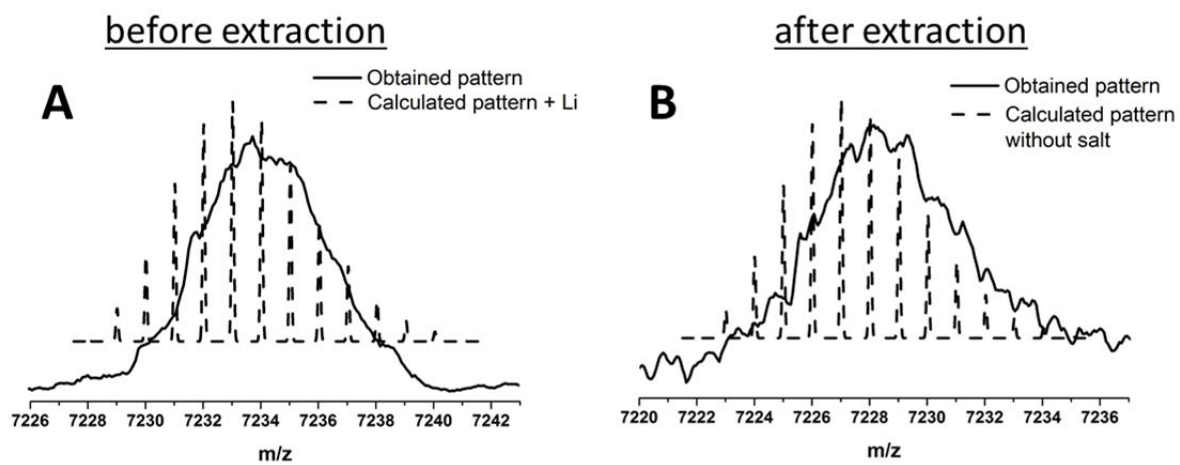


Figure S3: Comparison of the measured and the calculated MALDI-TOF MS spectra for P2VP<sub>68</sub>-FGE-OH before (A) and after (B) extraction to remove the lithium counterion.



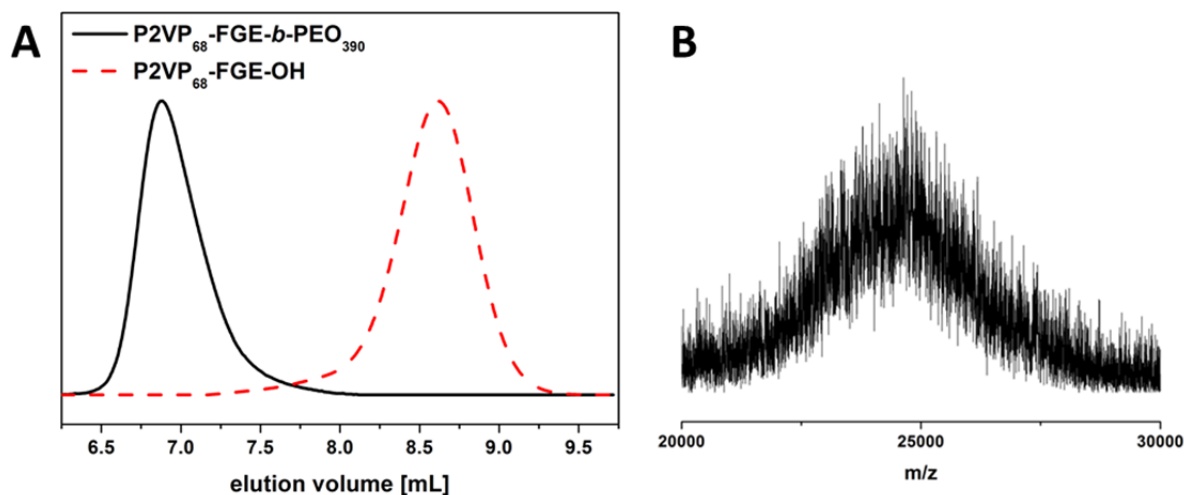


Figure S4: Comparison of the SEC traces for for P2VP<sub>68</sub>-FGE-OH (dashed line) and for P2VP<sub>68</sub>-FGE-*b*-PEO<sub>390</sub> (A) and MALDI-TOF MS spectra of P2VP<sub>68</sub>-FGE-*b*-PEO<sub>390</sub>.

Table S1: Characterization of the functionalized homopolymer (P2VP<sub>68</sub>-FGE-OH), block copolymer (P2VP<sub>68</sub>-FGE-*b*-PEO<sub>390</sub>) and the functionalized P2VP<sub>68</sub>-FGE-*b*-PEO<sub>390</sub>.

Polymer	$M_n^a$ [g mol <sup>-1</sup> ]	PDI <sup>a</sup>	$M_p^d$ [g mol <sup>-1</sup> ]
P2VP <sub>68</sub> -FGE-OH <sup>b</sup>	8 700 <sup>c</sup>	1.08 <sup>c</sup>	7 200
P2VP <sub>68</sub> -FGE- <i>b</i> -PEO <sub>390</sub> <sup>b</sup>	19 000	1.11	24 500
P2VP <sub>68</sub> -azo- <i>b</i> -PEO <sub>390</sub>	16 000	1.24	-
P2VP <sub>68</sub> -pyr- <i>b</i> -PEO <sub>390</sub>	17 000	1.22	-

a) SEC (CHCl<sub>3</sub>/*iso*-propanol/triethylamine) (PEO-calibration)

b) Determination by a combination of <sup>1</sup>H-NMR and MALDI-TOF MS

c) SEC (CHCl<sub>3</sub>/*iso*-propanol/triethylamine) (PS-calibration)

d) MALDI-TOF MS

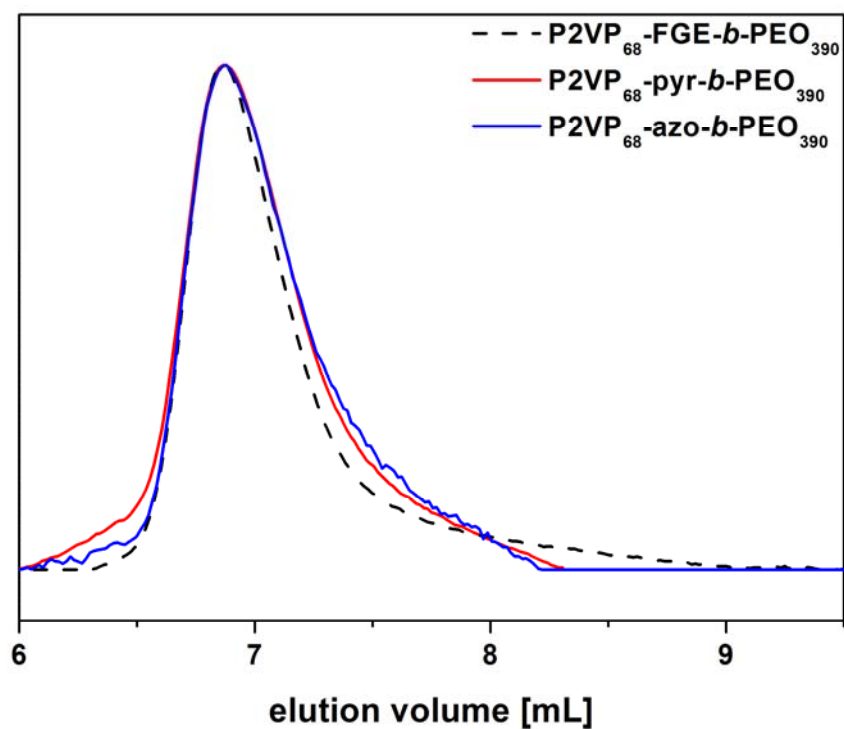


Figure S5: Comparison of SEC traces for the P2VP<sub>68</sub>-FGE-*b*-PEO<sub>390</sub> (black dashed curve), P2VP<sub>68</sub>-pyr-*b*-PEO<sub>390</sub> (red curve), and P2VP<sub>68</sub>-azo-*b*-PEO<sub>390</sub> (blue curve).

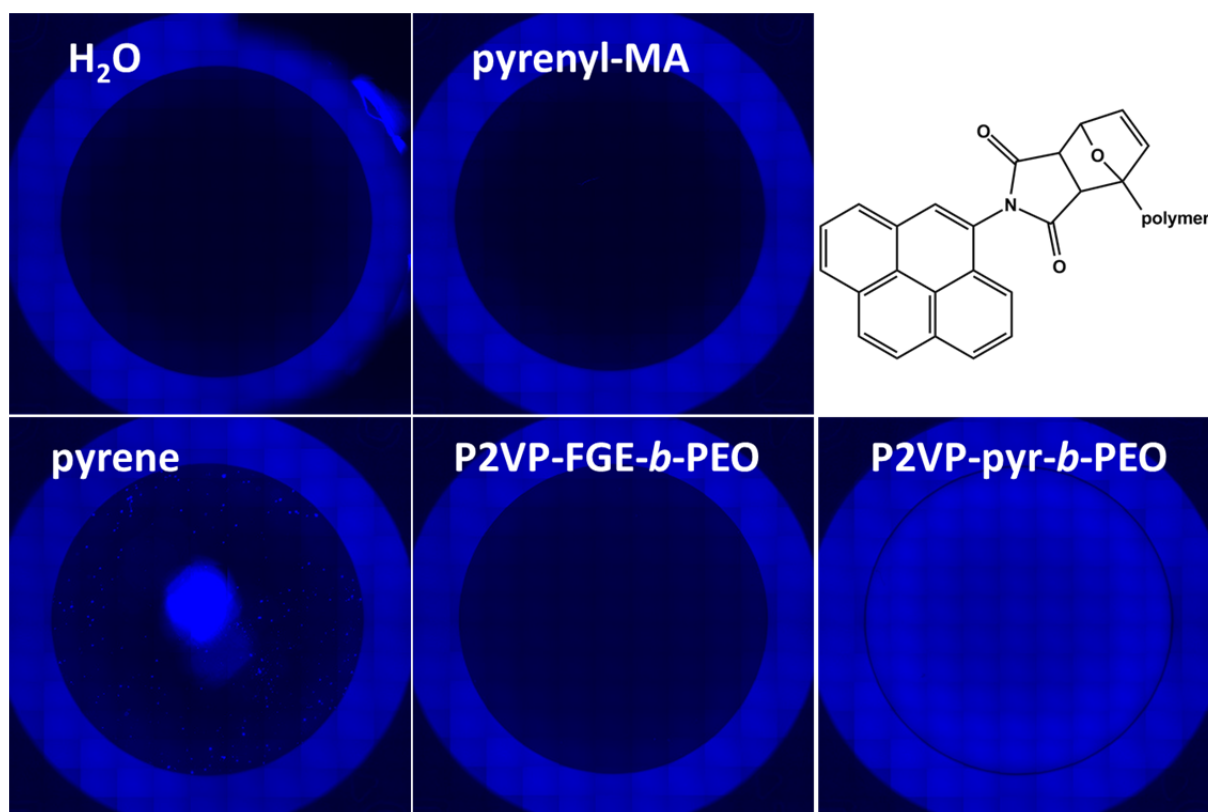
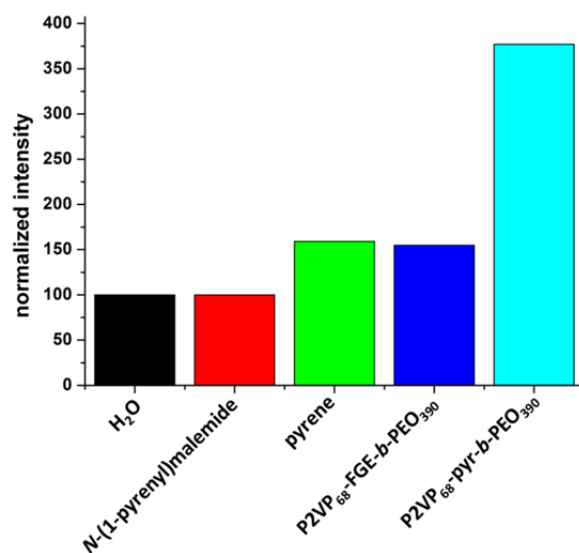


Figure S6: Comparison of fluorescence micrographs for water (A), pristine *N*-(1-pyrenyl)maleimide (B), pyrene (C), P2VP<sub>70</sub>-FGE-*b*-PEO<sub>380</sub> (5 mg mL<sup>-1</sup>), and P2VP<sub>70</sub>-pyr-*b*-PEO<sub>380</sub> (5 mg mL<sup>-1</sup>) in water (at pH 7) under comparable conditions (same gain, excitation 357 nm; emission filter 460 nm).



**Figure S7:** Comparison of the fluorescence measurements normalized in comparison to H<sub>2</sub>O (black) for *N*-(1-pyrenyl)-maleimide (red), pyrene (green), P2VP<sub>68</sub>-FGE-*b*-PEO<sub>390</sub> (blue, 5 mg mL<sup>-1</sup>) and P2VP<sub>68</sub>-pyr-*b*-PEO<sub>390</sub> (cyan, 5 mg mL<sup>-1</sup>) in water (at pH 7) under comparable conditions (same gain, excitation 357 nm; emission filter 460 nm).

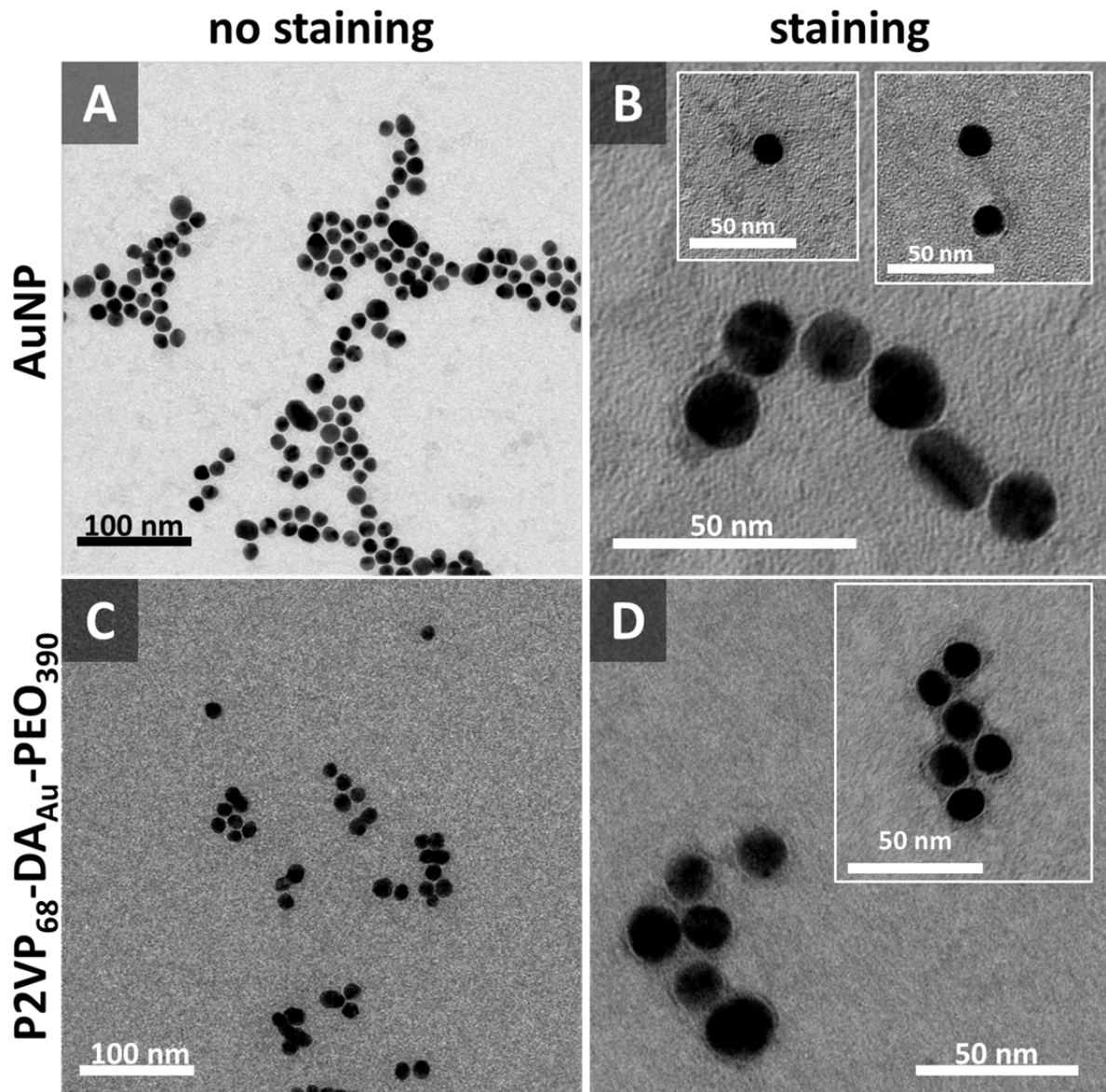


Figure S8: Comparison of TEM micrographs of the maleimide-coated AuNPs (A and B) and P2VP<sub>68</sub>-DA<sub>Au</sub>-PEO<sub>390</sub> (C and D): before (A and C) and after (B and D) staining with uranyl acetate.

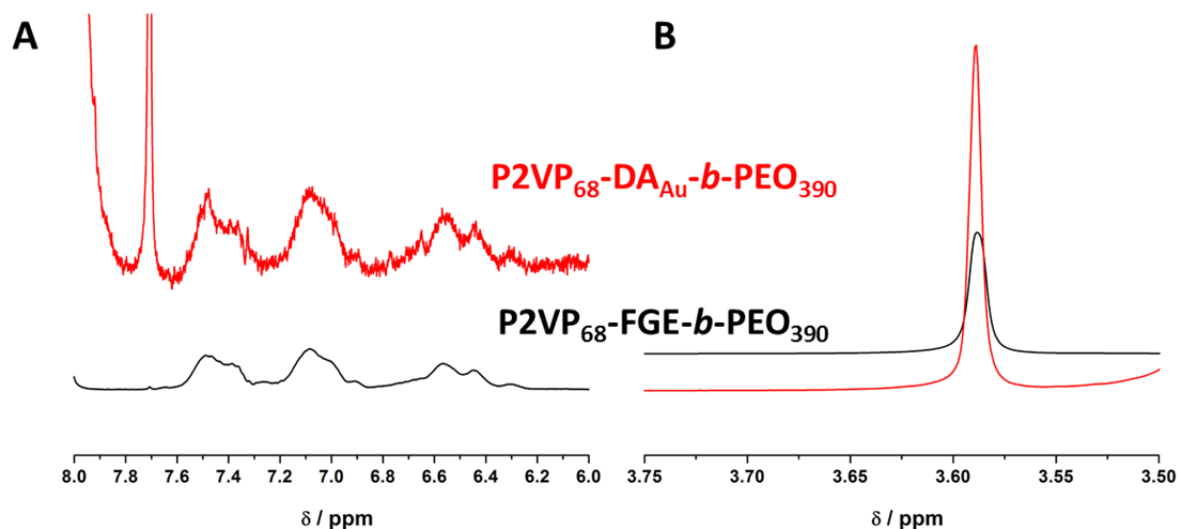


Figure S9: Comparison of NMR spectra for P2VP<sub>68</sub>-FGE-*b*-PEO<sub>390</sub> (black curve) and P2VP<sub>68</sub>-DA<sub>Au</sub>-*b*-PEO<sub>390</sub> (black curve) in the characteristic regions for P2VP (A) and PEO (B).

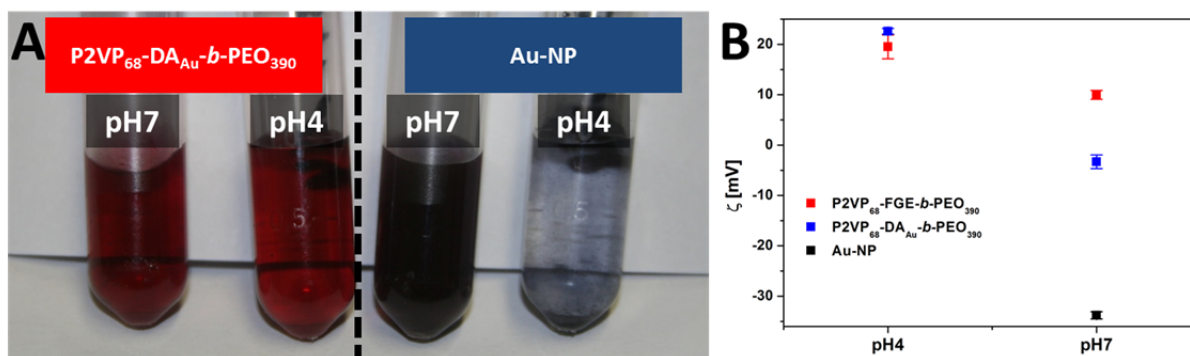


Figure S10: A) Comparison of images for P2VP<sub>68</sub>-DA<sub>Au</sub>-*b*-PEO<sub>390</sub> (left) and AuNP (right); B) Zeta potential measurements for P2VP<sub>68</sub>-DA<sub>Au</sub>-*b*-PEO<sub>390</sub> (blue dots; ~0.2 mg mL<sup>-1</sup> polymer), P2VP<sub>68</sub>-FGE-*b*-PEO<sub>390</sub> (red dots; 0.5 mg mL<sup>-1</sup>) and Au-NP (black dot) after transfer into water at different pH 4 and 7.

## References

- 1 H. Normant, B. Angelo; *B. Soc. Chim. Fr.*, 1960, 354.
- 2 M. J. Barthel, T. Rudolph, S. Crotty, F. H. Schacher, U. S. Schubert; *J. Polym. Sci. Part A: Polym. Chem.*, 2012, 50, 4958-4965.
- 3 H. Y. Song, M. H. Ngai, Z. Y. Song, P. A. MacAry, J. Hobley, M. J. Lear, *Org. Biomol. Chem.*, 2009, 7, 3400-3406.
- 4 F. Kretschmer, U. Mansfeld, S. Hoepfner, M. Hager and U. S. Schubert, *Chem. Commun.*, 2013, 50, 88-90.